UNDERSTANDING THE CO_2 CYCLE IN THE NORTH PACIFIC OCEAN USING INVERSE BOX MODELS

By

Richard James Matear

B.Eng., (Geophysics) University of Saskatchewan

M.Sc., University of British Columbia

A THESIS SUBMITTED IN PARTIAL FULFILMENT OF THE REQUIREMENTS

FOR THE DEGREE OF DOCTOR OF PHILOSOPHY

IN

THE FACULTY OF GRADUATE STUDIES

(DEPARTMENT OF OCEANOGRAPHY)

We accept this thesis as conforming

to the required standard

THE UNIVERSITY OF BRITISH COLOMBIA

June 1993

In presenting this thesis in partial fulfilment of the requirements for an advanced degree at the University of British Columbia, I agree that the Library shall make it freely available for reference and study. I further agree that permission for extensive copying of this thesis for scholarly purposes may be granted by the head of my department or by his or her representatives. It is understood that copying or publication of this thesis for financial gain shall not be allowed without my written permission.

(Signature) _____

Department of Oceanography

The University of British Columbia
Vancouver, Canada

Date July 3/93

ABSTRACT

Tracer transports across 35°N were computed using the hydrographic data from a synoptic section (INDOPAC) and from the Levitus annual mean section. The tracer transports calculated from the INDOPAC section were better able to close the tracer budgets in the North Pacific than the Levitus section. The transport calculations showed that highly resolved hydrographic data are necessary to accurately determine the tracer transports, and pointed out the sensitivity of the calculation to errors in the Ekman transports and air-sea exchanges of fresh water.

The inverse box model was applied to data generated from the Hamburg LSGOC-biogeochemical model. For this data, the mixing transports of the tracers were important for closing the tracer budgets. Applying the inverse box model to the temperature, salinity, total CO_2, alkalinity, phosphate, oxygen, POC, calcite, and ^{14}C fields produced poor results. With the addition of velocity shear information, the inverse box model extracted the correct velocity fields and produced air-sea exchanges and detrital rain rates consistent with the known values from the Hamburg model.

A model of the nutrient and carbon cycles in the North Pacific north of 24°N is formulated, and water flow rates, eddy mixing coefficients, particle fluxes and air-sea exchange rates of fresh water, heat, CO_2 and O_2 are calculated. The model incorporates geostrophy, wind-driven Ekman transports and budget equations for a suite of seven tracers. Geostrophic transports are based on two highly resolved synoptic sections across the North Pacific at 24°N (Roemmich *et al.,* 1991) and 47°N (Talley *et al.,* 1991). Tracer

distributions are obtained from historical station data. Budgets of mass, heat, salt, oxygen, phosphate, silicate, CO_2 and alkalinity are satisfied simultaneously in the North Pacific. The water transports in the model are in agreement with other transport calculations for the Pacific. The calculated heat transport showed that the subtropical North Pacific transfers heat into the atmosphere while the subarctic ocean gains heat. The net heat lost by the North Pacific ocean was 0.12 ± 0.08 PW. The North Pacific Ocean was calculated to be a sink of 0.1 ± 0.1 Gt C yr^{-1} of atmospheric carbon. The calculated maximum values of new production for the subarctic and subtropical regions are 42 g C m^{-2} yr^{-1} and 12 g C m^{-2} yr^{-1} respectively. The influence of the dissolved organic matter on the nutrient and carbon cycles is investigated using the data reported by Suzuki *et al.,* (1985). The model showed that the dissolved organic matter had little influence on the carbon and nutrient cycles. More data for the dissolved organic matter should be collected to verify this result.

TABLE OF CONTENTS

LIST OF TABLES

LIST OF FIGURES

LIST OF SYMBOLS AND ABBREVIATIONS

AABW	Antarctic Bottom Water
AAIW	Antarctic Intermediate water
$CaCO_3$	Calcium Carbonate
CO_2	Carbon dioxide
CO_3^{-2}	Carbonate ion
DIC	Dissolved inorganic carbon
DOC	Dissolved organic carbon
DOM	Dissolved organic matter
DON	Dissolved organic nitrogen
HCO_3^-	Bicarbonate ion
H_2O	Water
K_1	First apparent dissociation constant for carbonic acid
K_2	Second apparent dissociation constant for carbonic acid
k_h	isopycnal mixing coefficent
k_v	diapycnal mixing coefficent
K_w	Ionization constant for water
LP	Linear Programming
LSG	Large Scale Geostrophic
LSGOC	Large Scale Geostrophic Ocean Circulation
LSI	Least Squares with inequality constraints
NPBW	North Pacific Bottom Water

NPIW	North Pacific Intermediate Water
NODC	National Oceanographic Data Center
O_2	Oxygen
pCO_2	Partial pressure of carbon dioxide
POC	particulate organic carbon
PW	10^{15} Watts
S	Salinity
T	Temperature
TCO_2	Total Dissolved inorganic carbon
α	Solubility of carbon dioxide in water
μ	10^{-6}

ACKNOWLEDGEMENT

I would like to thank my committee members for their inspiration and guidance during the work on this thesis. I would especially like to express my gratitude to Dr. K. Holmen for our interesting discussion on applying inverse models to geochemical cycles, and for providing me with the opportunity to spend six months in Stockholm Sweden. Both of which were instrumental in shaping the research presented in this thesis. To Dr. C. S. Wong I wish to acknowledge the patience and encouragement he provided when discussing my doctorial research.

To my wife Rhonda, I immensely appreciate the sacrifices she made and the moral support she has provided.

This research was supported by a Joint Venture Agreement between the Institute of Ocean Sciences, Department of Fisheries and Oceans, and the Department of Oceanography at the University of British Columbia.

CHAPTER 1. INTRODUCTION

Since the start of the industrial age, the concentration of CO_2 in the atmosphere has increased dramatically (Bacastow and Keeling, 1981). This increased CO_2 concentration in the atmosphere is expected to lead to significant global climatic changes during the coming decades (Dickinson, 1986; Ramanathan, 1988; Washington and Meehl, 1989). After 35 years of measurements of CO_2 in the atmosphere and oceans, the global CO_2 budget is still surprisingly uncertain. An improved understanding of the CO_2 cycle is essential to predict the future rate of CO_2 increase in the atmosphere and the future climatic changes, as well as to plan for a strategy to reduce CO_2 emissions.

The three most important reserves in the global carbon cycle are the atmosphere, the terrestrial ecosystem and the oceans. At present, the combustion of fossil fuels outputs 5.3 Gt/yr (10^{15} g/yr) of carbon into the atmosphere (Tans *et al.*, 1990). This is a major contributor to the rise in atmospheric CO_2 concentrations. The measured rise in CO_2 was about 57% (3 Gt/yr) of the fossil fuel input for 1981-87. The excess CO_2 must be removed from the atmosphere by the ocean and by the terrestrial ecosystem.

The effect of the terrestrial ecosystem on the atmospheric CO_2 concentration is not well understood. Houghton (1986), Bolin (1986) and Wong (1978) consider that the terrestrial ecosystem is a source of CO_2 due to a deforestation. Contrary to this, Tans *et al.*, (1990) believe that it is a significant sink of carbon due to unknown processes.

Estimates of the uptake of CO_2 by the ocean have been made using "box" models and 3-dimensional ocean circulation models (Siegenthaler, 1983; Maier-Reimer and Hasselmann, 1987; Bacastow and Maier-Reimer, 1990; Toggweiler *et al.*, 1989a and 1989b; Bolin, 1986). From these models, the uptake of CO_2 ranges between 26 - 44% (1.3 - 2.3 Gt/yr) of the fossil fuel output. This shows that the ocean is an important sink of atmospheric CO_2, but its absolute magnitude is poorly determined. Better understanding of the role of the ocean in the CO_2 cycle is necessary to balance the CO_2 budget and to allow one to better assess the importance of the terrestrial ecosystem.

The research in this thesis is based on the study of the CO_2 cycle of the North Pacific Ocean through the use of inverse box models. From previous work it is not clear if the North Pacific Ocean is a sink of carbon (Tans *et al.*, 1990) or a source (Broecker *et al.*, 1986). The goal of this work is to improve the understanding of the carbon cycle in the North Pacific and to assess the role of this ocean basin in modulating the CO_2 in the atmosphere. This requires that one quantify the processes that transport carbon in the ocean. Related to these questions, I will address the effectiveness of the box model in extracting information about the CO_2 cycle by making use of data generated by a general circulation model (GCM) of Bacastow and Maier-Reimer (1990).

1.1 INVERSE BOX MODELS

The box model is a classical method used for developing a quantitative picture of the role of an ocean in transporting heat, salt, carbon and other tracers. The studies of

Wunsch and Minster (1982) and Bolin *et al.*, (1983) provide the foundation for formulating this problem as an inverse problem. In these studies, the conservation constraints are applied to a set of boxes for the observed distribution of physical and biochemical tracers. This process generates a set of equations by which inverse methods are used to extract a solution, giving values for rates of the processes which govern the tracer distributions. The work of Wunsch and Minster and Bolin *et al.*, has been followed by other studies that use the inverse methodology with various tracers to quantify the advective, biological and air-sea processes affecting the tracer distributions (Bolin *et al.*, 1987; Schlitzer, 1988 and 1989; Wunsch 1984; Garçon and Minster, 1989; Metzl *et al.*, 1989; Metzl *et al.*, 1990, plus others not mentioned). In the studies referenced, questions concerning the problems of including different tracers, of including different processes, of considering different model regions, of considering the seasonal scale, and of choosing the spatial scale (the box sizes) in the inverse models are addressed. For example, Rintoul (1988) looked at the compatibility of heat and nutrient transports in the South Atlantic. Garçon and Minster (1987) addressed the question of introducing heat transport in the Bolin *et al.*, (1983) model. Schlitzer (1988, 1989) looked at the carbon cycle in the North Atlantic and Bolin *et al.*, (1987) for the whole Atlantic Ocean. Metzl *et al.*, (1990) looked at the processes that must be included in inverse methods when one uses biogeochemical tracers; the application was made in the Indian Ocean. The common ingredient of all these models is the desire to quantify the advective and biological processes from tracer distributions through the use of the inverse methodology. The

models differ in the processes that are considered unknown, the tracer fields used, and the additional equations generated from dynamical principles (e.g. geostrophy).

From the past studies, it is useful to emphasize some of the important philosophical differences in applying these models to tracer data. The main differences are 1) the data used to calculate the mean circulation field, 2) how the geostrophic constraint is applied, 3) how the tracer transports are determined, and 4) the algorithm employed to solve the inverse problem.

The two different types of hydrographic data employed in the box models for the computation of geostrophic velocities are synoptic sections (Rintoul and Wunsch, 1991; Meméry and Wunsch, 1990), and Levitus annual mean temperature and salinity data (Schlitzer, 1988, 1989). The advantage of using the Levitus data set is the flexibility in defining the boxes of the model (sampling of 1° in latitude and longitude). The drawback to using the Levitus data set is the question of whether this data set is adequate for calculating the mass and tracer transports. This question will be further explored in chapter 2.

Setting aside the question of the "best" data to use in calculating the geostrophic transports, important differences exist among the various models in how the geostrophic transports are applied in the model. In Bolin *et al.*, (1987) much effort is spent on determining the weighting to be used for the geostrophic constraints. Such a question can never be satisfactorily answered, and in Matear (1989) I also devote much effort to the question of weighting the equations. The conclusion reached in Matear (1989) and in Bolin *et al.*, (1987) is that a simple weighting be employed that reflects the relative

information content of the equations. In part, the question of weighting constraints can be circumvented by assigning acceptable errors to the constraints and by using the linear programming routine to solve the problem. This will be discussed further in chapter 3. The problem of weighting of the geostrophic constraints arose in the Bolin *et al.*, (1987) work; by demanding that geostrophy be exactly satisfied, the errors in the conservation of the tracers were greatly increased. In Bolin *et al.*, (1987), only one reference velocity was determined for each horizontal section used to defined the boxes; in part, the difficulties experienced may have been resolved by determining more reference level velocities. Just such an approach was used by Rintoul and Wunsch (1991), in their application of geostrophy. They allowed an unknown reference level velocity for each station pair in the section defining the boxes. Such an approach generates a large underdetermined system of equations (number of unknowns greatly exceeds the number of constraints). In order to solve such a system, one typically invokes the additional constraint that the square of the magnitude of the unknowns be minimized. The problem in such an approach is that the individual velocities are poorly resolved by the tracer data, and thus the added degrees of freedom introduced by having many reference level velocities are not justified. The results of Rintoul and Wunsch (1991) showed that, except for the areas of significant topography, the reference level velocities were nearly constant. Schlitzer (1988, 1989) realized that the tracer fields did not provide adequate information to resolve the small scale reference velocities (e.g. reference velocity for each station pair) and so allowed only several reference velocities for each section defining the boxes (length scale of 1000 km). By doing it this way he ensured that the model was still

overdetermined (more equations than unknowns). This is the approach I take in applying my inverse model to the North Pacific data.

How the tracer transports are calculated varies significantly with the different studies. In Bolin *et al.*, (1983), Garçon and Minster (1988), and Metzl *et al.*, (1990), the advective transport is determined as the average transport through the box face times the average concentration between the two adjacent boxes. In the work of Schlitzer (1988 and 1989) and Rintoul and Wunsch (1991), the advective transport is calculated from the tracer concentrations along the section. The other major difference in the tracer transports is whether turbulent mixing transports are considered in the model. In the studies with reference level velocities determined at each station pair, the mixing terms are omitted. In the work of Schlitzer (1989) and Bolin *et al.*, (1987), the turbulent mixing terms are parameterized by an apparent eddy diffusion term times the tracer gradient normal to the box face. The two approaches are either to determine many reference level velocities and omit mixing or to limit the number of reference velocities but include mixing transports. It is unclear which approach is better. I will use the latter approach because, by ensuring that the problem is overdetermined, it is possible to determine the unknown parameters most consistent with the constraints. If too many unknown parameters were to be considered, the inverse model would be unable to resolve all the unknowns. Therefore, it seems logical to try and restrict the number of unknowns to a number that can be resolved by the model. The inclusion of the mixing transports is in recognition of the fact that the model will not resolve the small-scale transports.

The choice of the algorithm in many ways reflects what one expects to answer by the model. At this point I will only present and briefly discuss the two most common algorithms employed in the cited references above, the least squares with inequality constraints (LSI) and linear programming (LP) algorithms. In the LSI routine, one essentially determines the "best" solution to the observed tracer properties. The solution obtained in such a way may have more meaning physically and may be more easily compared to other observations than the LP solutions. In the LP routine, one determines the maximum or minimum value of a given quantity that is consistent with the observed property distribution and constraints. I will employ both algorithms to extract information from the model.

The one common ingredient missing from all the cited references is the application of the inverse models to the North Pacific. With the extensive studies of JGOFS and WOCE, it is an ideal time to look at the situation in the North Pacific. Such a research effort can provide tools to use the data that will be generated by these experiments to further advance our understanding of the carbon and nutrient cycles.

1.2 OCEAN CARBON CYCLE

Carbon is present in the ocean in the form of dissolved inorganic carbon (DIC), organic compounds (particulate organic carbon and dissolved organic carbon) and calcium carbonate ($CaCO_3$). The DIC in the ocean accounts for about 97% of the carbon in the ocean (Post *et al.*, 1990). The ocean contains about 50 times more carbon than the

atmosphere (Post *et al.*, 1990). The main reason for the abundance of carbon in the ocean is its chemical reactivity with water. The average surface water in the ocean contains only 0.5% of the DIC in the form of dissolved CO_2 gas the remaining DIC is composed of bicarbonate ions, HCO_3^- ($\approx$90%) and carbonate ions, CO_3^{-2} ($\approx$10%). Thus the atmosphere only sees a tiny fraction of the carbon present in sea water, enabling the ocean to be a relativelty large reservoir of carbon. The partition of carbon between the atmosphere and the ocean and the distribution of DIC within the ocean is affected by the ocean circulation, by the biological activity and by the air-sea exchange of CO_2.

The atmosphere-ocean exchange of carbon is related to the difference in partial pressure of CO_2 between the atmosphere and ocean (ΔpCO_2). The partial pressure of carbon dioxide (pCO_2) in water depends on its solubility, α, and its concentration in water:

$$pCO_2 = \frac{[CO_2]}{\alpha} \tag{1.1}$$

The solubility of CO_2 increases as temperature or salinity decreases (Weiss, 1974). The dissolving of CO_2 in water is described by the following reaction, (the concentration of carbonic acid is very small and is ignored)

$$CO_2 + H_2O \leftrightharpoons H^+ + HCO_3^- \tag{1.2}$$

Bicarbonate ion then dissociates into hydrate proton and carbonate ion

$$HCO_3^- \rightleftharpoons H^+ + CO_3^{-2} \ . \tag{1.3}$$

These two reactions reach equilibrium in less than a few minutes (Broecker and Peng, 1982) and this requires that the concentrations of the species in these reactions obey the laws of chemical equilibria. The equilibria of these reactions is given by

$$K_1 = \frac{[H^+]\ [HCO_3^-]}{[CO_2]} \tag{1.4}$$

$$K_2 = \frac{[H^+]\ [CO_3^{-2}]}{[HCO_3^-]} \tag{1.5}$$

where K_1 and K_2 are called the first and second apparent dissociation constants of carbonic acid, respectively. In writing these equilibria equations, the concentration of water (H_2O) is assumed constant. The hydrogen ion is also involved in the ionization of water:

$$H_2O \rightleftharpoons [H^+] + [OH^-] \ . \tag{1.6}$$

The equilibrium of this reaction is given by

$$K_w = [H^+]\ [OH^-] \tag{1.7}$$

where K_w is called the ionization constant of water.

Typically when studying the carbon cycle in the ocean one measures DIC and alkalinity. The DIC in water is given by

$$[DIC] = [CO_2] + [HCO_3^-] + [CO_3^{-2}] \ . \qquad (1.8)$$

Since the equilibrium constants K_1, K_2, and K_w vary with temperature, salinity and pressure, a water parcel undergoing a change of state will experience variations in CO_2, HCO_3^-, CO_2^{-2}, H^+, and OH^-. However, a change of state will not affect DIC because carbon will simply be redistributed among the three carbon species.

The point at which all buffering species in seawater are neutralized by the added acid is called the alkalinity. A simple equation for alkalinity is given by

$$ALK = [HCO_3^-] + 2[CO_3^{-2}] + [OH^-] - [H^+] + [B(OH)_4^-] \ . \qquad (1.9)$$

A more rigorous treatment, as by Peng *et al.* (1987), should include the silicate phosphorus-containing ions. In the equation for alkalinity, the borate ion concentration can be computed from the $[H^+]$ and the salinity (Peng *et al.*, 1987).

One now has a system of equations (1.1, 1.4, 1.5, 1.7 1.8, 1.9) to solve. If DIC and alkalinity along with temperature and salinity are specified, all unknowns can be completely determined. This system of nonlinear equations can be used to look at the variability of the partial pressure of CO_2 in seawater as a function of temperature, salinity, DIC and alkalinity. For pCO_2 as a function of T and S under average surface conditions (DIC=2000 μmol kg^{-1}, ALK = 2300 μEq kg^{-1}), pCO_2 increases with increasing DIC and with decreasing ALK with approximately the same sensitivity (Najjar, 1992). DIC and ALK can be changed by the exchange of freshwater at the air-sea interface. The freshwater flux can produce large variations in DIC and ALK, however, these variations

produce nearly equal but opposite effects on the dissolved CO_2 resulting in negligible impact on the seawater pCO_2.

Sizeable variations in the surface water partial pressure of CO_2 occur from place to place in the ocean. The variation of the CO_2 partial pressure in the surface ocean stems from the complex interplay between the seasonal temperature cycles, the mixing dynamics of the upper ocean, and the biological cycles of the sea. The CO_2 transfer between the air and sea tends to eliminate these differences but the time constant to achieve equilibrium is about 1 year (Broecker and Peng, 1982).

The marine biological productivity in the surface waters is primarily controlled by the availability of nutrients, particularly nitrogen and phosphorous, and is not significantly influenced by changes in DIC. Biological activity in the well-lit upper layers of the ocean (the euphotic zone) converts DIC into $CaCO_3$ and organic carbon. This material is transported to the deeper, dark layers of the water column (the aphotic zone) and to the sediments by particle settling. In the aphotic zone and in the sediments, chemical and biological processes dissolve $CaCO_3$ and remineralize organic carbon to DIC. This biological cycling of carbon in the ocean is known as the biological pump because it maintains vertical gradients in DIC and many other chemical species in the ocean (eg. phosphate). It can be separated into an organic matter pump and a calcium carbonate pump.

The photosynthesis due to the uptake of nitrate transported into the euphotic zone by the ocean circulation is known as new production (Dugdale and Goering, 1967). The total phytoplankton production, or primary production, is usually significantly higher than

new production. The f-ratio is used to define the proportion of new production to primary production. New production is very important when considering the organic matter pump. Over seasonal time scales, new production must balance the input of nutrients into the euphotic zone as well as the export of organic matter. In the absence of new production, all the primary production would be recycled within the euphotic zone, and the atmospheric CO_2 would be much higher.

Calcium carbonate ($CaCO_3$) is a mineral solid that plays an important role in the marine carbon cycle. Some plants and animals living in the euphotic zone have $CaCO_3$ skeletons which they precipitate from dissolved calcium and carbonate ions. The $CaCO_3$ formed in this manner eventually sinks and is dissolved back into calcium and carbonate ions in the deeper parts of the water column and in the sediments. Ocean circulation closes the loop and transports these ions back to the surface waters. This cycling of the $CaCO_3$, known as the carbonate pump (Volk and Hoffert, 1985), creates a surface depletion and a deep enrichment of DIC and alkalinity. Since variations due to the carbonate pump are twice as great on alkalinity as on DIC, an increase in the strength of the carbonate pump will increase atmospheric CO_2.

To use tracer distributions to quantify the cycling of carbon in the ocean requires that this data provide information on the ocean circulation, biological processes and air-sea exchanges that affect the distribution of carbon in the ocean. All tracers will be affected by the physical processes but only certain tracers will contain information on the latter two processes. Alkalinity and DIC are essential tracers to understanding the carbon cycle. The nutrient data - phosphate, nitrate, and oxygen tracers - provide additional information

on the organic matter pump. Temperature, salinity, and silicate tracers are useful to provide additional constraints on the ocean circulation. By using several different tracers, one attempts to overcome the limitation that no one tracer can adequately describe all the relevant processes affecting the cycling of carbon in the ocean. However, in using several different tracers it important to realize that the different tracer fields may contain redundant information.

The work presented in this thesis divides into three parts. In the first part (chapter 2), the question of the best hydrographic data to use to determine the horizontal tracer transports is studied by looking at the tracer transports across 35°N in the Pacific. The results of this study are reflected in how the inverse model is applied to the data from the North Pacific. In the second part (chapter 3), I apply the inverse model to a data set generated by the Hamburg biogeochemical model. The purpose of this study is to provide a means with which to assess the ability of the inverse model to determine air-sea exchanges. In the third and final part (chapters 4-5), I use the tracer data from the North Pacific to formulate an inverse model. The model is used to investigate the nutrient and carbon cycle in the North Pacific as well as the circulation fields. The role of dissolved organic matter in the carbon and nutrient cycles is examined using a model which includes the dissolved organic nutrient measurements of Suzuki *et al.*, (1985).

CHAPTER 2. TRACER TRANSPORTS ACROSS 35°N IN THE PACIFIC OCEAN

2.1 INTRODUCTION

The use of inverse models has been one approach to estimate the uptake of CO_2 by the ocean (Bolin *et al.*, 1983; Bolin *et al.*, 1987; Schlitzer 1988 and 1989). The air-sea exchanges calculated from these models need an accurate determination of the transport of carbon by the horizontal flow field. The situation arises because one utilizes the imbalances in the horizontal transport to estimate the air-sea exchange of CO_2. To reliably determine the importance of the oceans as a sink of anthropogenic CO_2, therefore, requires an accurate calculation of the horizontal transport which is orders of magnitude larger than the air-sea exchange.

In applying inverse models to the problem of estimating the air-sea exchange of CO_2, it is typical to assume that the horizontal transport is geostrophic. The unknown reference level velocities are adjusted in a manner that conserves mass, carbon and other tracers. An initial specification of the horizontal transport is required because the tracer fields do not possess enough information to fully constrain the flow (Schlitzer, 1988). The initial mass transport is usually determined using geostrophic equations with either synoptic data or the Levitus Climatological data (Levitus, 1982). The choice of data used

for this initial mass transport calculation depends on which type of data one considers more appropriate for calculating the tracer budgets in an ocean basin. This question has been debated but not satisfactorily resolved, with proponents of both approaches still existing. Meméry and Wunsch (1990) argue that the use of the Levitus dataset in the North Atlantic inverse box model produced unrealistic meridional heat fluxes at mid-latitudes. They feel that these difficulties can only be resolved by either introducing large lateral mixing terms or by assuming the Ekman fluxes in serious error as done by Schlitzer (1988). Schlitzer (1988) maintains that even though the Levitus dataset may not represent the average ocean circulation it still describes the average circulation better than synoptic sections and does a better job of balancing the long term nutrient budgets. The difficulty with these two statements is that they are based on the results of inverse models which have the tendency to blur the inconsistencies present between the mass and tracer fields. Thus it makes it difficult to state clearly what data are more appropriate.

In this chapter, the problem is simplified by considering only one section across the North Pacific at latitude 35°N. This can be thought of as a one box model of the North Pacific. The annual mean tracer transports calculated from a synoptic section are then compared to the annual mean tracer transports calculated from the annual mean Levitus section. The transport of heat, salt, dissolved inorganic carbon (DIC), alkalinity, phosphate, nitrate, oxygen and silicate through the two sections are used to compare the sections. The goal is to show clearly which approach is most consistent with the data. The simplified approach of dealing with only one section will provide insight into

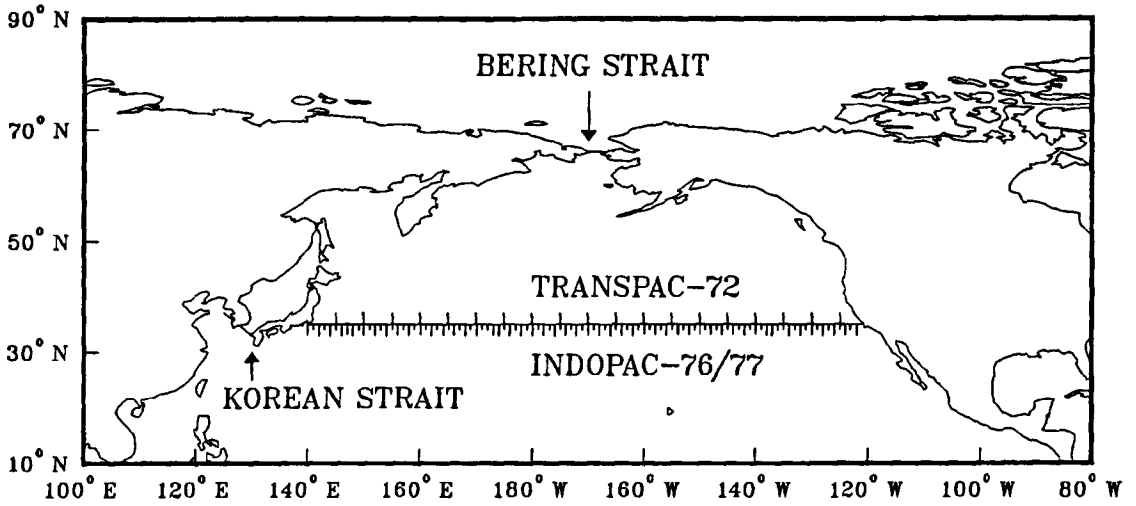

Figure 2.1: Location of stations for the trans-Pacific sections. The long ticks above the line at 35°N indicate the locations of the TRANSPAC stations; the long ticks below, the deep stations; and the short ticks the 1200-m stations, both for INDOPAC.

problems that one will encounter in applying inverse models to nutrient data to quantify the carbon cycle processes and the limitation of these models. The analysis will also be applicable to attempts to determine the air-sea exchanges of CO_2 by using the transport through a section (Brewer *et al,* 1989).

2.2 SECTIONS

For this chapter, three sections across 35°N are used, the Levitus annual mean section, the INDOPAC section and the TRANSPAC section (Fig 2.1). Additional tracer data from the NODC archives is included to create mean tracer fields along 35°N. In this

study the INDOPAC section and Levitus section have comparable horizontal resolution of about 1 degree longitude.

2.2.1 INDOPAC Section

The INDOPAC section consists of data from INDOPAC Cruises 1 and 16 of Mar.-Apr. 1976 and July 1977 respectively (Scripps Institution of Oceanography, 1978; Kenyon 1983). The data from the July 1977 cruise are only used to augment the deep data missing in the original section (depth deeper than 1000 m). The data were collected at 98 stations of 1 degree spacing with alternating casts to 1000 m and casts to the ocean bottom. The tracer data collected included temperature, salinity, dissolved inorganic carbon (DIC), alkalinity, oxygen, nitrate, phosphate and silicate. Because the last station in the INDOPAC section was well east of the Japanese coast in water of depth of 2300 m, an additional station closer to the coast was added to the section from the NODC files (NODC cruise number 1847, station RY4761). The station in the Kuroshio, 80 km west of the last INDOPAC station preceded the INDOPAC station by only 4 days and provided additional measurements of temperature, salinity, oxygen and phosphate. The tracer properties of the INDOPAC section are shown in Figure 2.2. In general, the contours of the property fields are zonal with evidence of increased eddy activity in the western boundary region. The eastern part of the section has slightly greater concentrations of silicate, phosphate, nitrate, and salinity than the western portion of the section.

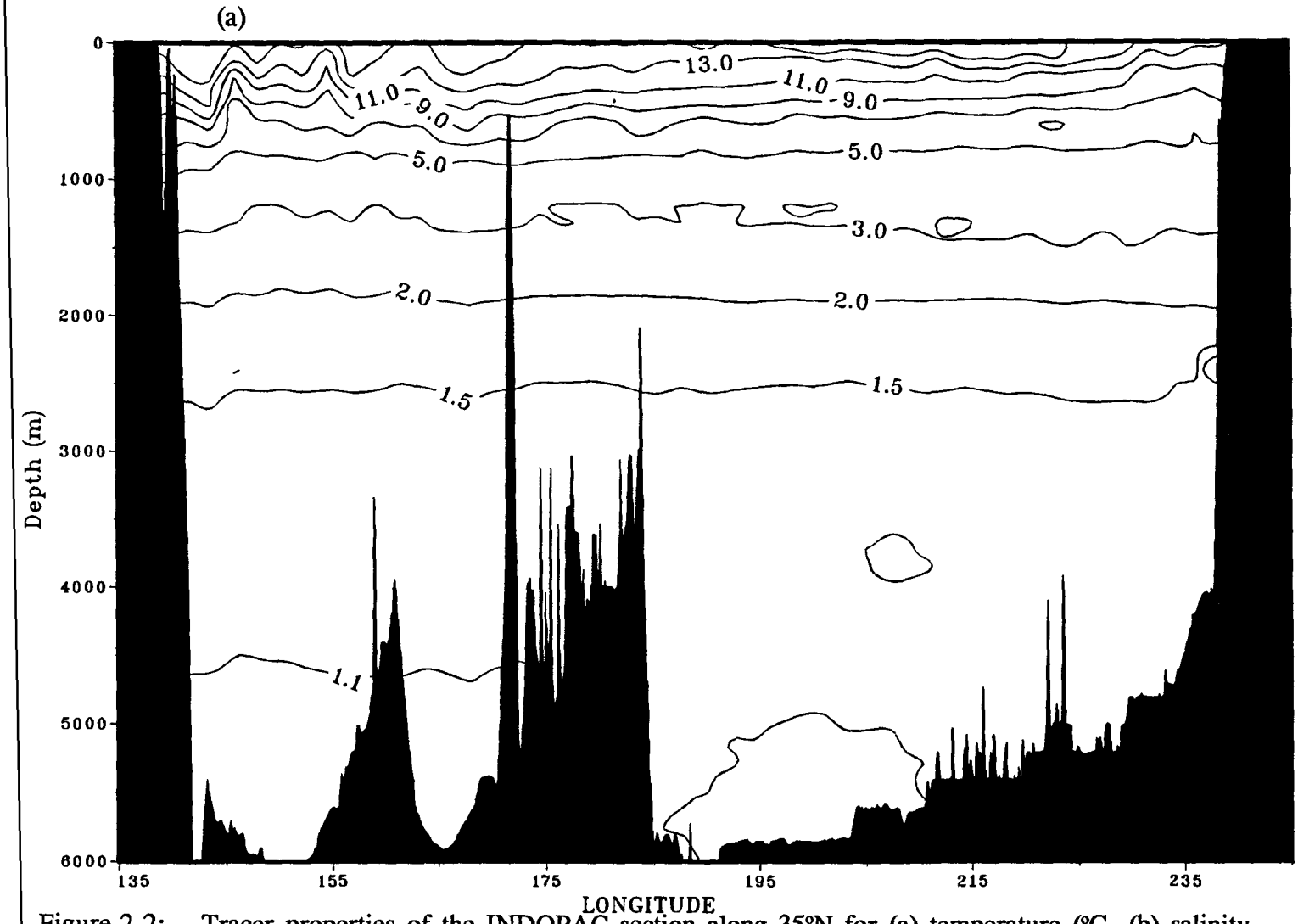

Figure 2.2: Tracer properties of the INDOPAC section along 35°N for (a) temperature (°C, (b) salinity (pss), (c) phosphate (μmol/kg), (d) nitrate (μmol/kg), (e) oxygen (μmol/kg) , (f) silicate (μmol/kg), (g) DIC (μmol/kg), and (h) alkalinity (μEq/kg).

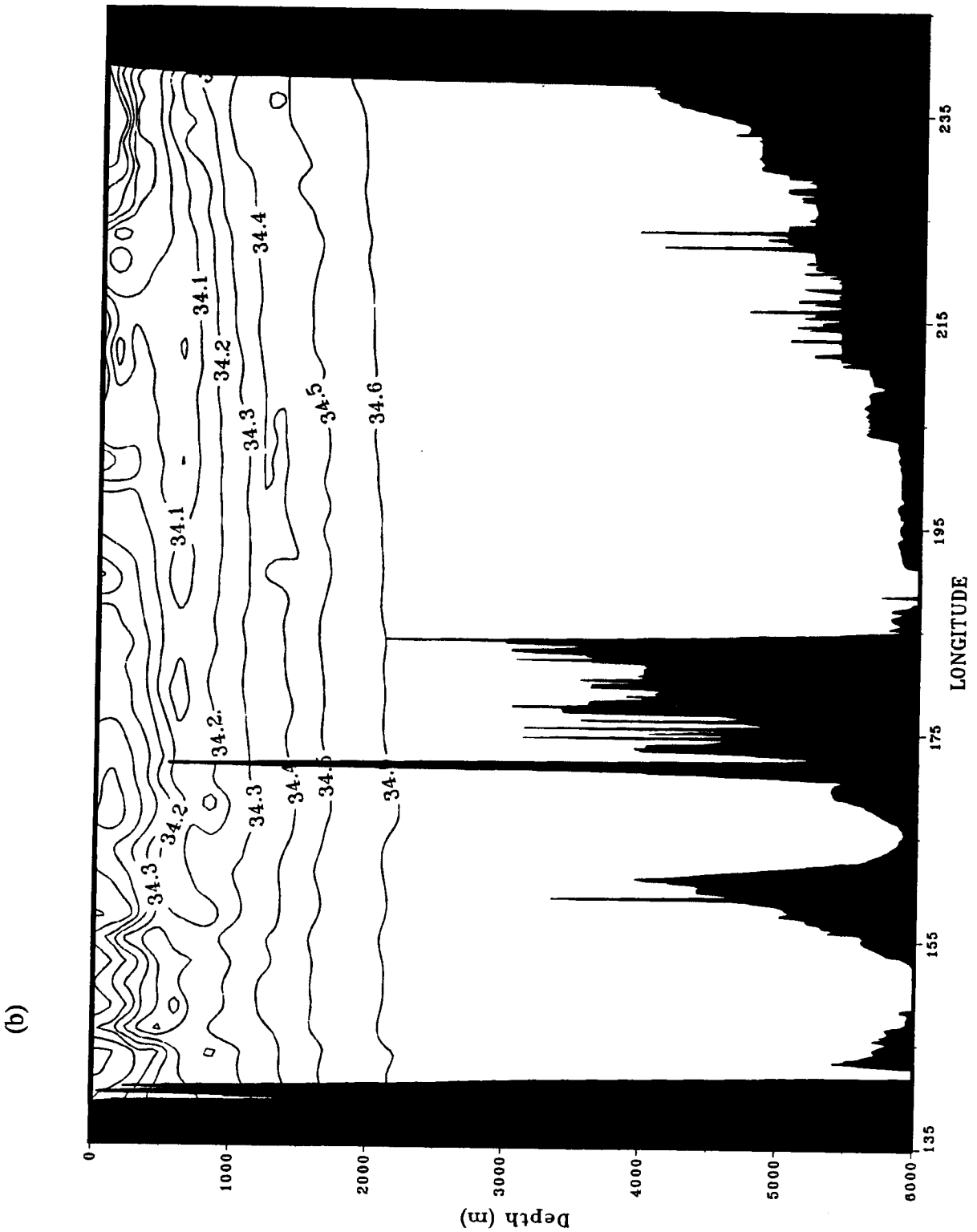
(b)
Depth (m)
0
1000
2000
3000
4000
5000
6000
135
155
175
195
215
235
LONGITUDE
34.1
34.2
34.3
34.4
34.5
34.6

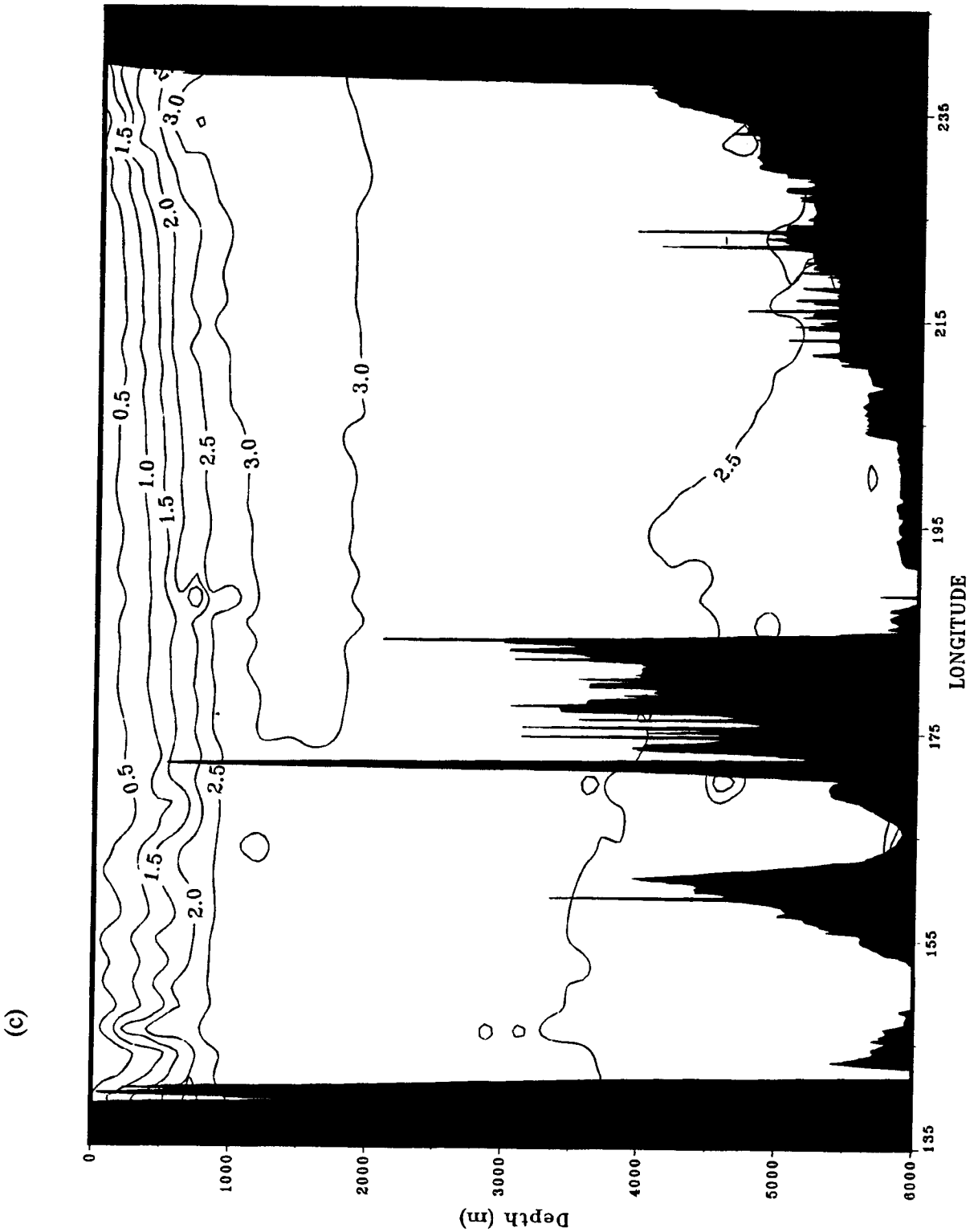
(c)
Depth (m)
0
1000
2000
3000
4000
5000
6000
135
155
175
195
215
235
LONGITUDE
0.5
1.0
1.5
2.0
2.5
3.0

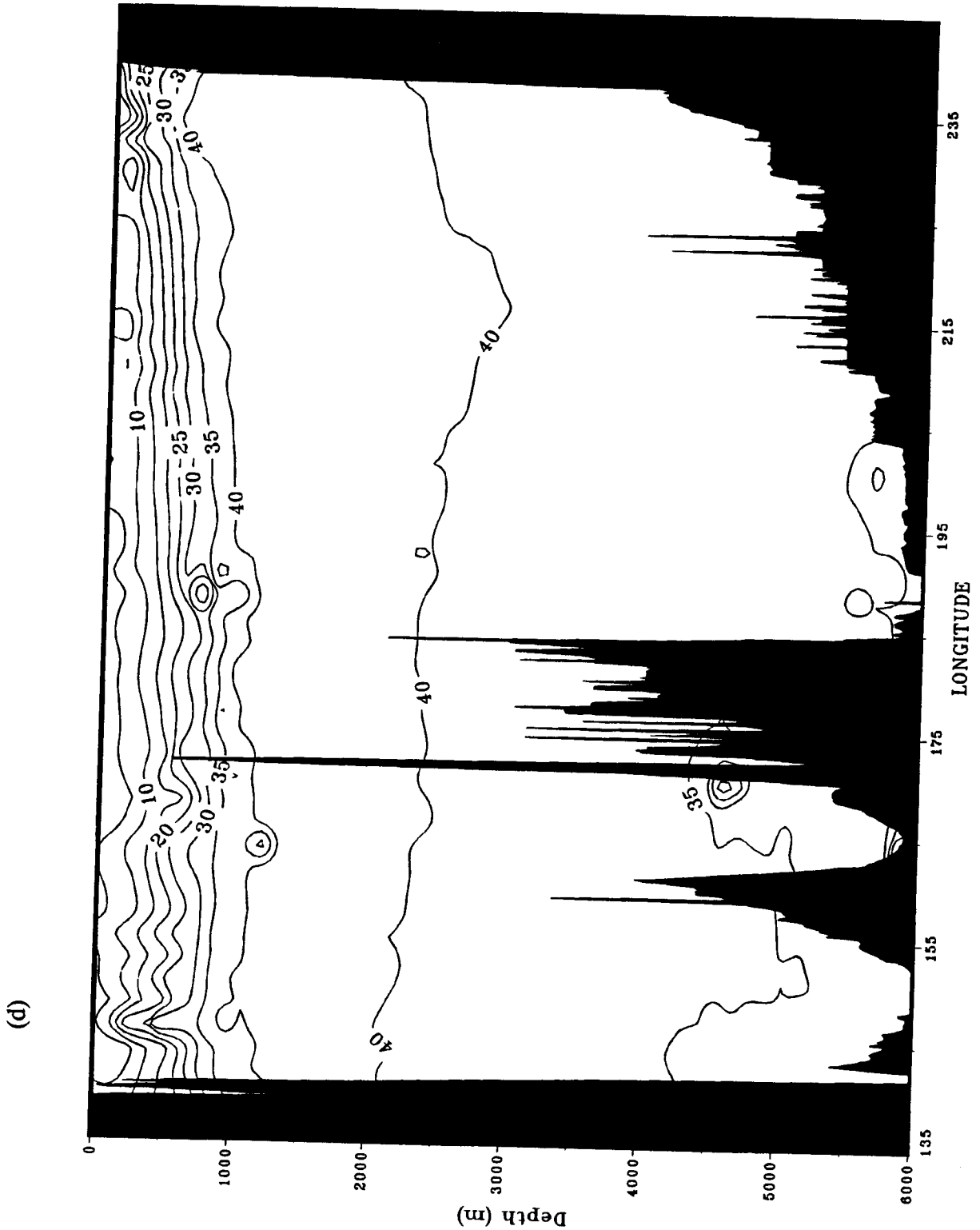
(d)
Depth (m)
0
1000
2000
3000
4000
5000
6000
135
155
175
195
215
235
LONGITUDE
40
0
40
35
40
10
20
30
35
10
25
30
35
40
10
25
30
40

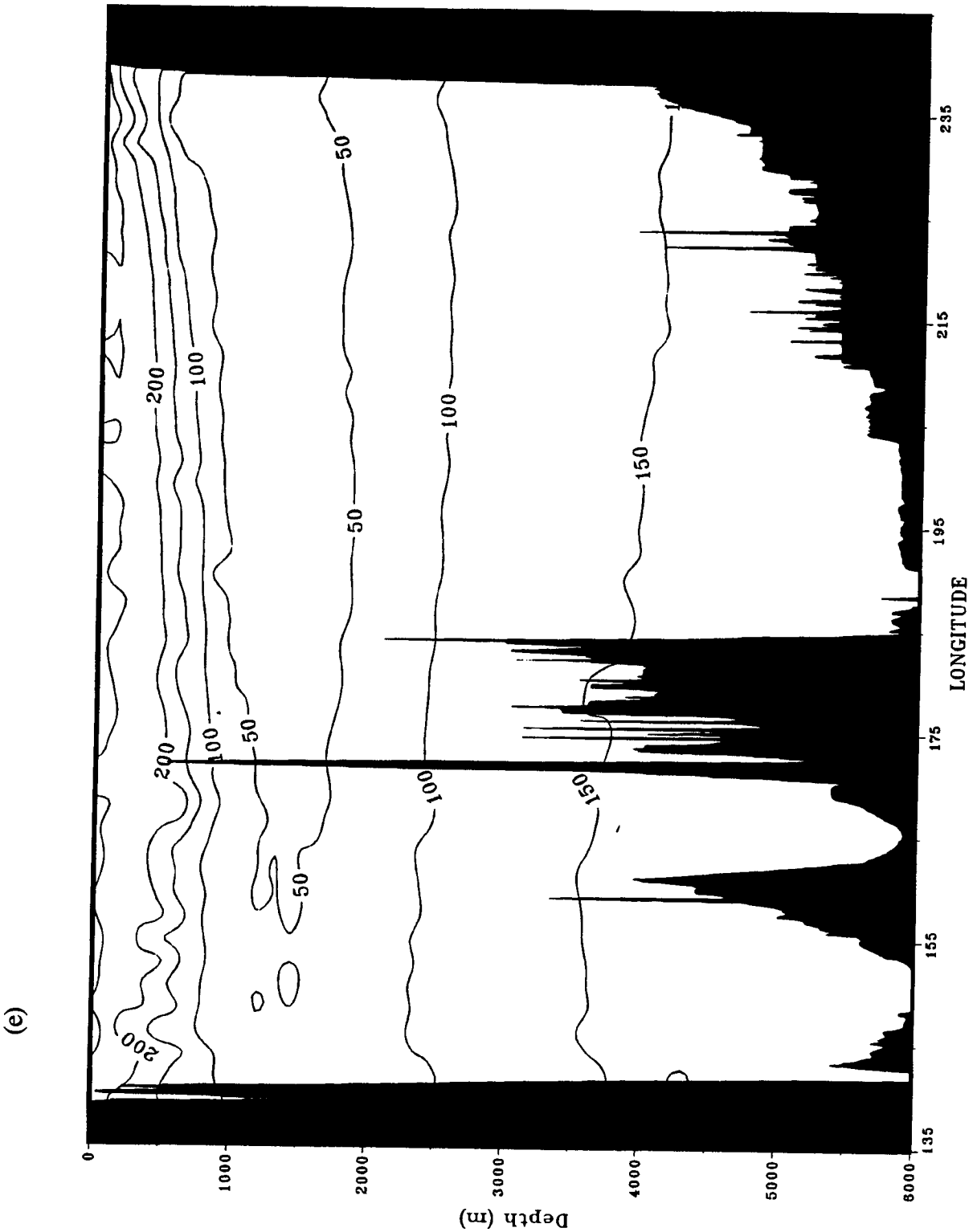
(e)
Depth (m)
0
1000
2000
3000
4000
5000
6000
135
155
175
195
215
235
LONGITUDE
200
100
50
150

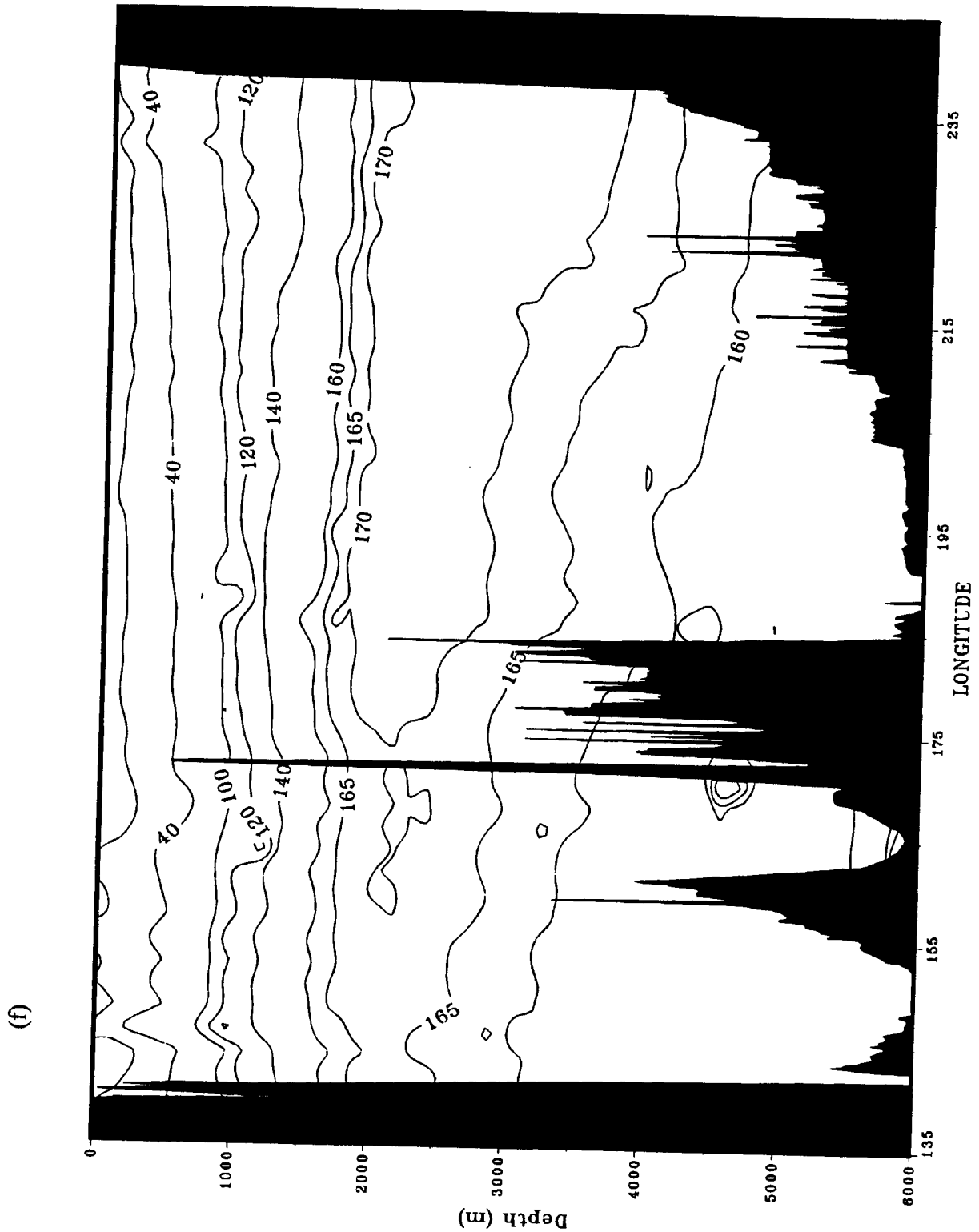
(f)
Depth (m)
0
1000
2000
3000
4000
5000
6000
135
155
175
195
215
235
LONGITUDE
40
120
140
160
165
170
100

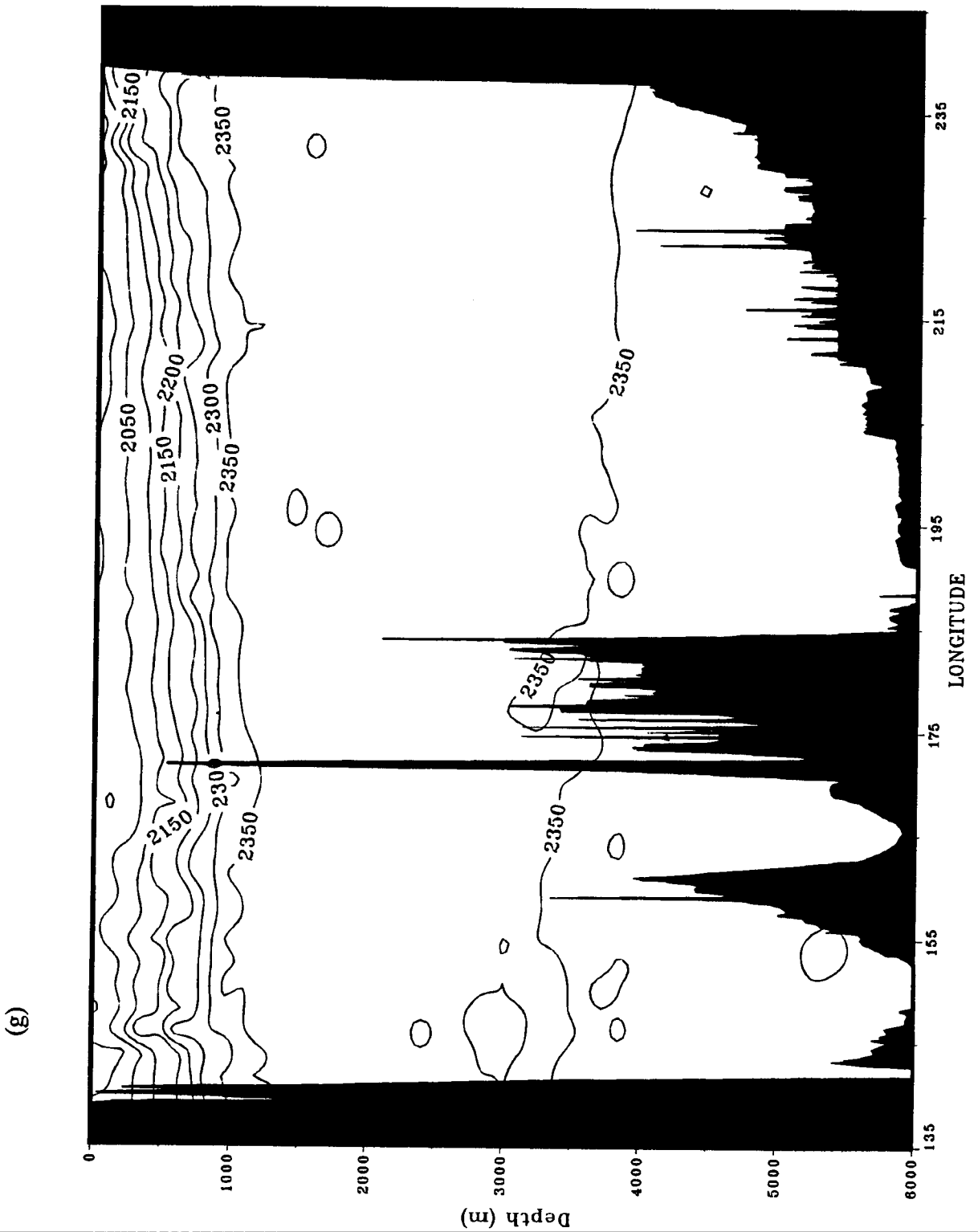
(g)
Depth (m)
0
1000
2000
3000
4000
5000
6000
135
155
175
195
215
235
LONGITUDE
2150
2350
2050
2200
2300
2350
2150
2350
2350
2350
2350

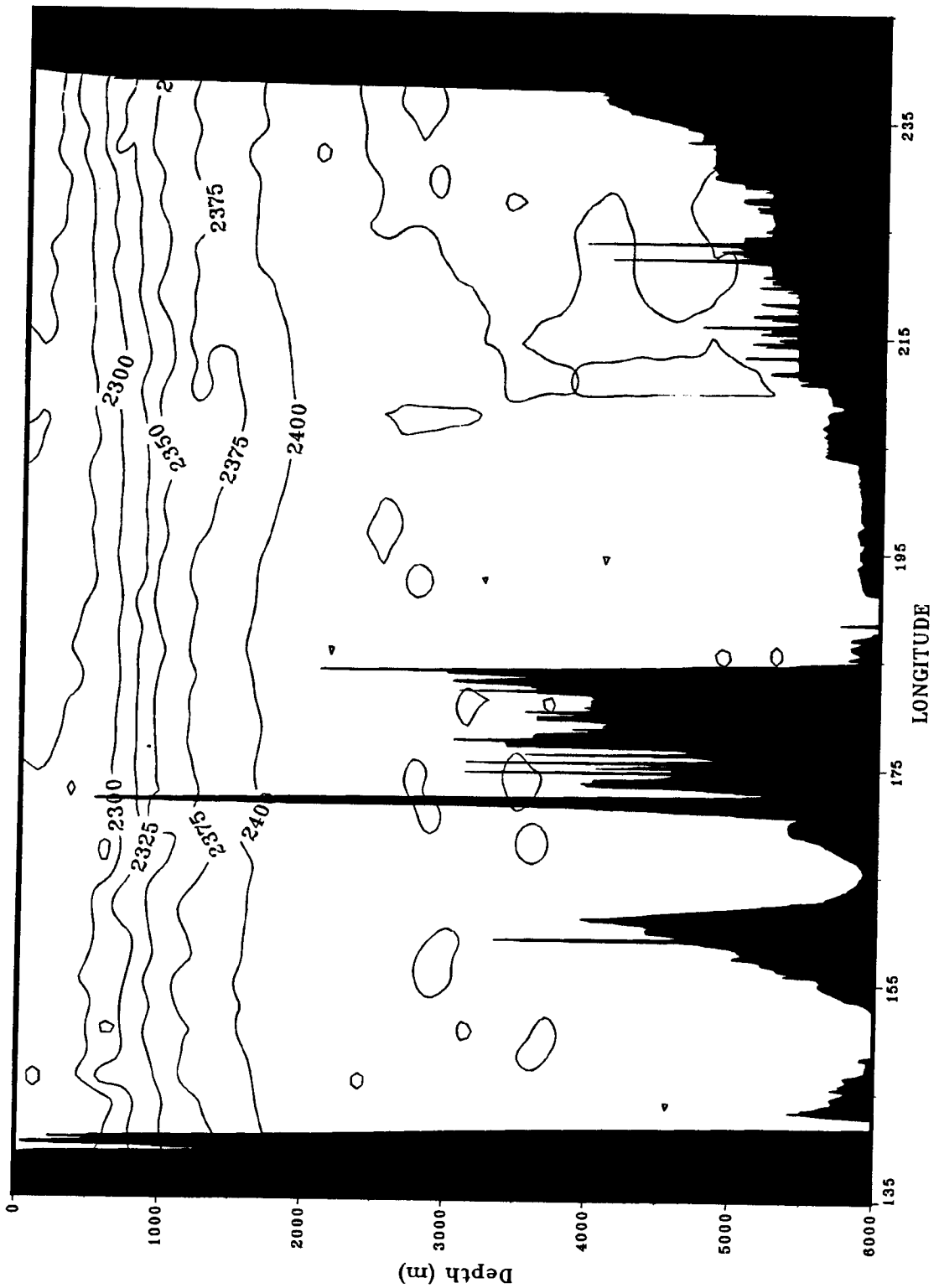
(h)
Depth (m)
0
1000
2000
3000
4000
5000
6000
135
155
175
195
215
235
LONGITUDE
2300
2350
2375
2400
2325
2375
240

2.2.2 TRANSPAC Section

The TRANSPAC section data were collected during Oct. 1972 (Wong, unpublished cruise report; Wong *et al.*, 1974). The data consisted of casts to a maximum depth of 5000 m at every 5 degrees longitude along 35°N. The tracers measured were temperature, salinity, DIC, alkalinity, oxygen, nitrate, and silicate. As with the INDOPAC section, an additional station in the Kuroshio was added to the section from the NODC files (NODC cruise number 994, station RY4204). The Kuroshio station preceded the most westerly TRANSPAC station by 9 days and included additional measurements of temperature, salinity, oxygen, phosphate, and silicate.

2.2.3 Levitus Section

The Levitus section consisted of the annual mean temperature and salinity measurements with 1 degree longitude spacing in the latitude band 34°N - 35°N compiled by Levitus (1982). For this section, the average concentration of oxygen, phosphate, nitrate and silicate were computed from the NODC files, which included INDOPAC and TRANSPAC data. To determine these average tracer fields between 34-35°N, a procedure similar to what was done with the temperature and salinity in the Levitus annual

mean dataset was followed. The data was objectively mapped to a one degree spacing (Roemmich, 1983). Because the NODC files did not contain DIC and alkalinity measurements, the average annual mean fields for these tracers were obtained by averaging the INDOPAC and TRANSPAC data. The DIC and alkalinity measurements of the TRANSPAC cruise were systematically less than the INDOPAC cruises (Fig. 2.3). An offset of 41 μEq kg^{-1} and 42 μmol kg^{-1} for alkalinity and DIC respectively were added to the TRANSPAC measurements to correct for the systematic differences between the two cruises for the deep water measurements. The two cruises displayed very similar features despite systematic differences.

2.3 COMPUTATION OF THE TRANSPORTS

Instead of the traditional station pair calculation of geostrophic shear, the approach prescribed by Roemmich (1983) was followed. Using an objective mapping routine (Roemmich, 1983), all tracer fields and the specific volume anomaly were interpolated to a constant 1 degree horizontal spacing and to the 33 depth levels used in the Levitus dataset. The shear in the geostrophic velocity was calculated from the gridded values of the specific value anomaly. By using the objective mapping approach, one makes use of both the vertical and horizontal features of the field to extrapolate to the ocean bottom. Such an approach does a better job of calculating the geostrophic shear where there are large changes in the depth of the ocean bottom between stations (Roemmich and McCallister, 1989).

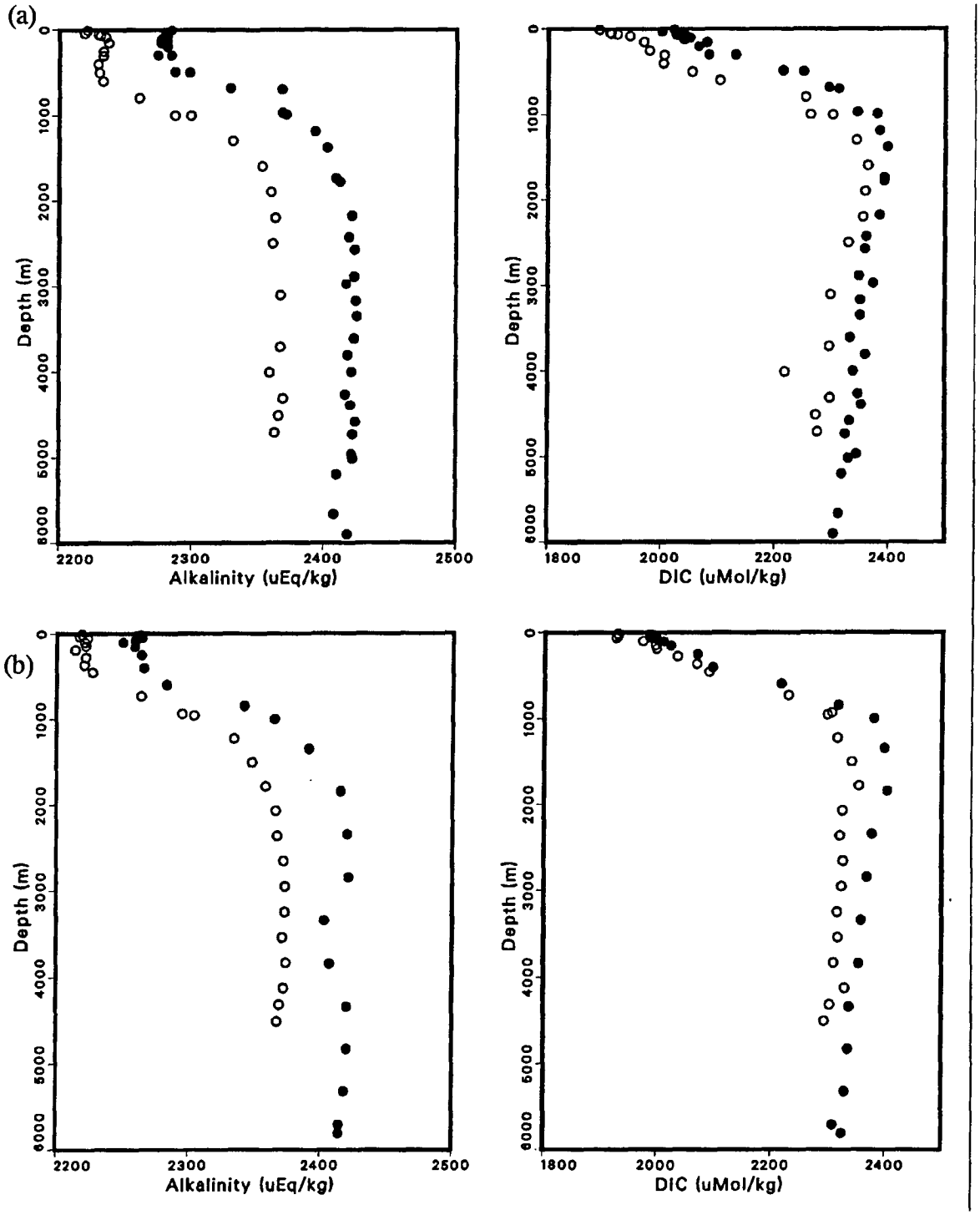

Figure 2.3: A comparison of the alkalinity and DIC measurements of the INDOPAC cruise (●), and the TRANSPAC cruise (○), at (a) 35°N and 164°E, and (b) 35°N and 170°W.

For each section a reference level was chosen and the relative geostrophic transport was calculated by integrating the geostrophic shear.

$$v(z) = \frac{g}{\rho_o f}\int_{z_o}^{z} \frac{\partial \rho}{\partial x} dz + v_o = v_g + v_o \qquad (1.1)$$

where v_o is the velocity at the reference level z_o. The Ekman transport across 35°N was calculated using Hellerman and Rosenstein (1983) annual mean wind stress values. The Ekman transports of the tracers were assumed to be confined to the upper 50 m of the ocean (Gill 1982). The total mass transport across the section is given by

$$\rho M_e + \int \rho v_r dA + \rho v_o A = 0 \qquad (1.2)$$

where M_e is the total Ekman transport through the section, and the integral is over the area of the section, A. By assuming no net mass transport across the section, the velocity at the specified reference level (v_o) is determined. Only one reference level velocity is determined for the section and this is added to the relative geostrophic transport to obtain the geostrophic transport. The tracer transport through the section is determined by

$$X = \int \rho C(v_g + v_o)\, dA + \int \rho C m_e\, dS \qquad (1.3)$$

where C is the tracer concentration and m_e is the Ekman transport along the section. The first integral is over the entire section while the second integral is only for the upper 50 m of the section.

2.4 MASS TRANSPORT

The depth of the reference level (z_o) chosen for all sections was 2500 m. The 2500 m depth corresponds to the depth of the silicate maximum and the ^{14}C minimum which are considered to represent the oldest and slowest moving water (Bien *et al.*, 1965). Although the choice of the reference level is somewhat arbitrary, it was clear in the transport across the INDOPAC section that a reference level shallower than 2000 m would produce a southward flow of water in the deepest layer (Fig 2.4). In the Pacific, the abyssal water can be traced back to water of North Atlantic origin (Reid and Lynn, 1971); there is no source of deep water in the North Pacific (Warren 1981). The maps of Mantyla and Reid (1983) indicate the northward spreading of the bottom water at 35°N. These observations all suggest that the deep water should be flowing northward at 35°N. The variation in transports between the 2000 m and 3000 m reference levels were used to estimate the transport errors generated by the choice of reference level. With a reference level of 2500 m the INDOPAC section had approximately 10 Sv of deep water flowing north (2500 m to the bottom). The geostrophic velocities for the three sections are shown in Figure 2.5 . The two synoptic sections show much greater eddy activity than the annual mean Levitus section.

The integrated geostrophic transport from 139°E for the three section showed significant differences between the sections (Fig 2.6). However, Figure 2.6 showed that between 139°E and 240°E the integrated transport of the INDOPAC section was very similar to the Levitus section suggesting that the Levitus dataset poorly represents the

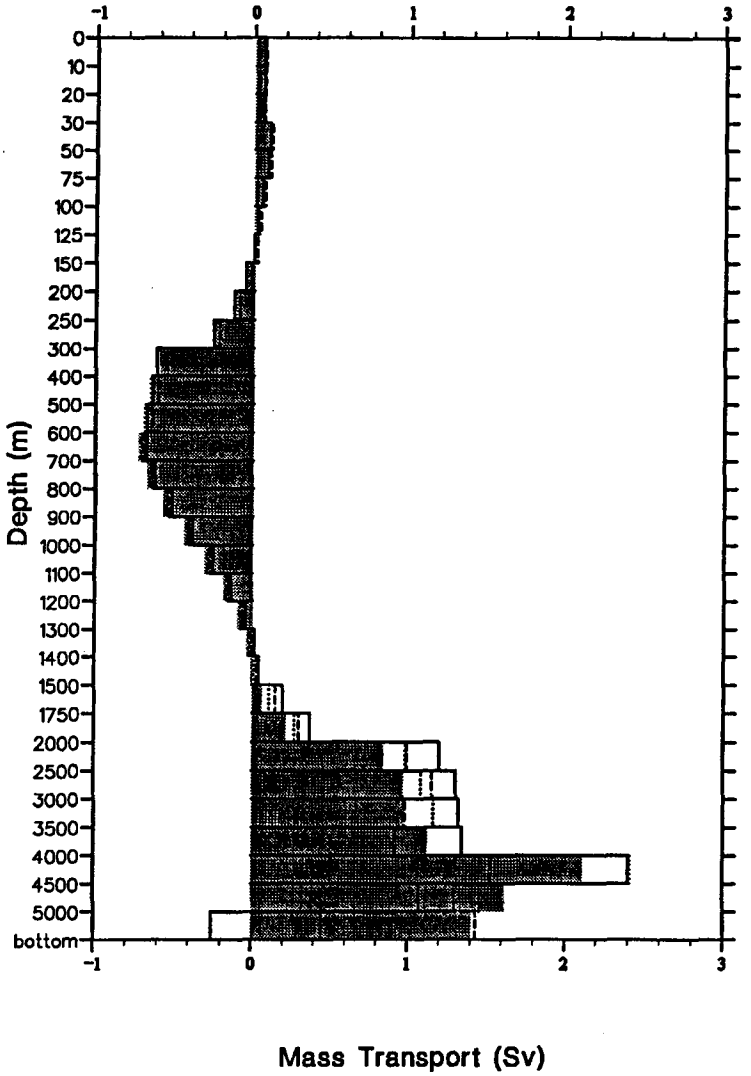

Figure 2.4: Layer transports for the INDOPAC section at the following reference levels, 2500 m (shaded), 1750 m (solid line), 2000 m (dotted line), and 3000 m (dashed line). A positive value indicated a northward transport.

western boundary current. A depth profile of the total transport across the section (Fig 2.7a), further elucidates some of the differences between the three sections. This profile reveals that in the upper 2000 m, the INDOPAC and TRANSPAC section are remarkably

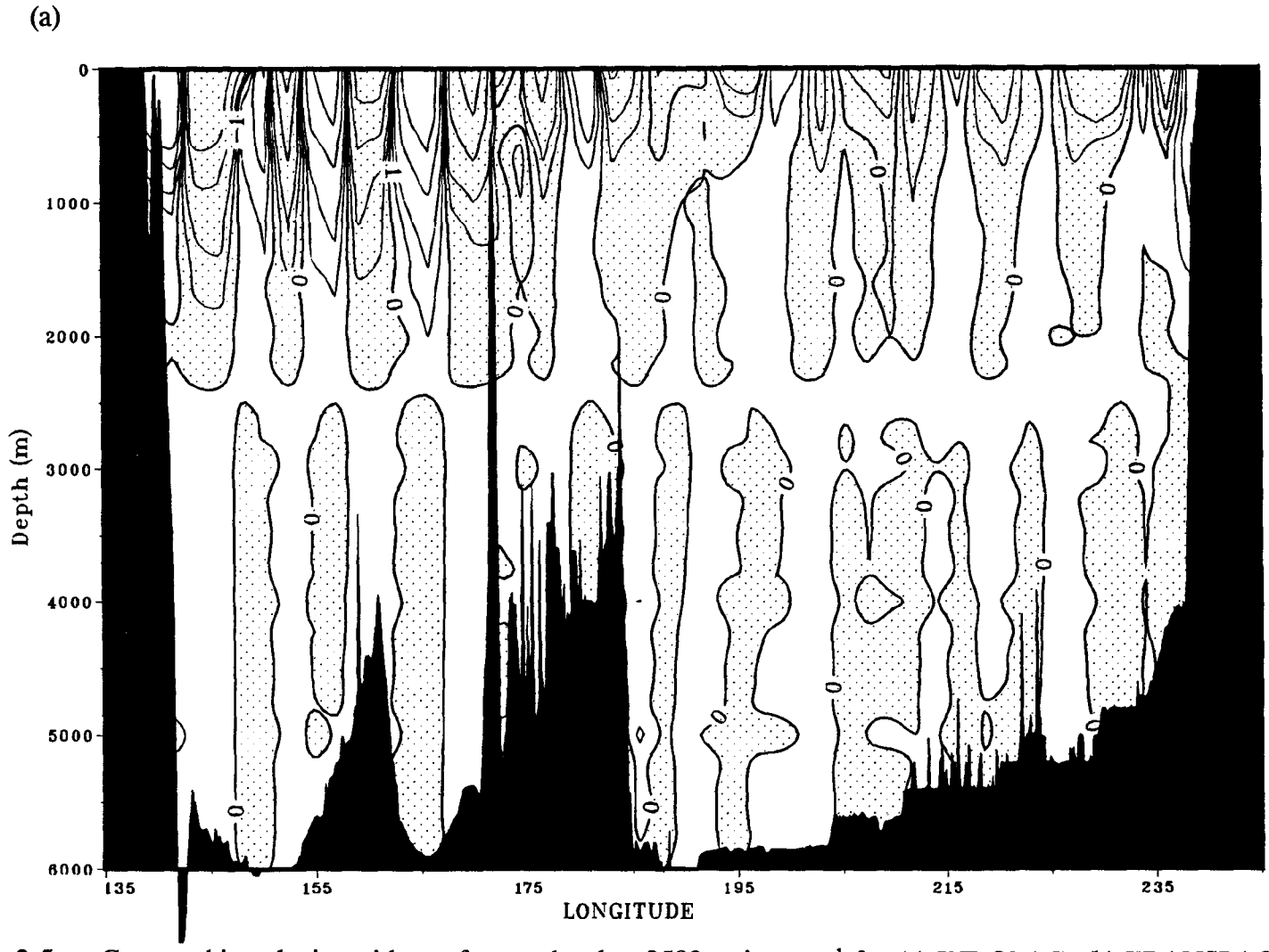

Figure 2.5: Geostrophic velocity with a reference level at 2500 m in cm s^{-1} for (a) INDOPAC, (b) TRANSPAC, and (c) Levitus sections.

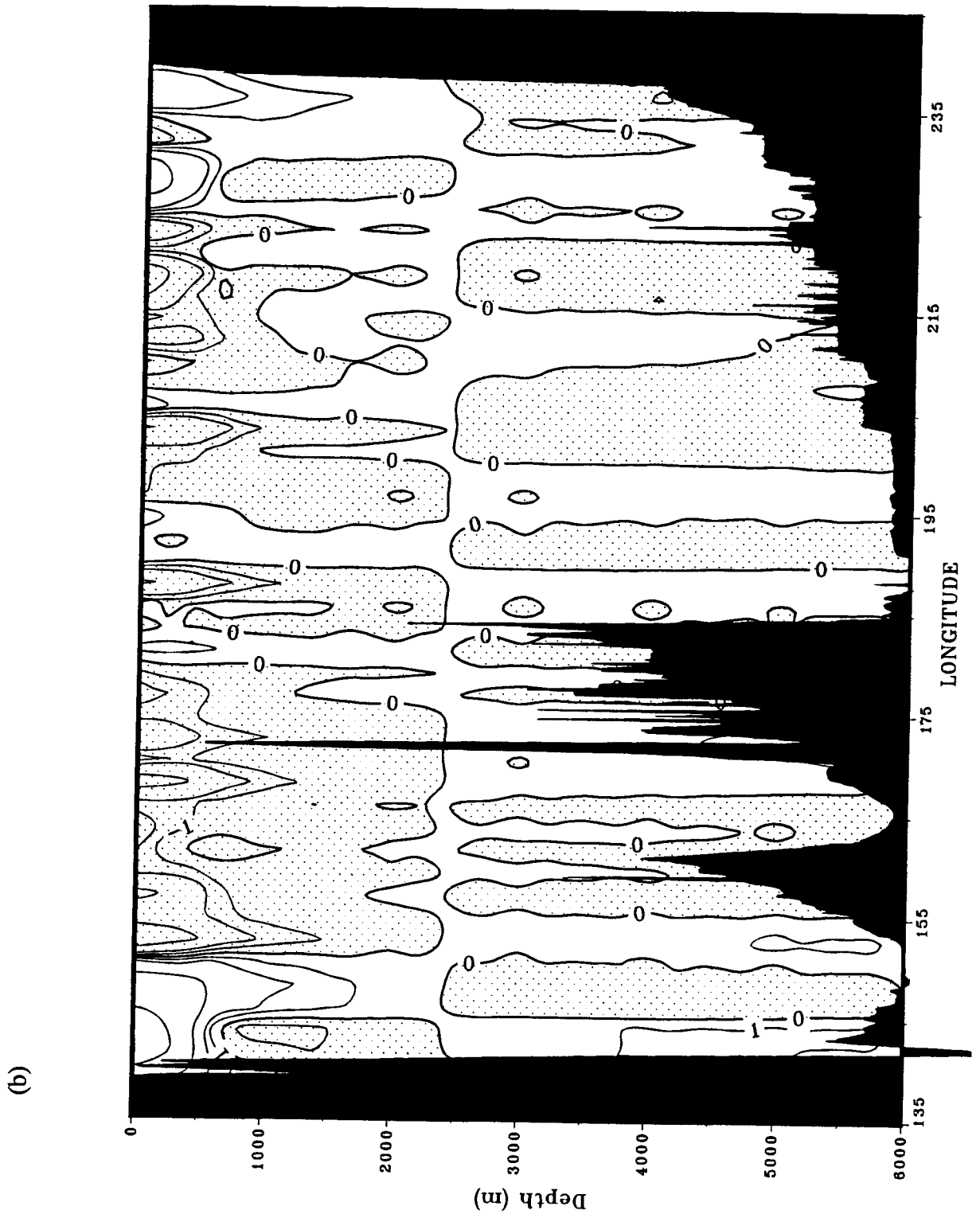
(b)
Depth (m)
0
1000
2000
3000
4000
5000
6000
135
155
175
195
215
235
LONGITUDE

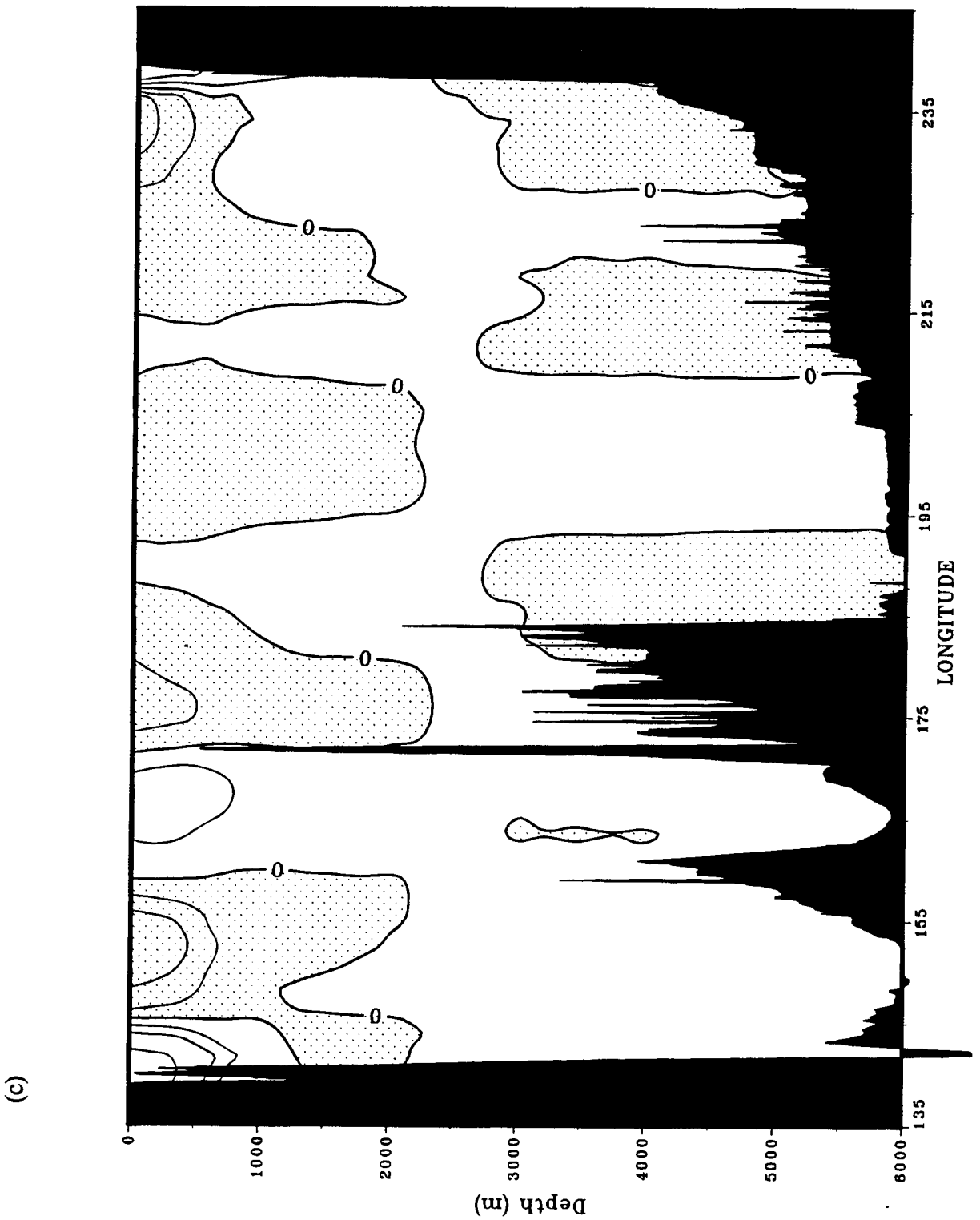
(c)
Depth (m)
0
1000
2000
3000
4000
5000
6000
135
155
175
195
215
235
LONGITUDE
0
0
0
0
0
0

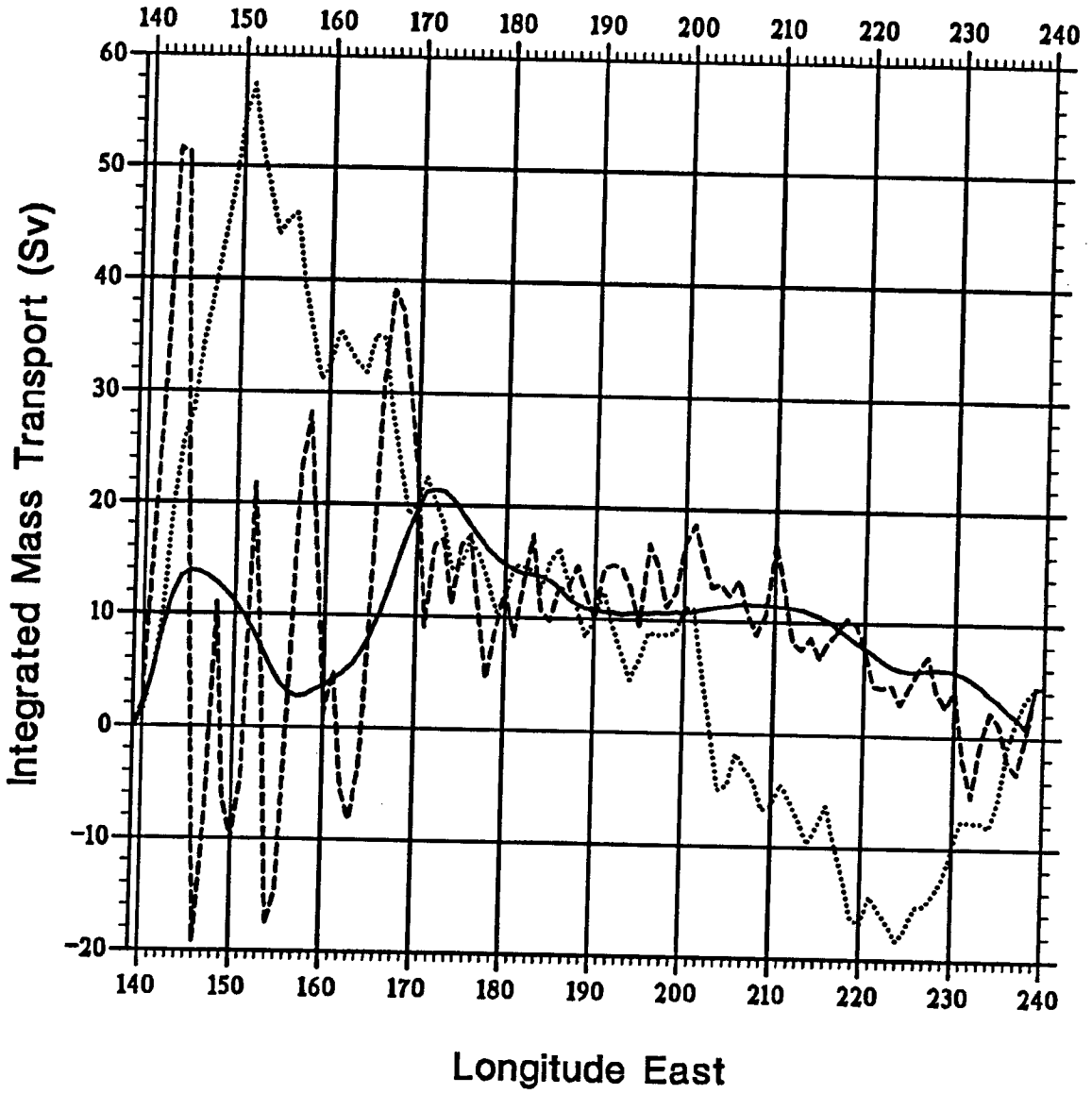

Figure 2.6: The integrated mass transport along 35°N for the Levitus section (solid), the INDOPAC section (dashed) and the TRANSPAC section (dotted). A positive value indicates a northward transport.

similar considering how different they appeared in the integrated transport plot. It is the deep layers where the transports differ significantly between the two sections. This clearly reveals the problem of insufficient deep casts in the TRANSPAC section, with no stations having data deeper than 5000 m. Based on these findings, the transports obtained from the TRANSPAC section will be disregarded and only the tracer data from this section will be used. The similarity of these two sections in the upper ocean suggests that the synoptic section does represent the gross features of the annual circulation. The depth profile of the Levitus section showed no similarity with the INDOPAC section.

The integrated layer transports for the western part of the section (139 - 170°E) and eastern part of the section (170 - 240°E) (Fig. 2.7b and 2.7c) reinforces the idea that the TRANSPAC section poorly resolves the deep layer transports. The number of deep casts for the TRANSPAC section is insufficient to determine the deep geostrophic shear. However, in the upper ocean the TRANSPAC section has similar features to the INDOPAC section. The Levitus transport in Figure 2.7c clearly shows differences in the western boundary flow. The western boundary flow is more reduced in the Levitus section than the INDOPAC section. Away from the western boundary, the Levitus transports are very similar to the INDOPAC section for the upper 2500 m of the ocean.

2.5 TRACER TRANSPORTS

In the previous section, it was obvious that there were significant differences between the mass transport of the INDOPAC section and the mass transport of the Levitus

a)

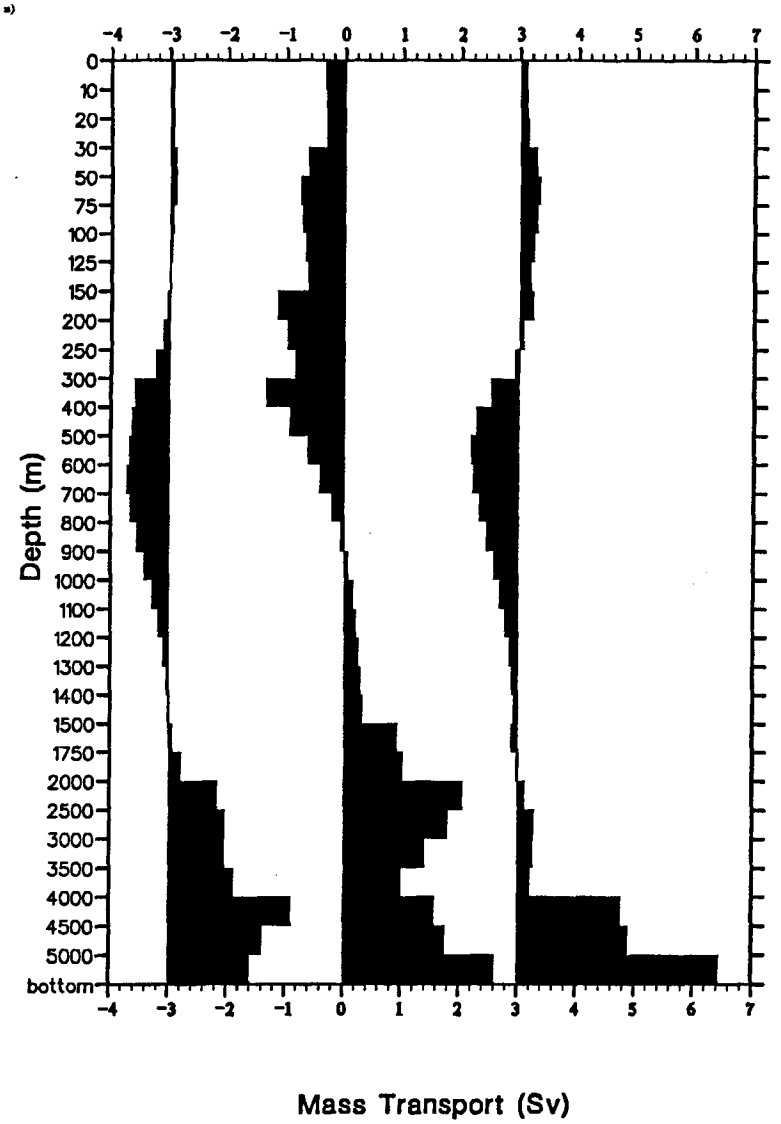

Figure 2.7: The integrated layer transport for the three section, with each section shifted by 3 Sv for clarity. The left plot is the INDOPAC section with zero at -3 Sv, the middle plot is the Levitus section and the right plot is the TRANSPAC section. The Figure show: a) the transport for the entire section, b) the transport for the western part of the section (139°E to 170°E) and c) the transport for the eastern part of the section (170°E to 240°E). A positive value indicates a northward transport.

b)

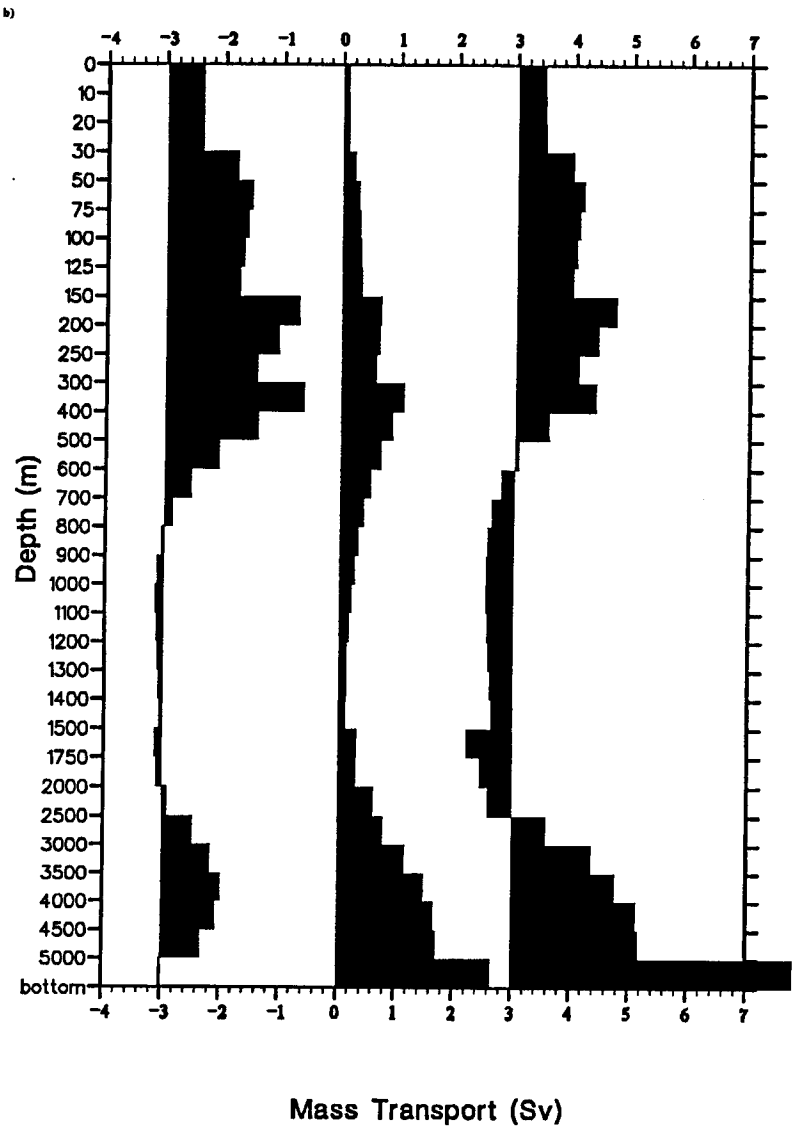
b)
-4 -3 -2 -1 0 1 2 3 4 5 6 7
0 10 20 30 50 75 100 125 150 200 250 300 400 500 600 700 800 900 1000 1100 1200 1300 1400 1500 1750 2000 2500 3000 3500 4000 4500 5000 bottom
Depth (m)
-4 -3 -2 -1 0 1 2 3 4 5 6 7
Mass Transport (Sv)

c)

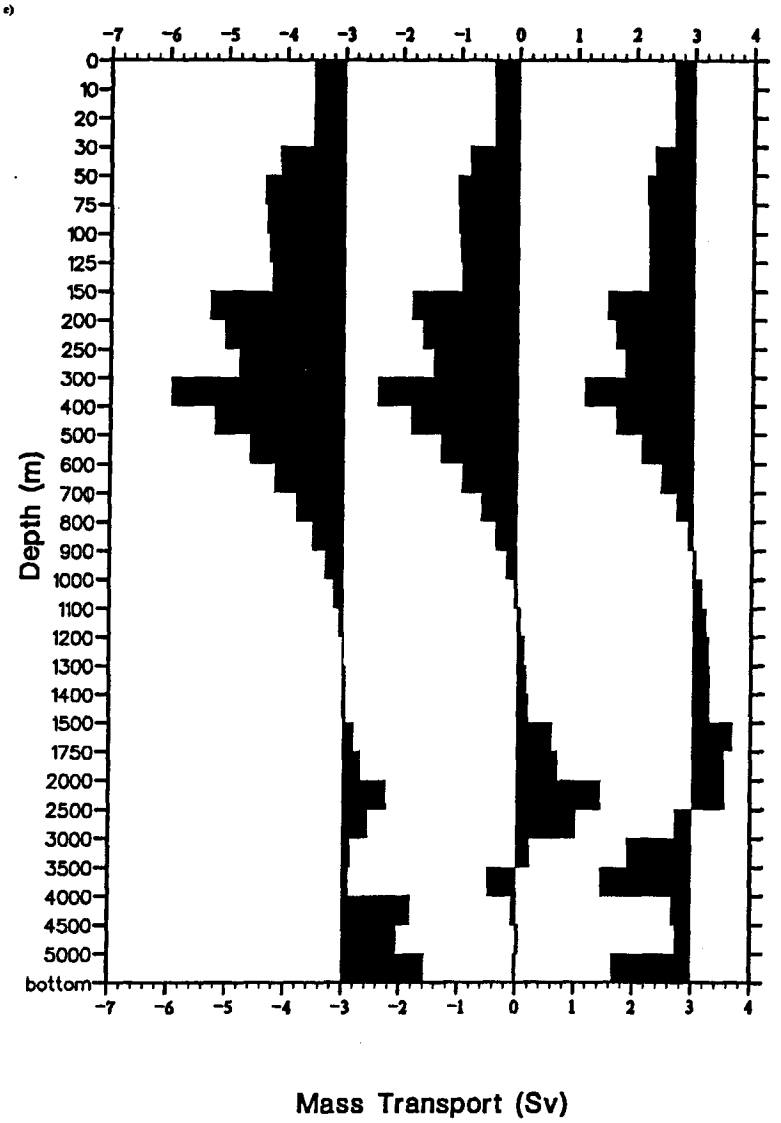

section. We will now investigate the ability of the two sections to close several different tracer budgets. First, we will compare the salt and heat transport through the two sections. Second, we will compare the calculated transport of DIC, alkalinity, oxygen, phosphate, nitrate and silicate of the two sections. Finally, we will correct the tracer

transports through the section to obtain the corresponding tracer budgets for the Pacific Ocean north of 35°N.

2.5.1 Heat and Salt

The calculated salt transport for the synoptic and climatological section (Table 2.1) is comparable, with both appearing to be consistent with expected values needed to close the freshwater budget (Baumgartner and Reichel, 1975). The freshwater inputs implied by these salt transports will be calculated in the next section. The calculated heat transport using the two sections is drastically different. The Levitus section gives an unrealistically large southward transport of heat which is not in agreement with the heat transport determined from air-sea exchanges (Talley, 1984). Part of this discrepancy can be attributed to the underestimated flow in the west boundary which reduces the northward transport of heat across the section. The heat transport determined from the INDOPAC section is much more believable but it is in the lower range of the oceanic heat flux estimated by Talley (1984).

Table 2.1: The tracer transports through the 35°N section for a) salt and heat, b) alkalinity and DIC, c) phosphate and nitrate and d) oxygen and silicate. These transports are determined with the assumption that there is no net mass transport through the section. Positive values indicate transport into the North Pacific. The errors in the transports are determined from the integrated layer transports multiplied by the variability of the tracers within those layers plus the estimated errors arising from the choice of reference level.

a)

	Salt (10^6 kg s^{-1})		Heat (10^{15} W)	
Transport	Levitus	INDOPAC	Levitus	INDOPAC
Geostrophic	160.2	163.7	4.446	4.920
Ekman	-151.5	-151.3	-5.139	-5.083
Total	8.7	12.4	-0.693	-0.163
	±5.3	±2.8	±0.075	±0.130

b)

	Alkalinity (k mol s^{-1})		DIC (k mol s^{-1})	
Transport	Levitus	INDOPAC	Levitus	INDOPAC
Geostrophic	12,178	11,056	12,175	10,042
Ekman	-9,9767	-9,9767	-8,789	-8,789
Total	2,200	1,080	3,390	1,250
	±380	±320	±790	±700

c)

	Phosphate (k mol s^{-1})		Nitrate (k mol s^{-1})	
Transport	Levitus	INDOPAC	Levitus	INDOPAC
Geostrophic	26.7	15.9	331.3	36.7
Ekman	-0.9	-0.9	-7.8	-7.8
Total	25.8	15.0	323.5	28.9
	±6.0	±5.0	±94.0	±76.0

d)

	Oxygen (k mol s^{-1})		Silicate (k mol s^{-1})	
Transport	Levitus	INDOPAC	Levitus	INDOPAC
Geostrophic	-682	-845	1,847	684
Ekman	-1,144	-1,144	-26	-26
Total	-1,826	-1,989	1,821	658
	±510	±540	±197	±158

2.5.2 Nutrient Tracers, DIC and Alkalinity

The difference in the heat transport for the two sections was amplified further when comparing the transport of nutrient tracers, DIC and alkalinity (Table 2.1b, c, and d). With the exception of oxygen, the Levitus section produced values 2-3 times greater than the INDOPAC section. It should be recalled that for the Levitus section the annual mean nutrient tracer fields were determined from the NODC archives, and the DIC and alkalinity fields were calculated from the average of the INDOPAC and TRANSPAC data.

Table 2.2: The transport of phosphate and silicate across the 35°N using the hydrography from the Levitus seasonal data (FMA) and the tracer measurements of INDOPAC.

	Phosphate (K mol s^{-1})	Silicate (K mol s^{-1})
Transport	Levitus (FMA)	Levitus (FMA)
Geostrophic	35.9	2356
Ekman	-1.7	-50
Total	35.2	2,307
	±6.0	±197

Although the study was meant to evaluate the annual mean tracer transports, it was interesting to see if the use of seasonal Levitus hydrography (Feb., Mar., Apr.) corresponding to the time of the INDOPAC cruise (Mar.) applied to the INDOPAC tracer fields would produce more comparable transports with the INDOPAC section. For the phosphate and silicate transports, the use of the seasonal hydrography (Table 2.2) did not reduce the difference between the INDOPAC section and the Levitus section. To assess the significance of the tracer transports given in Table 2.1, one must consider additional transports to obtain the corresponding tracers budgets for the North Pacific.

2.5.3 Corrections to the Tracer Transports due to Bering Strait Flow, Korean Strait Flow and Freshwater Exchanges

In the North Pacific, the northward movement of water through the Bering Strait, Korean Strait and freshwater exchanges produce significant changes to the tracer transports estimated from the 35°N section, using the assumption of zero net mass transport through the section. The necessity of including these transports arises because of the significant differences in tracer concentrations between the Bering Strait water, the Korean Strait water, the freshwater input, and the average water along the 35°N section. The freshwater exchange is considered to have no tracer concentration (air-sea exchanges of heat, CO_2, and O_2 are treated separately). The Bering Strait is very shallow (50 m or less), as is the Korean Strait (200 m), and therefore they have significantly different average tracer concentrations than the average concentrations in the 35°N section.

By using the Bering Strait salt transport of Anderson *et al.* (1983), the Korean Strait transport of Yoon (1982) and the average salinity in the Korean Strait, the salt and mass budgets are closed. By closing the budgets, one obtains a freshwater exchange and a mass transport correction for each of the sections. The freshwater exchange is an estimate of the net input of freshwater into the Pacific Ocean north of 35°N. The mass transport correction for the section is introduced as a correction to the

Table 2.3: The corrections to the tracer transports, the value in the "Difference" column should be added to the tracer transport given in Table 2.1 to obtain the tracer budgets. *In the table the heat transport assumes the water transport through the Bering Strait is replace by water with an average temperature of 5°C.

Tracer	Bering Strait Transport	Korean Strait	35°N Section Correction Transport	Difference
Alkalinity (kmol s^{-1})	-2,978	4,975	-3,086	-1,089
DIC (kmol s^{-1})	-2,835	4,457	-3,002	-1,380
Oxygen (kmol s^{-1})	-405	541	-152	-16
Nitrate (kmol s^{-1})	0.0	13.6	-47	-33
Phosphate (kmol s^{-1})	0.0	1	-3	-2
Silicate (kmol s^{-1})	-31	20	-182	-193
Heat (10^{15}W)	-1.48	2.52	-0.94*	0.100

reference level velocity necessary to produce the required mass transport. The following values are used for this calculation along with the salt transports determined by the section. The volume transport through the Bering Strait is 1.35 Sv northward with an average salinity of 31.963. The transport through the Korean Strait is 2.2 Sv northward with an average salinity of 34.2 . The average salinity of the 35°N section is 34.55 . For the Levitus section the freshwater input into the North Pacific is 0.33 Sv with a mass transport correction of 1.18 Sv out of the North Pacific. For the INDOPAC section, the freshwater input is 0.44 Sv and the mass transport correction is 1.29 Sv out of the North Pacific. The freshwater input calculated by Baumgartner and Reichel (1975) for the

Pacific Ocean north of 35°N was 0.42 Sv which is very comparable to the values determined for the two sections.

By using the appropriate transport corrections for the two sections and the average tracer concentrations in the Bering Sea and the Sea of Japan, the correction to the tracer transport through the section necessary to obtain the tracer budgets for the North Pacific north of 35°N is calculated (Table 2.3). The values given in the 'difference' column should be added to the net tracers transports through the 35°N section in order to obtain the tracer budgets.

2.5.4 Tracer Budgets for the Pacific Ocean north of 35°N

The tracer budgets for the various tracers clearly show that the synoptic section does a better job at balancing these budgets than the climatological data (Table 2.4). For the INDOPAC section, one succeeds in closing the budgets for all tracers except oxygen, phosphate and silicate. For the Levitus section, none of the tracer budgets are closed with the imbalances being 3 times larger than the estimated errors in these budgets and, with the exception of oxygen, more than double the INDOPAC imbalances.

It is interesting to investigate further the tracer imbalances in the sections for oxygen, phosphate and silicate budgets. For oxygen, part of the imbalance can be attributed to air-sea exchanges. To balance the oxygen budget would require an air-sea exchanged of 2.0 Mmol s^{-1} into the ocean which is considerably greater than the 0.8 Mmol s^{-1} that were calculate from Craig and Hayward (1987) data. The difference could

Table 2.4: Tracer budgets for the North Pacific Ocean north of 35°N for the two sections. A positive value indicates input into the North Pacific.

Tracer	Levitus		INDOPAC	
Heat (10^{12}W)	-593	±130	-63	±75
Salt (kg s^{-1})	0	±5.3	0	±2.8
Alkalinity (Kmol s^{-1})	1,111	±380	-9	±320
DIC (Kmol s^{-1})	2,010	±790	-130	±700
Oxygen (Kmol s^{-1})	-1,846	±510	-2,006	±540
Nitrate (Kmol s^{-1})	291	±94	-4	±76
Phosphate (Kmol s^{-1})	24	±6	13	±5
Silicate (Kmol s^{-1})	1,628	±197	465	±158

be explained by a flux of dissolved organic matter (DOM) out of the North Pacific. By using the air-sea exchange value calculated from Craig and Hayward (1987) data (0.8 Mmol s^{-1}) the estimated DOM value required to balance the oxygen budget is +1.2 ± 0.54 Mmol s^{-1} of oxygen. By using the following the constant molecular ratio from Takahashi *et al.* (1985) (P:N:C:O = 1:16:103:-172) for the composition of DOM, the DOM transport of nitrate, phosphate, and carbon were calculated. Broecker *et al.*, (1985) showed that the ratio of O_2 utilization to phosphate production in the sea is equal to 175 ± 6, with no significant changes with depth or location. The estimated DOM transport of 1.2 ±0.54 Mmol s^{-1} necessary to close the oxygen budget would alter the nitrate budget by -112 ± 50 Kmol s^{-1}, the phosphate budget by -7 ± 3.1 Kmol s^{-1} phosphate and the

carbon budget by -720 $\pm$ 400 Kmol s^{-1}. For the INDOPAC section, such a DOM flux would be sufficient to balance the phosphate and the nitrate budgets.

By using the results of Sugimura and Suzuki (1988), the apparent oxygen utilization (AOU) of the INDOPAC section was calculated and used to obtain a dissolved organic carbon (DOC) field for the section. From the DOC field, the transport across 35°N is 2.253 Mmol s^{-1} southward. With the Bering Strait and Korean Strait having an average DOC value of 300 μmol m^{-3} and the 35°N section average DOC value being 110 μmol m^{-3}, this translated into a correction to the carbon budget of -1.733 Mmol s^{-1}. The calculated correction is double the value necessary to close the oxygen budget. From the tracer budgets, one could argue that there is a significant DOM transport but the results are probably not sufficient to prove this idea. The AOU - DOC relationship formulated by Sugimura and Suzuki (1988) defines an upper limit for the transport of DOM.

Recent measurements of the DOC concentration by Martin and Fitzwater (1992) show no evidence of the AOU - DOC relationship. However, in the equatorial Pacific they did observe strong gradients in DOC between surface water at the equator (130 μM) and 9°N (230 μM), and strong vertical gradients at 9°N between the surface water (230 μM) and 250 m (150μM). It is the existence of these strong gradients in the DOC field which are important in the net transport of DOC out of the North Pacific because they cause significant differences in the DOC concentration between the Bering Strait and Korean Strait and the average value along the 35°N section.

Without considering the transport DOM, the carbon budget calculated for the INDOPAC section implies that the North Pacific is a weak sink of atmospheric CO_2, 0.05

$\pm$ 0.2 Gt C yr^{-1}. Contrary to this, the Levitus section shows the North Pacific to be a source of 0.76 $\pm$ 0.2 Gt C y^{-1}. Tans *et al.*, (1990) calculated the air-sea flux of CO_2 into the North Pacific north of 15°N to be 0.44 Gt C y^{-1} (Jan.-Apr.) and -0.33 Gt C y^{-1} (Jul.-Oct.) with an estimated annual mean of 0.06 Gt C y^{-1}. The potential source/sink of CO_2 between 15°N and 35°N is small (ΔpCO_2 is close to zero Broecker *et al.*, 1986; Takahashi 1989). This enables one to compare the Tans *et al.*, (1990) air-sea exchange estimates with the values determined in this study from the carbon budget. The INDOPAC section estimate of air-sea flux of CO_2 agrees with the annual mean value of Tans *et al.*, (1990). The large flux of CO_2 out of the ocean calculated from the Levitus sections appears unrealistic when compared to the estimates of Tans *et al.* If one includes the estimate transport of carbon as DOM that was required to close the oxygen budget (720 Kmol s^{-1} of carbon), the air-sea flux of CO_2 into the ocean is increased by 0.3 Gt y^{-1}. Even with the additional transport of carbon as DOM, the Levitus section still shows the North Pacific ocean to be a large source of CO_2.

The excess in the silicate budget of 465 Kmol s^{-1} for the INDOPAC section is more difficult to explain. If this silicate is removed by sedimentation, the calculated deposition on the sea floor would be 70 mg m^{-2} d^{-1} (area of the ocean taken as 2 X $10^{13}m^2$). This value is significantly greater than the average detrital flux of biogenous silica at 3800 m of 17 mg m^{-2} d^{-1} from station P (of which about 1% is permanently deposited on the sea floor). What other processes may affect the silicate budget? Could the time lag between when the silicate is removed from the surface water and redissolved back into the water be important? This process may be significant because most of the

silicate removed from the surface water is dissolved slowly at the ocean bottom introducing an apparent time lag. The variability of the surface silicate at station P in the North Pacific (50°N and 145°W) showed seasonal fluctuations of 20 μmol kg^{-1} (C.S. Wong unpublished data). The estimated southward mass transport between 170 -240°E in the upper 100 m is about 10 Sv (7 from geostrophy and 3 Sv from Ekman transport). This would produce a seasonal fluctuation of 200 Kmol s^{-1} in the transport of silicate in the upper ocean. This value is large and is nearly enough to close the silicate budget. This brings about the question, on what time scale do we expect the tracer budgets to be balanced?

Two other effects must be considered in assessing these imbalances in the oxygen, phosphate and silicate budgets. First is the resolution of the data. The resolution of the INDOPAC section is such that it may have missed significant transport at the east, west, and bottom boundaries of the ocean (Roemmich and McCallister, 1989). The errors introduced by these effects are difficult to determine but cannot be discounted as an explanation for the imbalances in the tracer budgets. Second, the calculation of the tracer budgets are sensitive to the prescribed Ekman transport. The Ekman transport does not greatly affect the salt and heat budgets because the vertical structure of salinity and temperature (°K) is relatively constant (deviations of only a few percentages from the mean value). However, for nutrient tracers, DIC and alkalinity, the tracer concentration in the upper ocean is significantly different from the mean value for the water column.

In the 35°N section a 1 Sv change in the Ekman transport would produce a change of 144 Kmol s^{-1} in the silicate budget, 2 Kmol s^{-1} in the phosphate budget, 45 Kmol s^{-1} in

the nitrate budget, 76 Kmol s^{-1} in the oxygen budget, 131 Kmol s^{-1} in the alkalinity budget and a 300 Kmol s^{-1} in the carbon budget. A 1 Sv error in Ekman transport corresponds to a 0.1 GT of carbon error in the air-sea exchange for the North Pacific. This places limitations on trying to estimate the air-sea exchange of carbon from the synoptic section due to uncertainties in the windstress. The calculation above shows that errors in the mass field can translate into important uncertainties in the nutrient budgets.

2.6 DISCUSSION AND CONCLUSION

In this chapter, I have shown that the annual mean Levitus section and the synoptic INDOPAC section produced significantly different mass and tracer transports. The results provided strong evidence of the inadequacy of using the Levitus dataset in trying to evaluate tracer budgets. It was not unexpected to find that the Levitus' mass transport poorly represented boundary transports (west, east, and bottom). However, it appears that these inadequacies are not attenuated but rather amplified in the nutrient tracer transport calculations. In hindsight it is not surprising that a flow field determined from the average temperature and salinity fields does not represent the average geostrophic flow because of the non-linear nature of the equation of state. The clear structural similarities in the mass transport field between the INDOPAC and the TRANSPAC sections in the upper 2000 m of the ocean emphasize the idea that synoptic sections do represent the general circulation in the ocean.

The tracer budgets calculated from the synoptic section for the North Pacific are better able to close the tracer budgets than the Levitus section. However, the INDOPAC section tracer budgets reveal several interesting results. One, the DOM transport may play an important role in the nutrient budgets. It is accepted that this section does not have high enough resolution to confidently resolve this problem. However, it is clear that if the DOM has a definite vertical structure at any time of the year it will be a significant component to the nutrient budget in the North Pacific. Two, one may need to consider the time-scale that is applicable to the conservation of tracers in the North Pacific. The imbalance caused by the non-steady-state nature of the tracer is postulated to be most important for the silicate budget because of the significant time lag between when the silicate is removed from the surface water as detrital rain and when it is re-dissolved back into the water column at the ocean bottom. Three, variations in the Ekman transport have significant effect on the tracer budgets. Any errors in the Ekman transport will produce large discrepancies in the nutrient budgets because of the large vertical gradients in the nutrient tracers. A similar argument holds for the freshwater exchange processes because they introduce only a small amount of nutrient tracers due to continental runoff, but may generate significant nutrient tracer transport because of alterations to the mass field. The limitations in trying to determine the air-sea exchange of carbon are closely associated with deviations in the Ekman transport and freshwater exchanges. Therefore, it is important that one has an accurate determination of the flow field before one tries to determine the air-sea exchanges that affect the nutrient tracers. Small modifications to the mass field may be acceptable dynamically but the implications on the nutrient budgets will

be much more profound. This will be especially true for air-sea exchanges making it difficult to obtain meaningful results. Such a question forces one to critically assess the best approach to take to understand the CO_2 cycle and what type of data would be most useful in providing information on this cycle. A formal inverse inverse approach considering several tracers simultaneously would help reduce the errors in the tracer budgets cause by uncertainties in the Ekman transport and air-sea exchanges.

The study reinforces the need for highly resolved hydrographic sections in order to properly calculate the geostrophic and tracer transports. The inability of either the INDOPAC or Levitus section to close the tracer budgets to within the prescibed error suggest that these sections omit significant volume transports at in the western boundary and ocean bottom due to their limited resolution. As a consequence, the inverse model formulated for the North Pacific (chapters 4 and 5) will not uses these sections but rather I will use the only two highly resolved hydrographic sections across the Pacific (at 24°N and 47°N) to constrain the horizontal transports.

CHAPTER 3. VALIDATING AN INVERSE BOX MODEL USING DATA GENERATED FROM THE HAMBURG CARBON MODEL

3.1 INTRODUCTION

The box model is a classical method used in developing a quantitative picture of the role of an ocean basin in transferring heat, salt, carbon and other tracers. In this method, one applies conservation constraints to a set of boxes for the observed distribution of physical and biochemical tracers. This process generates a set of equations by which an inverse method is used to extract a solution for rates of the processes which govern the tracer distribution. Additional equations can be generated by considering other constraints, such as geostrophy, to further restrict the solution. To better understand the ability of the inverse box model and provide guidance in attacking the problem of understanding the CO_2 cycle in the ocean, the inverse box model was applied to data generated from a biogeochemical-ocean circulation model.

In this chapter, the annual fields produced by the Hamburg Large Scale Geostrophic Ocean Circulation (LSGOC)-biogeochemical model (Maier-Reimer and Bacastow, 1990) were used as data for an inverse box model of the North Pacific. The goal was to investigate the ability of the inverse model to determine the air-sea exchange of heat and carbon and the new production of organic and shell material. By performing inversions in this controlled setting one can test the ability of the inverse box model.

3.2 HAMBURG MODEL

3.2.1 Model Description

The global ocean circulation model used for validating the inverse box model was the Hamburg Large Scale Geostrophic (LSG) ocean circulation model (Maier-Reimer and Bacastow, 1990). The Hamburg LSG ocean circulation model has evolved from an original concept of Hasselmann (1982). The model was based on the observations that, for climate studies with a large scale ocean circulation model, the relevant characteristic times scales are large compared with the periods of gravity modes and barotropic Rossby wave modes. From these scaling conditions, the baroclinic velocity field can be determined from the density field through local geostrophy. The barotropic velocity field and surface elevation, for a given density field, are determined as the equilibrium barotropic response to the prescribed surface windstress forcing and bottom torque. In this model, the advection equations for temperature and salinity are solved using an implicit upwind differencing scheme. Coupled to this physical model is a biochemical model that computes the distributions of nutrient tracers using the transport field and computed biochemical source and sink terms. A brief discussion of the physical and biotic parts of the model are discussed in the next two sections.

3.2.1.a. Physical Model

Applying the standard hydrostatic and Boussinesq approximations and neglecting vertical friction, the prognostic equations of the model are given by:

1) the horizontal momentum equation

$$u_t - 2v\Omega \sin\phi + \frac{1}{\cos\phi}\frac{P_\lambda}{\varrho_o} = \frac{\tau^\lambda}{\varrho_o} + A \Delta u \tag{3.1}$$

$$v_t + 2u\Omega \sin\phi + \frac{1}{R}\frac{P_\phi}{\varrho_o} = \frac{\tau^\phi}{\varrho_o} + A \Delta u \quad ; \tag{3.2}$$

2) the equation for the evolution of potential temperature (θ) and salinity (S) (neglecting diffusion terms)

$$\theta_t + \frac{u}{R\cos\phi}\theta_\lambda + \frac{v}{R}\theta_\phi + w\theta_z = q^\theta \tag{3.3}$$

$$S_t + \frac{u}{R\cos\phi}S_\lambda + \frac{v}{R}S_\phi + wS_z = q^S \tag{3.4}$$

(the source q^θ and q^S only occur in the surface layer);

and 3) the evolution equation of the surface elevation ς, given by the surface boundary conditions,

$$\zeta_t = w \quad at \quad z=0. \tag{3.5}$$

The prognostic equations are complemented by the diagnostic relations consisting of:

1) the continuity equation

$$w_z + \frac{1}{R}\left[(v\cos\phi)_\phi + \frac{u_\lambda}{\cos\phi}\right] = 0; \tag{3.6}$$

2) the hydrostatic pressure

$$p = g\varrho_o\left[\zeta + \frac{1}{\varrho_o}\int_0^z \varrho(z')dz'\right] ; \tag{3.7}$$

and 3) the equation of state

$$\varrho = \varrho(S,T,P) , \tag{3.8}$$

where T is the in-situ temperature.

The velocity terms were solved for by separating horizontal velocities into barotropic and baroclinic components. The equations of motions for both the baroclinic and barotropic components are solved using a rigorous Euler-backward method. The advection of temperature and salinity (3.3 and 3.4) is then computed using an upwind method which is implicit in time,

$$T^t = T^{t-\Delta t} + \Delta t \sum_i u_i^t (T_i^t - T^t)/\Delta x_i \tag{3.9}$$

where the summation is over all neighbouring points for which u_i is directed towards the point of computation. The apparent diffusivity of this upwind scheme is derived in Appendix A and is equal to

$$K = |u|\frac{\Delta x}{2}\left(1 + \frac{|u|\Delta t}{\Delta x}\right) \tag{3.10}$$

The implicit upwind scheme numerical diffusion is $u^2\,\Delta t$ greater than the explicit upwind scheme (Smolarkiewicz, 1983) (see Appendix A for more details).

3.2.1.b Biotic model

The basic details of the biotic model are presented by Maier-Reimer and Bacastow (1990). Formally the model is characterized by a set of differential equations

$$\frac{\partial C_i}{\partial t} + v_j \frac{\partial C_i}{\partial x_j} + A_i C_i = \sum_k B_i^k, \tag{3.11}$$

where C_i denotes the components of the chemical cycle, v_j is the three-dimensional velocity from the LSGOCM, A_i denotes the intrinsic processes like radioactive decay, and B_i^k denotes the source/sink of tracer i due to metabolic processes (ie. the formation/dissolution of shell and organic material). The advection of the tracers are calculated by the same implicit upstream scheme used for temperature and salinity in the physical model. The model tracers are total dissolved inorganic carbon (TCO_2), alkalinity, phosphate, dissolved oxygen, particulate organic matter (POC), calcium carbonate of shell material, silicate, radiocarbon and ^{13}C (in the model ^{14}C and ^{13}C concentrations have been normalized by their fractions in the atmosphere).

The biotic cycle of the model is driven by a phosphate-limited primary productivity. In the model, photosynthesis of organic matter is assumed to be restricted to the surface layer. In the layers below the surface, remineralization of the carbon flux is accompanied by a reduction in oxygen concentration corresponding to its Redfield ratio. The following generalized ratios are used in the LSGOC model for the changes associated with the photosynthesis of organic matter and its subsequent remineralization: P: N: C: O_2: Ca: = 1:16:122:-172:30.5 . An additional flux of calcium carbonate from shell material is assumed

to sink from the surface layer. In this model, $CaCO_3$ is allowed to undergo dissolution at all depths.

The system is closed by the boundary conditions, which for all tracers except TCO_2, oxygen, ^{14}C, and ^{13}C, is vC=0 across all boundaries where vC denotes diffusive and advective fluxes of any tracer concentration C. The carbon tracer exchange CO_2 with a well mixed atmosphere of 280 ppm, using the calculated partial pressure of CO_2 in the surface boxes and the gas transfer rates determined by Merlivat *et al.*, (1991). In the model, the mass conservation is fulfilled for the number of carbon, phosphate, and oxygen atoms and for alkalinity.

The model was run on two staggered 5° x 5° global grids with 15 vertical levels (Fig. 3.1). The use of the staggered grid separates the model into two grids which are linked through the use of an explicit horizontal diffusion (200 m^2 s^{-1}) in the advection equations for the various tracers (Bacastow and Maier-Reimer, 1990). The vertical levels were defined as the mid-point of each layer and the layers were defined by the following depths: 0, 50, 100, 150, 200, 250, 300, 400, 525, 700, 900, 1500, 2500, 3500, 4500, and 6000 m. The output from the model used in the inverse box model consists of the annual mean velocity and tracer fields averaged over 2 years after the model has been completely spun-up (4000 years with a one month time step).

3.2.2 Tracer Transports

In a time varying flow one can separate the velocity, v(t), and the concentration, c(t),

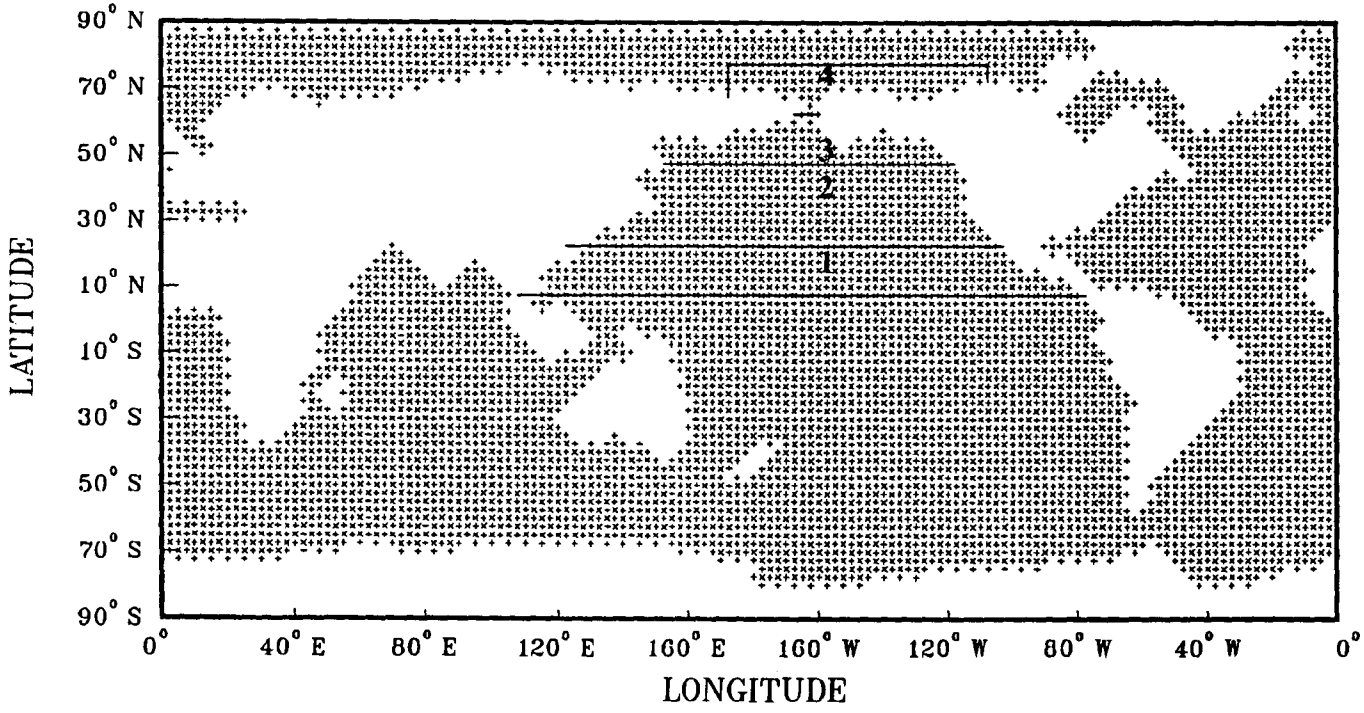

Figure 3.1: The Hamburg model grid where the * denotes the points where the u and v are determined, and + denotes the location of the tracer concentrations and w. In the figure, the regions used in the 4-region inverse model are denoted by the highlighted areas and are labelled.

a of some quantity into a time-average part and a fluctuating part according to:

$$v(t) = \bar{v} + v'(t), \qquad c(t) = \bar{c} + c'(t). \tag{3.12}$$

An overbar indicates an average over a chosen time (2 years in our case). The time-average tracer flux (per unit area) is then given by

$$F_c = \overline{vc} = \bar{v}\,\bar{c} + \overline{v'c'} \tag{3.13}$$

where the first term to the right is the transport by the mean advection, $\bar{v}$, and the second term gives the "turbulent" (eddy) flux. The horizontal transport by the mean advection into the North Pacific was calculated from the annual mean velocity and tracer fields by integrating (3.13) along a specified latitude (Table 3.1). The resulting calculation for the North Pacific produced some surprising results. One, the heat and salt transports are significantly different for the two grids even though they differ by only 2.5° latitude in their definition of the North Pacific. Two, for tracers with no air-sea exchange (phosphate, silicate, alkalinity, and salt), the mean advective transport does not close the budgets of these tracers in the North Pacific. These results imply that, in the model, the horizontal eddy transports play an important role in closing the tracer budgets. The implicit numerical diffusion of the upwind scheme may also work to increase the horizontal eddy transport.

Table 3.1: Mean Advection transport into the North Pacific (positive value). The first column gives the transports through 25°N into the North Pacific, this grid has no outflow into the Arctic Ocean. The second column gives the net transports into the North Pacific between 22.5°N and the Bering Strait.

Tracer	Transport 1	Transport 2
Volume	-0.099 Sv	-0.07 Sv
Temperature	-0.10×10^{15}W	0.02×10^{15}W
Salinity	-1.69×10^{6} kg s^{-1}	0.01×10^{6} kg s^{-1}
Phosphate	3.03 kmol s^{-1}	2.93 kmol s^{-1}
Silicate	352.82 kmol s^{-1}	406.44 kmol s^{-1}
Alkalinity	10.0 kmol s^{-1}	132.35 kmol s^{-1}
Oxygen	-17.9 kmol s^{-1}	-62.56 kmol s^{-1}
DIC	-15.6 kmol s^{-1}	-24.26 kmol s^{-1}
DIC 14	-881.4 kmol s^{-1}	-944.61 kmol s^{-1}
POC	-59.8 kmol s^{-1}	-53.52 kmol s^{-1}
calcite	-0.01 kmol s^{-1}	0.095 kmol s^{-1}

The horizontal eddy transports of the tracers can be calculated using the "known" annual exchanges air-sea exchanges of the various tracers from the LSG ocean circulation model. For tracers with no air-sea exchanges (salinity, phosphate, silicate and alkalinity) the eddy transports must equal to but of opposite sign to the values given in Table 3.1. For heat, to produce the LSGOC model air-sea exchange of 0.25 PW into the atmosphere requires the horizontal eddy transport of heat to be approximately 0.25 PW into the North Pacific. The eddy transport of heat is significantly greater than the mean advective transport of heat. The LSGOC model air-sea exchange of CO_2 is 780 Kmol s^{-1} into the North Pacific which implies

an eddy transport of CO_2 of approximately 780 Kmol s^{-1} out of the North Pacific. The eddy transport of CO_2 is much greater than the calculated from the mean advective transport of CO_2.

One critical test for the inverse box model is to see whether it can recover these horizontal eddy transports from the mean tracer distributions to produce a consistent estimate of the air-sea exchanges.

3.3 INVERSE BOX MODEL

3.3.1 Model Topology

The inverse box model is applied by dividing the ocean into boxes. For this study, the boxes consist of large regions bounded by two depth surfaces. It was necessary to consider large regional areas in the inverse box model in order to ensure that tracer gradients between the boxes were greater than the tracer variability. The ability of the model to extract a solution rapidly degrades as the number of regions is increased and forces one to use large regions in the inverse model.

The inversions were performed on the Hamburg model data from the North Pacific Ocean. For comparisons with studies with actual measured data, the boxes were defined to reflect the inverse box models that will be pursued with this measured data. The inverse model was first configured using a 6 layer model with 4 regions of the North Pacific. The North Pacific was divided into 4 regions by the latitude bands 7.5°, 22.5°, 47.5°, 62.5°, and

77.5°N (Fig. 3.1), and 6 layers by the depth surfaces 0 m, 50 m, 200 m, 525 m, 900 m, 3500 m, and 6000 m. For the model, two of these regions are necessary to handle the open boundaries at the north and south. With this box configuration, several sets of experiments were performed to investigate the information content in the tracer fields.

3.3.2 Model Constraints

The basic constraints of the inverse box model are the continuity of tracers and freshwater within the defined boxes. The general continuity equations applied to a box for any given scalar tracer C are :

$$V\frac{\partial C}{\partial t} = \int (\nabla\cdot(\vec{u}C) - \nabla\cdot(k\nabla C))dv + Q_{bio} + Q_{air\text{-}sea} - Q_{decay} = 0 \qquad (3.14)$$

$$\int (\nabla\cdot\vec{u})dV + Q_{air\text{-}sea} = 0 \qquad (3.15)$$

The rate of change of the concentration C in any box with volume V, ($\partial C/\partial t$), is affected by the net flux of the tracer C due to horizontal and vertical advection, horizontal and vertical mixing, biological processes (Q_{bio}), air-sea exchanges ($Q_{air\text{-}sea}$), and radioactive decay (Q_{decay}). In the model, all tracers are assumed to be steady state and the density of the water is constant (to be consistent with the LSGOC model). In (3.14) and (3.15), the $Q_{air\text{-}sea}$ term only affects boxes in contact with the surface. The advective transport is calculated by multiplying the velocity through the box face by the average concentration of the two connected boxes (like Bolin *et al.*, 1987).

In (3.14) the eddy transports are parameterized by an eddy diffusion approach which assumes that the turbulent flux is proportional to the mean tracer gradient. The definition of the eddy transport is obtained by separating the time average flow into a space-average term and a part fluctuating in space:

$$\bar{v} = <\bar{v}> + \bar{v}^*, \quad \bar{c} = <\bar{c}> + \bar{c}^*, \tag{3.16}$$

where $< >$ denotes a space averaging and * the spatial fluctuation. The flux in (3) can now be written as :

$$F = <\overline{vc}> = <\bar{v}><\bar{c}> + <\bar{v}^*\bar{c}^*> + <\overline{v'c'}> \ . \tag{3.17}$$

The average flux consists of a transport by mean advection $<\bar{v}>$; a transport by the spatial fluctuations of the time-average circulation, that is standing eddies v^*; and a transport by transient eddies v'. The eddy diffusion approach followed here assumes that the turbulent flux is proportional to the mean tracer gradient. The eddy transports are determine by multiplying the mixing coefficient (k) on the box face by the difference in tracer concentrations between the two boxes and dividing by the distance between the centre of the two connected boxes. This parameterization of the eddy transports is a critical ingredient of the box model and will be evaluated in this chapter.

The biological source parameter, Q_{bio}, in (3.14) represents the formation of soft and hard shells in the surface boxes and the subsequent remineralization of the particulate matter in the deeper layers of the model. In the inverse model, the sedimentation rate is zero; all particulate matter formed in the surface boxes is redissolved in the underlying boxes (consistent with the LSGOC-biogeochemical model). For this problem, the molecular ratios

linking the biological source/sink for the various tracers are known, and in the inverse box model, they are set equal to the values used in the LSGOC-biogeochemical model.

In applying the box model, several additional inequality constraints were included to improve the solutions. One, the model was forced to satisfy exactly the freshwater budget in all the defined boxes. Two, in the defined regions, the model conserved all tracers exactly. This required that the total amount of tracer leaving a region plus any radioactive decay be equal to the air-sea exchange. Three, the mixing transports are assumed to only transport tracers down-gradient ($k>0$). With the inverse box model it is relatively easy to augment the problem with additional constraints in order to further investigate the problem.

3.3.3 Inversions

The formulated constraints (3.14) and (3.15) are applied to the defined boxes and available tracers to generate a set of equations. This set of equations can be represented by the equation

$$Gx = b \pm \epsilon \tag{3.18}$$

where the coefficients matrix **G** contains tracer concentrations and gradients, **x** is the vector of unknowns

$$x = (u_i, v_i, w_i, k_{h_i}, k_{v_i}, Q_{bio}, Q_{air\text{-}sea}) \tag{3.19}$$

and the vector **b** is a zero. Due to errors in the approximations in the model, the constraint equations are not expected to be exactly satisfied but only to be within a specified tolerances ϵ_i. The estimation of the tolerances will be discussed in later in this section.

To solve this system of equations, I relied on two different algorithms: the least squares algorithm with inequality constraints (LSI) and linear programming (LP). For details on how these routines work, refer to Lawson and Hanson (1974) for the LSI routine and Luenberger (1984) for the LP routine. The implementation of these routines in NAG library is ideal for solving this problem using either algorithm. The only difference between the two approaches is the objective function that one wishes to minimize. In the LSI routine, one determines a solution **x** by minimizing in a least squares sense

$$\Phi = \| Gx - b \|^2 \tag{3.20}$$

subject to

$$b - \epsilon \leq Gx \leq b + \epsilon \tag{3.21}$$

$$x^- \leq x \leq x^+ \tag{3.22}$$

A priori bounds x^- and x^+ are applied to the unknowns to restrict their numerical values to physically meaningful ranges, like allowing only positive mixing coefficients. To properly apply this inversion algorithm it is essential that the set of equations ($\mathbf{G\,x = b}$) be properly weighted. The need for weighting the equations arises because each tracer possesses a different signal to noise ratio. A proper weighting of the equations must reflect the

significance of the tracer concentrations, and force the model to rely most heavily on the most significant tracers. A simple row normalization only works if one can assume the information content of all tracers in all boxes is equal.

In an inverse problem, one typically weights the i^{th} equation by dividing this equation by the error in b_i, δb_i. The difficulty of attempting this for our problem is that the errors in **b** are functions of the unknown transport terms. An appropriate estimate of $\delta\mathbf{b}$ was thought to be determined by only considering the error in **b** due to advective transports by using the following equations:

$$\begin{aligned} b' &= \sum_i x_i C_i \\ \delta b' &= \sum_i \delta x_i C_i + \sum_i \delta C_i x_i \end{aligned} \tag{3.23}$$

where x_i represents the volume transport through the i^{th} box face, C_i represents the concentration on the i^{th} box face, and δ denotes the errors in these terms. The first term on the rhs of (3.23) was dropped because for flow that is forced to conserve mass, the sum of the δx_i's for the box is zero and hence the error from this term will be small. The second term on the rhs of (3.23) was evaluated by using the standard deviation of the tracers in the defined boxes to determine the tracer errors on the box faces (δC_i) and multiplying this value by the known volume transports (x_i). It should be noted that to properly weight the equations, the exact determination of $\delta\mathbf{b}$ is not required but rather only the relative weighting of different equations. By using just the δC's to weight the problem, one produced nearly identical results to the weighting given by (3.23). Another quantity one can make use of

when weighting the equations by the standard deviation in **b** is that the chi-squared error (X^2) should approximately equal the number of equations (N):

$$X^2 = \sum_{i=1}^{N} \left| \frac{Gx - b}{\delta b} \right| \approx N \tag{3.24}$$

If the X^2 is much less than N, the data are overfitted, and if X^2 is much greater than N, then one is underfitting the data. If one wishes to produce reasonable results, then care should be taken to ensure that X^2 is not significantly different from N. In this problem small variations in the known velocities (less than $\pm 0.2\%$) were allowed in order to produce solutions with X^2's approximately equal to N.

In the LP approach one finds a solution to **x** which minimizes

$$\Phi = \sum w_i x_i \tag{3.25}$$

subject to the same set of inequality constraints given in (3.21) and (3.22). If there is a solution to the set of constraints, the solution is said to be feasible; it usually is not a unique solution but an infinite number of solutions may exist. Running the model repeatedly with a convenient set of chosen objective functions allows one to explore the whole range of possible solutions.

The great utility of the LP routine is its ability to provide solutions to any objective function that is made up of a linear combination of the unknown **x**. A common set of objective functions that are used in analysing the model are ones that minimize and maximize each individual unknown by setting one w_i to 1 or -1 and all the other w_i to zero. By minimizing and maximizing such objective functions one obtains the maximum and minimum

values of the model parameters that satisfy the constraints. This reveals how well the model determines the different model parameters.

It is a common feature of LP solutions that to obtain a maximum or minimum value for the objective function many of the constraints are pushed to their lower and upper bounds. The dual solution reveals the sensitivity of the objective function to changes in the bounds of a constraint (Luenberger, 1984). Those constraints that limit the value of the objective function are represented in the dual solution by non-zero values. The larger value the more sensitive the object function is to the bounds on the respective constraint. The examination of the dual solution reveals the importance of the constraint in determining the value of the objective function.

The solutions that are calculated with LP algorithm are extremal solutions in the sense that they maximize or minimize a conveniently chosen linear objective function. As a consequence, as mentioned above, many of the constraints are pushed to their upper and lower bounds in order to minimize the value of the objective function. Thus the corresponding solution may exhibit certain features that may not be realistic. This is why the LSI routine is used to look at the "best" solution. The main goal of the LP routine is not to produce one "best" solution but to explore the range of solutions that are possible given the model's constraints. This approach demonstrates which oceanographic parameters are well-determined and which are not, and it indicates which constraints have the largest errors.

The ranges determined for the various objective functions are dependent on the errors prescribed to the tracer budgets. The determination of these errors is intimately related to the weighting of the LSI problem. For LP solutions, the errors in the equations are

determined using (3.23) but are increased by a constant factor equal to the maximum factor determined from the LSI solution. One should observe that the weighting of the equations has no effect on the LP solution because the objective function is linear. However, the errors in the equations are derived in a manner analogous to the weighting of the equations in the LSI routine and thus have similar ambiguities. In addition to providing ranges for the unknowns, the LP routine also provides information on which equations are most important in determining these ranges through the dual solution. This gives clear information on how one could reduce the acceptable ranges for the different unknowns in the inversion.

3.4 INVERSE SOLUTIONS

3.4.1 Tracer Studies

The first set of experiments was performed to assess the information content of the various tracer fields. In these experiments, the horizontal velocity field was considered well-determined (prescribed error of less than 0.2%) and LSI inversion was used to solve the system of equations.

If only the temperature (T) and salinity (S) fields are included in the inverse box model, the resulting solution produces a poor estimate of the air-sea exchange of heat for the North Pacific (0 PW compared to the LSGOC model value of -0.25 PW). By including total CO_2 (TCO_2), phosphate (P), and alkalinity (A) fields in the model, the model is better constrained and the solution begins to reflect the known air-sea exchange of heat (-0.17 PW).

The addition of oxygen (O_2) and radiocarbon (^{14}C) to the model does surprisingly little to the solution, it only slightly increases the detrital rain rate of organic matter. The addition of the POC and calcite fields to the model increases the air-sea exchange of CO_2, O_2 and ^{14}C by 100, 240 and 30 kmol s^{-1} respectively, and increase the heat exchange to -.184 PW. To include POC and calcite fields in the model required that (3.14) be modified for TCO_2, alkalinity, phosphate, oxygen and ^{14}C to address the transports of these tracers as organic and shell material. To include the effect of organic and shell material on the tracer budgets, the following terms were added to (3.14):

$$\begin{aligned} &+R_i\ [(\nabla\cdot(\vec{u}[POC]))\ -\ \nabla\cdot(k(\nabla[POC]))] \\ &+S_i\ [(\nabla\cdot(\vec{u}[CaCO3]))\ -\ \nabla\cdot(k(\nabla[CaCO3]))]\ . \end{aligned} \tag{3.26}$$

The R and S are determined from the Hamburg model's Redfield's ratios and are given in Table 3.2 for the various tracers. This will be called the reference model and will be used for comparison with other inverse box models.

3.4.2 Reference Model

Table 3.3 summarizes the different models studied. The circulation and mixing fields obtained from the reference box model are shown in Figure 3.2. This model made use of T, S, TCO_2, P, A, O_2 ^{14}C, POC and calcite fields to constrain the model; in all subsequent models all these tracer fields are used. With the T, S, TCO_2, P, A, O, ^{14}C, POC, and calcite fields, the inverse box model was able to produce consistent estimates for the heat and CO_2

Table 3.2: The molecular ratios for organic matter (R's) and shell material (S's).

Tracer	Organic Matter (R)	Shell Material (S)
TCO_2	1.0	1.0
Alkalinity	0.3525	2.0
Phosphate	1/122	0
Oxygen	-1.409	0
^{14}C	1.0	1.0

Table 3.3: Summary of the various inverse box models used

Model	Model Definition
I	Reference Model
II	Reference Model but allowing negative eddy diffusion
III	Model with an unknown barotropic flow
IV	Model III with limits on the fresh water fluxes of 0 - 2 Sv into the ocean
V	Reference Model but allowing Redfield's ratios to vary by $\pm 20\%$
VI	Model III but allowing Redfield's ratios to vary by $\pm 20\%$
VII	Model IV but allowing Redfield's ratios to vary by $\pm 20\%$

exchange of the North Pacific when compared to the known values from the LSGOC model (model I in Table 3.4). The consistent results support the use of the eddy diffusion term with

a positive k as a means of parameterizing the eddy transport. In contrast, the LSI inversion of a model that allowed negative k's (model II in Table 3.4) greatly underestimated the heat and the CO_2 exchange. Furthermore, by allowing just a small error in the known velocities, a model with positive k's satisfies the problem equally as well as the model which allowed for negative k's. These results suggest that the use of an inverse box model with positive k's is sufficient to produce useful results.

The LP solutions obtained from the reference model with positive k's express the ability of the inverse model to estimate the unknown detrital rain rates and air-sea exchanges (model I in Table 3.4). The errors used for the LP problem were 3.215 times the $\delta\mathbf{b}$'s used to weight the LSI problem. This value, 3.215, was equal to the maximum error in the equations obtained from the LSI solution. The transport of freshwater, heat and CO_2 by the inverse model is plotted with the corresponding values from the LSGOC-biogeochemical model (Fig 3.3a-c). In general the acceptable ranges for these transports determined from the inverse model were in good agreement with the unknown values.

The acceptable ranges for the mixing coefficients are shown in Figure 3.4 along with the apparent numerical diffusivity of the upwind advection scheme used by the LSGOC-biogeochemical model (derived in Appendix A). The horizontal mixing terms are not well-determined but they are consistent with the apparent numerical diffusivities of the original model. The inverse results suggest that k_h is enhanced in both the surface layers and the bottom layer. The inverse results for k_z show an exponential-like increase in vertical mixing with depth for both the inverse model results and the apparent diffusivities of the original model.

(a)

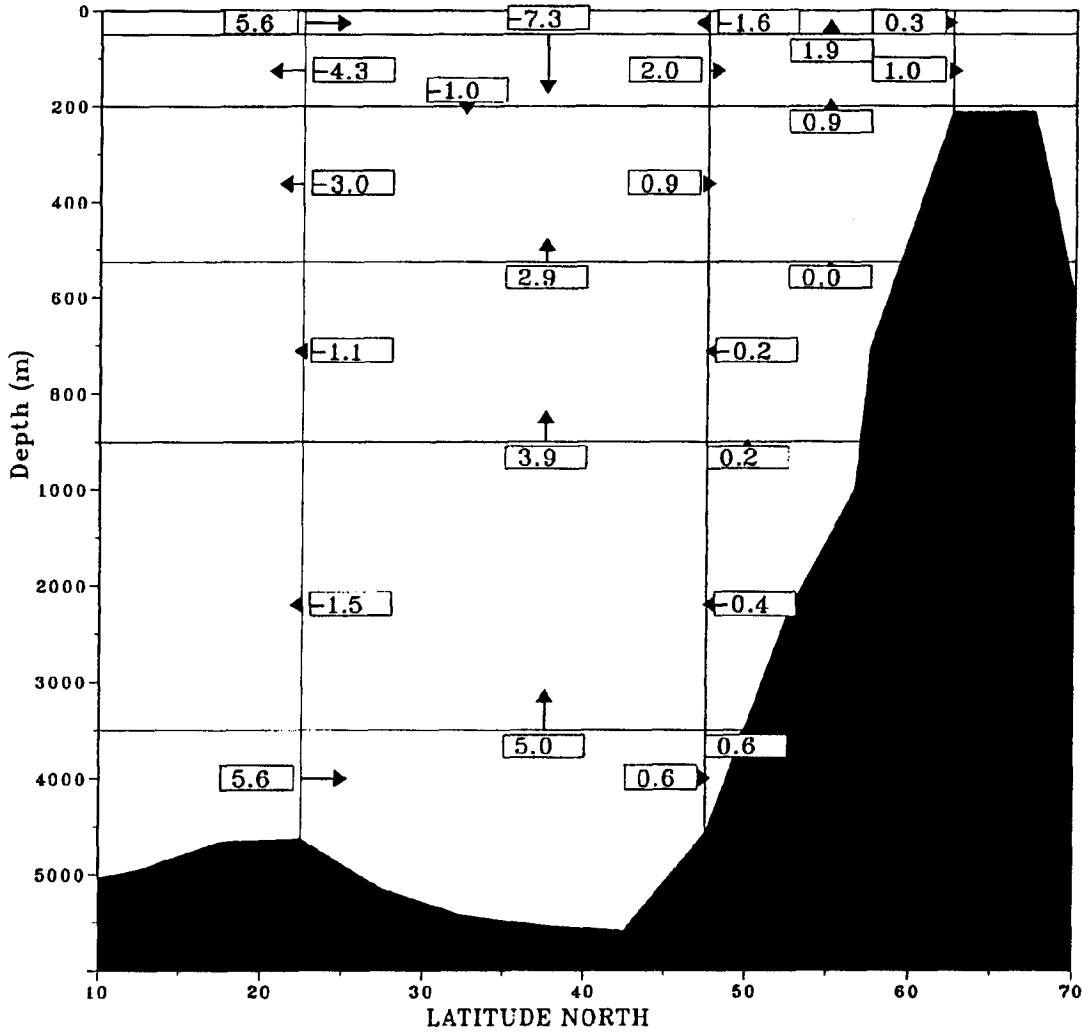

Figure 3.2: The circulation field for the reference model where (a) shows the volume transports (Sv) across the box faces, and (b) shows the mixing transports as k * area / distance in Sv.

(b)

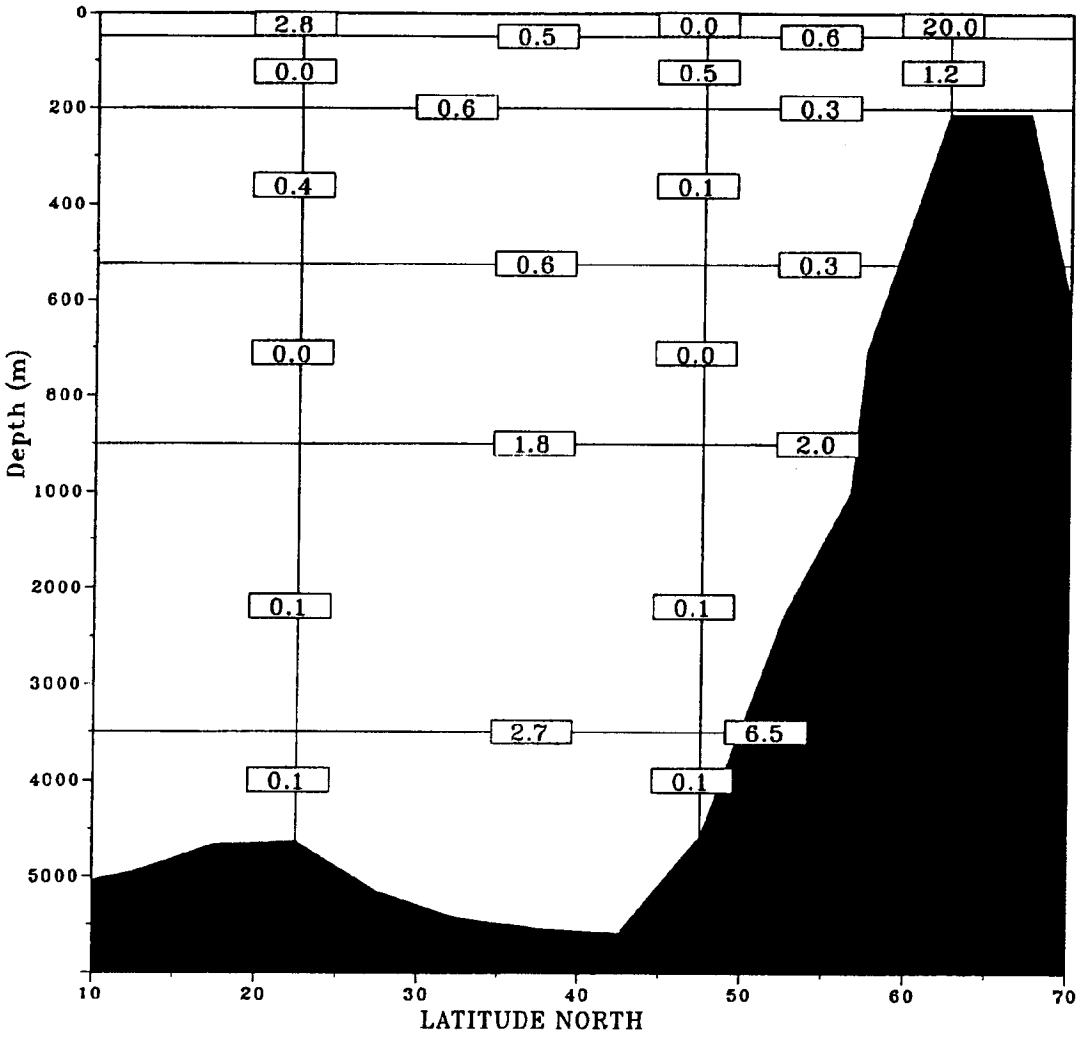
2.8
0.5
0.0
0.6
20.0
0.0
0.5
1.2
0.6
0.3
0.4
0.1
0.6
0.3
0.0
0.0
1.8
2.0
0.1
0.1
2.7
6.5
0.1
0.1
Depth (m)
0
200
400
600
800
1000
2000
3000
4000
5000
10
20
30
40
50
60
70
LATITUDE NORTH

(a)

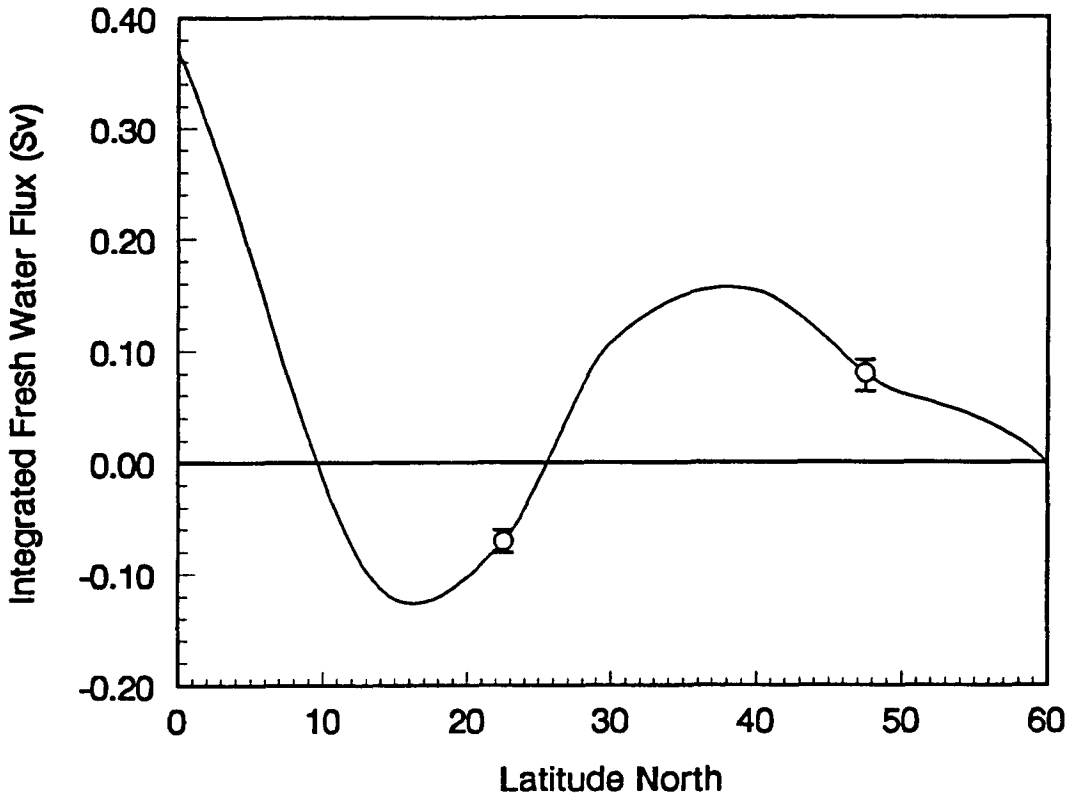

Figure 3.3: The integrated northward transport of (a) freshwater, (b) heat, and (c) CO_2. The curve in (a) shows the freshwater exchanges calculated by Baumgartner and Reichel (1975), and in (b) and (c) the curve denotes the values from the LSGOC model. In three plots the circles denote the values determined by the LSI inversion of the model and the error bars are corresponding the maximum and minimum values determined from the LP inversions.

(b)

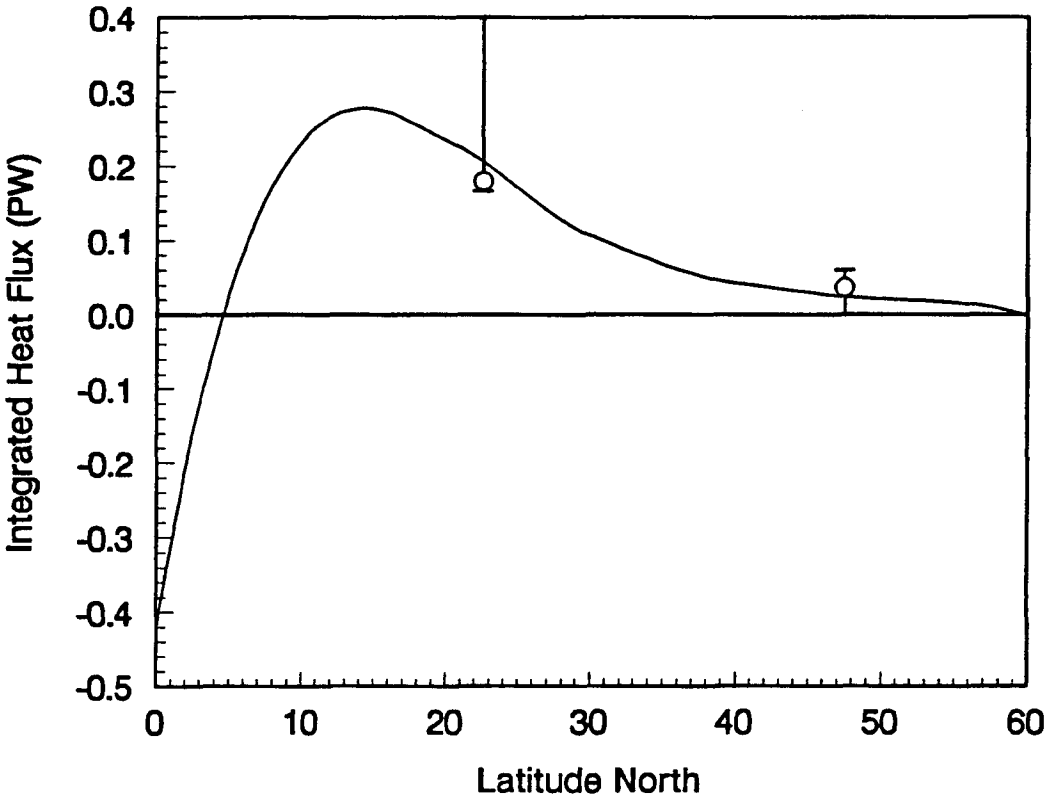
0.4
0.3
0.2
0.1
0.0
-0.1
-0.2
-0.3
-0.4
-0.5
Integrated Heat Flux (PW)
0
10
20
30
40
50
60
Latitude North

(c)

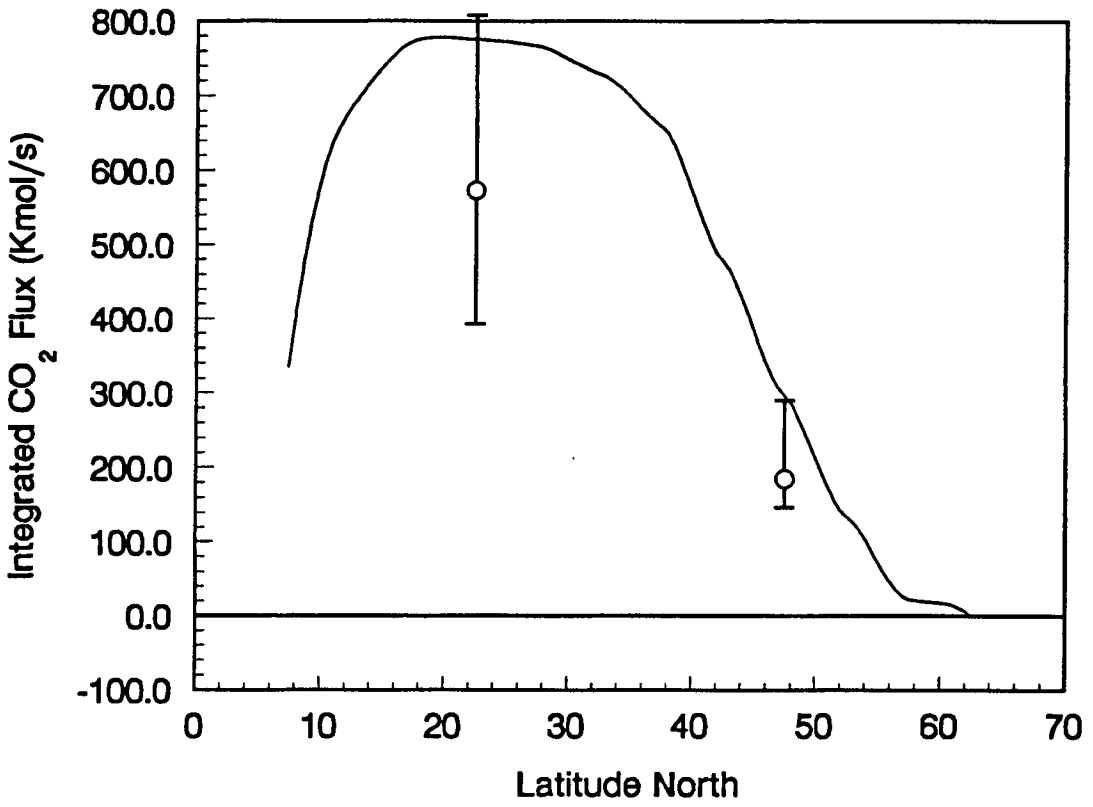
800.0
700.0
600.0
500.0
400.0
300.0
200.0
100.0
0.0
-100.0
Integrated CO_2 Flux (Kmol/s)
0
10
20
30
40
50
60
70
Latitude North

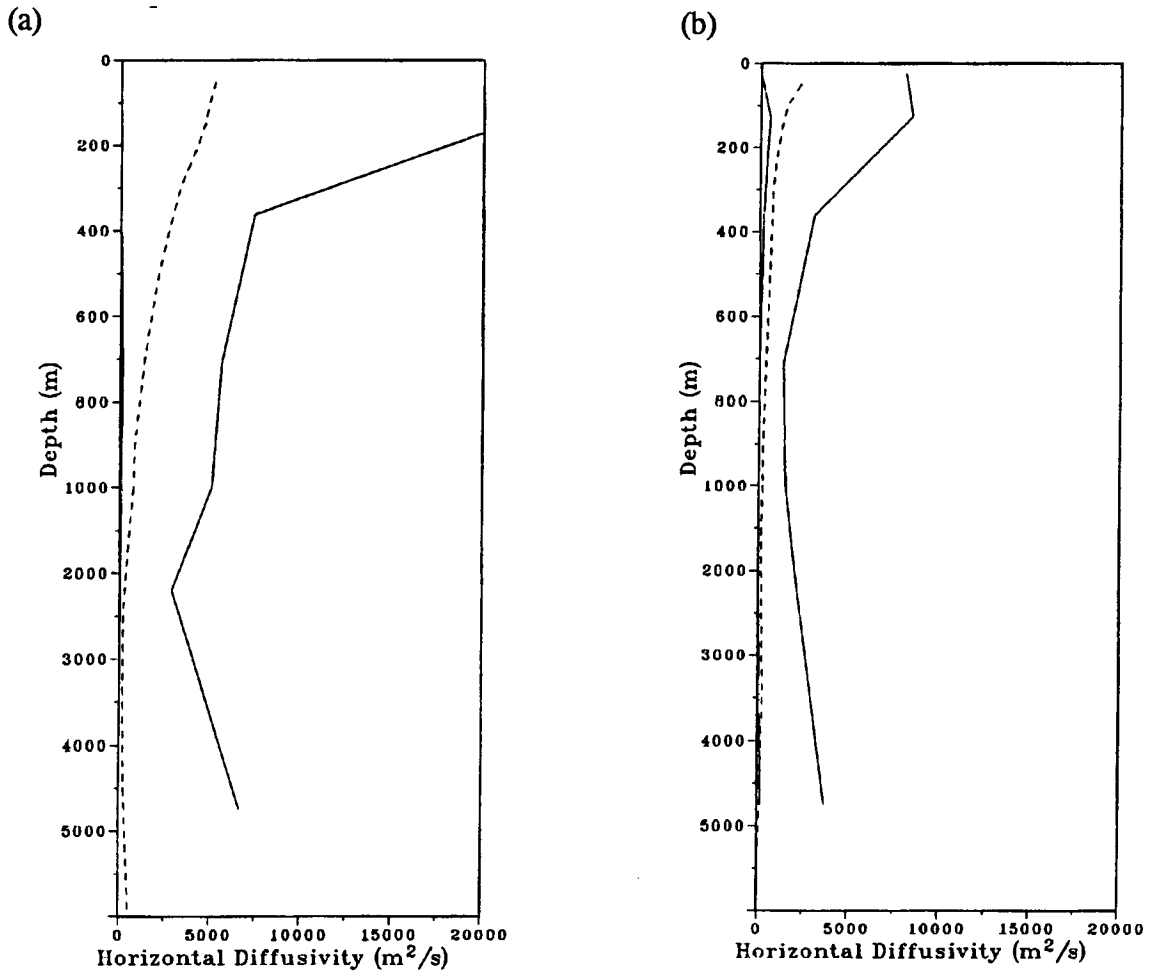

Figure 3.4: The acceptable ranges for the horizontal mixing coefficients for (a) region 1, and (b) region 2, if only one line is present then the lower range is zero. The dashed line is the calculated numerical diffusivity of the upwind advection scheme used in the LSGOC-biogeochemical model.

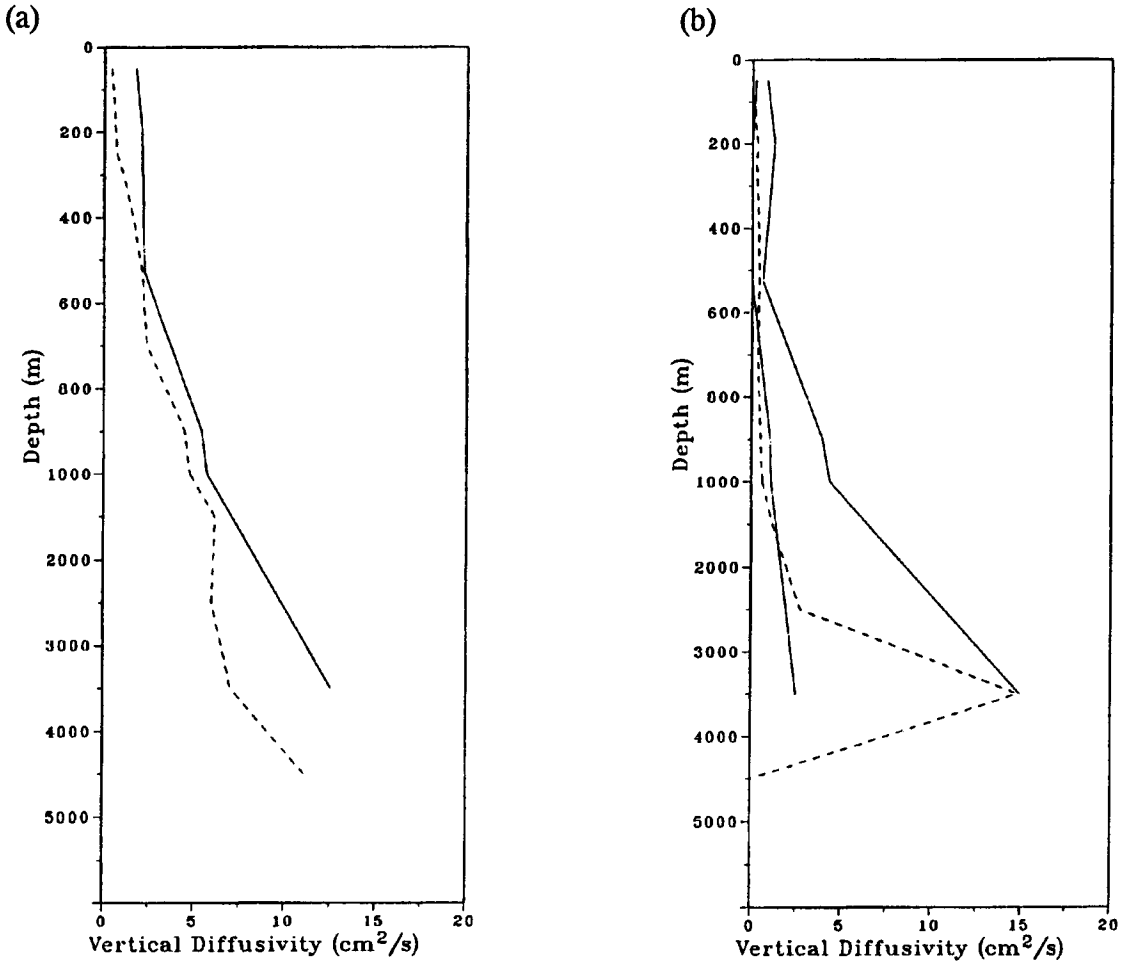

Figure 3.5: The acceptable ranges for the vertical mixing coefficients for (a) region 1, and (b) region 2, if only one line is present then the lower range is zero. The dashed line is the calculated numerical diffusivity of the upwind advection scheme used in the LSGOC-biogeochemical model.

The range in acceptable values for the particle fluxes in the different layers revealed that the individual values are not well-determined (Fig. 3.6). For example, both the upper two layers are capable of dissolving all the particulate matter produced in the surface layer.

The area of regions 1 and 2 are 25 x 10^{12} and 7 x 10^{12} m^2 respectively. Like the original model (Fig 3.7), the new production in the two regions is of similar magnitude (14 g m^{-2} y^{-1}). From the inverse model the new production is estimated to be 17 $\pm$ 17 g m^{-2} y^{-1}.

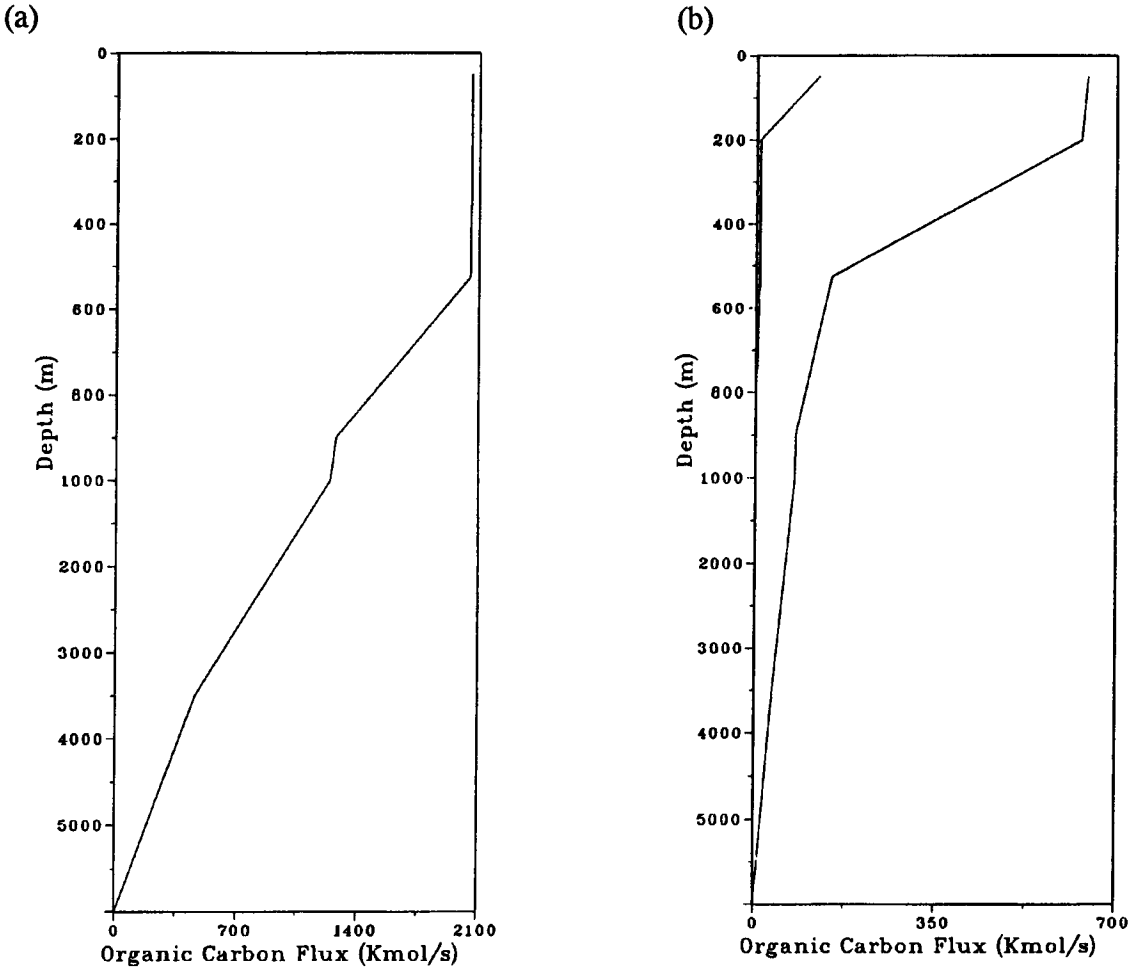

Figure 3.6: The acceptable ranges of the particle fluxes of organic and shell material, the minimum value is zero. The organic carbon flux for region 1 and 2 is shown in (a) and (b) respectively, and the flux of shell matterial for region 1 and 2 is shown in (c) and (d) respectively.

(c)

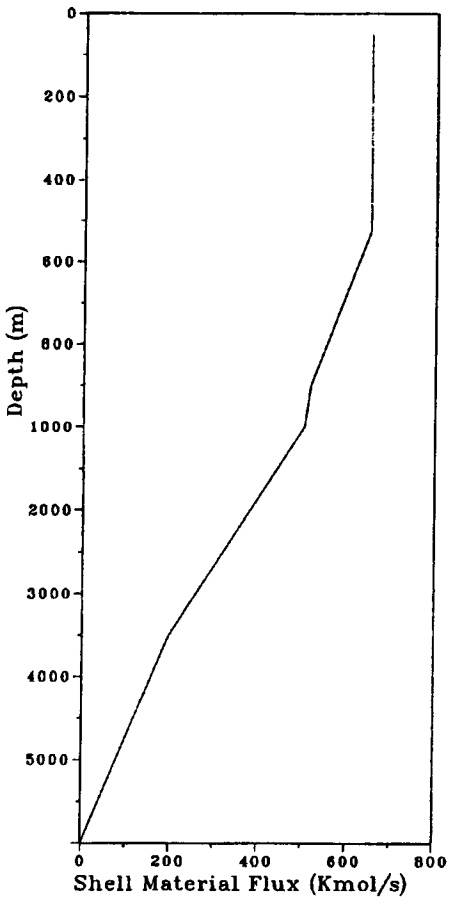
0
200
400
600
800
1000
2000
3000
4000
5000
Depth (m)
0
200
400
600
800
Shell Material Flux (Kmol/s)

(d)

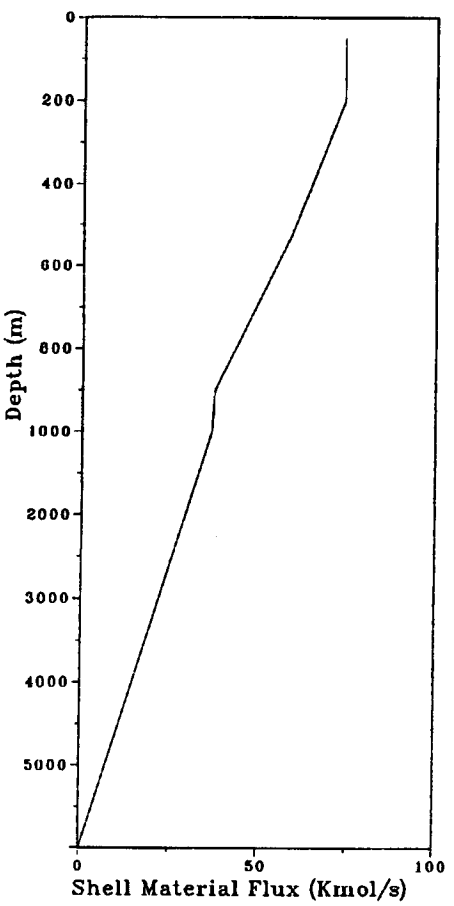
0
200
400
600
800
1000
2000
3000
4000
5000
Depth (m)
0
50
100
Shell Material Flux (Kmol/s)

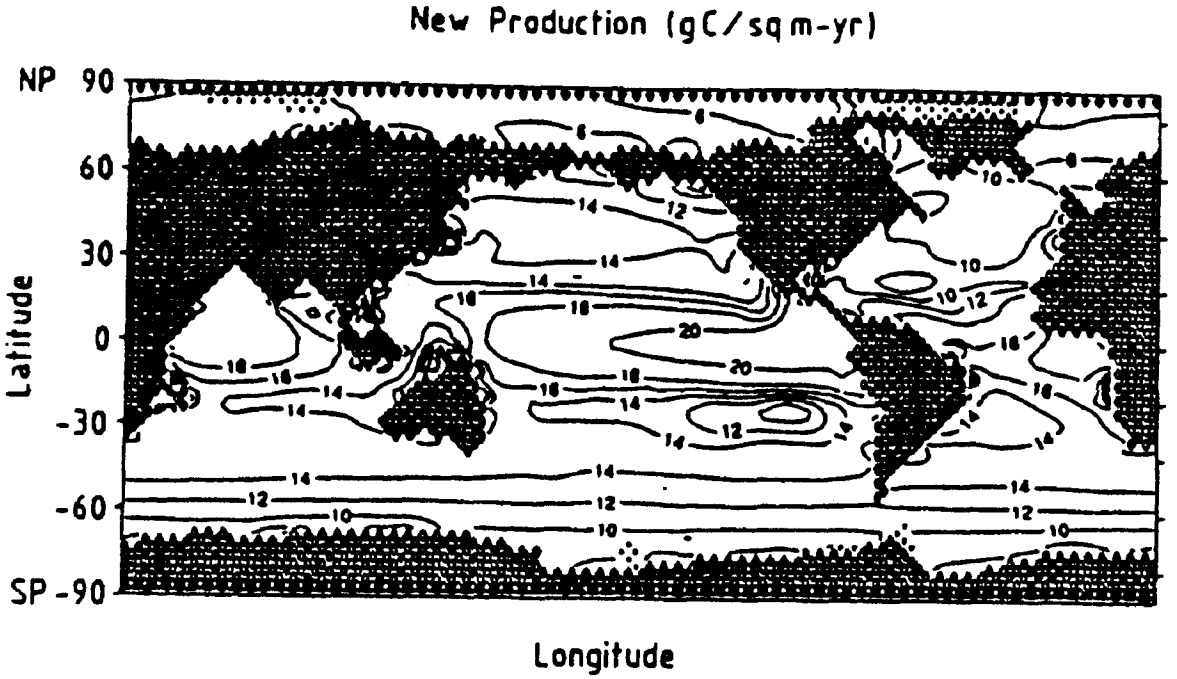

Figure 3.7: Map of the new production from the LSGOC-biogeochemical model taken from Bacastow and Maier Reimer (1990).

In the discussion of the LP solutions, the importance of the prescribed error cannot be overlooked. Further investigation of the prescribed errors shows that, if the errors are doubled, the effect on the unknown air-sea exchanges would be less than 10%, but the detrital rain-rates would nearly double, k_z would increase by 80% and k_h would increase by 20%. The vertical structure of the k_h and k_z would be unaffected by the increased errors.

3.4.3 Model Sensitivity

To examine the sensitivity of the inverse model to the various model constraints several different experiments were performed using different model constraints. The different models are summarized in Table 3.3.

To see how well the inverse box model performs when the horizontal velocity information is less well-determined, two experiments were tried. First, the inverse box model was formulated to allow the horizontal volume transports to vary by $\pm 100\%$ from the known values. The circulation and mixing fields from the LSI inversion (Fig. 3.8) showed that without additional velocity information the circulation is grossly underestimated. For this inverse box model one relies on the ^{14}C tracers to force the model since all of the other tracers are compatible with the null solution. Second, the inverse box model was formulated to only determine an unknown barotropic flow through each section in the model (model III in table 3.4). In this case the information in the tracer fields is very capable of determining the unknown barotropic flows. The volume transports calculated from this model were nearly identical to the circulation given in Figure 3.2, however, the k's, detrital rain rates and air-sea exchanges differed from the reference solution. Using the same errors as the reference model, the LP solutions were obtained to give the acceptable ranges for the air-sea exchanges and detrital rain rates. The detrital rain rates and heat exchange results were reasonably consistent with the reference model but the air-sea exchanges of CO_2, O_2, and ^{14}C exhibited a much larger range. Most of the increased ranges were attributed to the increased acceptable range for the freshwater exchange. This shows that considerable uncertainty in the air-sea

Table 3.4: The inverse results for the 4-region 6-layer models given in Table 3.3. The maximum acceptable errors are 3.215 times greater than the errors used to weight the LSI inversions.

Model	Inversion	Detrital Rain Rate		Air-sea exchange			
		Organic Matter (Kmol/s)	Shell Material (Kmol/s)	Heat PW	CO_2 Kmol/s	O_2 Kmol/s	^{14}C Kmol/s
I	LSI[1]	835	53.3	-0.18	573	314	1915
	LP[2]	120 to 2667	0 to 671	-0.4 to -0.16	392 to 807	-46 to 899	1230 to 2587
II	LSI	1120	134	-0.08	365	9	1722
	LP	13 to 2881	0 to 804	-0.4 to 0.1	-98 to 735	-792 to 923	81 to 3649
III	LSI	523	17.8	-0.24	852	735	2008
	LP	66 to 2950	0 to 724	-0.56 to -0.09	40 to 1503	-951 to 1939	1112 to 2879
IV	LP	66 to 2814	0 to 677	-0.48 to -0.09	353 to 1068	-353 to 1342	1112 to 2862
V	LSI	872	136.8	-0.18	558	295	1943
	LP	92 to 2820	0 to 935	-0.4 to -0.16	392 to 808	-45 to 899	1226 to 2587
VI	LSI	613	34.8	-0.23	843	689	2045
	LP	54 to 3395	0 to 1065	-0.56 to -0.03	-13 to 1505	-1636 to 1941	1108 to 3111
VII	LP	54 to 3186	0 to 962	-0.5 to -0.04	338 to 1110	-640 to 1340	1108 to 2934

[1]Refer to section 3.3.3 for a discusion of the LSI and LP inversion routines.

exchange unknowns can arise from uncertainties in the freshwater exchanges. If the freshwater exchanges were constrained to be more consistent with the reference model by restricting the freshwater exchange for the North Pacific to be between 0 and 0.2 Sv, the acceptable ranges in the unknown air-sea exchanges are greatly reduced (model IV in Table 3.4).

In the inversions already discussed, the molecular ratios linking the C:P:O in the formation and remineralization of organic matter were specified according to the values used in the Hamburg model. To observe how well the inverse model can predict these ratios, an inversion was performed using a model which allowed the Redfield ratios to vary by $\pm 20\%$ from their known values. If the horizontal volume transport was specified, the inverse box model returned the correct ratios. The acceptable ranges determined from the LP solution showed that the air-sea exchanges were unaffected by a variable molecular ratio (model V in Table 3.4). The detrital rain rates calculated from this model experienced a slight increase in the acceptable ranges from that of the reference model. If the horizontal volume transport was specified with an unknown barotropic component, the inverse box model (model VI) was still capable of returning the correct ratios and producing the same circulation field as the reference model. The acceptable ranges for heat, CO_2, and ^{14}C were the same as for the model with an unknown barotropic term (model III). The acceptable ranges for the detrital rain rates and O_2 exchange increased significantly over that of model III. By including the mass constraint as was done in model IV, the uncertainty in air-sea exchanges was greatly reduced (model VII in Table 3.4).

(a)

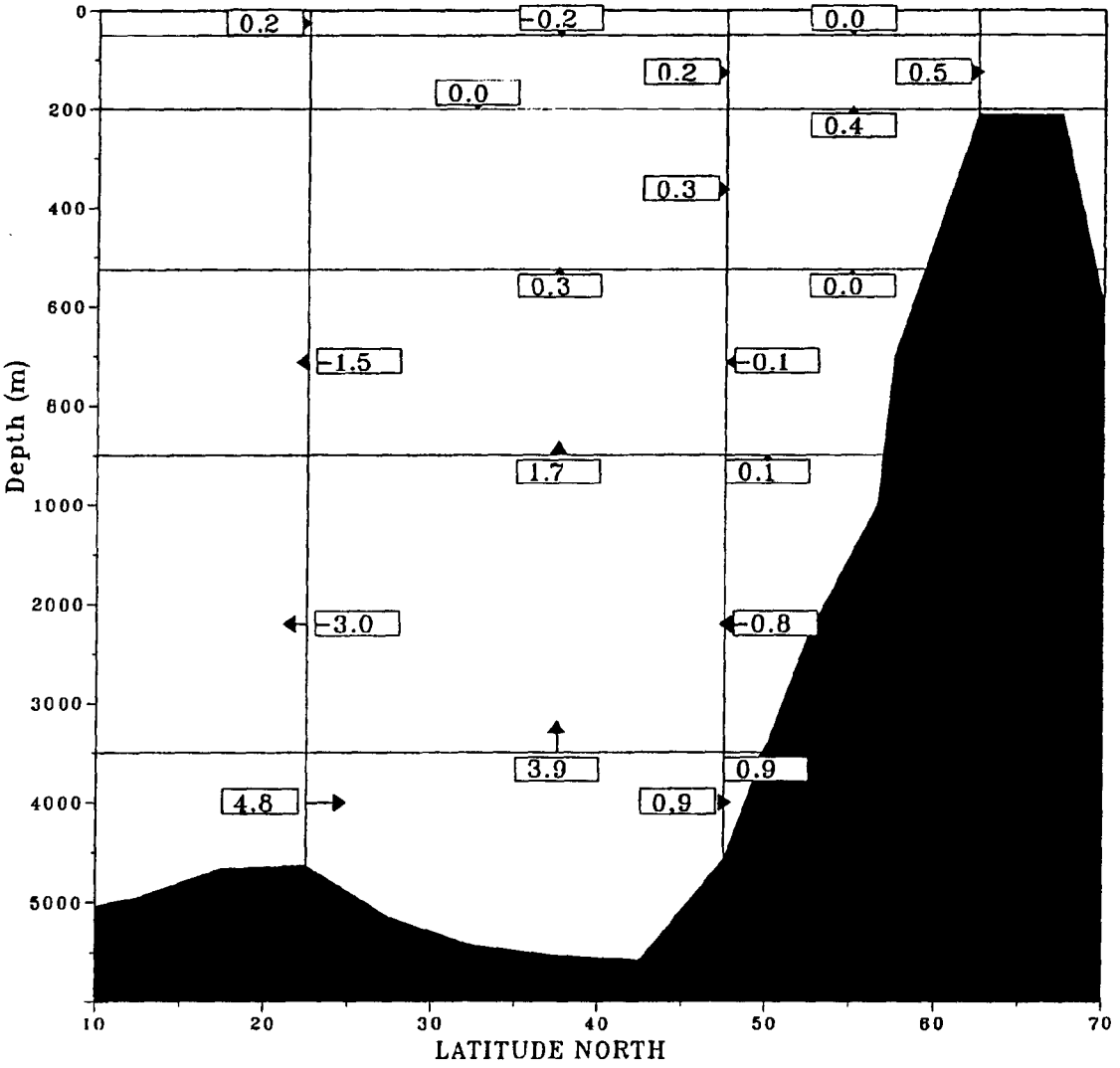

Figure 3.8: The volume transports, (a), and mixing transports, (b), in Sv of a model forced only by the tracer fields.

(b)

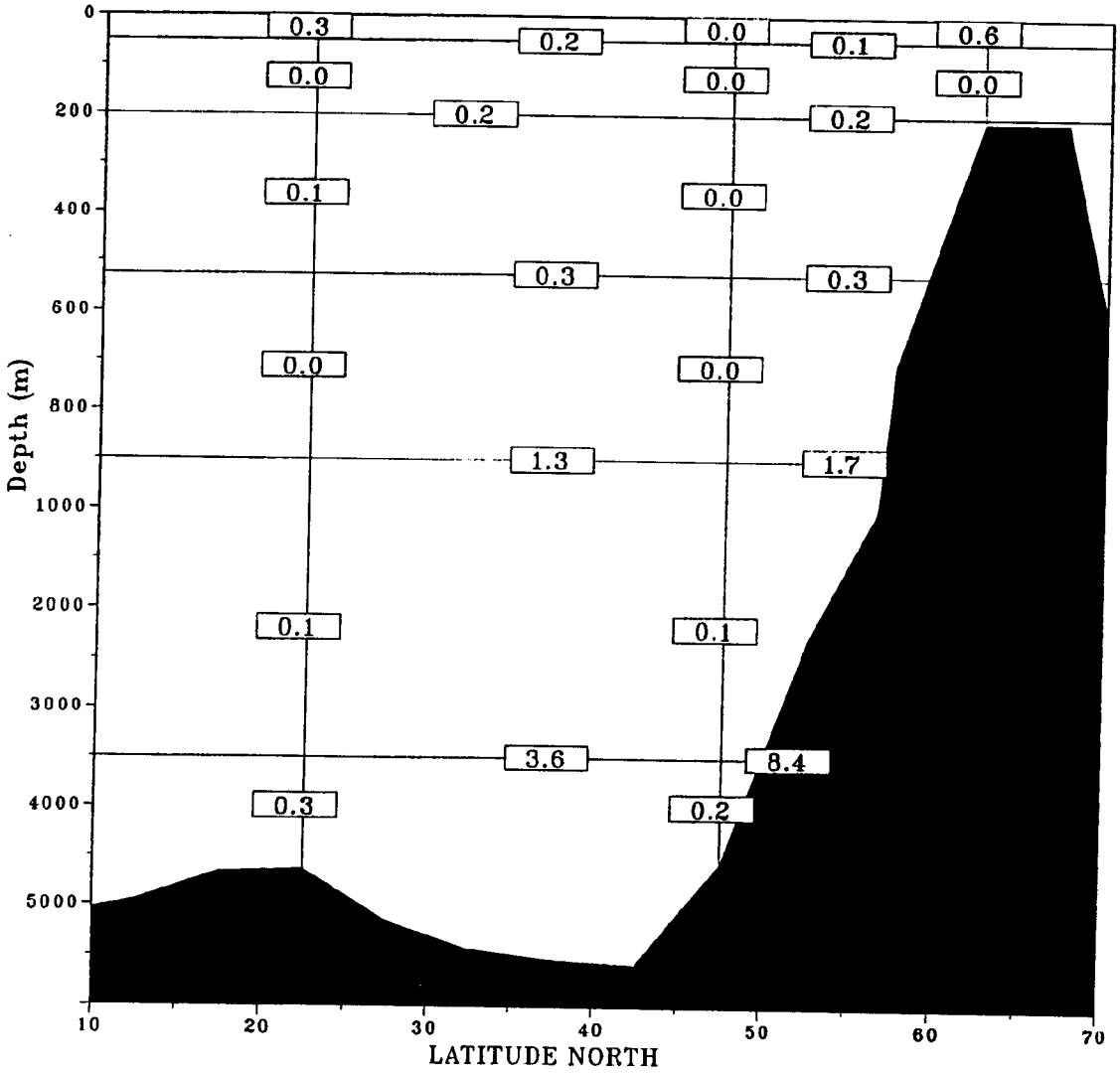
0.3
0.2
0.0
0.1
0.6
0.0
0.0
0.0
0.2
0.2
0.1
0.0
0.3
0.3
0.0
0.0
1.3
1.7
0.1
0.1
3.6
8.4
0.3
0.2
0
200
400
600
800
1000
2000
3000
4000
5000
Depth (m)
10
20
30
40
50
60
70
LATITUDE NORTH

3.4.4 Effects of Model Geometry

The last set of experiments performed investigated the sensitivity of the solution to the configuration of the inverse box model. By including more layers in the 4-region model, it was observed that the uncertainties in the unknowns change very little (Table 3.5). A 15-layer model, (same number of layers as Hamburg model), produced a slightly different LSI solution but the uncertainties in the unknowns were very similar to the 6-layer model. By reducing the number of layers, the effect on the solution was more profound, and it was decided that a 6-layer model was a good compromise between producing results consistent with more layers and limiting the computations.

The sensitivity of the solution to how the regions of the North Pacific were drawn was investigated with several different models (Table 3.5). A 5-region model was formulated by dividing the 22.5°-47.5° region into 22.5°-32.5°-47.5°. The model was purposely configured so that the mean advective fluxes in the inverse model did not reflect the values determined from the Hamburg data. The results from this model appear to have shifted the air-sea exchanges heat, CO_2, ^{14}C from that of the 4-region model. To remove this ambiguity inversions performed on the real data will use the actual tracer concentrations along the box interface rather then the average tracer concentration from the two adjacent boxes. The range in uncertainties for the unknowns given in Table 3.5 are generally increases as the number of regions in the model is increased. By dividing the 5-region model into 10 regions by a meridional line at 175°W, the resulting model produced results more consistent with the 4-

Table 3.5: Inverse solutions obtained from experiments that change the definitions of the boxes. The numbers under the model heading give the number of regions and layers in the respective model.

Model	Inversion	Detrital Rain Rate		Air-sea exchange			
		Organic Matter (Kmol/s)	Shell Material(Kmol/s)	Heat PW	CO_2 Kmol/s	O_2 Kmol/s	^{14}C Kmol/s
4x6	LSI[1]	835	53.3	-0.18	573	314	1915
	LP[1]	120 to 2667	0 to 671	-0.40 to -0.16	392 to 807	-46 to 899	1230 to 2587
4x15	LSI	536	71.6	-0.15	471	153	1851
	LP	0 to 2306	0 to 877	-0.44 to -0.08	271 to 854	-187 to 883	660 to 1960
5x6	LSI	678	53.6	-0.12	377.6	-173	1450.6
	LP	203 to 1930	0 to 580	-0.2 to -0.01	164 to 571	-329 to -46	622 to 2125
5x15	LSI	589.3	109.3	-0.03	213	-208	1443
	LP	66 to 1330	0 to 590	-0.2 to 0.05	149 to 601	-374 to -34	306 to 1886
10x6	LSI	903	29.7	-0.26	855.9	-91	2348
	LP	0 to 3229	0 to 1030	-0.75 to -0.04	385 to 1746	-553 to 822	859 to 3440
15x6	LSI	870	37.8	-0.20	840	68.5	2173
	LP	0 to 3841	0 to 3841	-1.28 to -0.04	316 to 1890	-508 to 1393	-25 to 4023

[1] Refer to section 3.3.3 for a discussion of the LSI and LP inverse routines.

region model than the 5-region model. By dividing the 5-region model by meridional lines at 190°W and 155°W, a 15-region model was produced. The results from the 15-region model were more consistent with the 4-region model than the 5-region model. The increasing range in uncertainty observed for the 10- and 15-region model reflects limited information in the tracer fields at these scales. The annual tracer fields provided by the Hamburg model are only suitable for providing information at the scales equivalent to the regions in the 4- or 5-region inverse box model. A similar scaling of the regions of the North Pacific will apply to the inversions performed on the real data.

3.5 DISCUSSION AND CONCLUSION

The annual mean velocity and tracer fields produced by the Hamburg LSGOC-biogeochemical model were used to evaluate an inverse box model. The tracer fields from the LSGOC model showed that the eddy transports played an important role in the conservation of the tracer in the North Pacific. It was satisfying to see that, given the importance of the eddy transports in the data, the inverse box model performed so well. By using the known velocity fields, a simple diffusive mixing parameterization with positive mixing coefficients for the eddy transports, and several tracer fields - the inverse box model produced consistent estimates of the air-sea exchange of heat and CO_2. The inverse box model did not require negative k's to produce reasonable results. Furthermore, a LSI inversion with negative k's did not significantly reduce the errors in the conservation

equations. These two results clearly suggest that it is not necessary to allow negative k's in the inverse model to produce good results.

An inverse model that uses only the tracer fields to predict the velocity field revealed that, by themselves, the tracer fields are insufficient to determine the velocity field. If additional information on the velocity field, like the velocity shear, can be included in the model the inverse model is quite capable of extracting the missing velocity information from the tracers fields. With the addition of the velocity shear information, the inverse box model produced air-sea exchanges and detrital rain-rates comparable to the model where the velocity fields were well-determined. An inverse box model was formulated to allow the molecular ratios of C:P:O to vary by $\pm 20\%$ from their known values in the formation/remineralization of organic matter. The results of this model show that the air-sea exchanges are not sensitive to the variable molecular ratios. The maximum detrital rain rate of organic matter for the inverse box model with variable molecular ratios is only 5% greater than the model with constant molecular ratios.

A set of experiments to investigate the sensitivity of the inverse box model topology show that results did depend on the box configurations. In drawing the boxes, it is important that the mean advection transports through the box faces adequately reflect the data. By increasing the number of regions, a point is quickly reached where the concentration differences between boxes becomes insignificant. This is most obvious in the LP inversions by the large range in the acceptable values for the various unknowns. The penalty one pays for including too many regions is a poorly determined solution.

CHAPTER 4. DEVELOPING THE INVERSE BOX MODEL OF THE NORTH PACIFIC

In this chapter I will discuss how the inverse box model is formulated and applied to the North Pacific Ocean. In the first section the data used by the inverse box model will be presented. The second section, discusses the division of the North Pacific Ocean into boxes. The third section presents the model constraints and applies these constraints to generate the model equations. The fourth section deals with the different algorithms used to solve the set system of equations. The chapter will conclude with a discussion of how the data are used to prescribe the acceptable errors in the equations generated in section 3.

4.1 DATA

The inverse model requires tracer concentrations and concentration gradients on the box faces and geostrophic velocity shears along the sections as inputs. The datasets used in the model were obtained from many different sources. First, I will discuss the hydrographic sections used in determining the geostrophic transports. Second, I will summarize all the tracer used in the model and discuss how the data were combined to produce a dataset for the inverse box model.

4.1.1 Geostrophic Velocity Sections

The conclusion reached in chapter 2 pointed out the need to accurately determine the mass transport field in order to obtain reliable estimates of the horizontal tracer transports and ultimately determine the air-sea exchanges. At the present time, two high density hydrographic sections have been obtained across the North Pacific at 24°N and 47°N (Figure 4.1). The high density of sampling of these sections should ensure accurate estimates of the geostrophic velocities. By using this data to constrain the large scale flow features, it is assumed that the volume transports computed are representative of the mean ocean circulation through these two sections.

The CTD/hydrographic transect across the centre of the subtropical North Pacific Ocean at 24°N was carried out by the R. V. Thomas Thompson in the spring of 1985 (Roemmich *et al.*, 1991). The cruise will be referred to as TPS24. The first station was occupied off San Diego, California on March 30 and the ship proceeded westward ending in the East China Sea on June 1. A total of 206 full-depth CTD/hydrographic cast were completed on the long crossing. All CTD/hydrographic casts used a modified Neil Brown Instrument System Mark III CTD and rosette package carrying 36 10-litre Niskin bottles. All samples were obtained and analyzed by the Scripps Physical and Chemical Oceanographic Data Facility, providing measurements of temperature, salinity, oxygen, silicate, nitrate, and phosphate. The estimated sampling errors and random measurement errors in these measurements for salinity, oxygen, phosphate, nitrate and silicate were

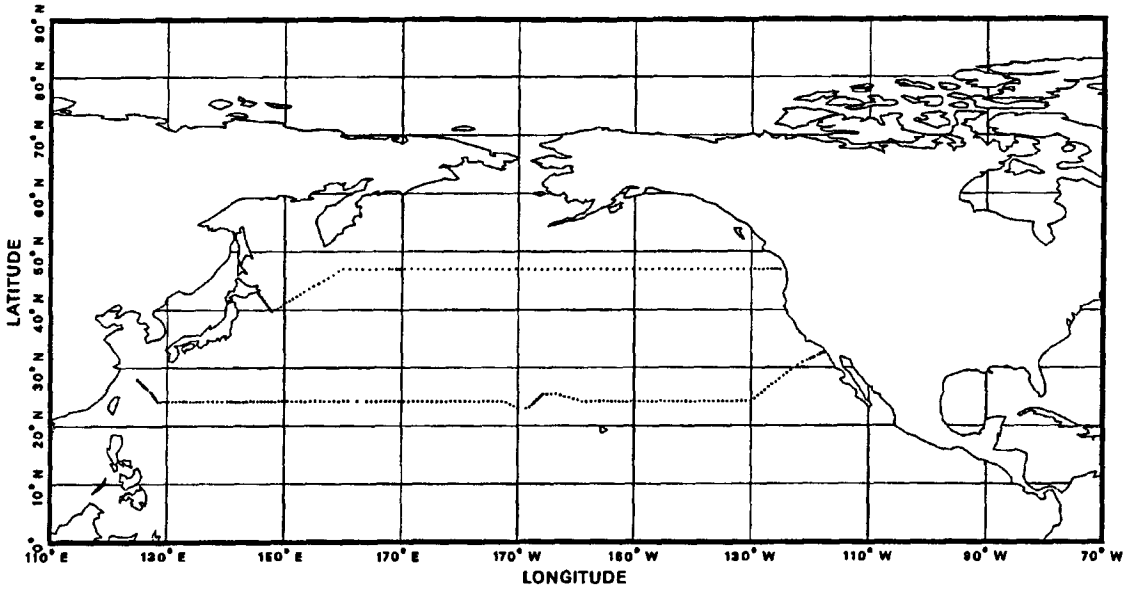

Figure 4.1: Map showing the hydrographic sections used in the model (TPS24 and TPS47).

0.001 psu, 0.021 ml l^{-1}, 0.036 μmol l^{-1}, and 2.0 μmol l^{-1} respectively (from Table 2, Roemmich *et al.*, 1991).

In August of 1985, 115 relatively closely spaced CTD/hydrographic stations were occupied by the R. V. Thomas Thompson along the nominal latitude of 47°N in the subpolar North Pacific (Talley *et al.*, 1991). The cruise is henceforth referred to as TPS47. The data from TPS47 were collected and processed by the Oceanographic Data Facility at Sripps Institue of Oceanography an a full data report on the cruise is given by Talley *et al.*, (1988). All stations consisted of a CTD/rosette cast, with a Neil Brown Mark III CTD and a rosette package of 36 10-litre Niskin bottles. Salinity, oxygen, nitrate, phosphate, and silicate were measured at every bottle. The temperature precision for a given station was 0.001°C. The precision of the salinity was 0.001 to 0.002 psu. The oxygen measurement were made by Winkler titration, with accuracies of 1% and station precision of 0.01 ml l^{-1}. The precision of the silicate, phosphate, and nitrate measurements were 1%, 2% and 2-3% respectively. The nutrient measurements from both these cruises are include in the NODC archive of nutrient data that is used in the next section.

The geostrophic velocities for both sections are determined from the objectively mapped values of specific volume anomaly using the objective mapping routine presented by Roemmich (1983). The geostrophic velocity relative to reference levels of 3000 m and 4000 m for TPS24 and TPS47 respectively are shown in Figure 4.2a-b.

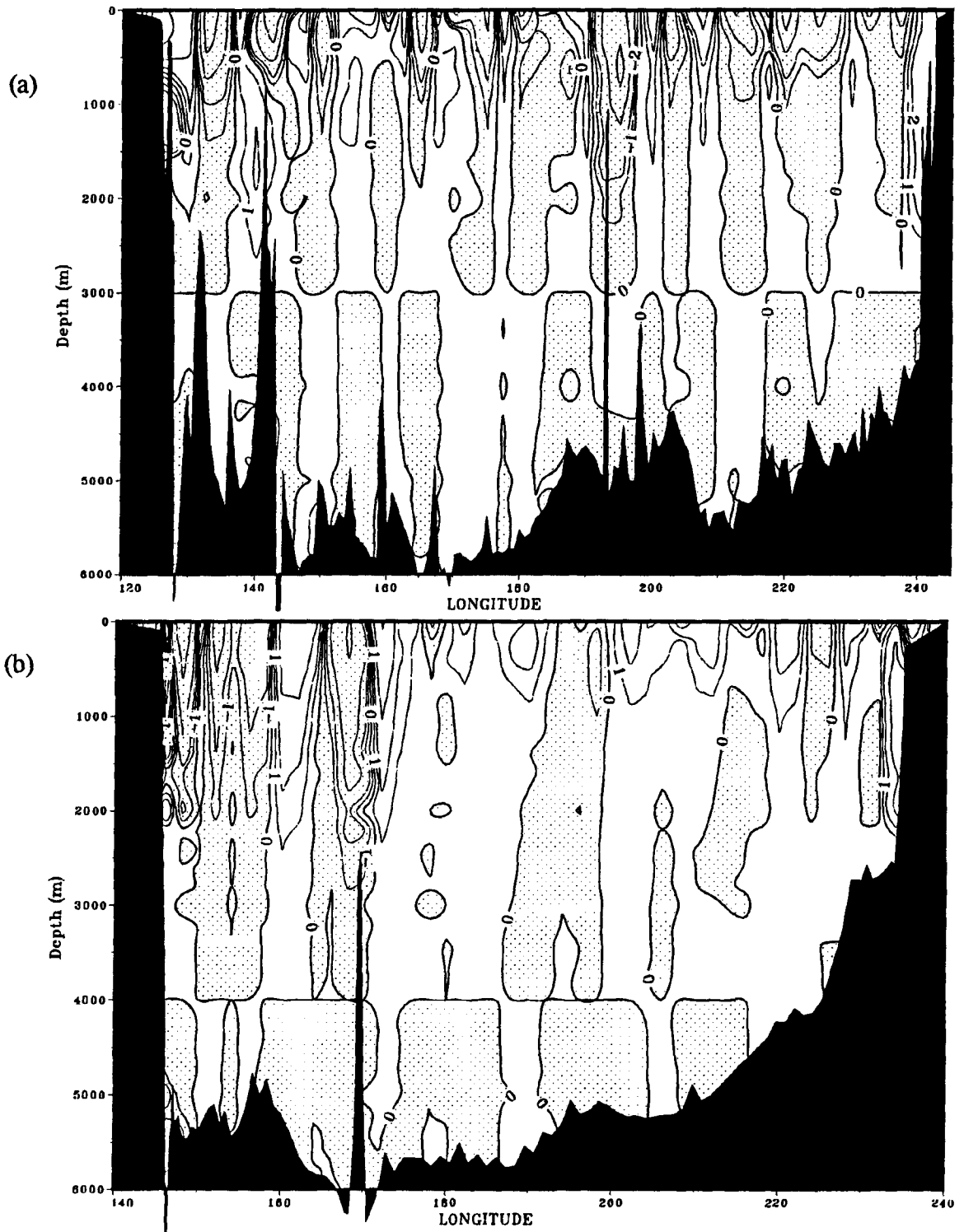

Figure 4.2: Geostrophic velocities (cm s^{-1}) of the transpacific sections, shaded areas denote southward velocities, (a) TPS24, and (b) TPS47.

4.1.2 Tracer Data

The data that are essential for this research are tracer data. This data must provide information on the physical, biological and air-sea processes that affect the carbon distribution in the ocean. All tracers will be affected by the physical processes by only certain tracers will contain information on the latter two processes. Alkalinity (ALK) and dissolved inorganic carbon (DIC) are essential to understanding the carbon cycle. The nutrient data - phosphate and oxygen tracers - provide additional information on the biological processes affecting carbon distribution in the ocean. Temperature, salinity and silicate tracers are also included to provide additional information on the physical processes affecting the carbon distribution. This provides for seven tracers to describe the carbon cycle. By using more than one tracer, one attempts to overcome the limitation that no one tracer can adequately describe all the relevant processes affecting the carbon cycle in the ocean.

The values of potential temperature, salinity, DIC, alkalinity, phosphate, oxygen, and silicate used in the model are taken from many sources. It is necessary to use all these data sources to provide sufficient coverage of the North Pacific. This is especially true for alkalinity and DIC. The following is a brief description of the data used in the model and summarized in Table 4.1.

1) IOS Data - Useful data collected by IOS ships consists of four cruises: the Hudson 70, Transpac 72, Pan 75 and Hudson 81 plus data from station P. Additional data from the joint Canadian-Russian expeditions (GEMS) in the summer of 1991 are also

used. The stations occupied by these cruises are shown in Figure 4.3. At all of these stations, temperature, salinity, alkalinity, DIC, and nutrient data were collected. The data collected at station P provides additional information for assessing the annual and interannual variability of the tracer concentrations in the North Pacific.

2) The GEOSECS cruises provide an essential source of data for the North Pacific (Fig 4.3). At all of the stations, all the relevant tracer were collected. The GEOSECS cruises will serve as the standard to which other cruises will be compared to ensure that all the data form the different cruises are consistent. A correction of -15 μmol kg^{-1} has been made to the DIC measurements as suggested by Takahashi *et al.*, (1980).

3) The NOAA 82 Discoverer Cruise provides an important source of data for alkalinity and DIC measurements from the western Pacific (Fig. 4.3).

4) The INDOPAC cruises provide data from the western Pacific south of Japan and across the Pacific. However, it was only the INDOPAC 1 cruise where DIC and alkalinity measurements were made (Fig. 4.3).

5) The Japanese cruises are another source of data (Fig. 4.3). Only data collected after 1970 are used. The drawback to these cruises is that DIC was not measured. However, pH and alkalinity were measured which enables one to determine DIC from these measured values. Although this introduces possible errors in the DIC

Table 4.1: The list of cruises used to determine nutrient concentrations.

Number on Plot	Cruise	Source of Data
0	FGGE	IOS Cruise
1	GEOSECS	GEOSECS Pacific data
2	HUD70	IOS Cruise
3	HUD81	IOS Cruise
4	INDOPAC1	INDOPAC (Scripps Institute of Oceanography)
5	INDOPAC2	"
6	INDOPAC3	"
7	INDOPAC7	"
8	INDOPAC8	"
9	INDOPAC15	"
10	INDOPAC16	"
11	JAPAN	Collection of Japanese cruises (1970-1989)
12	NOAA82-Chen	Chen pH and alkalinity
13	NOAA82-Feely	Feely alkalinity and DIC
14	PAN75	IOS Cruise
15	TRANSPAC72	IOS Cruise
16	GEMS91	IOS-Russian Cruise

The NOAA82-Feely data comes from Feely *et al.*, (1984) and the estimated uncertainties are $\pm$ 5μEqu kg^{-1} and $\pm$12μmol kg^{-1} for alkalinity and DIC respectively.

(a)

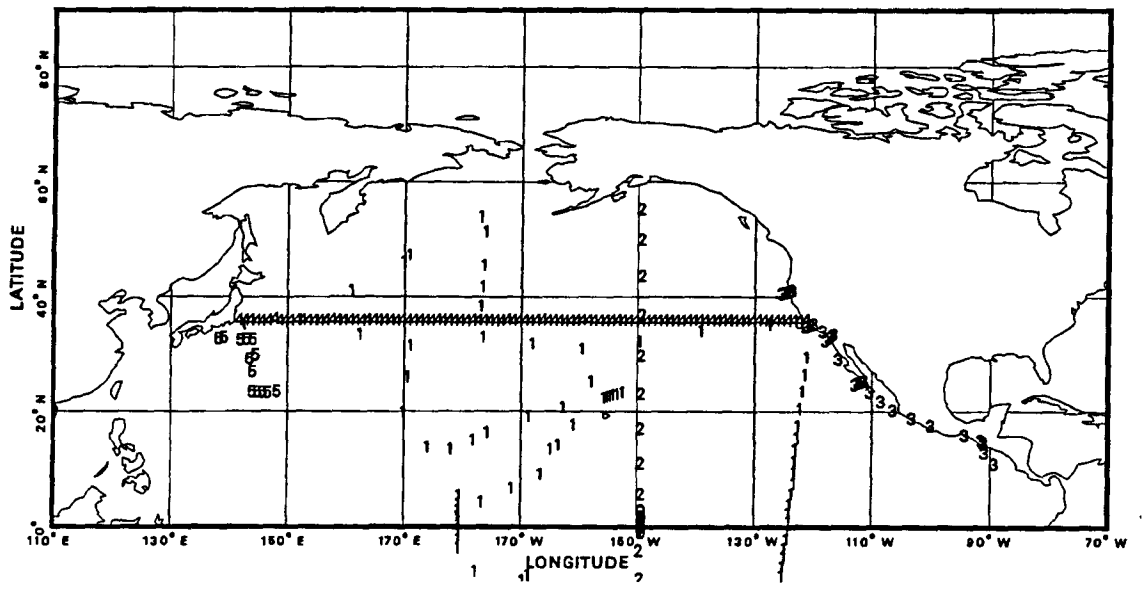

(b)

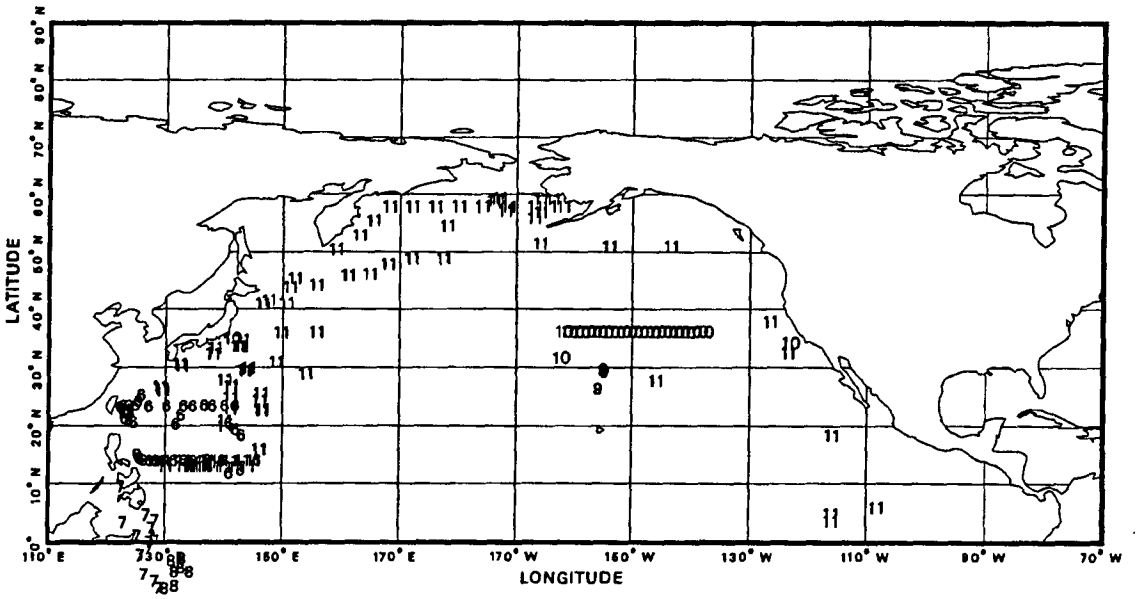

Figure 4.3: Station maps (a-c) of data from the IOS, GEOSECS, NOAA82, INDOPAC, and Japanese datasets, refer to Table 4.1 to identify the different datasets.

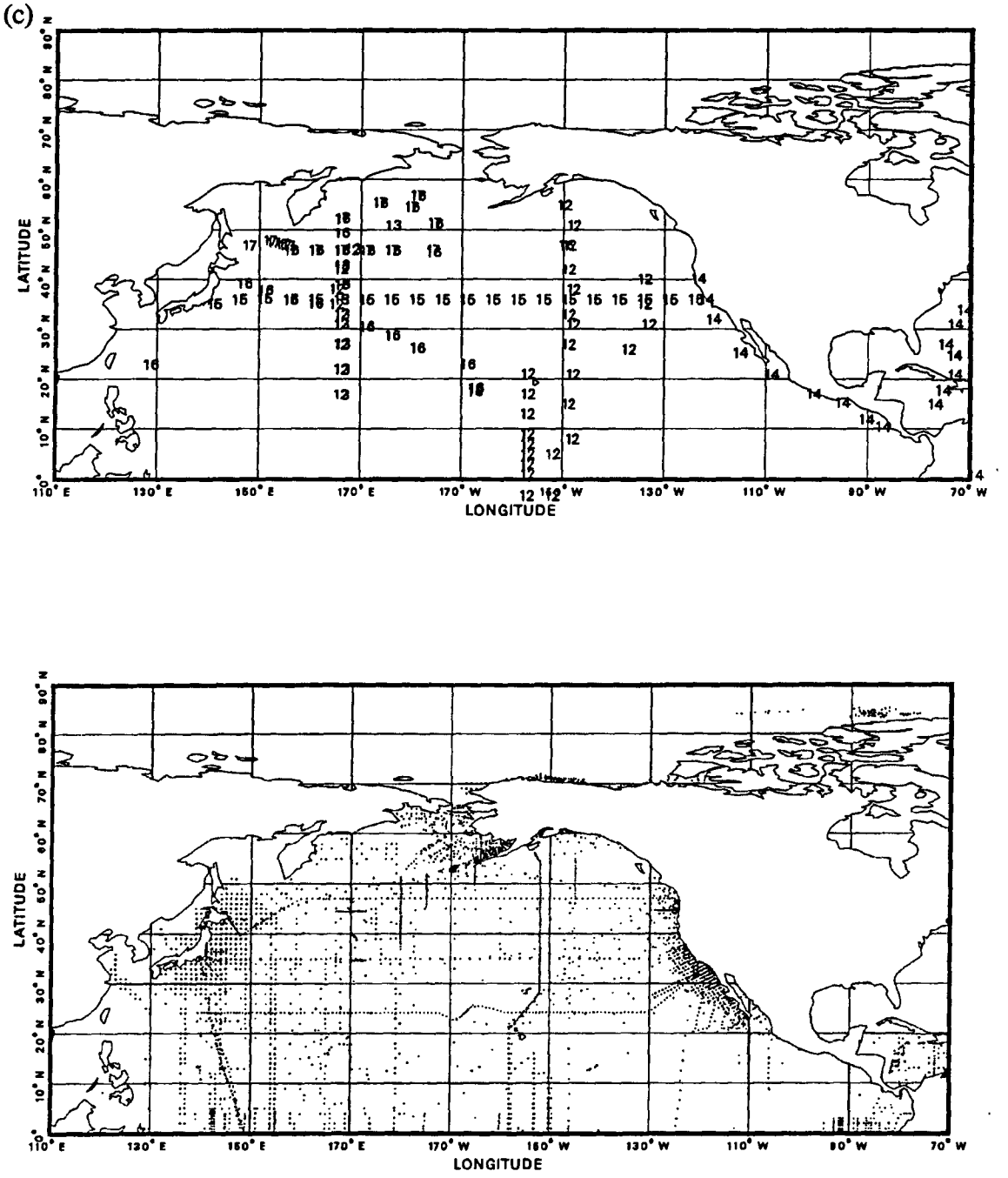

Figure 4.4: Station map of data in the NODC archive from 1970 and onward.

measurements, the data from these cruises are essential in order to provide adequate coverage of all areas of the North Pacific.

6) The NODC dataset provides temperature, salinity and nutrient data from 1970 and onward, but not alkalinity and DIC. The NODC dataset is extensive, providing good coverage of all the North Pacific (Fig. 4.4). The nutrient data from the TPS24 and TPS47 cruises are contained in this dataset. This dataset provides more reliable calculations of the average nutrient distribution than can be made from the previous five datasets alone.

The first step in using the data was to check the data for errors and systematic differences. To compare the alkalinity and DIC data, six different regions in the North Pacific were selected and the results are shown in Figures (4.5). In these plots, Table 4.2 can be used to identify the appropriate dataset. The comparisons of the different datasets showed that the alkalinity data from the HUD70, HUD81, PAN75 and TRANPAC72 cruise are suspect and were omitted.

In dealing with large data sets like the NODC archives, the data were processed in 10-degree squares in an attempt to remove obvious error in the data. The approach was similar to what Levitus (1982) used in creating his annual mean temperature and salinity fields. The data were passed twice through a filter that removed outlying points more than 5 standard deviations away from a mean curve calculated from a least squares cubic spline approximation to the data (de Boor, 1978). If more than 30% of a particular cast were considered "bad", the entire cast was omitted. Next, the remaining data were

Table 4.2: The regions used for comparing the data from the different cruises.

Region	Cruises
1) 33°N - 165°E	GEOSECS, INDOPAC1, NOAA-Chen, NOAA-FEELY, TRANS72
2) 34°N - 150°W	HUD70, INDOPAC1, INDOPAC16, NOAA-Chen, TRANSPAC72
3) 32°N - 150°W	GEOSECS, NOAA-Chen
4) 34°N - 122°W	HUD81, INDOPAC1, PAN75
5) 32°N - 139°E	GEOSECS, INDOPAC2, INDOPAC16, JAPAN, TRANSPAC72
6) 22°N - 128°E	INDOPAC3, GEMS
7) 12°N - 140°E	INDOPAC3, JAPAN
8) 45°N - 166°E	JAPAN, NOAA-Chen, NOAA-Feely, GEMS

interpolated to a one-degree horizontal spacing and vertical sampling as that of the Levitus data (I used one more depth, 6000 m). This was done by first interpolating the points vertical to the Levitus depths and then using a gaussian weighting function to combine the data from different stations.

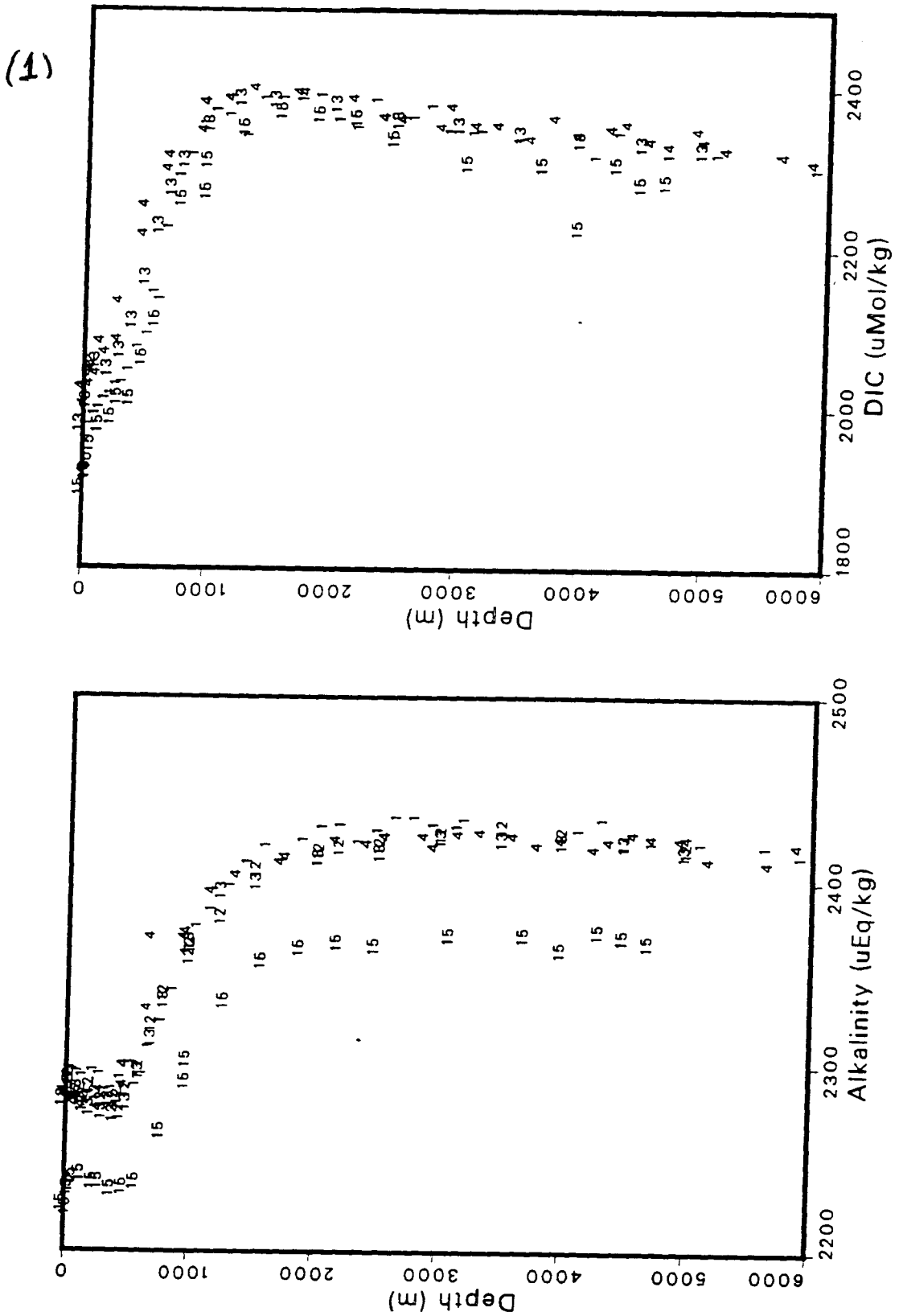

Figure 4.5: Comparison plots of alkalinity and DIC for the six selected regions in Table 4.2; use Table 4.1 to identify the different datasets.

(2)

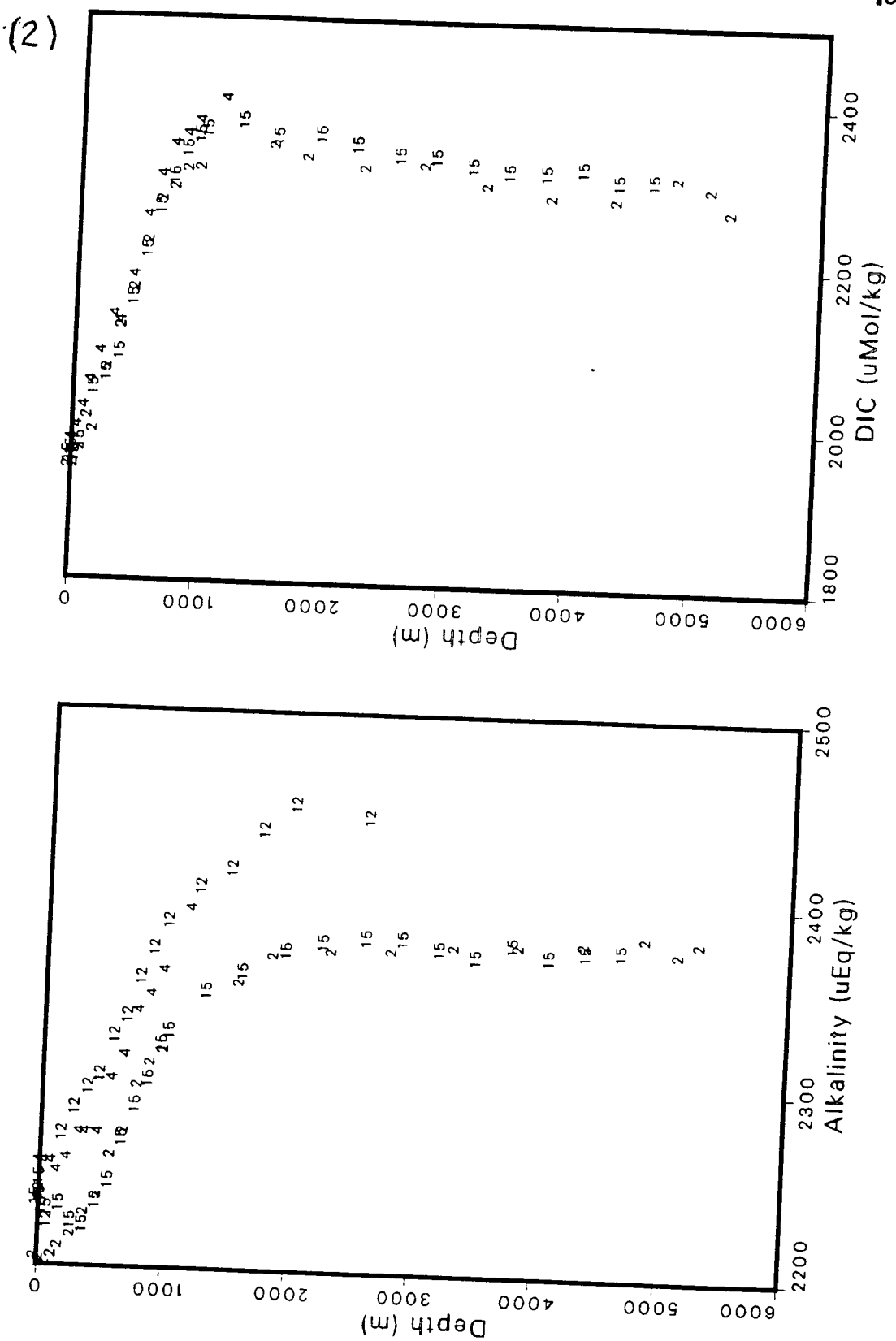
Depth (m)
0
1000
2000
3000
4000
5000
6000
DIC (uMol/kg)
1800
2000
2200
2400
Alkalinity (uEq/kg)
2200
2300
2400
2500

#3

Depth (m)
0
1000
2000
3000
4000
5000
6000
2200
2300
2400
2500
Alkalinity (uEq/kg)

Depth (m)
0
1000
2000
3000
4000
5000
6000
1800
2000
2200
2400
DIC (uMol/kg)

(4)

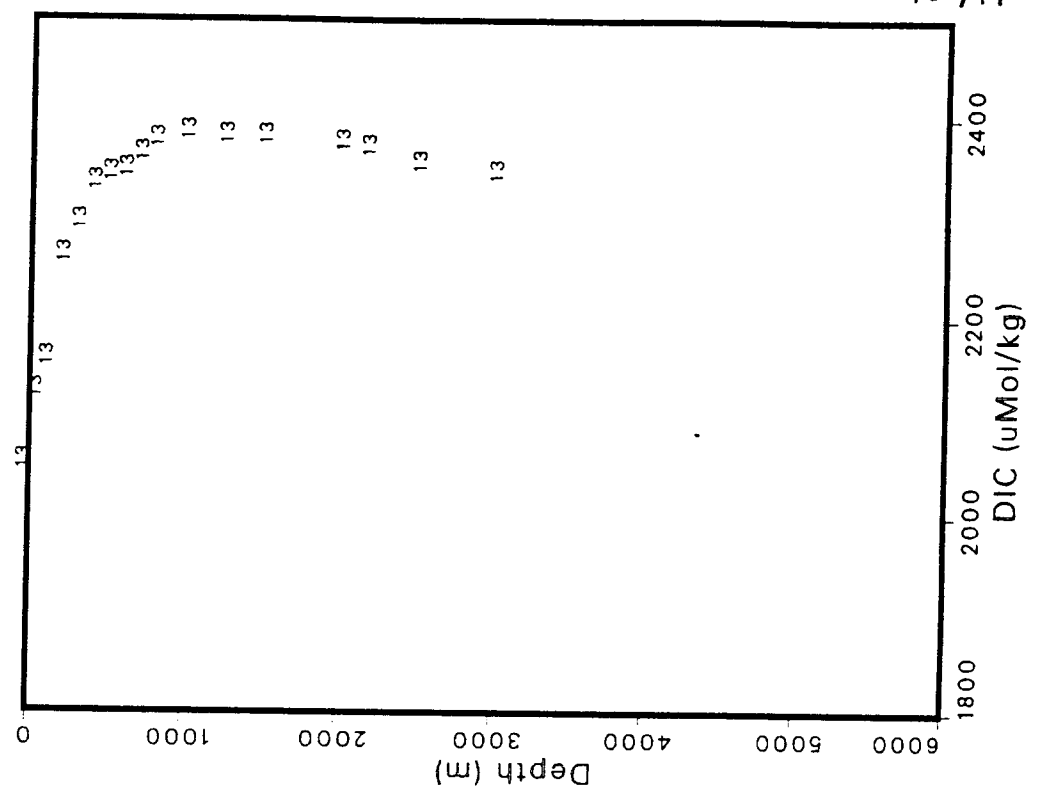
Depth (m)
0
1000
2000
3000
4000
5000
6000
DIC (uMol/kg)
1800
2000
2200
2400

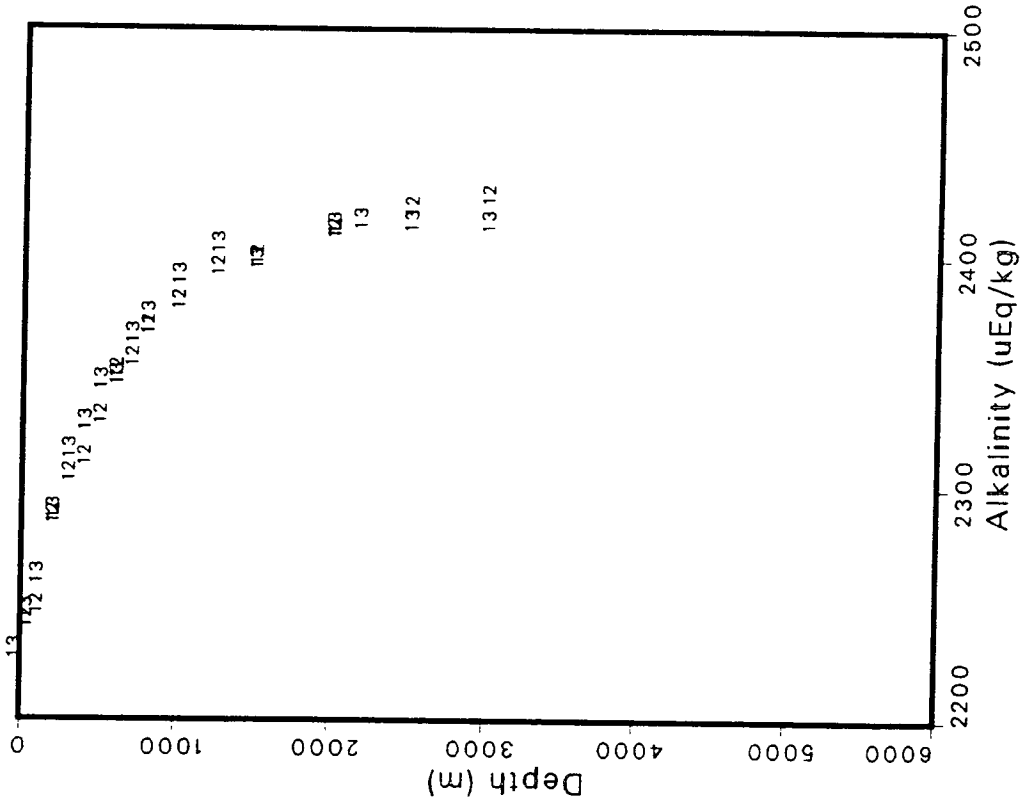
Depth (m)
0
1000
2000
3000
4000
5000
6000
Alkalinity (uEq/kg)
2200
2300
2400
2500

(5)

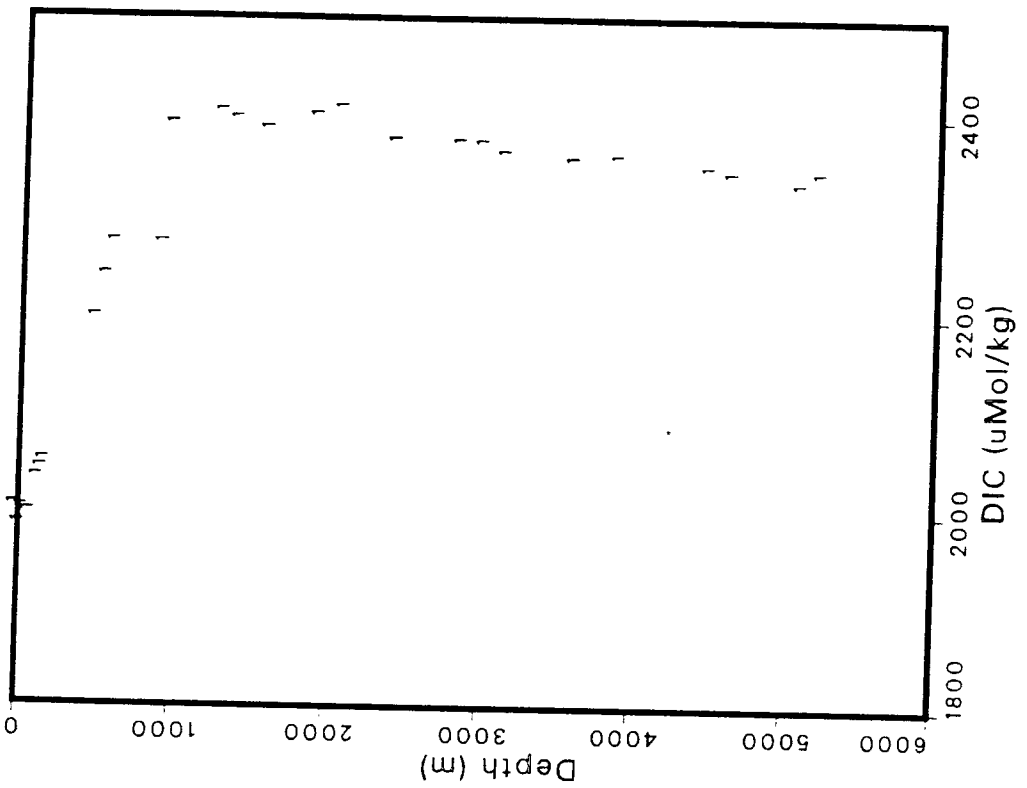
Depth (m)
0
1000
2000
3000
4000
5000
6000
DIC (uMol/kg)
1800
2000
2200
2400

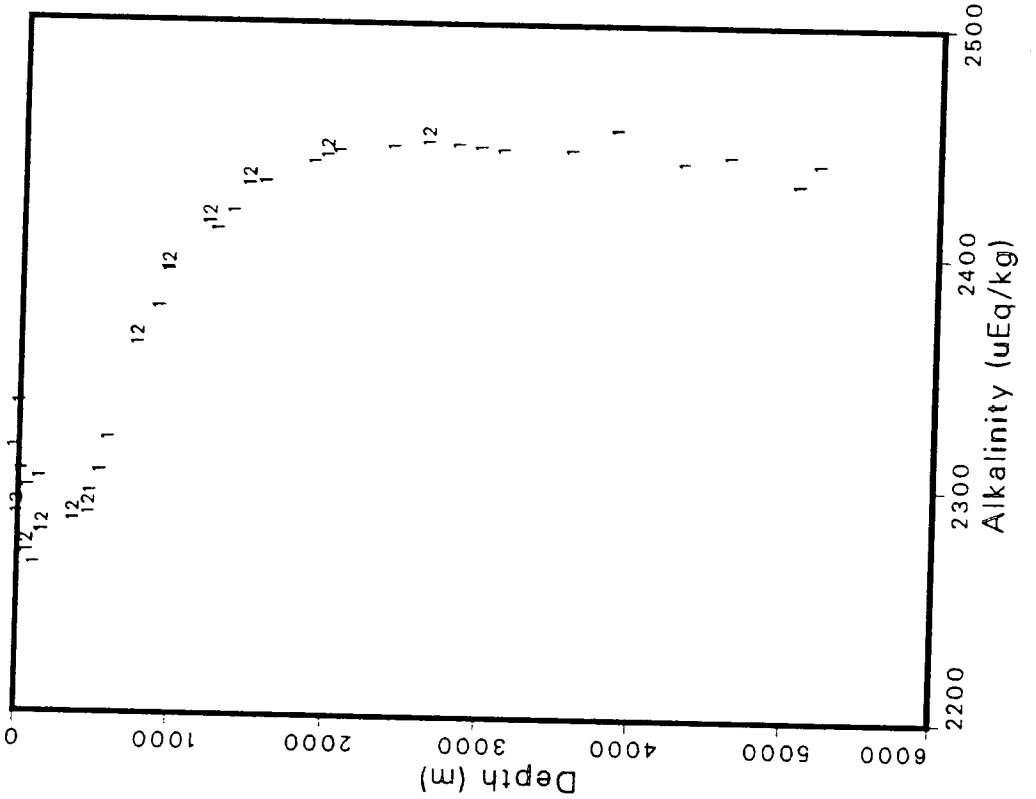
Depth (m)
0
1000
2000
3000
4000
5000
6000
Alkalinity (uEq/kg)
2200
2300
2400
2500

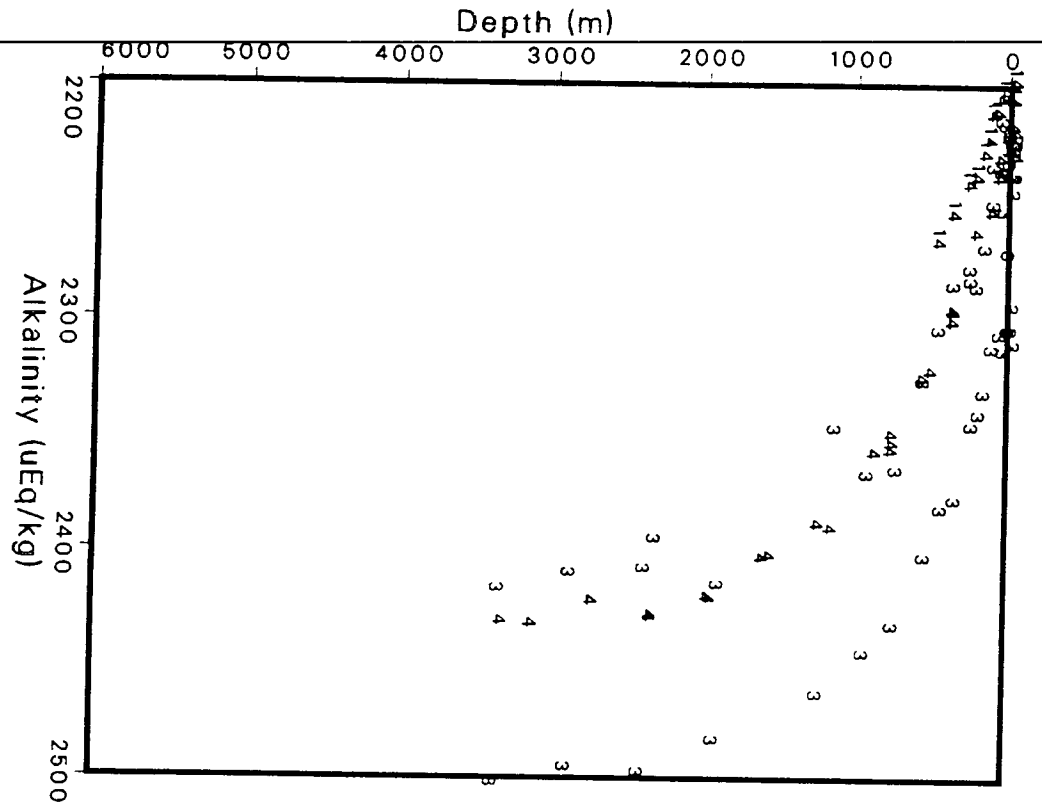
Depth (m)
6000
5000
4000
3000
2000
1000
0
2200
2300
2400
2500
Alkalinity (uEq/kg)

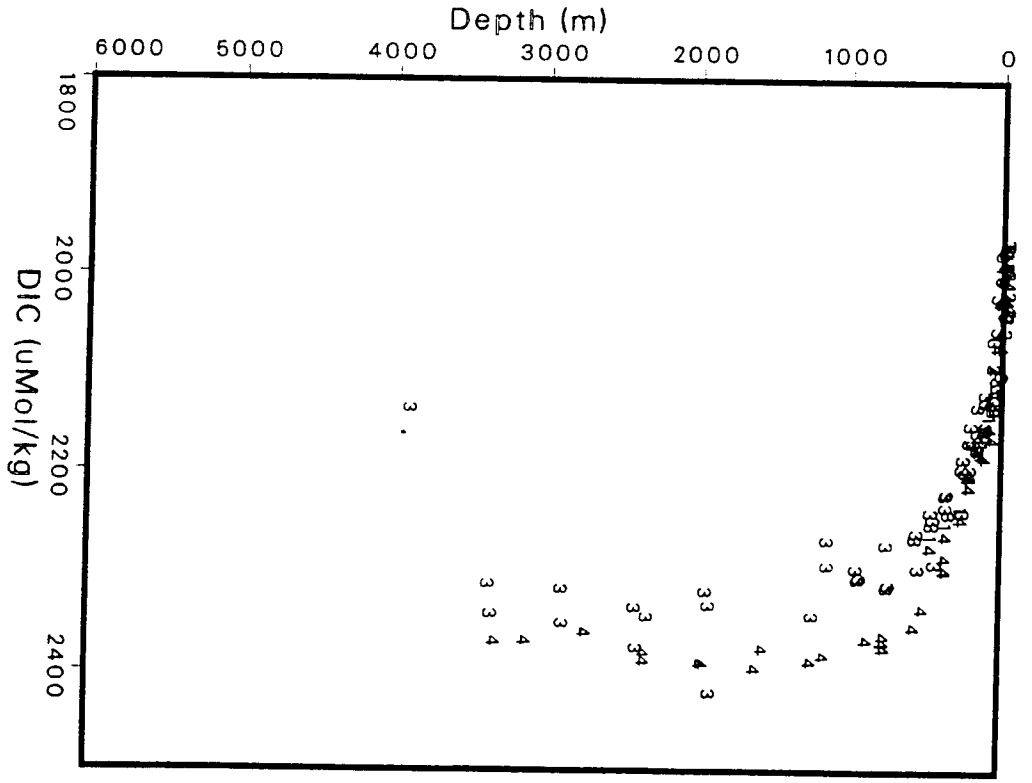
Depth (m)
6000
5000
4000
3000
2000
1000
0
1800
2000
2200
2400
DIC (uMol/kg)

(9)

108A

The tracer concentration $c(x_o,y_o,z_o)$ at the interpolation point was calculated as a weight average of all the stations "near" (x_o,y_o)

$$c(x_o,y_o,z_o) = \frac{\sum_i W(\Delta x_i,\Delta y_i)\, c(x_i,y_i,z_o)}{\sum_i W(\Delta x_i,\Delta y_i)} \tag{4.1}$$

where $c(x_i,y_i,z_o)$ is the tracer concentration of the original data linearly interpolated to the depth z_o and

$$W(\Delta x_i,\Delta y_i) = \exp - \left(\frac{\Delta x_i^2}{r_x^2} + \frac{\Delta y_i^2}{r_y^2}\right) \tag{4.2}$$

is the gaussian weighting function. Data points with a distance greater than $(2r_x, 2r_y)$ from the interpolation point were assigned a weighting of zero. Two passes of the interpolation scheme were used. On the first pass, the r_x and r_y values of the gaussian weighting function were both 5 degrees. The goal of the first pass was to reduce the biasing of the highly sampled Japanese and Californian coasts on the interior ocean. The second pass of the gaussian weighting function used the data from the first pass with r_x and r_y equal to 10 degrees. The larger length scale produced a smoother interpolated field. The interpolated fields for all tracers were used as input into the inverse model. In general the zonal variations in the tracers are small as shown by the plots of the interpolated silicate and phosphate distributions (Fig. 4.6). For a more detailed display of the nutrient distributions, one can refer to the atlas of the GEOSECS Pacific survey which

contains a comprehensive overview of the tracer fields in the Pacific (Craig et al., 1981). The averaged meridional distributions of interpolated silicate and phosphate distribution are shown in Figure 4.7. Silicate is especially suited to distinguish the high silicate concentration of the North Pacific Deep Water (NPDW) from the lower silicate concentration of the Antarctic Bottom Water (AABW) and Antarctic Intermediate Water (AAIW). The concentration differences between the Antarctic water and NPDW makes silicate an important tracer for studying large-scale deep circulation. The phosphate distribution reveals a northward spreading of a high phosphate concentration in the bottom water. The phosphate maximum at 1500 m is lying at a shallower than the silicate maximum at 2500 m because organic matter is less resistant to decomposition than opal material.

(a)

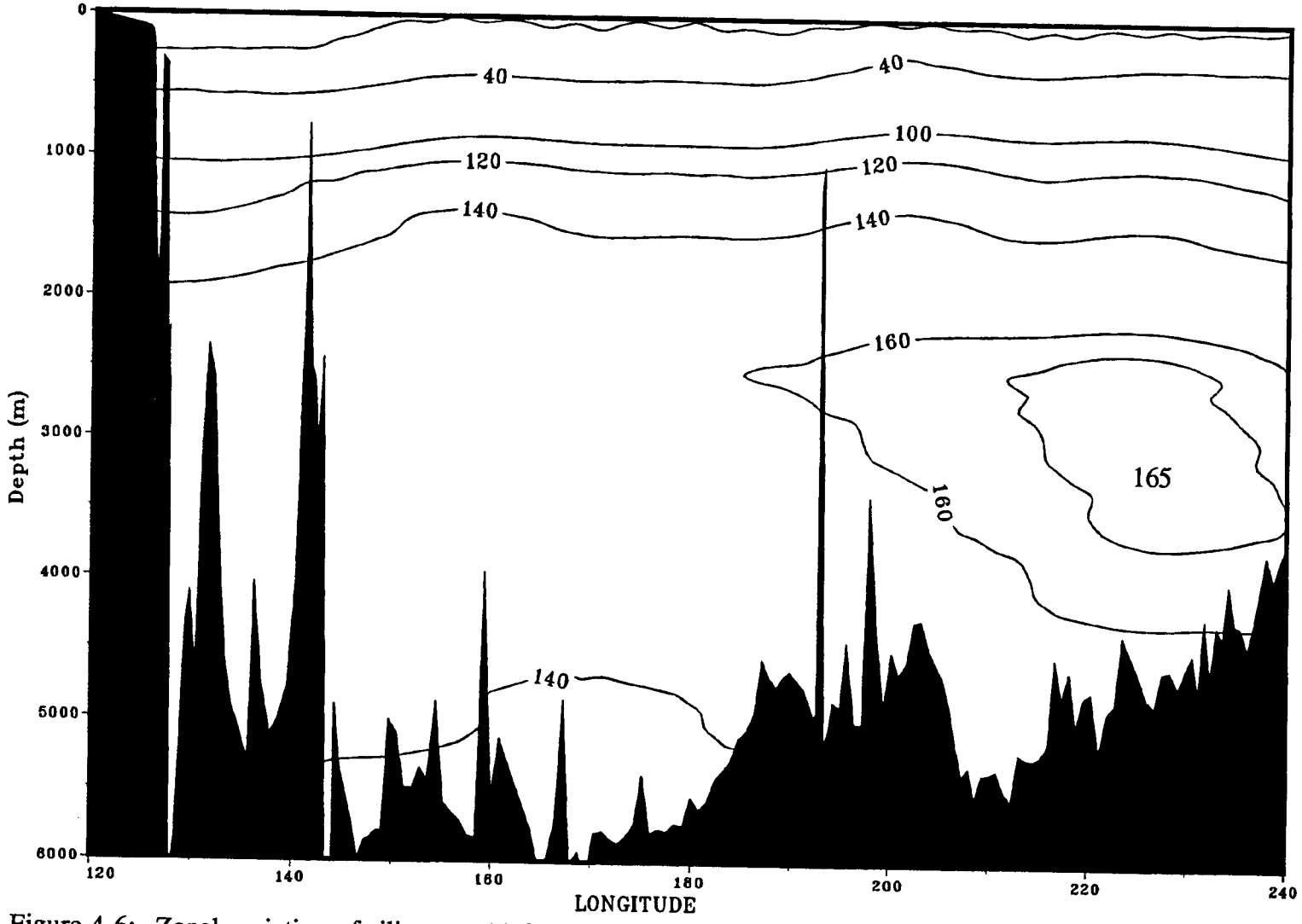

Figure 4.6: Zonal variation of silicate at (a) 24°N and (b) 47°N, and phosphate at (c) 24°N and (d) 47°N, all units are in mol kg^{-1}.

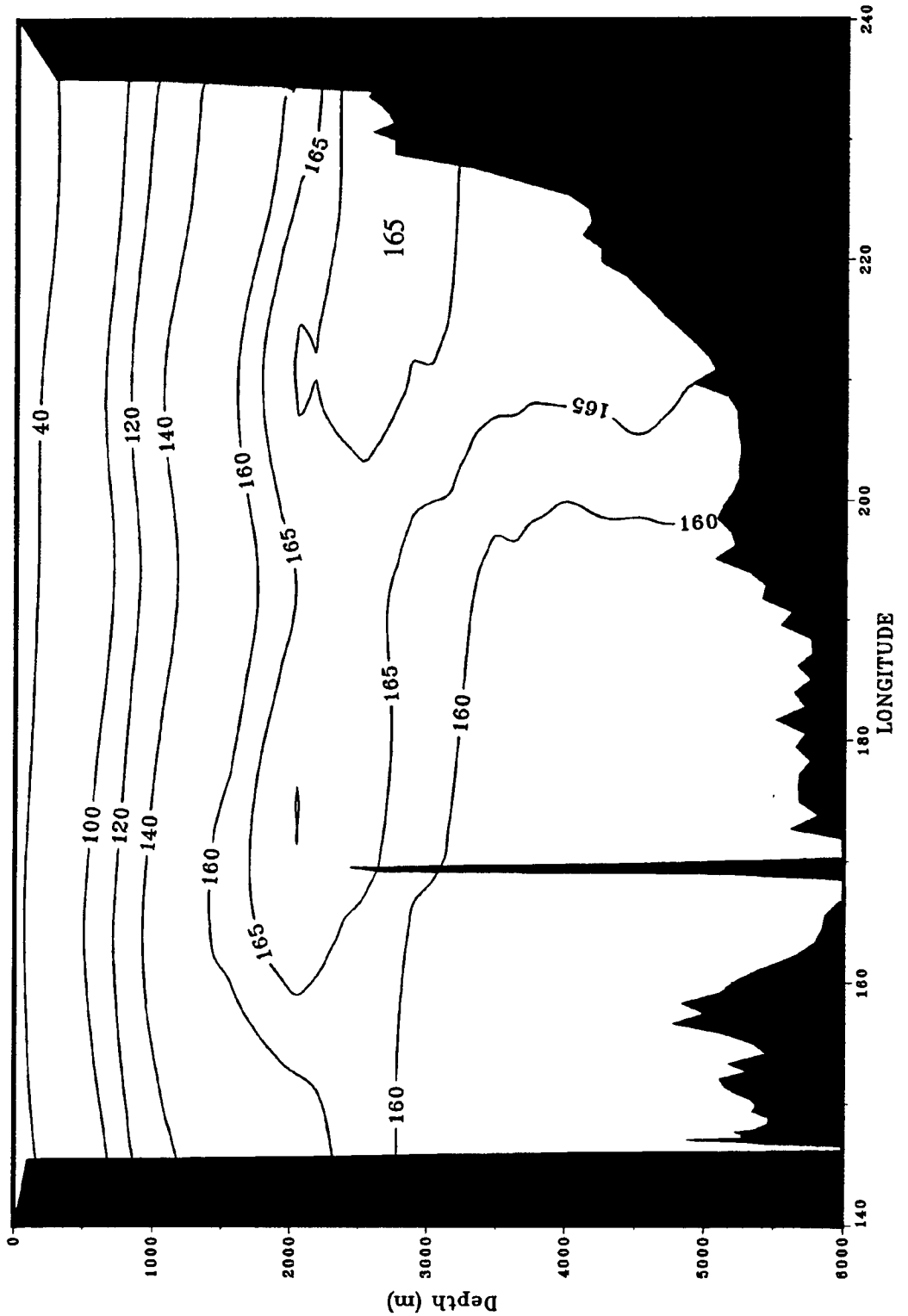
(b)
Depth (m)
0
1000
2000
3000
4000
5000
6000
140
160
180
200
220
240
LONGITUDE
40
100
120
140
160
165

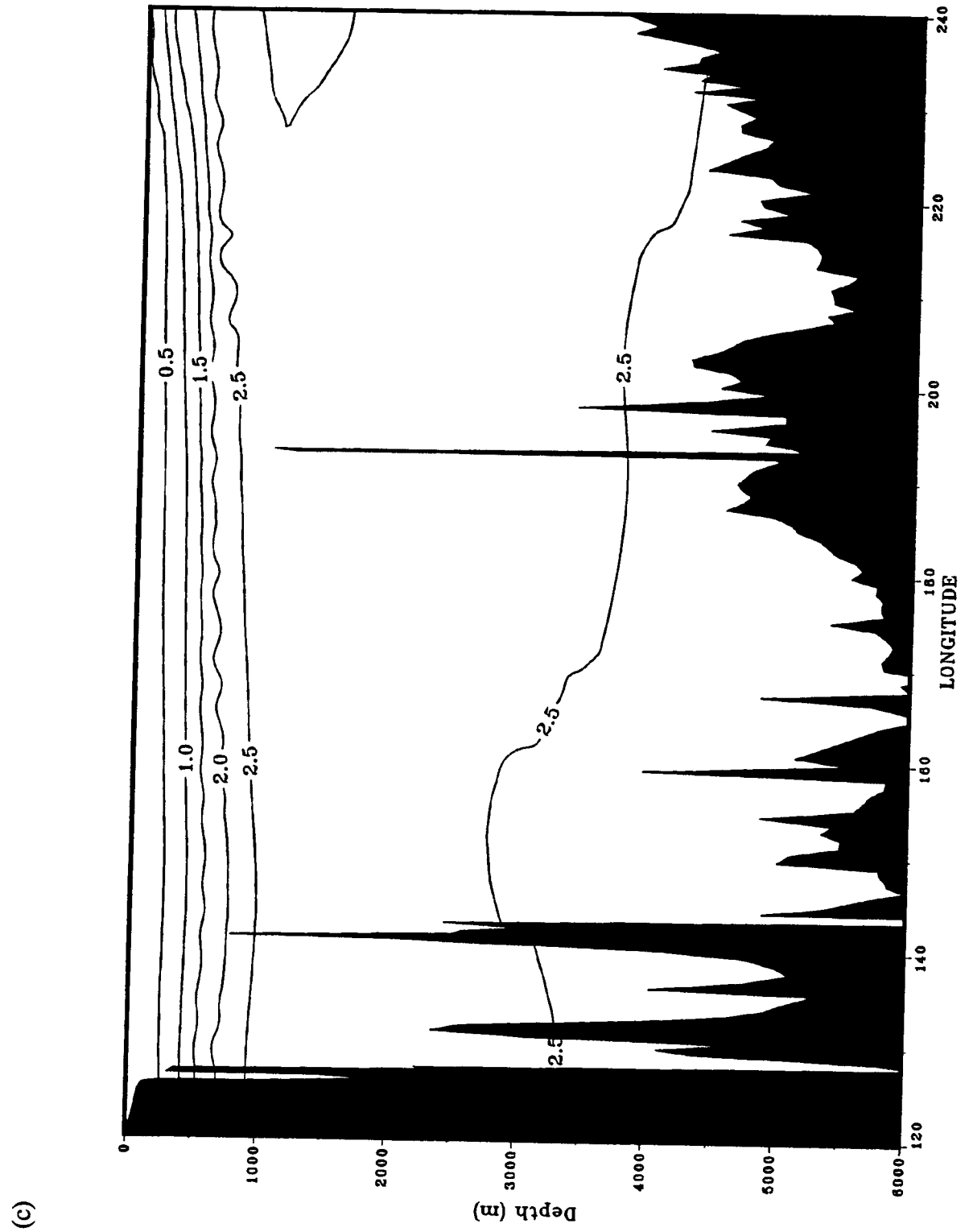
0.5
1.0
1.5
2.0
2.5
2.5
2.5
2.5
2.5
0
1000
2000
3000
4000
5000
6000
Depth (m)
120
140
160
180
200
220
240
LONGITUDE

(c)

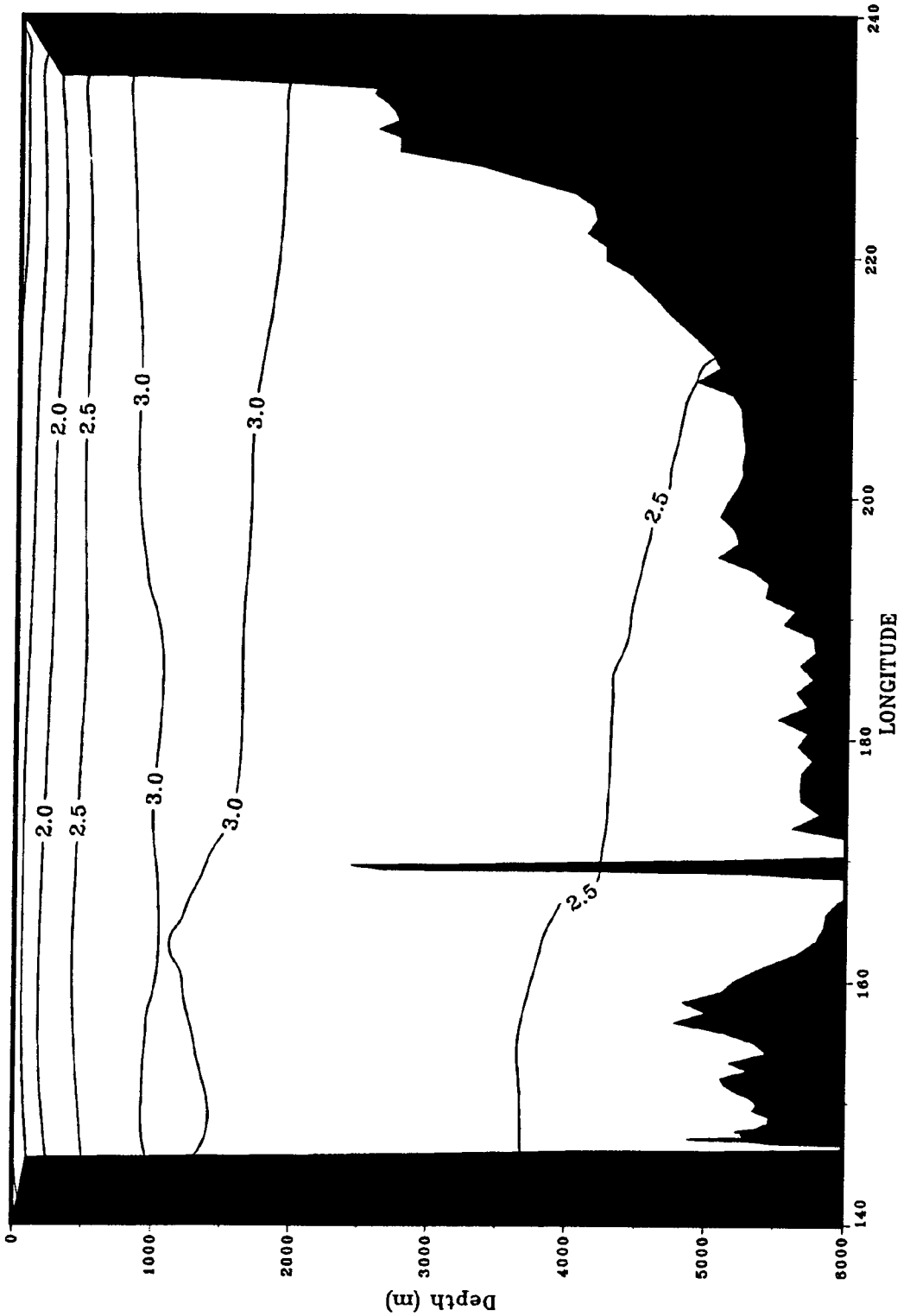
(d)
Depth (m)
0
1000
2000
3000
4000
5000
6000
140
160
180
200
220
240
LONGITUDE
2.0
2.5
3.0
2.0
2.5
3.0
3.0
2.5
2.5

4.2 MODEL GEOMETRY

In the model, the North Pacific is divided into a series of layers by depth and isopycnal surfaces and the ocean bottom (Figure 4.8 and Table 4.3). In the model, layer 1 represents the euphotic zone and it is assumed that all the biological production is restricted to this zone. Near the surface, the vertical resolution of the model is relatively high; the layer thicknesses of the top two layers are about 100 - 200 m. The deep layers of the model are relatively thick (1000-2500 m). They represent the major water masses in the North Pacific below the thermocline: the Antarctic Intermediate Water (AAIW), layer 4; the North Pacific Deep Water (NPDW), layer 5; and the Antarctic Bottom Water (AABW), layer 6. These layers are divided into boxes by zonal sections at 24°N, 47°N and 65°N (Fig. 4.9). The divisions of the model domain by the three sections produces two regions in the model (Fig.4.9). Region one, the subtropical Pacific region, is the largest region with a surface area of $2.48 \times 10^{13} m^2$. This region contains the Kuroshio system and splits the subtropical gyre. Region two, the subarctic Pacific region, is about one-third the size of region one (surface area of $7.4 \times 10^{12} m^2$); it contains the Alaska gyre. The subarctic region is suspected to play a role in the formation of the North Pacific Intermediate Water (NPIW). In this region, the model allows NPIW to come into direct contact with the euphotic layer. This is consistent with Riser and Swift (1989) who observed that the 26.8 potential density surface outcrops in the Sea of Okhotsk. Van Scoy *et al.*, (1991) also argue that the NPIW outcrops in the Alaska Gyre in the winter time.

Table 4.3: The ocean layering used in the model.

Water Mass	Upper surface	Lower surface
Photic Zone	0 m	100 m
Near Surface Water	100 m	σ_θ=26.8
NPIW	σ_θ=26.8 (or 100 m)	σ_θ=27.3
AAIW	σ_θ=27.3	σ_θ=27.7
NPDW	σ_θ=27.7	σ_θ=27.8
AABW	σ_θ=27.8	ocean bottom

The Arctic Ocean is connected to the North Pacific through the shallow Bering Sea and inflows from the surface layer into the Arctic are allowed.

The model shown in Figures 4.8, 4.9, and 4.10 is a compromise between the desire for higher vertical resolution and the necessity to keep the system solvable. The vertical resolution is highest near the surface where the biological activity is occurring and where the particle fluxes vary the most. In the deep water, only the major water masses AAIW, NPDW, and AABW are resolved. In region II, the nutrient concentrations in the surface water are high leading to high productivity and new production. Region I, is more typical of oligotrophic water where nutrients are the limiting ingredient to biological productivity.

(a)

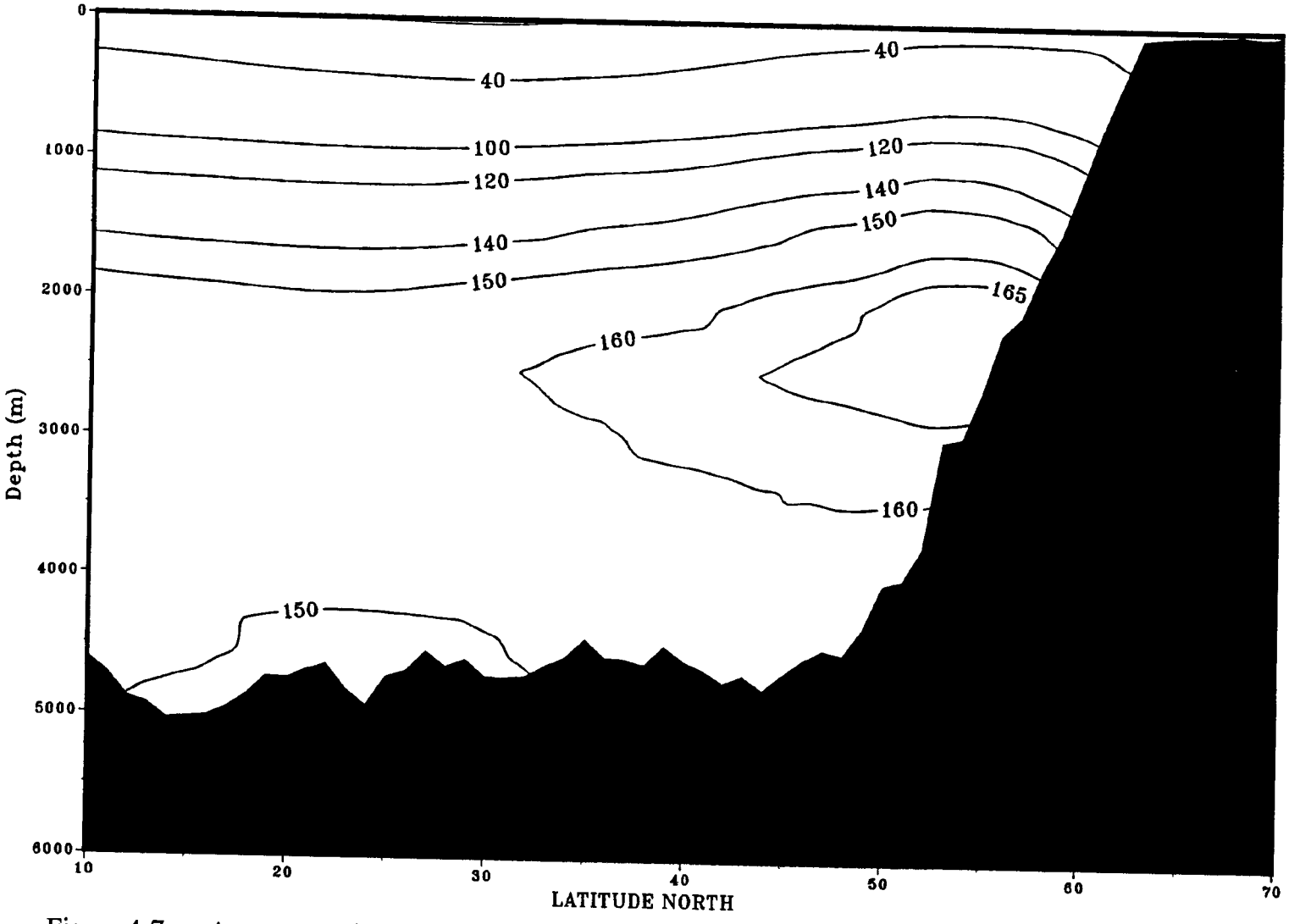

Figure 4.7: Average meridional section of (a) silicate and (b) phosphate in μmol kg^{-1}.

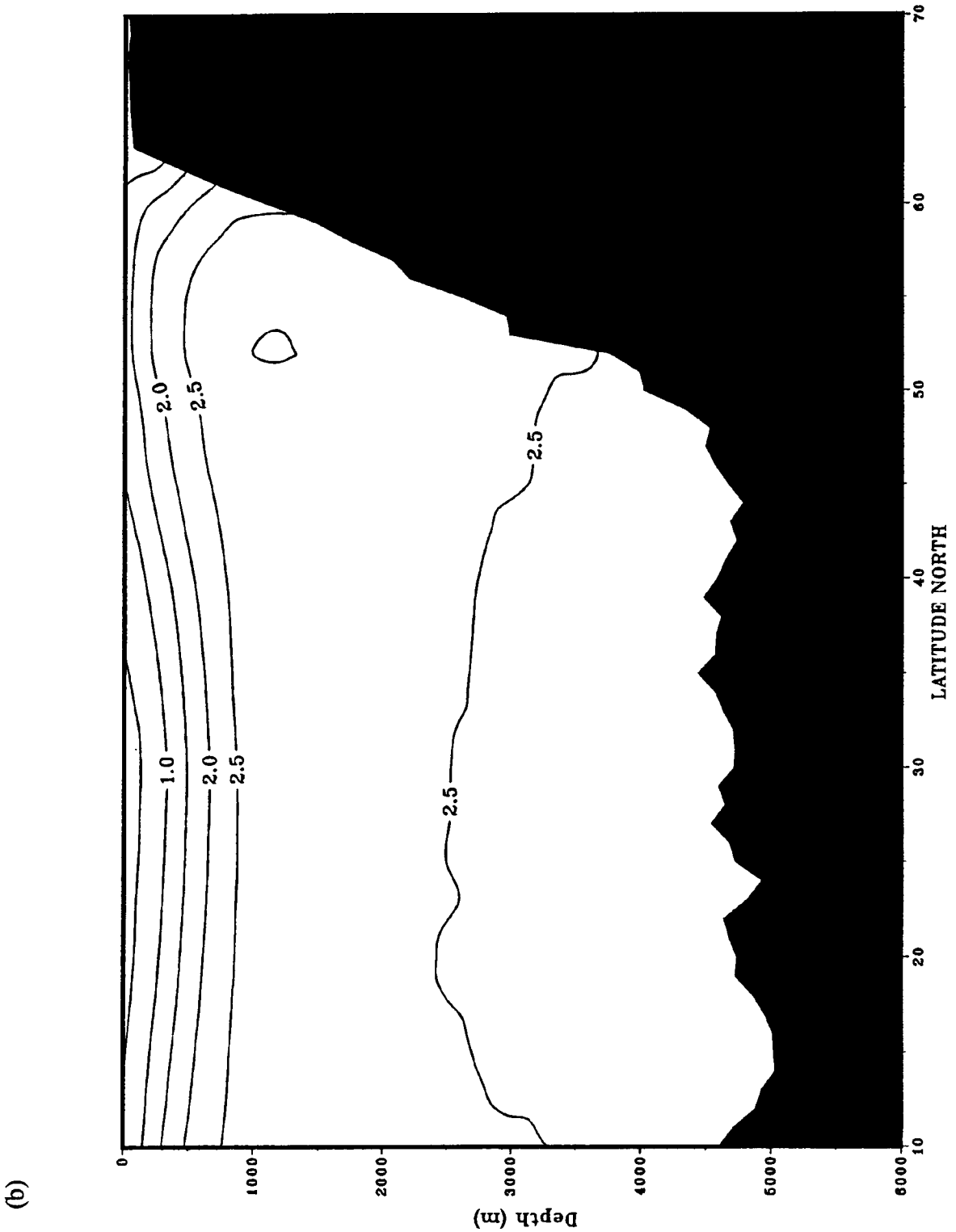
(b)
Depth (m)
0
1000
2000
3000
4000
5000
6000
10
20
30
40
50
60
70
LATITUDE NORTH
1.0
2.0
2.5
2.0
2.5
2.5
2.5

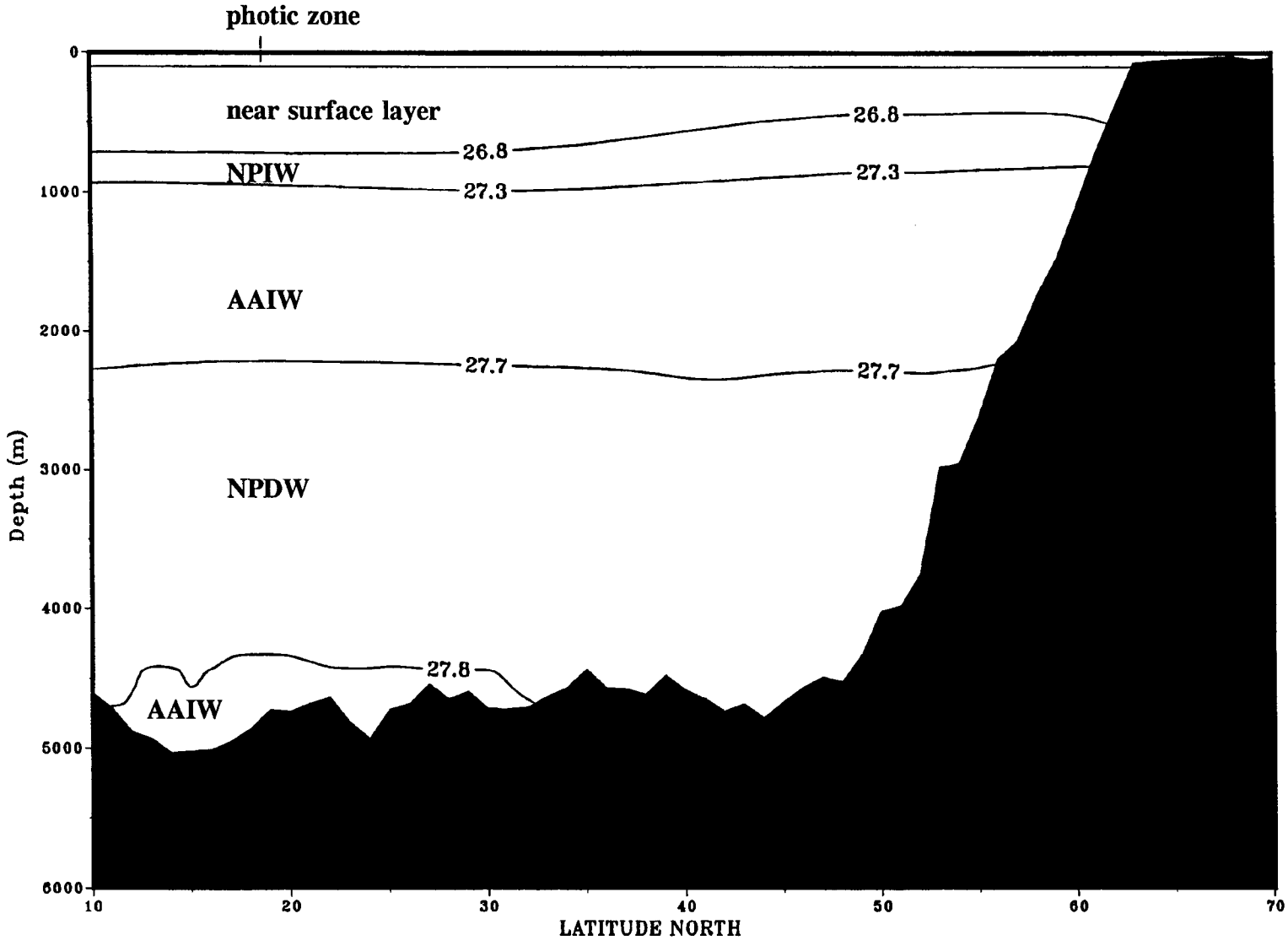

Figure 4.8: The meridional section showing the division of the model into layers.

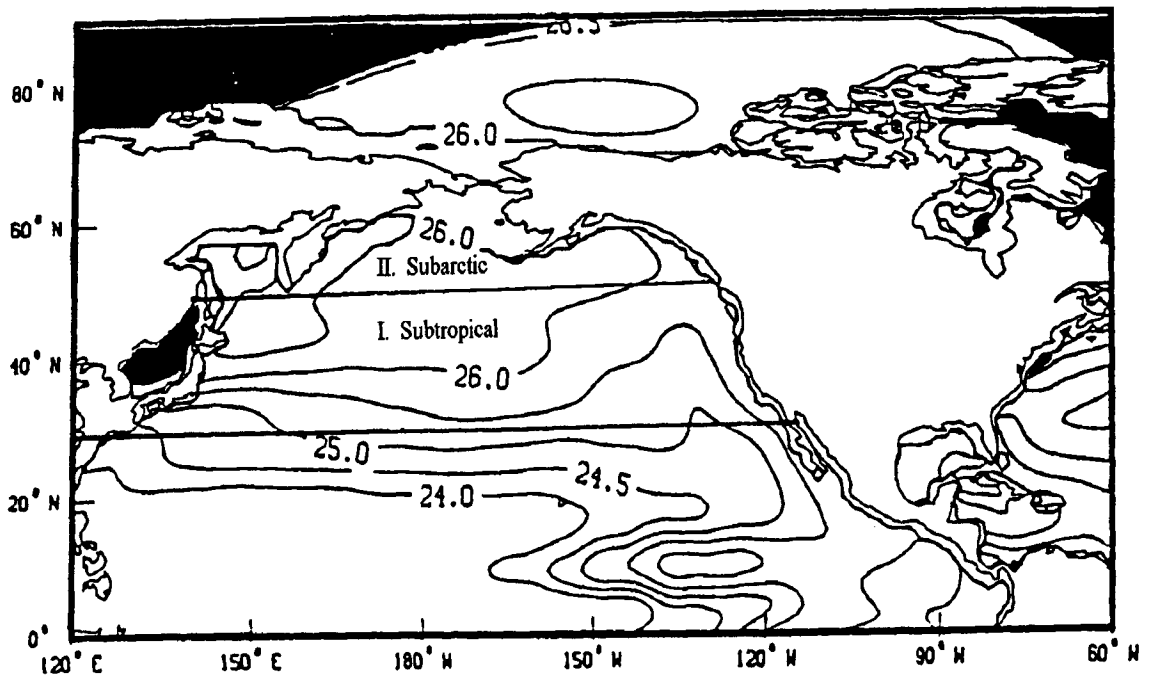

Figure 4.9: Map of potential density at 100 m with the division of the model into regions.

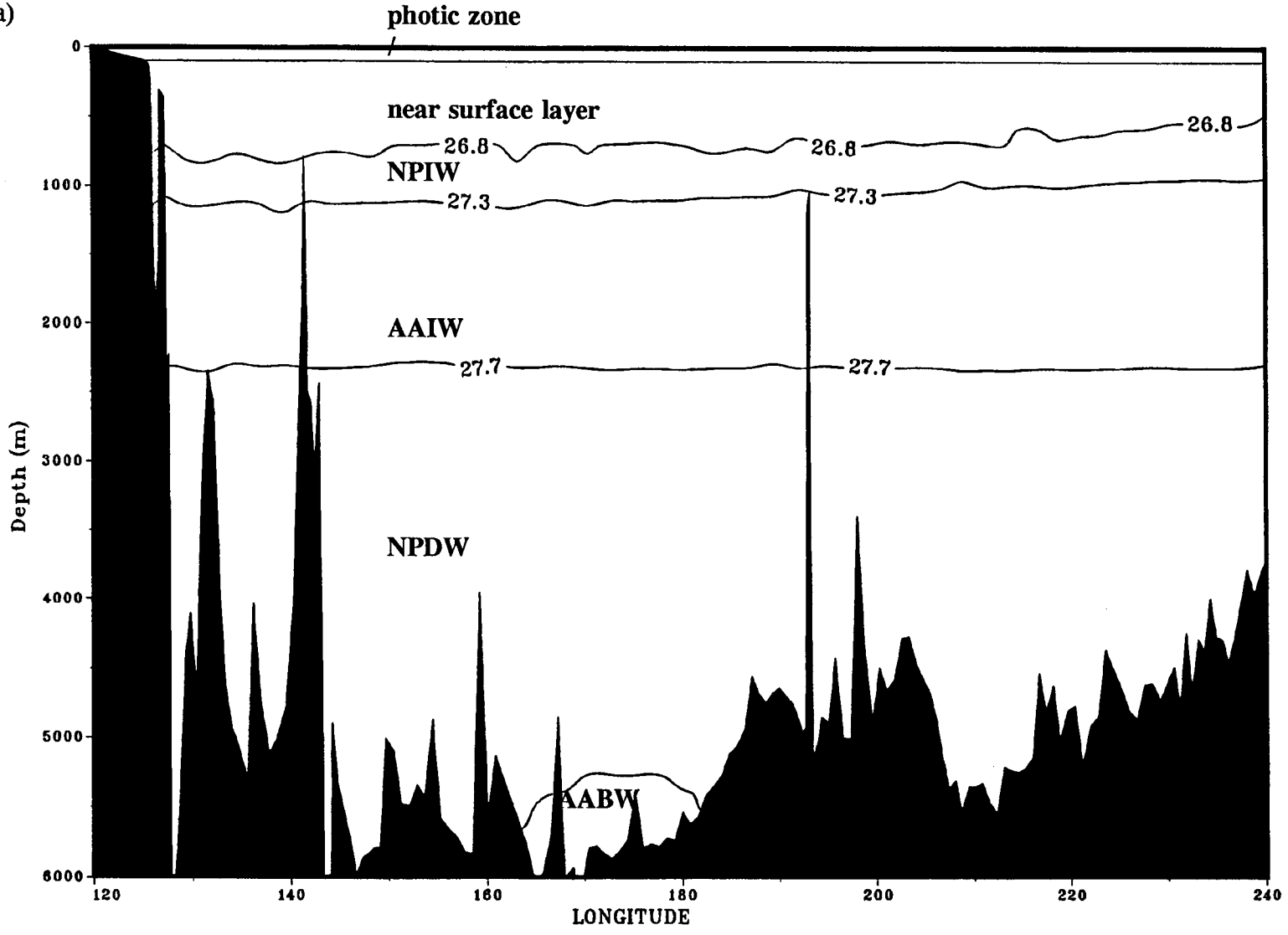

Figure 4.10: The zonal sections showing the layering used in the model, (a) 24°N, and (b) 47°N.

(b)

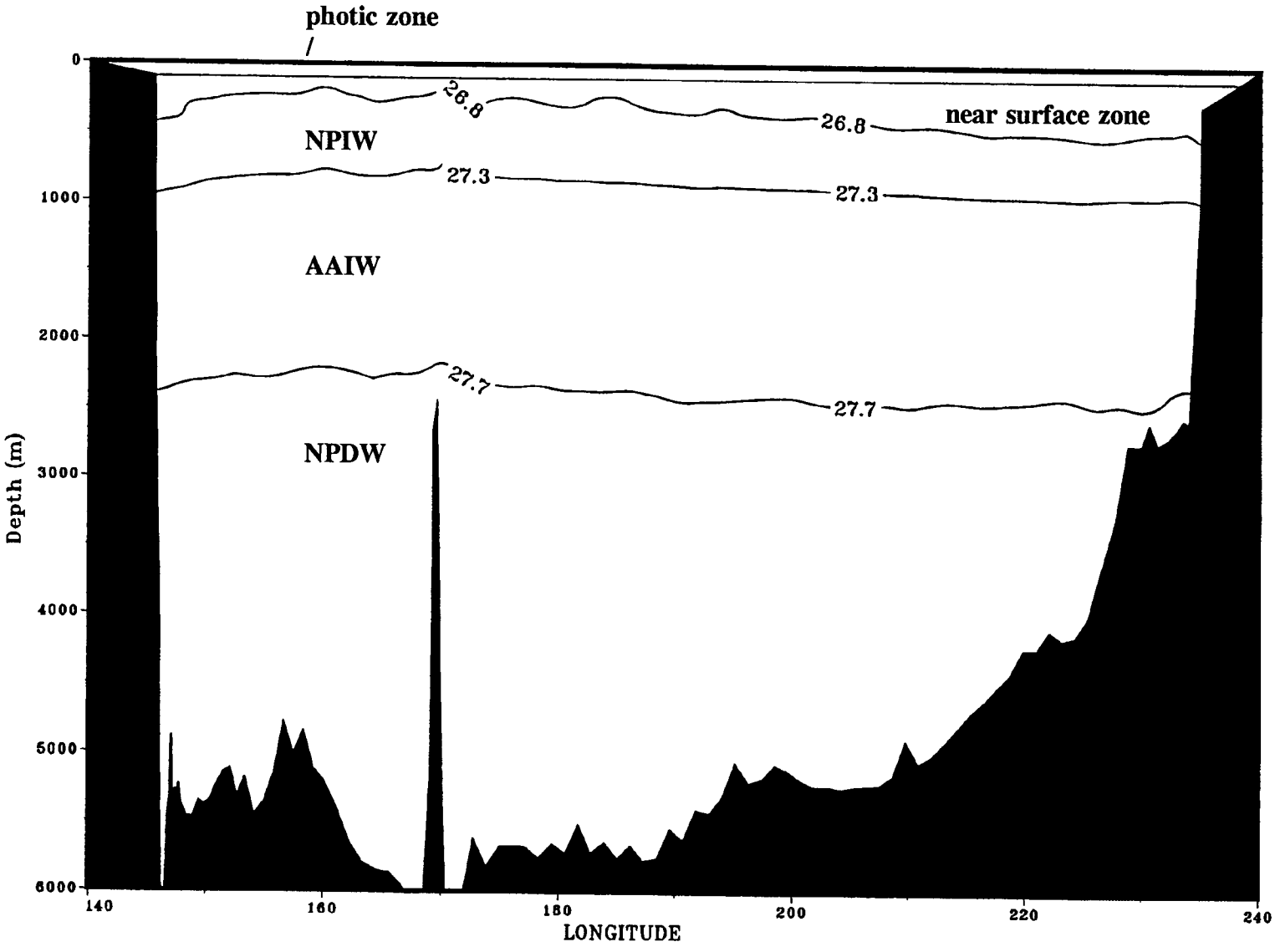
photic zone
near surface zone
NPIW
AAIW
NPDW
26.8
26.8
27.3
27.3
27.7
27.7
Depth (m)
0
1000
2000
3000
4000
5000
6000
140
160
180
200
220
240
LONGITUDE

4.3 MODEL CONSTRAINTS

The three basic principles applied in the model are: 1) continuity of mass within the boxes of the model, 2) continuity of tracers within the boxes of the model and 3) geostrophic flow through the sections. The continuity of equations for tracers and mass are given in the following two equations

$$\rho V\frac{\partial C}{\partial t} = \int[\nabla\cdot(\vec{u}C\rho) - \nabla\cdot(k\nabla C\rho)]dV + Q_{bio} + Q_{air\text{-}sea} = 0 \qquad (4.3)$$

$$\nabla\cdot(\rho\vec{u}) + \nabla\cdot Q_{freshwater} = 0 \qquad (4.4)$$

The tracer continuity equation states that the concentration of a tracer C within a volume V changes with time if the total (net) tracer transport does not balance internal sources and sinks (the Q's) of that tracer. The tracer transports are composed of advective parts which represent the tracer transport due to the 3-dimensional mean flow field (u, v, and w), and an eddy mixing term which describe the tracer transports due to temporal and spatial fluctuations of the flow fields and tracer concentrations. The usual approach of parameterizing these eddy transports as the product of the concentration gradient and apparent mixing coefficient is used in this model. By integrating both equations around the volume defined by a box and assuming steady-state, one can write the equations as a sum of transports through the surfaces of the box.

$$\sum_i (\vec{u}_i (C\rho)_i A_i) - \sum_i (k_i \frac{\partial (C\rho)_i}{\partial x_i} A_i + Q_{bio} + Q_{air\text{-}sea} = 0 \quad (4.5)$$

$$\sum_i (\rho \vec{u})_i A_i + Q_{freshwater} = 0 \quad (4.6)$$

The summation, i, includes all horizontal (isopycnal) and vertical (diapycnal) surfaces of the box. The parameter A_i refers to the surface area of the i^{th} surface, u_i is the average velocity through the i^{th} surface, $(C)_i$ and $(\partial C/\partial x_i)$ are the concentration and concentration gradient on the i^{th} surface. The concentration gradient is evaluated perpendicular to the surface. The values $Q_{air\text{-}sea}$ and $Q_{freshwater}$ are the net air-sea exchange of tracers and freshwater through the ocean surface, and Q_{bio} are net biological source/sink of tracers inside the box.

4.3.1 Horizontal water transports

The horizontal water flows through the box surfaces are assumed to be geostrophic; ie., the horizontal velocities satisfy the thermal wind equation:

$$v_g(z) = \frac{g}{\rho_o f} \int_{z_o}^{z} \frac{\partial \rho}{\partial x} dz + v_o \quad (4.7)$$

v_o is the unknown reference velocity at the reference level (z_o). The Ekman transports are added to the surface layer of each section. The Ekman transports are calculated from the integral equation

$$M_e = \oint \frac{1}{f}(\tau_y, -\tau_x) \cdot \hat{n}\, dS \tag{4.8}$$

where **n** is the unit vector normal to the vertical box face into the box; τ_x and τ_y are wind stress in the x and y direction respectively; and f is the coriolis parameter. The annual wind stresses from Hellerman and Rosenstein (1983) are used to calculate the Ekman transport. The total horizontal transport through the horizontal surface j, is

$$X_{H_j} = \sum_k \oint_{A_{jk}} \rho v_{g_k} dS + \sum_k \rho v_{o_k} A_{jk} + \sum_k M_{e_k} \tag{4.9}$$

Except for surface layers, the Ekman transport is zero (M_e=0). The total horizontal tracer transport through a surface j is

$$J_{H_j} = \sum_k C_k \oint_{A_{jk}} \rho v_{g_k} dS + \sum_k C_k \rho v_{o_k} A_{jk} + \sum_k C_k M_{e_k} \tag{4.10}$$

The first two terms represent the transport due to geostrophic flow and the third term is the contribution from the Ekman transport. The summation k is over all the parts in the section and A_{jk} denotes the corresponding area of that box face. The TPS24 and TPS47 sections are used to calculate the geostrophic velocities. Because it was believed that the tracer data which are used in the model did not contain information to resolve the individual station pairs reference velocities, no attempt was made to determine these individual velocities. Instead the sections are divided into four subsections and these reference velocities are determined. The inverse results of Rintoul and Wunsch (1991)

show how ill-conditioned the determination of the individual reference velocities are and, except in regions of large changes in bottom topography, their modelling results produce nearly constant velocities.

The total tracer transport into a box by horizontal and vertical advection is given by

$$J_a = \sum_j J_{H_j} + \sum_i w_i (\rho C)_i A_i \tag{4.11}$$

where the summation j is over all horizontal surfaces and the summation i is over all vertical surfaces. The parameter A_i denotes the surface area of the i^{th} box face.

4.3.2 Eddy transports

It has already been mentioned that the eddy transports in the model are parameterized by a diffusion term. In the model, the diffusive transport is broken down into diapycnal and isopycnal terms. The transport of mixing is

$$J_m = \sum_j K_{h_j} \frac{\partial(\rho C_j)}{\partial x_j} A_j + \sum_i K_{v_i} \frac{\partial(\rho C_i)}{\partial z_i} A_i \tag{4.12}$$

where the summation j is over all isopycnal surfaces and the summation i is over all vertical surfaces. The parameter A denotes the surface area of the box faces. The gradients on the surface are calculated from the average concentrations in the two connected boxes divided by the distance from the centre of the two boxes. In the model, the mixing terms are forced to be positive (in chapter 3 it was shown that it was

Table 4.4: The processes that contribute to the biological source/sink terms for the various tracers.

Tracer	Process
Mass	--
Heat	--
Salt	--
Oxygen (Q_O)	photosynthesis and remineralization of organic tissue
Phosphate (Q_P)	formation and remineralization of organic tissue
Silicate (Q_S)	opal formation and dissolution
Carbon (Q_C)	formation and remineralization of organic tissue and $CaCO_3$
Alkalinity (Q_A)	formation and dissolution of $CaCO_3$*

* Alkalinity is also slightly affected by the biological source/sink of nitrate.

unnecessary to have negative K's), making the coefficient physically meaningful (Olbers *et al.*, 1985).

4.3.3 Biological processes

The biological source parameter, Q_{bio}, in equation (4.3) is the net source (sink if negative) for the various tracers due to biological processes. This parameter for the different tracers is the result of various processes (Table 4.4). The biological uptake of dissolved nutrients, and the formation of organic tissue and calcareous and opaline shells

in the surface water represents a sink for nutrients and carbon and a source for oxygen. The subsequent remineralization of the particulate matter in the deeper ocean leads to a release of nutrients and carbon (sources) and the utilization of oxygen (sink). The use of the tracer pair, DIC and alkalinity, allows for the distinction between formation (dissolution) or organic matter and $CaCO_3$. Only the formation (dissolution) of $CaCO_3$ contributes to the alkalinity source term.

In the model, organic tissue and calcareous and opaline shells are formed in the surface boxes. This particulate matter formed in the surface box is assumed to be completely remineralized or dissolved in underlying deeper boxes of that same region. This assumption is reasonable because advective transport of particulate matter from one model region to another, as well as nutrient input from the continents and nutrient loss due to sedimentation, are small compared with the advective transport of the dissolved nutrients and uncertainties in the nutrient conservation equations.

The biological source terms for phosphate, nitrate, carbon and oxygen in the ocean are related. This is because of the relatively constant composition of organic matter. In the formation of organic tissue by photosynthesis, the uptake of phosphate is accompanied by a proportional uptake of nitrate and carbon and a release of oxygen. These proportionality factors were originally determined by Redfield and are called Redfield's ratios. The inverse model uses the values from Takahashi *et al* ., (1985) of $P:N:C:O_2$ = 1:16:103:-172. These differ slightly from Redfield's original values $P:N:C:O_2$ = 1:16:106:-138. Broecker *et al* ., (1985) showed that the $P:O_2$ = 1:-172 is applicable to all oceans. In the present model, constraints of the form

$$Q_c - R_{C/P} Q_p = 0 \pm \epsilon Q_c \quad (4.13)$$

$$Q_c - R_{C/O} Q_o = 0 \pm \epsilon Q_c \quad (4.14)$$

are used to allow the Redfield ratios to vary from the values of Takahashi by a given percentage, ϵ.

In addition to Redfield ratios, alkalinity of the ocean is not only affected by the formation/dissolution of $CaCO_3$ but by the following equation:

$$Q_A = 2 \times C_{carb} - 16 Q_P \quad (4.15)$$

where Q_A and Q_P are the biological source terms for alkalinity and phosphate respectively. The formation of $CaCO_3$ reduces the amount of dissolved inorganic carbon (C_{carb} is negative) and the ocean alkalinity. The formation of organic material alters the alkalinity by the uptake of nitrate.

In the ocean, one could restrict the formation of $CaCO_3$ to boxes above the lysocline and the dissolution to boxes below the 100% carbonate saturation level. However, in the North Pacific Ocean the situation is simplified because the 100% carbonate saturation level is so shallow, 500 m in the equatorial regions to shallower than 200 m in the high latitudes (Feely and Chen, 1982). In the model, $CaCO_3$ will form only in the surface boxes and will experience dissolution in all subsequent deeper boxes.

Table 4.5: The processes that contribute to the air-sea source/sink terms for the various tracers

Tracer	Process
Mass	precipitation, evaporation and river runoff
Heat	air - sea heat flux
Salt	--
Oxygen	gas exchange with the atmosphere
Phosphate	--
Nitrate	--
Silicate	--
Carbon	gas exchange with the atmosphere
Alkalinity	--

4.3.4 Air-sea exchanges

The air-sea processes that contribute to various tracer concentrations are given in Table 4.5. These processes only affect boxes that are exposed to the atmosphere. It is known that in order for CO_2 to enter the ocean, pCO_2 in the ocean must be less than the pCO_2 in the atmosphere. This information will be incorporated into the model to prescribe the direction of air-sea flux of CO_2 using the data from Tans *et al.*, (1990). The maps of the summer and winter ΔpCO_2 are shown in Figure 4.11. From this data one can

(a)

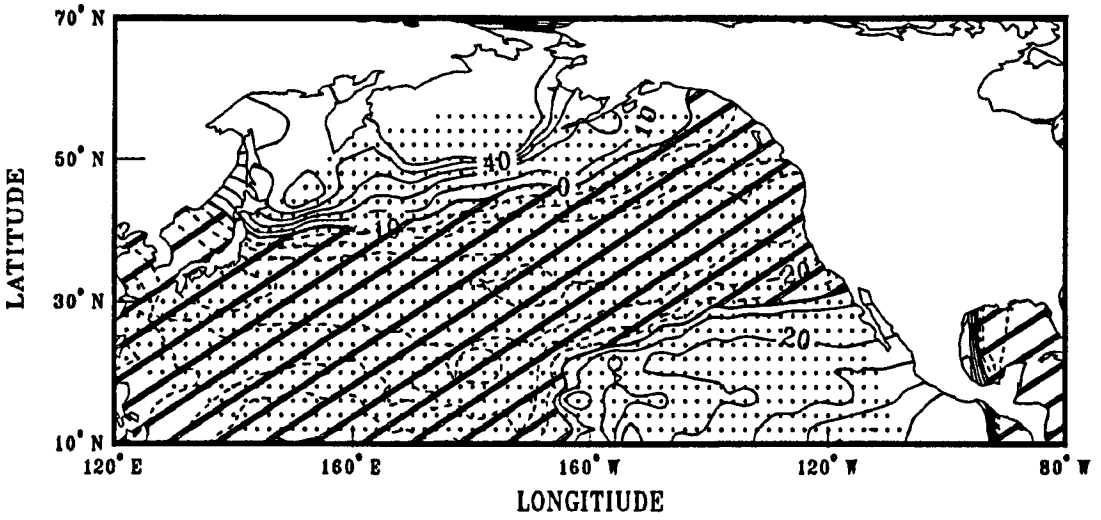

(b)

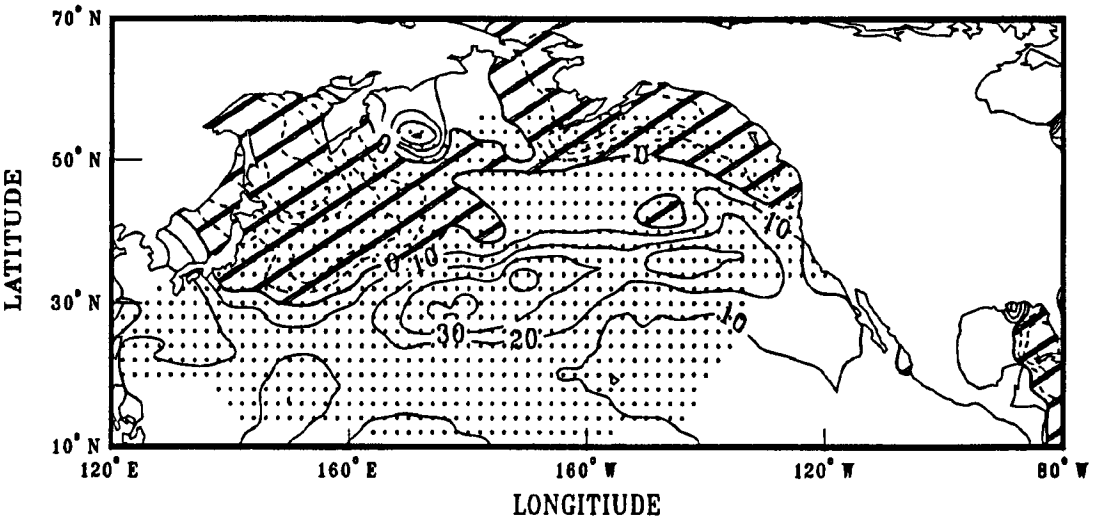

Figure 4.11: The ΔpCO_2 maps of the North Pacific (Tans *et al.*, 1990), the units are in μAtm, with negative regions (lined) denoting areas of the ocean that sinks of atmospheric CO_2, (a) winter (Jan.-Apr.) and (b) summer (Jul.-Oct.). The dots denote the regions where data are available.

see that in winter the subarctic Pacific is generally a source of atmosphere CO_2 and the subtropical Pacific is generally a sink of CO_2. In the summer, the situation is reversed, the subarctic is now a weak sink and the subtropics is a source. The net annual effect determined from these maps are that the subtropics behaves like a sink of CO_2 and the subarctic behaves like a source. The strong source of CO_2 in the high latitudes of the Pacific is somewhat surprising. Given the large seasonal fluctuation in the direction of the CO_2 in the subarctic Pacific and the limited data in the high latitudes, the sign of this flux was left undetermined. However, in the subtropics, the CO_2 flux is more definite and in the model this region is assumed to be a sink of CO_2.

4.4 INVERSE SOLUTIONS

From equations 4.5 and 4.6 one develops a set of equations that links the concentration data (C and the gradient of C) to the unknown reference velocities, mixing coefficients, biological parameters and air-sea exchanges. Mass and tracer balances for heat, salt, DIC, alkalinity, phosphate, oxygen and silicate are formulated for the individual boxes and for the two regions of the model. These continuity equations make up the largest part of the set of model constraints, but other constraints are added to exert more control on the model (Table 4.6).

Table 4.6: Summary of model constraints

Constraint	Number
Mass, heat, salt, phosphate, oxygen, silicate, $\sum CO_2$, alkalinity continuity for the individual boxes and regions of the model	112
Redfield constraints for phosphate and oxygen	20
Geostrophic constraints	12
Total	144

The model constraints represent a set of linear equations

$$Gx = b \pm \epsilon \tag{4.16}$$

where the coefficients matrix **G** contains tracer concentrations and gradients, x is the vector of unknowns

$$x = (v_{o_k}, u_i, w_i, k_{h_i}, k_{v_j}, Q_{bio}, Q_{air\text{-}sea}, Q_{freshwater}) \tag{4.17}$$

and the vector **b** contains the relative geostrophic components of the tracer fluxes across surfaces of the boxes. Due to errors in the data and approximations in the model, the constraint equations are not expected to be exactly satisfied but only to be within a specified tolerance ϵ_i. The estimation of the tolerances will be discussed in section 4.5. A priori bounds x^- and x^+ are applied to the unknowns to restrict their numerical values to physically meaningful ranges:

$$x^- \leq x \leq x^+ \tag{4.18}$$

Table 4.7: A priori bounds on the model parameters

Parameter	Lower Bound	Upper Bound
Reference velocities (v_o) cm s^{-1}	-5.0	5.0
Isopycnal mixing coefficients, k_h, m^2 s^{-1}	0	30,000
Diapycnal mixing coefficients, k_v, cm^2 s^{-1}	0	10
Air-sea exchange of CO_2 in the subtropics	0	∞
Water outflow through the Bering Sea, Sv	0	2.0
Korean Strait, northward flow, Sv	2.0	4.0

Table 4.7 summarizes these constraints. The outflow through the Bering Sea is based on the estimate of Coachman and Aagaard (1988) of 0.8 Sv annual mean transport with $\pm$0.6 Sv in seasonal variability. The flow through the Korean Straits (Tsushima Straits) was based on estimates of Bingham (1991), Yi (1966) and Nitani (1972). The advantage of this routine is that it can determine if feasible solutions exist and produce a realistic solution to the problem. This provides one with a clear visualization of the solutions being forced by the model. In this research, the LSI routine was extensively used to study different models and to assess how well the model was working. By studying the solutions from such models, one can see what information the data is providing to the model.

To solve these system of equations (4.18) and (4.19), I relied on two different algorithms: the least squares algorithm with inequality constraints (LSI) (Lawson and Hanson; 1974) and linear programming (LP) (Luenberger; 1984). Refer to §3.3.3 for a more detailed discussion of these two inverse methods.

4.5 TOLERANCES OF BALANCE EQUATIONS

The continuity equations (4.3) for the various tracers are not expected to be satisfied exactly but only to within certain tolerances ϵ. These tolerances reflect errors in the tracer data as well as simplifications in the model. In the present model, I assumed that the flow is geostrophic (with Ekman transport added to the surface layers) and that the reference velocities, v_o, vary only on large scales. Also, I assumed that the tracer transport through box surfaces can be decomposed into advective, diffusive and particle transports and that the diffusive transport can be parameterized by mixing coefficients. Though this approach is a standard method and frequently used, it is important to keep in mind that it is only an approximation to the correct tracer transports.

The effect of the approximations in (4.3) on the tracer budgets create part of the error in (4.16); however, these errors are difficult to assess quantitatively. An additional difficulty in determining the errors ϵ in (4.16) are that the errors in $\mathbf{b}$ are functions of the unknown transport terms. An appropriate estimate of these errors, $\delta\mathbf{b}$, was thought to be determined by only considering the error in $\mathbf{b}$ due to advective transports by using the following equations:

$$b' = \sum_i v_i A_i C_i$$
$$\delta b' = \sum_i \delta v A_i C_i + \sum_i \delta C_i v_i A_i \qquad (4.19)$$

where v_i represents the average velocity through the i^{th} box face, A_i the area of the i^{th} box face and C_i the concentration on the i^{th} box face, and δ denotes the errors in these terms. The first term on the rhs of (4.19) was dropped because for flow that is forced to conserve mass, the sum of $\delta v_i A_i$ for all boxes will be zero and hence the error from this term will be small. The second term on the rhs of (4.19) was evaluated by using the standard deviation of the tracers in the defined boxes to determine the tracer errors on the box faces (δC_i) and by multiplying this value by the rms volume transports of the relative geostrophic transports (x_i, the x_i approximately equalled 5.1 Sv). The tracers errors prescribed in (4.19) were 1.25 times greater than the temporal variability of the tracer data from Station P. Large fluctuations in some of the station P measurements resulted in the decision to use the values calculated from the boxes. It is felt that these values represent an upper limit of the errors expected in the tracers.

In the model, the mass continuity constraints are considered to be almost perfectly satisfied ($\pm$0.001 Sv). This approach was taken because large mass imbalances degrade the information content of the tracer continuity by introducing tracer imbalances. If large mass imbalances are allowed, one is in effect introducing artificial sources and sinks into the tracer's balances and corrupting these equations. Being aware that geostrophic transports across the surfaces of the boxes might be inconsistent with the principle of perfect mass balance, small errors in the thermal wind equations are allowed in the model

($\pm 1\%$). The model also forces the tracer continuity in the two regions to be nearly-perfectly satisfied. The logic for this comes from the fact that the steady-state assumption is assumed to be a valid approximation; then at least for the large regions of the model, this condition should be satisfied. Without this tightening of the regional constraints, the model would be allowing the equivalent of artificial air-sea exchanges to add and remove tracers from the model.

CHAPTER 5. MODEL RESULTS FOR THE NORTH PACIFIC OCEAN

In this chapter I will look at inverse solutions to models formulated for the North Pacific. The chapter is separated into three sections. In the first section, I attempt to understand and evaluate the model. The second section is devoted to discussing the results obtained from the inverse box model. In the third section, I aim to investigate the effect of dissolved organic matter on the tracer budgets by including the "new" DOM concentrations in the model in a simple way.

5.1 EVALUATING AND UNDERSTANDING THE MODEL

In this section I will evaluate the model to better understand how it works and to provide insight into the problem. In the discussion to follow, I will first look at the feasibility of several slightly different models, focusing on the change in the solutions obtained. Second, a study of the importance of the various tracers will be performed in order to evaluate the differences in the information content of the various tracers. Third, I will evaluate the model's sensitivity to the choice of layering and reference level.

5.1.1 Feasiblilty Studies

One powerful tool of inverse modelling is its flexibility. It is relatively easy to change the constraints of the model to investigate the effects on the solution. The flexibility of inverse models is exploited in the following analysis with four different inverse models. These models investigate the feasibility of the constraints and changes in the solutions of air-sea exchanges of freshwater, heat, CO_2 and O_2 and detrital rain rates of organic carbon, inorganic carbon and opal material.

The first model formulated satisfied the Ekman and Geostrophic transports to $\pm 1\%$, had positive unbounded mixing terms and satisfied the Redfield ratios for the formation/dissolution of organic matter exactly. The model had a feasible solution, showing that significant deviations in the Ekman or Geostrophic transports are not necessary for a feasible solution. The model's acceptable ranges for the unknown air-sea exchanges and maximum detrital rain rates are summarized in Table 5.1 and 5.2.

To further explore the feasibility of the constraints, a second model was formulated from the first model by including an upper limit on the diapycnal and isopycnal mixing terms of 10 $cm^2\ s^{-1}$ and 30,000 $m^2\ s^{-1}$ respectively. The acceptable ranges for the air-sea exchanges are sensitive to the bounds on the mixing terms and the ranges in these unknowns are better constrained in the second model (Table 5.1). The maximum detrital rain rates are considerably more sensitive to the a priori bounds on the mixing terms than the air-sea exchanges (Table 5.2). In the second model, the maximum detrital rain rates

Table 5.1: The acceptable ranges for the air-sea exchanges determined from the models used in the feasibility study.

Air Sea exchange	Region	Model I		Model II		Model III		Model IV (reference model)	
		MIN	MAX	MIN	MAX	MIN	MAX	MIN	MAX
Fresh water	1	0.04	0.53	0.07	0.33	0.0	0.42	0.0	0.42
(Sv)	2	-0.45	-0.02	-0.3	-0.05	-0.39	0.03	-0.40	0.03
Heat (PW)	1	-0.3	0.3	0.03	0.21	-0.04	0.31	-0.04	0.31
	2	-0.53	-0.11	-0.35	-0.17	-0.39	-0.02	-0.40	0.0
CO_2 (Kmol s^{-1})	1	-170.5	122.1	-132	62	-178	104	-178	105
	2	0	432.8	152	422	0.0	435	0.0	435
O_2 (Kmol s^{-1})	1	218	1749	272	996	-46	1139	-46	1149
	2	-1488	189	-925	85	-1434	253	-1446	253

Table 5.2: The maximum particle flux rate from the surface layer for the models used in the feasibility studies.

Particle Flux (Kmol s^{-1})	Region	Model I	Model II	Model III	Model IV (reference model)
Organic Carbon	1	802.7	452.5	594.6	730.3
	2	592.5	303.6	627.3	771.4
$CaCO_3$	1	355.3	201.4	264.4	275.8
	2	331.8	233.7	298.6	310.2
Opal	1	667.8	413.5	458.7	458.8
	2	134.9	84.5	157.4	157.7

are up to 50% less than the first model. The differences in the first two models for the maximum detrital rain rates provide some indication of the linkage between the unknown detrital rain rates and the unknown mixing terms. The second model shows that with good hydrographic data one does not need to have unreasonably large mixing terms or violate the Ekman transport significantly in order to obtain a feasible solution, as was the case with the Levitus dataset in the North Atlantic (Mémery and Wunsch, 1990)

In the first two models, one assumes that the Ekman transport was well determined but it must be recognized that the Ekman transports in the North Pacific exhibit significant seasonal variability (Table 5.3). Furthermore, there is doubt about the accuracy of these measurements. To account for these effects of seasonal variability and errors in the windstress data, a third model was formulated that allowed the Ekman velocities to vary

Table 5.3: The Ekman transport at 24°N and 47°N calculated from the Hellerman and Rosenstein (1983) monthly windstress measurements.

Section	Minimum (Sv)	Maximum (Sv)	Annual Mean (Sv)
24°N	4.6 (Jan.)	16.8 (Nov)	12.0
47°N	-2.0 (Jun-Jul)	-10.3 (Dec)	-5.8

by $\pm 25\%$ from their annual mean values. With the exception of the increased variance of the Ekman transports, model three is identical to model two. The acceptable range in the air-sea exchanges for model three (Table 5.1) are greater than model two, the heat fluxes range increased by approximately 0.1PW, the CO_2 flux by about 100 Kmol s^{-1}, and the oxygen flux by about 500 Kmol s^{-1}. By increasing the uncertainty in the Ekman transport, the ranges in the air-sea exchanges are still reasonably well-constrained. The maximum detrital rain rates are also greater than model two (Table 5.2). The organic carbon rain rate increased by 300 Kmol s^{-1} and 150 Kmol s^{-1} for regions one and two respectively. The increase in the inorganic carbon and opal rain rates from model two is approximately 60 Kmol s^{-1}.

The fourth model formulated was based on model three but allowed the Redfield ratios between phosphate, carbon and oxygen in the formation/dissolution of organic matter to vary by $\pm 20\%$ from the values given by Takahashi *et al.*, (1985). The acceptable ranges from this model for the air-sea exchanges were nearly identical with model three (Table 5.1). Allowing variable Redfield ratios are not important in determining the air-sea exchanges. The maximum rain rates of detrital material from the

euphotic layer (Table 5.2) are increased from model three. The organic carbon rain rate increased by 130 Kmol s^{-1} for both regions and the inorganic rain rates increased by 10 Kmol s^{-1} for region one. The opal rain rate did not change from model three. The fourth model formulation will henceforth be referred to as the reference model and will be used to further investigate the problem. The reference model makes use of the critical information in the geostrophic shear to constrain the horizontal transports. However, the model does allows some uncertainty in the Ekman transports to account for the seasonal variability in Ekman transports and variability in the Redfield's ratios to reflect uncertainty in the actual values of these ratios.

5.1.2 Tracer Studies

Before discussing the results of the reference model it will be helpful to have an idea of the importance of various tracers in the solution of the reference model. To investigate the effectiveness of various tracer fields, three models were formulated using a subset of the inorganic tracers. The following is a discussion of the solutions obtained from these models.

The first model only conserved mass, heat, and salt and the acceptable ranges for all unknowns in the solution are poorly determined. The acceptable ranges for the freshwater and heat flux into the North Pacific Ocean are -0.07 to 0.88 Sv and -.8 to .88 PW respectively. In part, the large amount of heat gained by the North Pacific can be attributed to the large freshwater flux into the North Pacific. The increased freshwater

flux causes an increased volume transport out of the North Pacific, and associated with this volume transport is an accompanying heat flux. Therefore, an increase in 0.1 Sv in the freshwater flux into the ocean produces an approximate 0.11 PW increase in the heat flux into the ocean. It is interesting to observe that the lower limit for the heat gained by the ocean is more consistent with the heat estimates made by Roemmich and McCallister (1989) of -0.75 PW and by Bryden *et al.*, (1991) of -0.76 PW. Both of these estimates were made using only the TPS24 cruise temperature and salinity data.

The second model conserves mass, heat, salt and silicate. With the addition of silicate to the model, the change in acceptable ranges for freshwater and heat exchanges between the ocean and atmosphere is slightly reduced. The freshwater flux into the North Pacific is -0.06 to 0.71 Sv and the heat flux is -0.60 to 0.27 PW. For this model, the maximum rain rate of opal from the euphotic zone is 304 Kmol s^{-1} (10.6 g Si m^{-2} yr^{-1}) and 530 Kmol s^{-1} (62.4 g Si m^{-2} yr^{-1}) for regions one and two respectively. The maximum rain rates of opal material are about double the values obtained using all of the tracers.

The third model formulated conserved heat, salt, mass, phosphate, oxygen, DIC, and alkalinity. The acceptable ranges from this model for freshwater flux and heat flux into the North Pacific are -0.04 to 0.45 Sv and -0.18 to 0.34 PW. The lower range for the heat flux into the North Pacific is consistent with the model of all the tracers. For this model the maximum rain rate of organic carbon from the euphotic zone is 1250 Kmol s^{-1} and 860 Kmol s^{-1} for regions one and two respectively. The maximum rain rate of inorganic carbon is 350 Kmol s^{-1} (6.8 g C m^{-2} yr^{-1}) and 370 Kmol s^{-1} (21.1 g C m^{-2} yr^{-1}) for regions one and two respectively. Both the rain rate of organic carbon and inorganic

are much greater in region one than for the model with all the tracers, while in region two the rain rates of organic and inorganic carbon have increased slightly.

5.1.3 Sensitivity to Model Layering and Choice of Reference Level

In developing the model several different layerings of the ocean were considered. In general, the effect of the model layering did produce different LSI solutions, however the acceptable ranges for the unknown air-sea exchanges and maximum detrital rain rates were very similar. The only exception to this was if the euphotic zone was defined to be 50 m or shallower. In this case, incompatibilities developed between the phosphate and carbon tracers and the silicate tracer. This was taken as an indication that the euphotic zone must be deeper than 50 m. Measurements compiled by Longhurst and Harrison (1989) place the euphotic depth at 75 m and 95 m for the Station P and the VERTEX location respectively. From Longhurst and Harrison (1989) analysis it is observed that most primary productivity occurs in the upper 100 m.

The reference levels used in the 24° and 47°N sections were varied between 1000 m and the ocean bottom. Again the LSI solution was sensitive to the prescribed reference level, and the fit to the data for these models varied significantly. The reference levels were chosen such that the chi-squared error of the LSI model was the smallest. The acceptable ranges for the air-sea exchanges and maximum detrital rain rates were not very

sensitive to the prescribed reference level. They all produced results similar to the reference model.

5.2 MODEL RESULTS

To help visualize and assess the standard model, I will first present the LSI solution of the model. This solution was obtained by minimizing the errors in the conservation equations in a least squares sense while being consistent with the inequality constraints on the conservation equations and the bounds on the unknowns. The equations in the model are weighted by the same errors used for the LP model. The solution calculated from this model was not unique but the minimum objective function was. This means that I have selected one solution produced by the model. This limitation does not affect the meridional transports but the effect on the mixing coefficients and detrital rain rates are more obvious and will be discussed below.

The meridional transport shown in Figure 5.1 is consistent with the general idea of meridional circulation in the North Pacific. In the bottom layer, AABW enters the North Pacific (NP); in layer 5, NPDW leaves the NP; and in layer 4, AAIW enters the NP. The NPDW is formed by the mixing of AABW and AAIW in both regions one and two. In the upper layers, the flow pattern is more confusing, reflecting the more zonal circulation in these layers. Two interesting features in the surface layer are the convergent flow in the subtropics and the upwelling of NPIW into the euphotic layer in

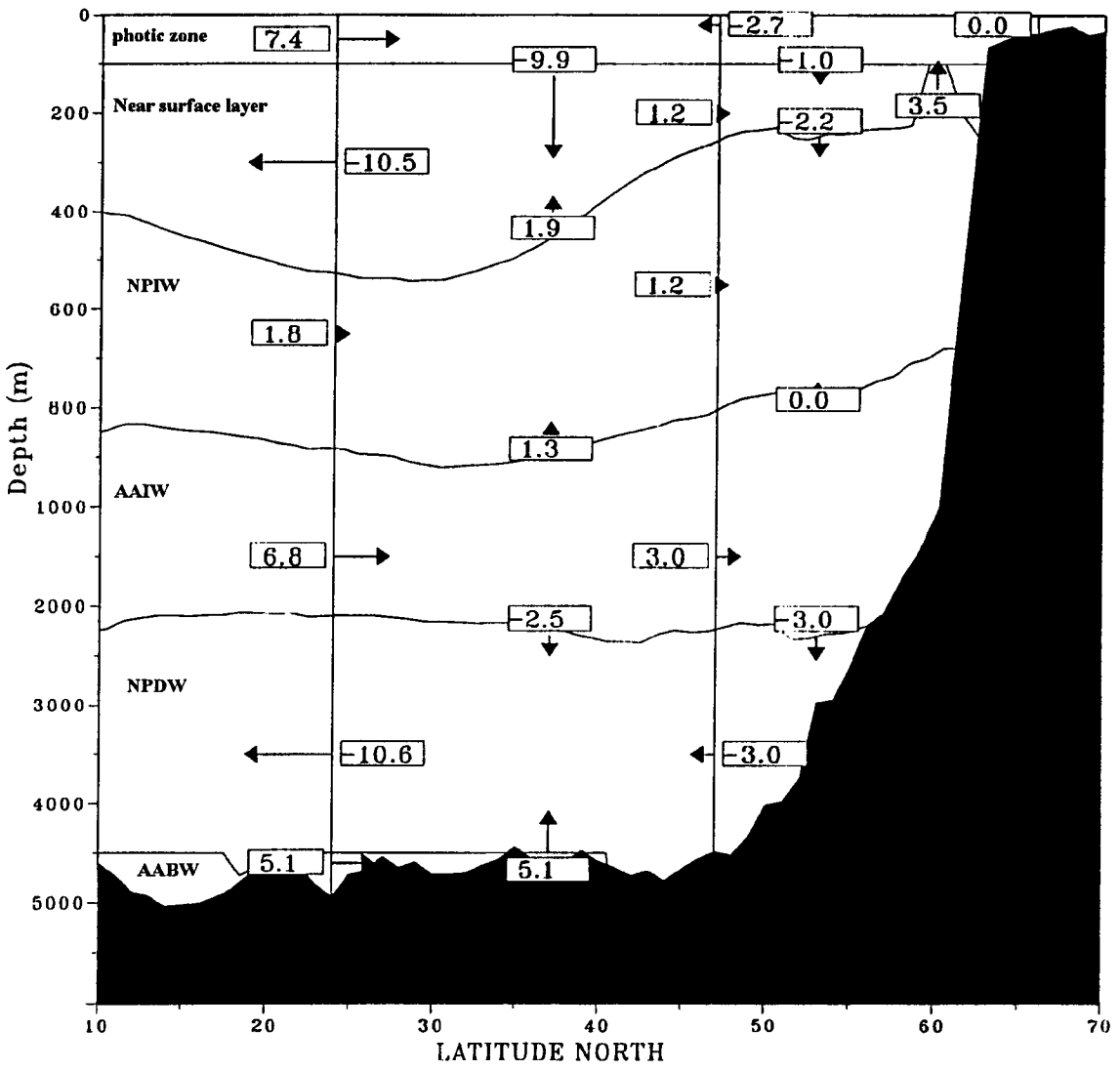

Figure 5.1: The integrated meridional transports calculated from the least squares solution in Sv.

the subarctic. In this model, the flow of water through the Japanese Sea into region two is 2.35 Sv. The outflow of water through the Bering Sea is at its lower bound of 0 Sv. The air-sea exchanges are summarized in Figure 5.2a-d. The freshwater fluxes for this model are small but the direction of the fluxes is consistent with the estimates of Baumgartner and Riechel (1975). The subarctic ocean gains freshwater while the subtropical ocean losses freshwater. The solution shows that heat leaves the ocean in the subtropics and enters the ocean in the subarctic. The values are in reasonable agreement with the bulk formula estimates of the annual mean air-sea heat fluxes calculated by Clark and Weare *et al.*, (Talley 1984). The net loss of heat by the North Pacific ocean at 24°Nis 0.1 PW. In the subarctic ocean there is a small outgassing of CO_2 into the ocean (0.005 Gt C yr^{-1}) but the North Pacific ocean is a net sink of atmospheric CO_2 (0.07 Gt C yr^{-1}). Oxygen outgasses into the atmosphere in the subtropics but enters the surface water of the subarctic. The flux of oxygen into the subarctic ocean is cause by the divergence in the horizontal and vertical oxygen transport of ocean in the surface layer.

The mixing coefficients calculated from the least squares inversion are in general small (Fig. 5.3). The notable exceptions are the large horizontal mixing terms in the surface layer of the subarctic Pacific and the large diapcynal mixing terms in the bottom layer of the subtropics region, and between layers 3 and 1 in the subarctic region. Both the horizontal mixing term for the Bering Sea and the mixing term between layers 1 and 3 are at their upper-bound limit. The relatively small values for the mixing terms are reflected in the equally small values for detrital rain rates. The total rain rates from the

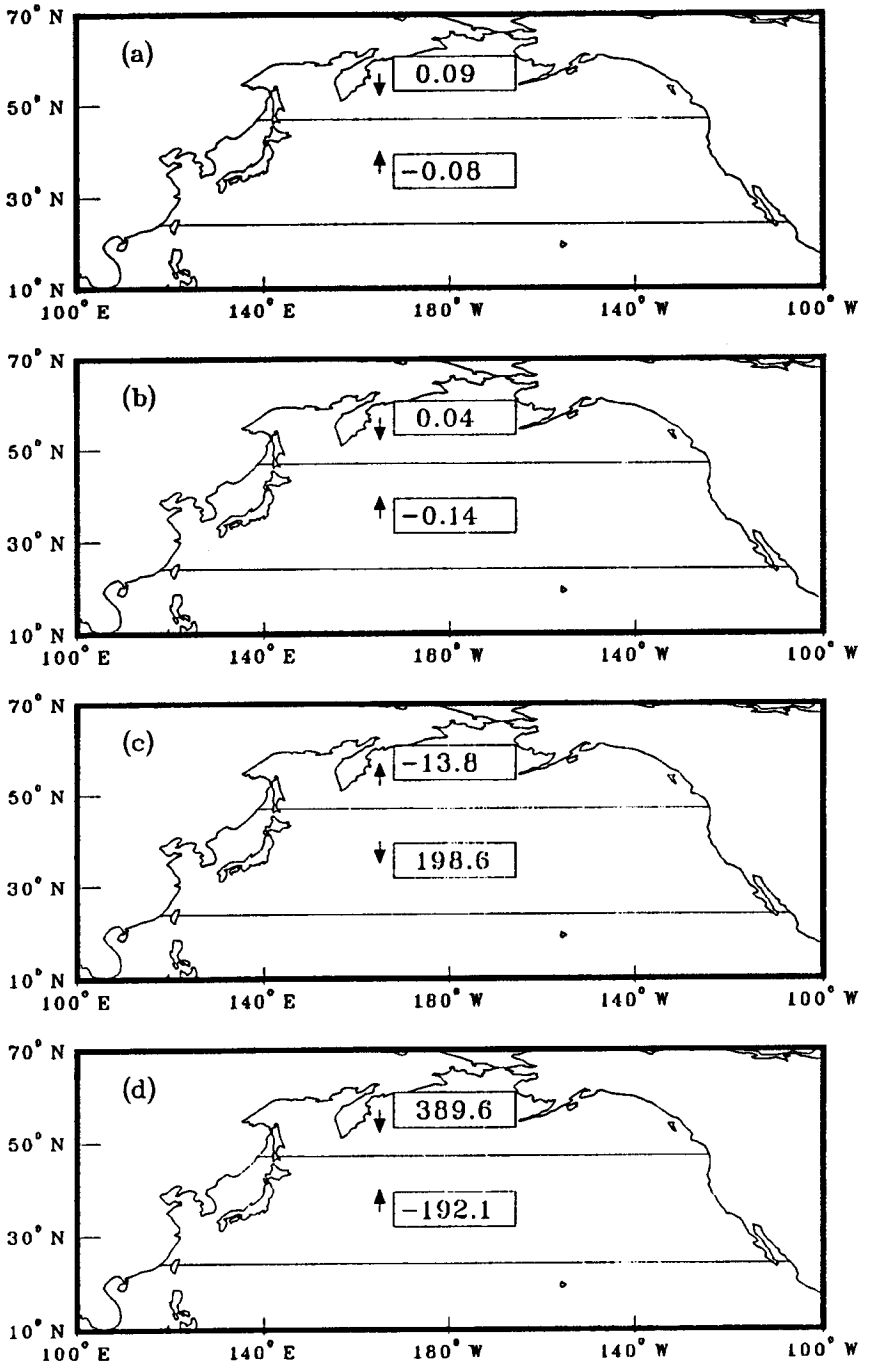

Figure 5.2: Maps of air-sea exchanges for a) freshwater (Sv), b) heat (PW), c) CO_2 (Kmol s^{-1}) and d) O_2 (Kmol s^{-1}) from the least squares solution.

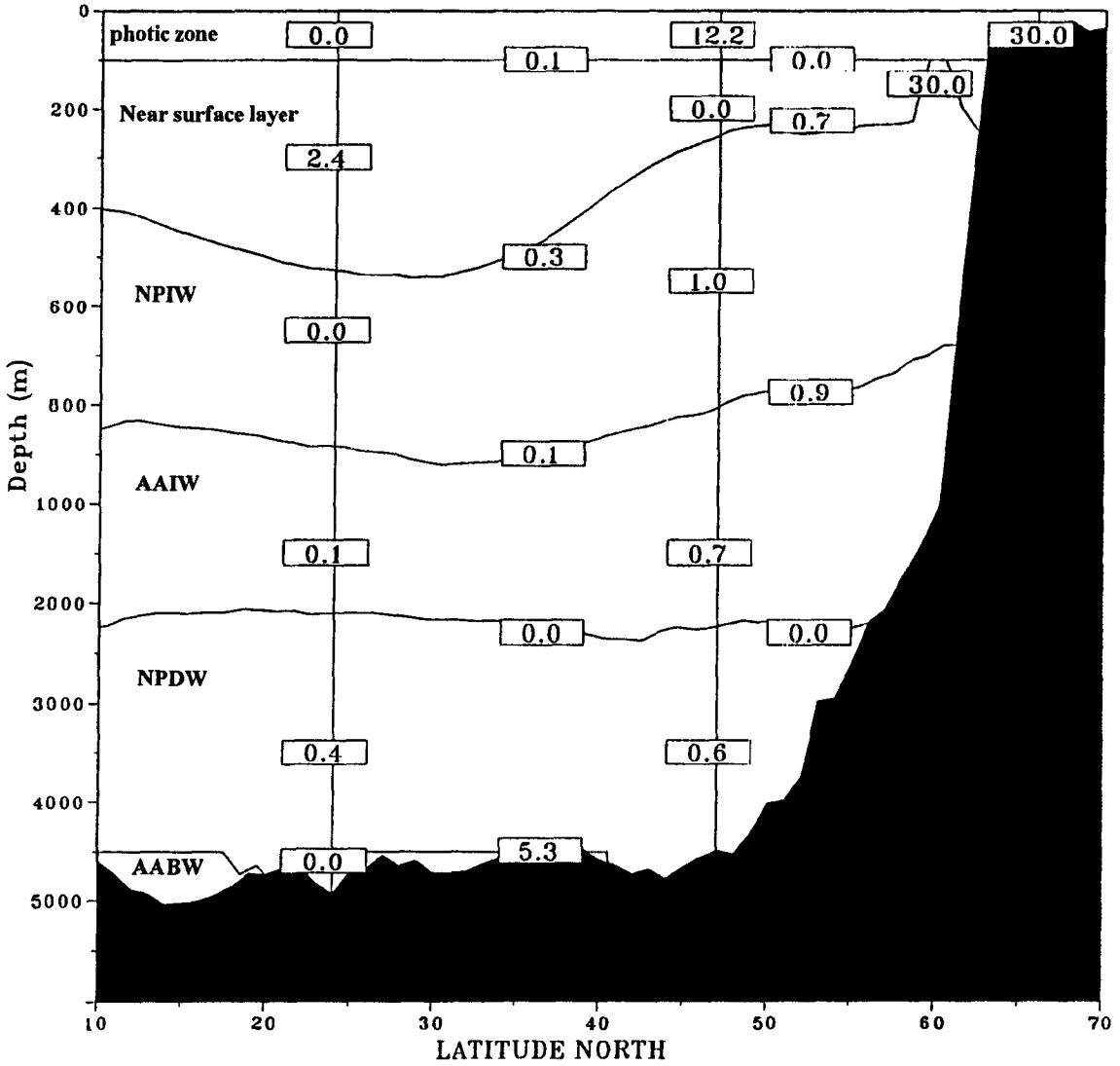

Figure 5.3: The mixing coefficients from the least squares solution, the isopycnal coefficients are in 10^4 m^2 s^{-1} and the diapycnal coefficients are in cm^2 s^{-1}.

surface layer for organic carbon, inorganic carbon and opal in the North Pacific are 97, 49 and 74 Kmol s^{-1} respectively. The algorithm used to solve the least squares problem has a tendency to place poorly constrained unknowns at their a priori bounds. This tendency is reflected in the mixing and detrital rain rates by the fact that most of these unknowns are at the a priori bounds and implying that the model has difficulty determining these unknowns.

5.2.1 Meridional Transports

Schlitzer (1988) showed that the specification of the geostrophic fluxes across a section does not determine the integrated layer transports through the section completely. The upper and lower bounds of the integrated layer transports depend on bottom topography, layer thickness along the section, bounds on the reference velocities and the tracer constraints. The upper and lower bounds of the zonally-integrated layer transports and diapycnal water fluxes have been calculated by using the linear programming routine with the appropriate objective functions. The results of these calculations are summarized in Figure 5.4. Typically the average of these ranges is comparable to the least squares solution in Figure 5.1. The meridional circulation pattern in the deep ocean is the samefor all possible solutions. AABW flows northward through the bottom layer of 24°N into the subtropical region where it mixes with AAIW and produces the NPDW which leaves the North Pacific through layer 5. The model does not show any deep water formation in the North Pacific.

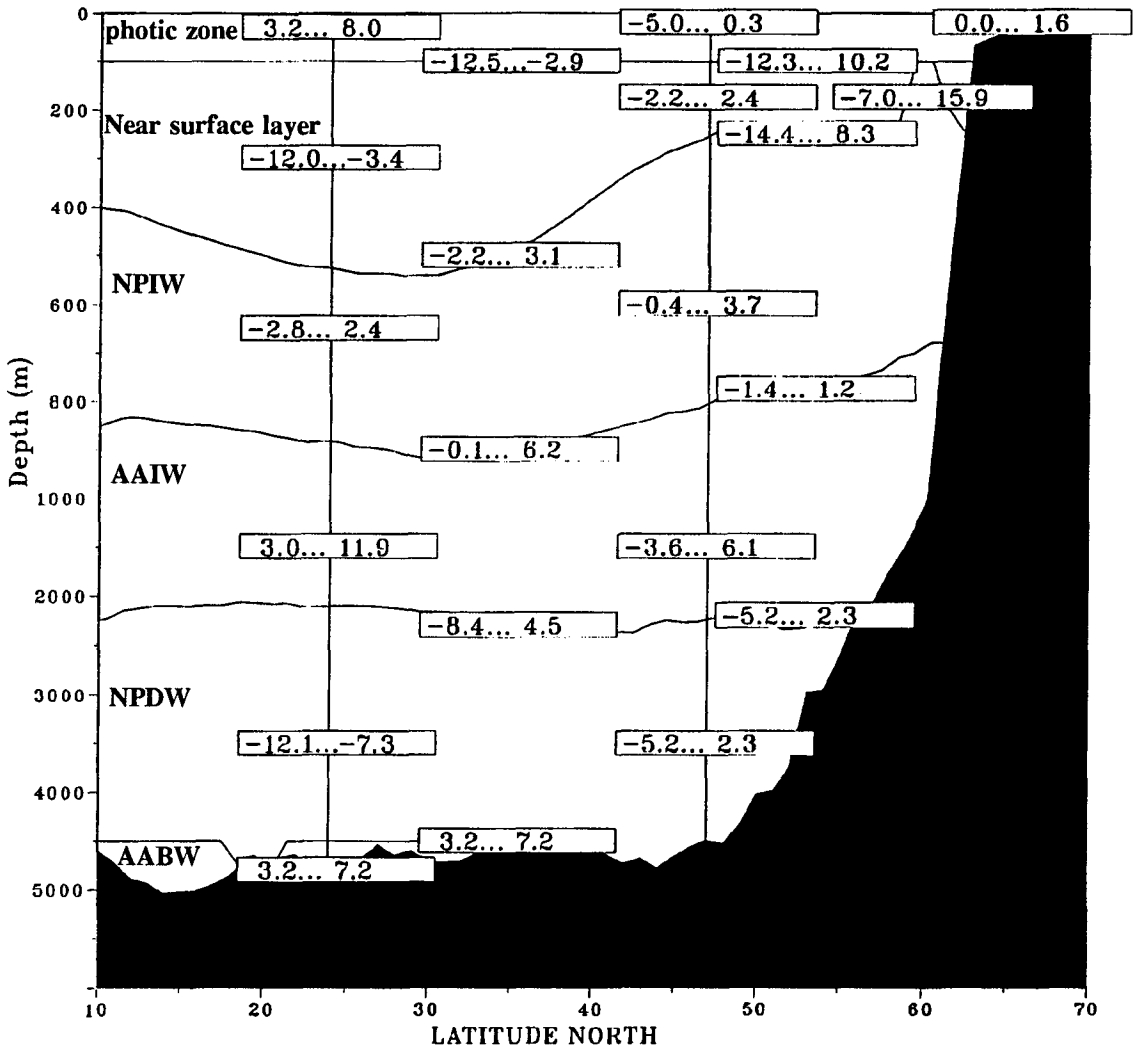

Figure 5.4: The acceptable bounds on integrated meridional transports in Sv.

The meridional water transports of the model and the results of other studies are compared in Table 5.4. The deep water transports across the 24°N section agree well with Bryden *et al.*, (1991) estimates. The northward transport of AABW determine by the inverse model also agrees with the transports of 8.4 Sv estimated by Johnson (1992) at 10°N.

In the upper layers the meridional circulation pattern is more confusing reflecting the more zonal circulation pattern of the upper ocean in the North Pacific. From the model the Kuroshio transport through 24°N is 25±5 Sv.

5.2.2 Freshwater transport

The minimal and maximal freshwater fluxes into the surface layer of the model are shown in Figure 5.5a. The freshwater input in the subarctic ocean is nearly balanced by a freshwater flux into the atmosphere in the subtropics. For comparison with freshwater flux estimates of Baumgartner and Riechel (1975), I have plotted their northward transport of freshwater along with the range of values determined by the model (Fig. 5.6). At 47°N the agreement between the two measurements is good but at 24°N the two measurements show a distinct difference in magnitude. McBean (1989) points out that care must be exercised in interpreting the freshwater estimates, such as Baumgartner and Riechel

Table 5.4: A compilation of meridional layer fluxes across 24°N.

	Section 1: 24°N		
Water Mass	Bryden[1]	Roemmich[2]	this study
AAIW	4.3		3.0 ... 11.9
NPDW	-8.4	-10.0	-12.1 ... -7.3
AABW	4.9	10.0	3.2 ... 7.2

[1]Hydrographic data from cruise TPS24 and the fluxes calculated by Bryden *et al.*, (1991).
[2]Hydrographic data from cruise TPS24 and the fluxes calculated by Roemmich and McCallister (1989).

(1975), due to the inherent difficulties in calculating the evaporation and precipitation values over the open ocean.

5.2.3 Heat Transport

The bounds on the air-sea exchange of heat are shown in Figure 5.5b. The air-sea exchanges of heat calculated from the model show that the subtropics can act as a important source of heat for the atmosphere. The heat flux into the atmosphere in the subtropical Pacific is in part balanced by a heat gain by the subarctic Pacific.

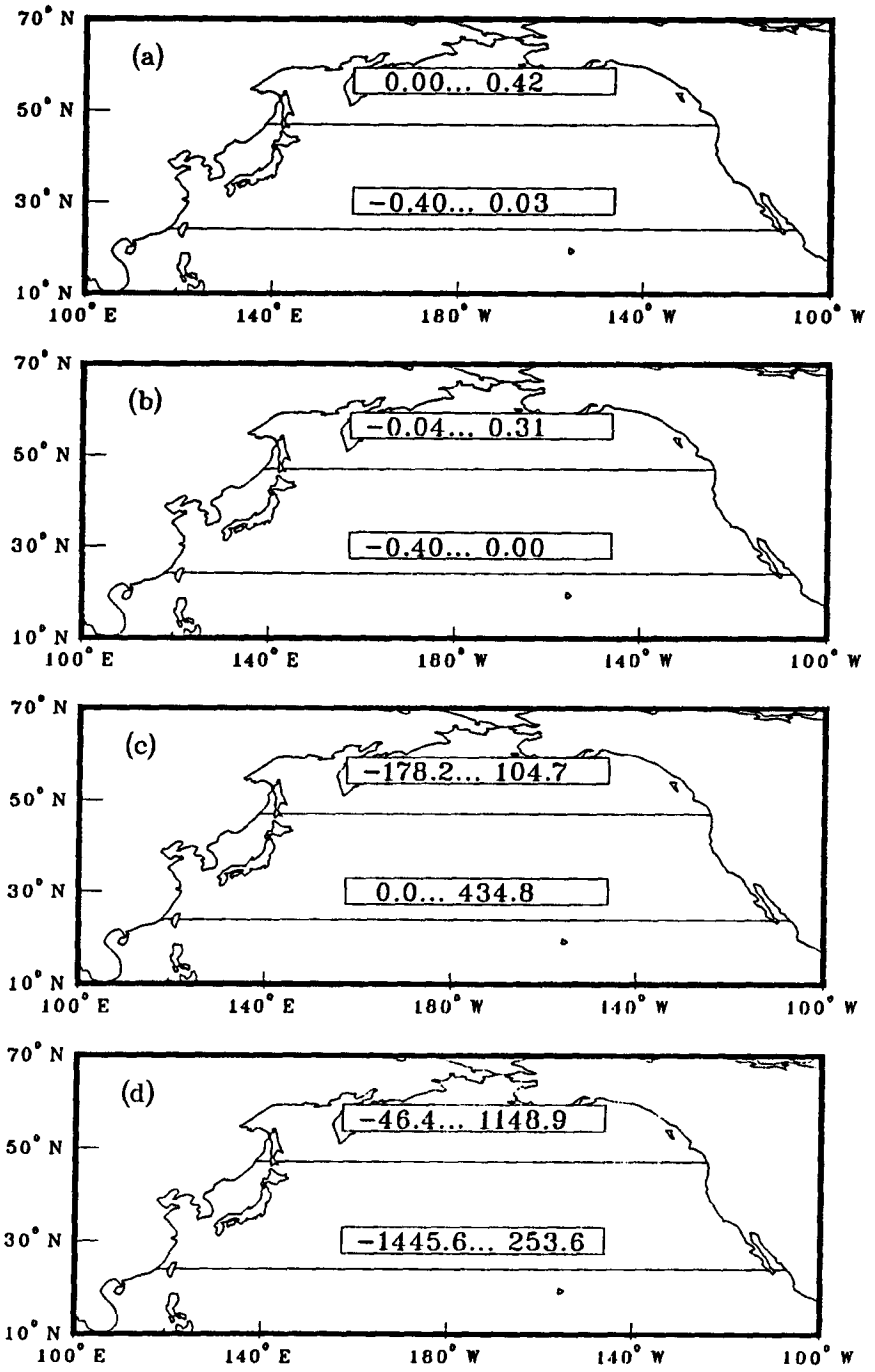

Figure 5.5: Maps of the bounds on the air-sea exchanges for a) freshwater (Sv), b) heat (PW), c) CO_2 (Kmol s^{-1}) and d) O_2 (Kmol s^{-1}).

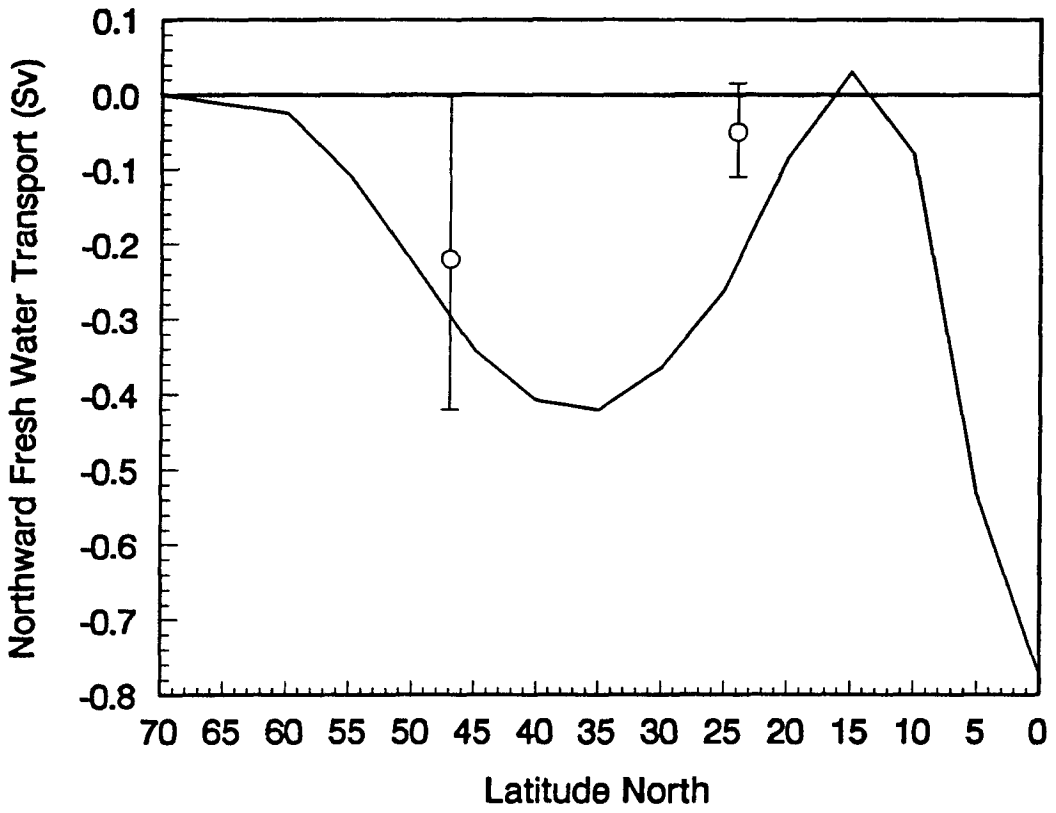

Figure 5.6: The meridional freshwater transport calculated from the model compared to the estimates of Baumgartner and Riechel (1975).

The meridional northward heat transport in the Pacific computed by Talley (1984) using Esbensen and Kushnir (1981), and Clarke and Weare *et al.*, (1981) heat flux measurements demonstrates even uncertainty in the sign of the northward heat transport in the Pacific (Fig 5.7a). The two curves for Clarke and Weare *et al.*, show the difference if the data poor regions of the Bering Sea and Sea of Okhotsk are neglected. The need to neglect these regions arises from the idea that the data are seasonally biased and shows a significant and unexpectedly large annual heat gain by these regions. The meridional heat transports determined by the model are plotted along with the heat transports calculated from Clarke and Weare *et al.*, by Talley (1984) (Fig 5.7b). The direct estimates of heat transport estimates of Bryden *et al.*, (1989), Roemmich and McCallister (1989), and McBean (1991) are also included in this Figure. At 47°N, the model results are consistent with the other measurements but the model does allow significantly more equatorial heat transport. The heat transport measurements at 24°N show considerably greater variability. Bryden *et al.*, (1989) calculated a northward heat flux of 0.76 PW, which is in better agreement with the values of EK in Figure 5.7a. My model estimate also shows a northward heat flux of about 0.2 PW, slightly greater than the measure from C WE. The comparison with Bryden *et al.*, (1989) measurement is of interest because both estimates were obtained using the TPS24 section but using different calculations. Bryden *et al.*, (1989) used a traditional station pair calculation using the temperature data from the

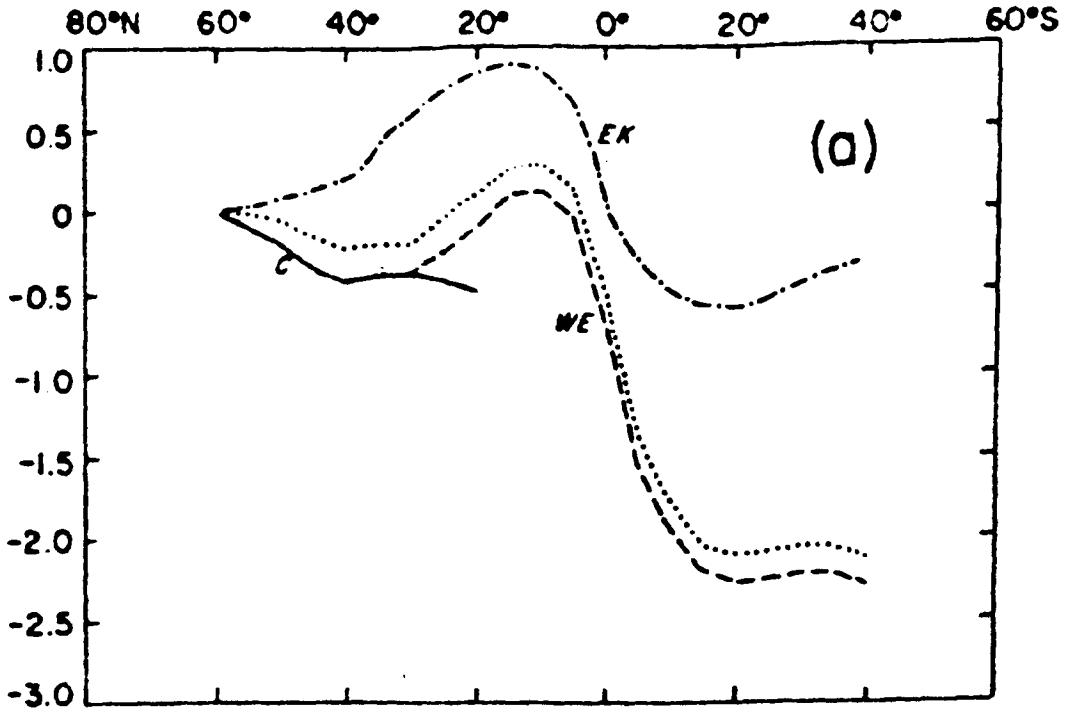

Figure 5.7: The annual mean meridional heat transport in the Pacific Ocean. (a) The values calculated by Talley (1984) for the heat fluxes of Clark and Weare *et al.*, (solid, dash and dot) and Ebsensen and Kushnir (dot-dash). The heat transport at 60°N is assumed to be zero. The solid curve is based on Clark's heat fluxes. The long dashes are based on heat fluxes of Weare *et al.*: The middle dotted curve deletes heat fluxes in the Bering Sea and Sea of Okhotsk. (b) The heat fluxes calculated from the model along with the direct estimates of heat by Roemmich and McCallister (1989) (RM), McBean (1991) (M), and Bryden *et al.*, (1989) (B), and for comparison the middle dotted line from (a) has been redrawn.

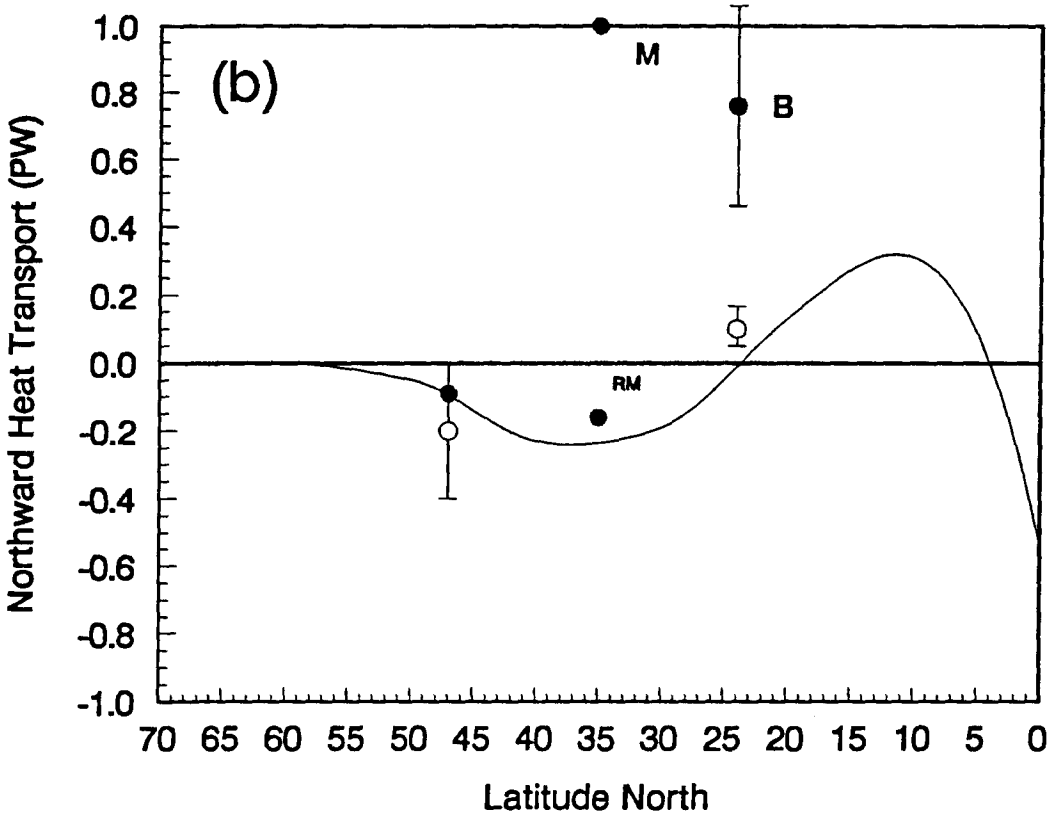
(b)
M
B
RM
Northward Heat Transport (PW)
1.0
0.8
0.6
0.4
0.2
0.0
-0.2
-0.4
-0.6
-0.8
-1.0
70 65 60 55 50 45 40 35 30 25 20 15 10 5 0
Latitude North

synoptic section for the heat transport; I averaged many different datasets to obtain the average temperature in the six layers along the section. In my calculation I employ a diffusive transport to parameterize the eddy transports. In the model run that only conserved mass temperature and salinity, the maximum northward heat transport is much larger (0.8 PW), negating the discrepancy between the two estimates. This suggests that the differences in the way we calculate the heat transport are not that significant. The smaller northward heat transport determined by the reference model is a direct result of the model trying to satisfy the conservation of phosphate, oxygen, DIC, alkalinity and silicate.

5.2.4 Air-sea exchange of CO_2

The model results for the bounds on the carbon input into the North Pacific are shown in Figure 5.5c. In the subtropics, the ocean can take up 0 to 0.2 Gt C yr^{-1}. The sign of the subarctic CO_2 air-sea exchange is uncertain but the exchange is not large (-0.07 to 0.04 Gt C yr^{-1}). As alluded to in the discussion of the ΔpCO_2 maps, the ΔpCO_2 data is questionable and incomplete in the subarctic Pacific making it difficult to draw conclusion from this data. The CO_2 fluxes calculated at station P showed that this point was a weak sink of atmospheric CO_2 of 0.7 mol m^{-2} yr^{-1} (Wong and Chan, 1991) or 0.06 Gt C yr^{-1} for the entire subarctic region of the model. The estimate of the CO_2 flux of Wong and Chan for the entire subarctic region is comparable to the model results. Wong and Chan data showed that the ocean at Station P could be a weak or neutral source of

CO_2 in July and August and predominantly a CO_2 sink in other months. Wong and Chan believe the temporal variation in the gas exchange of CO_2 in the eastern subarctic Pacific water around Station P may differ from that of other oceanic areas in the high northern latitudes. In the Bering Sea and the northwest subarctic Pacific the summer depression of pCO_2 in the surface water may exceed 100 μatm (Kelly and Hood, 1971; Gordon *et al.*, 1973; Wong, unpublished data). The strong summer sink of CO_2 in the Alaska gyre and Bering Sea is demonstrated in the pCO_2 maps of Tans *et al.*, (1990) that are redrawn in Figure 4.11. The net degassing of CO_2 from the North Pacific of 5 mol m^{-2} y^{-1} (1.9 Gt C yr^{-1} for the subarctic region of the inverse model) was calculated by Thomas *et al.*, (1988) using the seasonal programme data of Takahashi *et al.*, (1986). The critical factor observed by Thomas *et al.*, (1988) in the calculation of the air-sea flux of CO_2 was the need to use seasonally-sampled Δp_{CO2} data in deriving the annual fluxes.

In the subtropical region, the inverse model calculated a maximum of 0.2 Gt C yr^{-1} enters the Ocean. For the entire North Pacific region of the model, the bounds on the air-sea exchange of CO_2 are between 0-0.2Gt C yr^{-1}. Tans *et al.*, (1990) calculated that the North Pacific (>15°N; 110°E to 90°W) takes up 0.06 Gt C yr^{-1}. Although my maximum acceptable uptake of CO_2 is slightly larger than Tans *et al.*, estimate, it clearly shows that the North Pacific Ocean is not a significant sink of atmospheric CO_2. The results of the budget methods used in this model do show that this technique is able to make reasonable estimates of CO_2 uptake in large regions ($\pm$0.1GT C yr^{-1}). Recall from chapter two that the estimated air-sea exchange from the INDOPAC section was 0.05 $\pm$ .2 Gt C yr^{-1} for the North Pacific north of 35°N, which is very consistent with the inverse model.

5.2.5 O_2 gas exchange rates

The calculated bounds on the O_2 gas exchange rates between the ocean and atmosphere are shown in Figure 5.5d. In general, the subarctic Pacific can act as a large sink of atmospheric O_2 while in the subtropics, the North Pacific is an even bigger source for atmospheric O_2. The bounds on the O_2 gas exchange rate for the North Pacific region of the model are -467 to 497 Kmol s^{-1}. An obvious difference between the air-sea exchange of O_2 and CO_2 is the much larger ranges for the O_2 exchanges. The acceptable ranges for O_2 are more than four times greater than the CO_2 ranges. This demonstrates the difficulty the model has in determining the gas exchange rates of O_2.

At Station P in the northeast subarctic Pacific Ocean, Thomas *et al.*, (1990) calculated a net O_2 degassing of 5.6 mol m^{-2} yr^{-1} from monthly average gas transfer coefficients and O_2 concentrations. Thomas *et al.*, concluded from this data that the measured flux was uncertain due to undersampling and the uncertainty and natural variability of O_2. The one-dimensional modelling results of Thomas *et al.*, (1989) suggest that this degassing is the O_2 produced by biological activity in the mixed layer. However, the modelling was not able to provide a robust estimate of the annual air-sea exchange of O_2. Their modelling results suggest that episodic events modify the O_2 content by up to 4 mol m^{-3} in the mixed layer but that gas exchange later draws this content back towards a smooth evolution curve. This suggests that highly sampled O_2 data are necessary to resolve the gas exchange between the ocean and atmosphere. The inverse model results show that the subarctic region is a sink, 6.3 to -1.1 mol m^{-2} yr^{-1} of atmospheric O_2,

opposite in sign to the Thomas *et al.*, (1989) measurements from Station P. The input of O_2 into the subarctic region of the model is the result of a divergence in the O_2 horizontal transport in this region.

5.2.6 Mixing terms

Figure 5.8 shows the minimal and maximal values of the isopycnal and diapycnal mixing coefficients in the model solutions. The lower bounds in all the mixing coefficients are limited only by the a priori bound of zero. The upper bounds on the magnitude of the mixing coefficients are reasonable with the exception of the bottom layer at 24°N and the Bering Sea. The model does a reasonable job of resolving the isopycnal mixing terms. Profiles of the isopycnal mixing coefficients maximum bounds display a maximum value in the surface layer and a nearly constant or decreasing value with depth (except for the bottom layer of region one) (Fig. 5.9).

The upper bounds of the diapcynal mixing coefficients appear to be resolved by the model with the exception of the deep water and in the outcropping of layer 3 with 1 where the values attain their a priori bound of 10 $cm^2\ s^{-1}$. Profiles of the maximum diapycnal

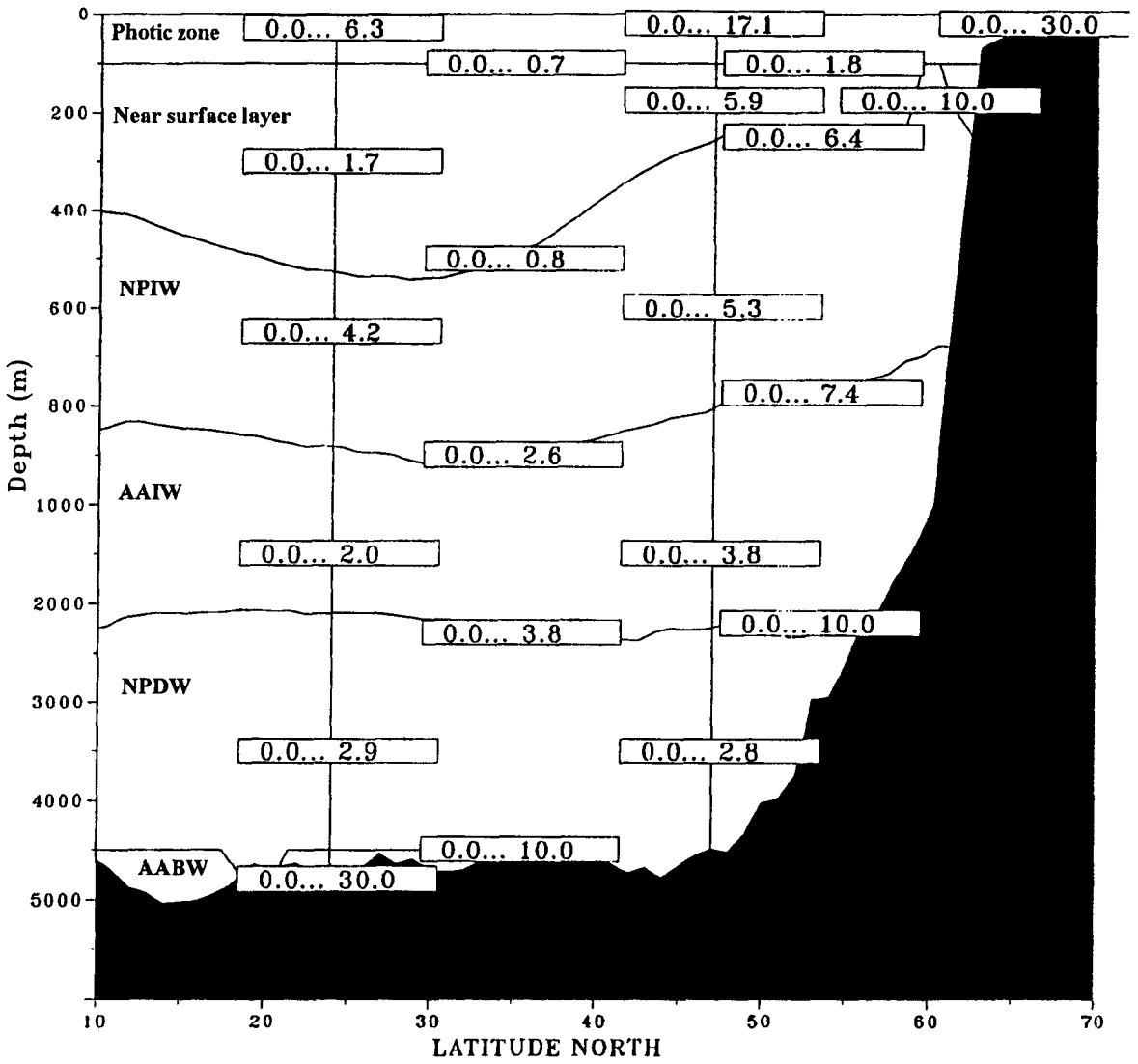

Figure 5.8: The bounds on the mixing coefficients, the units of the isopycnal and diapycnal coefficients are 10^4 m^2 s^{-1} and cm^2 s^{-1} respectively.

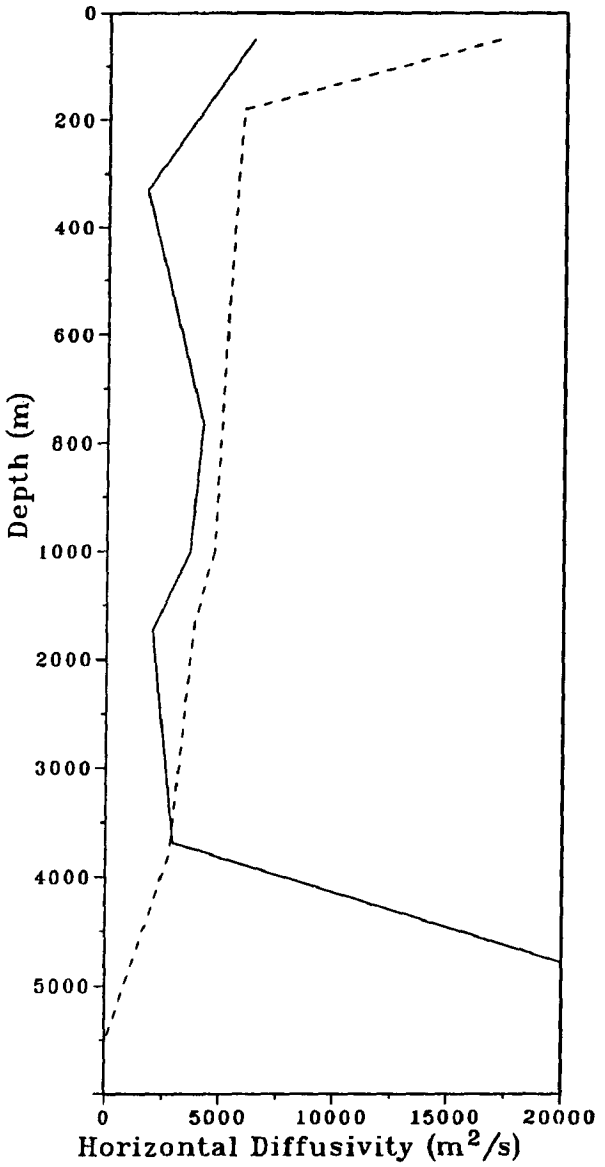

Figure 5.9: Profiles of the maximum bounds on the isopycnal mixing coefficient for a) subtropical region (solid line) and subarctic region (dashed line).

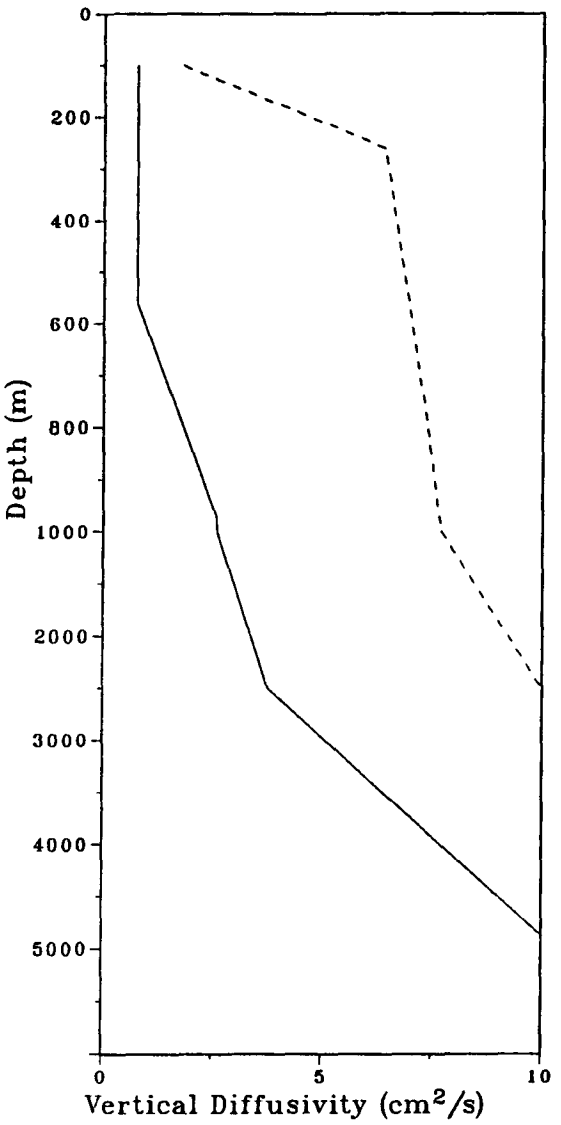

Figure 5.10: Profiles of the maximum bounds on the diapycnal mixing coefficient for the subtropical region (solid) and subarctic region (dash).

mixing coefficient show an increase in value with depth (Fig. 5.10). In region one the increase in mixing is quite gradual, however in region two, the diapycnal values increase rapidly in the upper two layers and then remain relatively constant.

The model's ability to determine the isopycnal and diapycnal mixing coefficients seems to depend on the relative size of the tracer fluxes induced by mixing compared with the advective tracer fluxes and thus depends on the size of the horizontal and vertical tracer gradient. The vertical and horizontal gradients in the upper ocean are large enough that varying the mixing coefficients has a significant effect on the tracer budgets, and consequently those mixing coefficients are well-determined. However in the deeper water, the vertical gradients are small and larger diapycnal mixing coefficients are necessary to produce significant differences in the tracer budgets. This explains why one sees a narrow range of diapycnal mixing coefficients in the upper ocean and a much larger range in the deeper layers. This same argument can be employed to explain the large coefficients of the isopycnal mixing in the Bering Sea and in the bottom water and the large diapycnal mixing coefficient in the outcropping of NPIW with the euphotic layer. The relatively small areas through which mixing occurs for these coefficients demands that much larger mixing coefficients are required in order for these transports to significantly affect the tracer budgets.

The solutions with the smallest and largest overall diapycnal and isopycnal mixing have also been calculated ($\phi = \sum kv, \sum kh$). The results of minimizing the diapycnal coefficients are that the mass, heat, salt, nutrient and carbon balances can be achieved with no diapycnal mixing and small particle fluxes. The solution with the maximum

diapycnal mixing coefficients also produces a solution with large particle fluxes. The linkage between the particle fluxes and diapycnal mixing is a reflection of the increase in nutrient concentrations with depth. This allows the downward transport of nutrients by particle fluxes to be compensated by the upward transport of nutrients by diapycnal mixing. By minimizing the isopycnal mixing coefficients, one generates a solution that requires very little mixing; only the surface layer has non-zero isopycnal mixing coefficients. This solution also has almost no particle fluxes. The solution that maximizes the isopycnal mixing coefficients generates a solution that has large particle fluxes.

5.2.7 New production

New production in the model has been studied by calculating the solutions that minimize and maximize the amount of organic carbon leaving the surface layer as detrital rain. Figure 5.11a shows the maximal values of new production in the model domain. The minimum values are zero for new production which is a reflection of the model's inability to constrain the lower bounds of the mixing terms. The maximum values of new production for the subarctic and subtropical North Pacific are 730 Kmol s^{-1} (42 g C $m^{-2}y^{-1}$) and 771 Kmol s^{-1} (12 g C m^{-2} yr^{-1}) respectively. This geographic pattern of the maximum new production is consistent with measurements of primary production (Koblentz-Mishke *et al.*, 1970 and Berger *et al.*, 1989). For comparison with the model output, estimates of the primary and new productions are shown in Table 5.5. Before

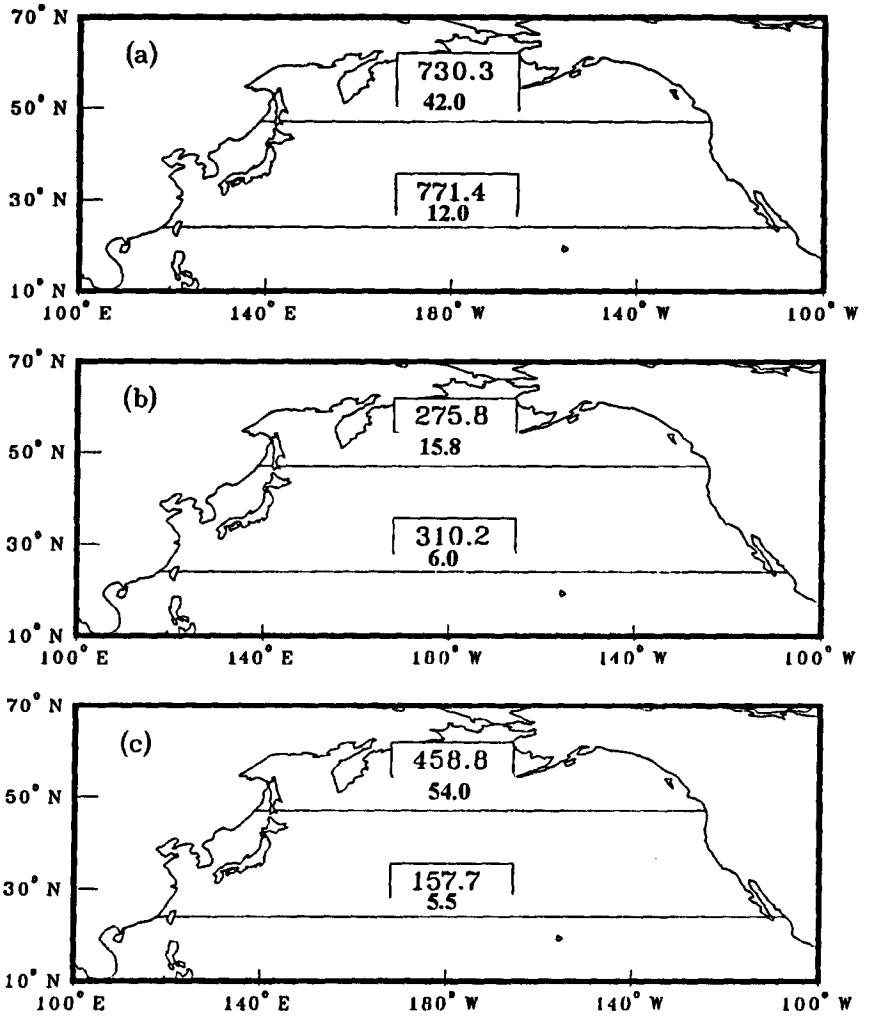

Figure 5.11: Maps of the maximum particle fluxes from the surface layer of the model for a) organic carbon, b) inorganic carbon, and c) opal. The top number is in Kmol s^{-1} and the bottom number is in mol m^{-2} yr^{-1}.

Table 5.5: Select production data for the North Pacific.

Location	Primary Production gC m^{-2} y^{-1}	New Production gC m^{-2} y^{-1}	f-ratio	Reference
Subtropic Ocean (Oligotrophic)	26	1.6	0.06	Eppley and Peterson (1979) [1,2]
Subtropics to Subpolar	51	6.6	0.13	Eppley and Peterson (1979) [1,2]
Subpolar	73	13.1	0.18	Eppley and Peterson (1979) [1,2]
Inshore	124	37.2	0.30	Eppley and Peterson (1979) [1,2]
Open Ocean Pacific	55	7.7	0.14	Eppley and Peterson (1979) [1,2]
N.E. Pacific (oligotrophic water)	130	18	0.14	Martin *et al.* 1987 [3]
N.E. Pacific Coastal Regions	250	42	0.17	Martin *et al.* 1987 [3]
N.E. Pacific (oligotrophic water)	121.4	13-17	0.11-.014	Knauer *et al.*, 1990 [3]
Subarctic North Pacific	219 - 365			Miller (1988) [4]
Bering Sea		100*	~1	Codispoti *et al*, 1986

[1]primary productivity data from Platt and Subbaa Rao (1975) and an empirical relationship between primary productivity and new productivity.
[2]primary productivity derived from the Koblentz-Mishke *et al.*, (1970).
[3]sediment trap data from the VERTEX experiment.
[4]productivity measurements from the SUPER experiment
*one spring bloom

Table 5.6: A variety of productivity measurements from Station P (50°N and 145°W).

McAllister (1969)	Maximum primary production	136 g C m^{-2} yr^{-1}
	Minimum primary production	12 g C m^{-2} yr^{-1}
	Peak production	July
Wheeler and Kokkinakis	f-ratio, June 1987	0.38 ± 0.06
(1990)	f-ratio, September 1987	0.52 ± 0.27
	f-ratio, October 1987	0.39 ± 0.11
	f-ratio, May 1988	0.41 ± 0.12
	f-ratio, August 1988	0.25 ± 0.05
Wong (unpublished)	primary production, August 1987	200 to 310 g C m^{-2} yr^{-1}
	annual mean particle flux, 200 m	5.6 g C m^{-2} yr^{-1}
	annual mean particle flux, 1000 m	2.7 g C m^{-2} yr^{-1}
	annual mean particle flux, 3800 m	1.3 g C m^{-2} yr^{-1}

comparing the model results of new production with the estimates given in the Table 5.5, it will be useful to first discuss these measurements in more detail. The global estimates of primary production have increased since about 1980 and new production even more. For example, several authors have suggested that the annual average f-ratio (new production/primary production) for oligotrophic central oceans may be higher than the 0.06 value for the oligotrophic central gyres proposed by Eppley and Perterson (1979).

Recent estimates from station P for the f-ratio in the summer and early fall (Table 5.6) produce much larger values than the f-ratio of 0.18 proposed by Eppley and Peterson for the subpolar ocean. These larger values for the f-ratio in part reflect the time of the year the measurements were made. During the year when the productivity is greater than the average annual mean value one expects the corresponding f-ratio to also be greater than the annual mean value. Production studies in the VERTEX program in the northeast Pacific by Martin *et al.* (1987) and Knauer *et al.* (1990) have much higher values of primary production and new production (Table 5.5) than earlier estimates by Eppley and Peterson (1979). In view of the present discrepancy in the literature, the values of primary production and new production require further study.

The average of the upper and lower bounds of new production from the model are greater than the values proposed by Eppley and Peterson but are less than newer estimates from oligotrophic water of the northeast Pacific. Modelling the O_2 cycle at Station P, Thomas *et al.*, calculated the new production to be 30 to 88 g C m^{-2} yr^{-1} (C/O=172/106). Wong (unpublished) calculated at Station P the primary productivity to 200 - 310 g C m^{-2} yr^{-1} for August 1987. Using the f-ratio calculated by Wheeler and Kokkinakis (1990) for August 1988, the estimated new production from Wong data is 50 - 70 g C m^{-2} yr^{-1}. From the values presented above it is clear that large differences exist in the estimates of primary and new production. In part, the difficulty in comparing measurements arises from the measurements different spatial and temporal sampling. The inverse model results for new production in the subarctic and subtropic Pacific are, in general, consistent

with various measurements; they are greater than the Eppley and Petersons estimates but less than some of the newer estimates from Station P and the VERTEX experiments.

5.2.8 Particle fluxes

The minimum and maximum particle fluxes of organic carbon, $CaCO_3$ and opal through each layer have been determined. For all the particle fluxes, the minimum value is zero. Figure 5.12 shows profiles of the maximum detrital rain rate of particulate organic carbon (Fig. 5.12a), $CaCO_3$ (Fig. 5.12b) and opal (Fig. 5.12c). Flux densities can be derived by dividing the rain rates by the surface area of the two regions; the surface areas of region one and two are 2.48×10^{13} m^2 and 7.4×10^{12} m^2 respectively.

The particle flux of organic carbon at 100 m is equal to the value of new production discussed in the previous section. The model results show a decreasing value of particle flux with depth; region two particle flux decreases faster with depth than region one. To get an idea of the values of the molecular ratios linking the particle flux of C,P and O that were being generated by the model, I looked at the solutions that maximized the particle flux of: 1) organic carbon, 2) phosphate, and 3) oxygen utilization. One, for the solution that maximized the particle flux of organic carbon, the $-O_2/P$ ratio equalled 170. The value shows good agreement with the value suggested by Takahashi *et al.*, (1985) and Broecker *et al.*, (1985). Two, the solution for the maximum particle flux of phosphate produced a C/O_2 ratio of -1.36. Three, the solution that maximized the oxygen utilization flux had a C/P ratio of 125. The three values determined in this manner are

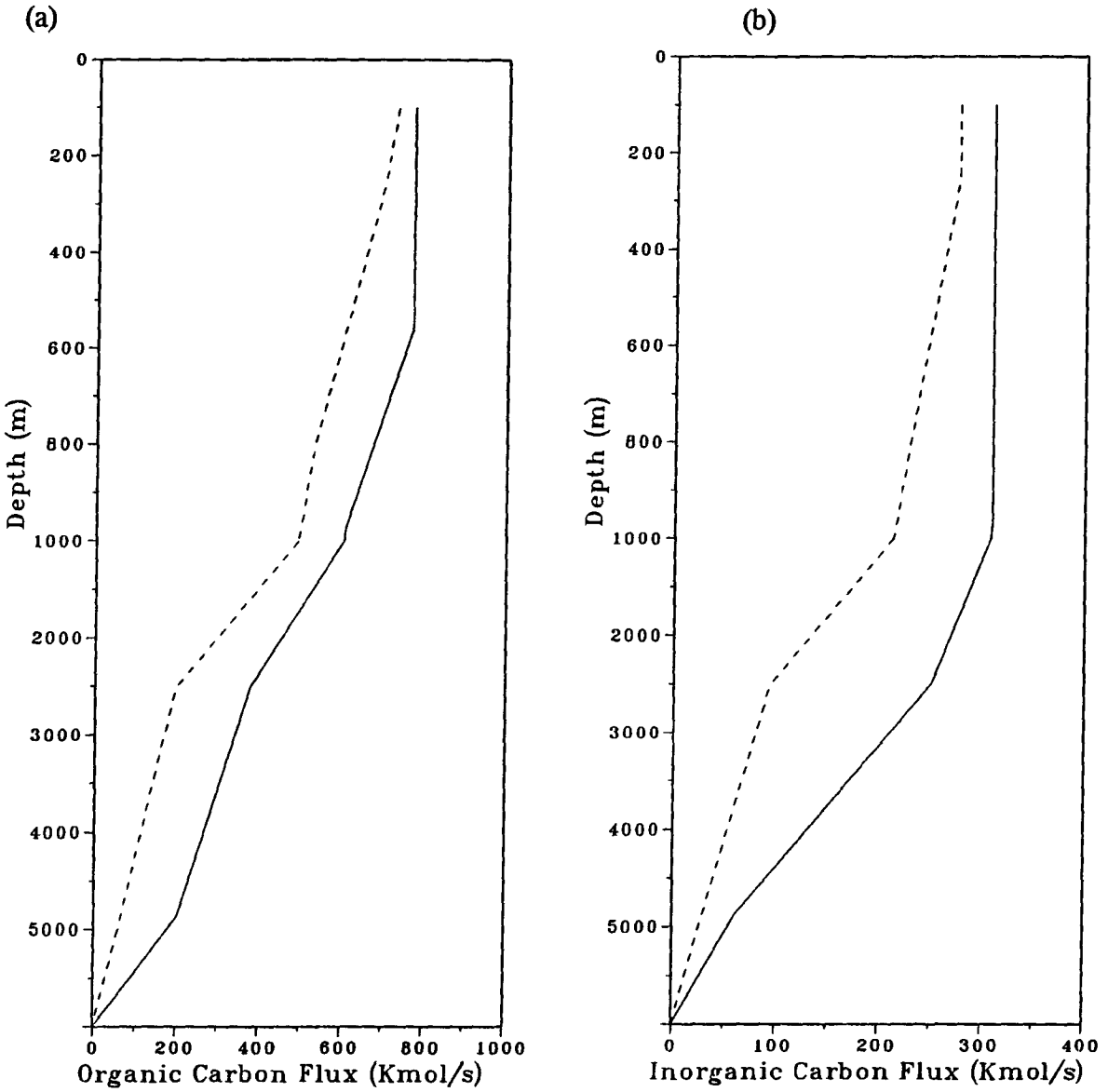

Figure 5.12: Profiles of the particle fluxes of (a) organic carbon, (b) inorganic carbon and (c) opal material. The solid lines denote the subtropical region and the dashed lines denotes the subarctic region.

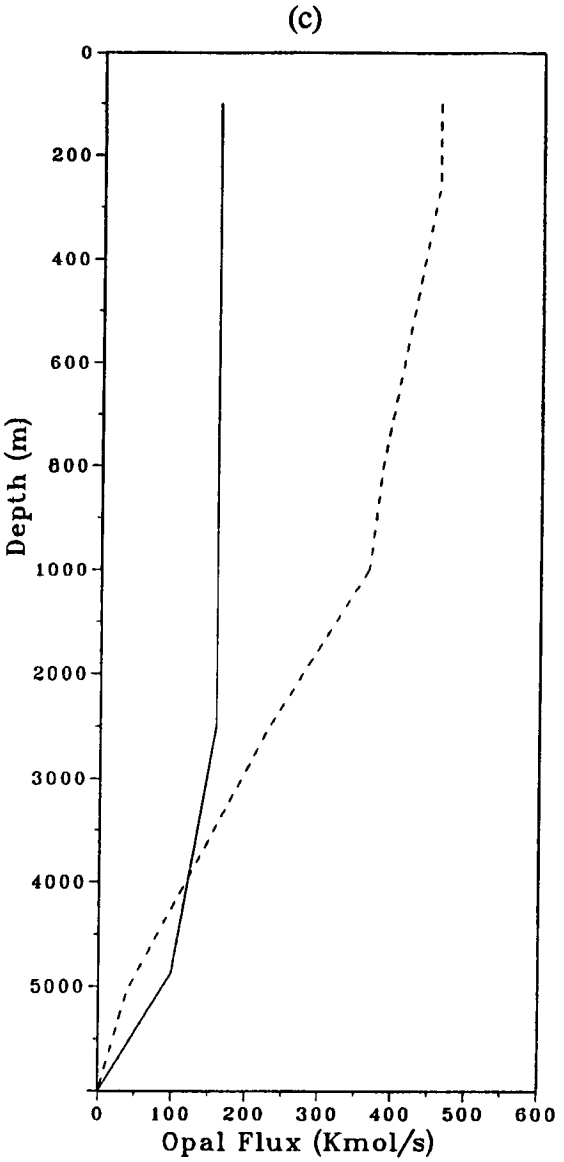
(c)
0
200
400
600
800
1000
2000
3000
4000
5000
Depth (m)
0
100
200
300
400
500
600
Opal Flux (Kmol/s)

internally consistent and produced molecular ratios linking organic matter of $P:C:O_2$ = 1:125:-170. The objective functions for this study were chosen to produce interesting solutions without requiring the desired unknowns in the ratio to be extremized. In this way the model is free to determine the selected unknowns in the desired ratio.

The maximum values for $CaCO_3$ fluxes gave particle fluxes of 6.0 and 15.8 g C m^{-2} yr^{-1} from the surface layers of the subtropics and subarctic respectively. The flux densities in the subarctic region are double the subtropical region. A comparison of particle fluxes of $CaCO_3$ with organic carbon showed that $CaCO_3$ was more resistant to dissolution than organic carbon. Table 5.7 presents a brief summary of $CaCO_3$ fluxes from sediment traps in the North Pacific. The sediment traps data from Noriki and Tsunogai (1986) do show indications that the $CaCO_3$ fluxes are greater in the subarctic Pacific than in the subtropics. The maximum particle fluxes in the model are significantly higher than the sediment trap data suggesting the values are poorly determined by the model. The slow redissolution of $CaCO_3$ with depth shown by the three sediment traps at Station P, is evident in the model results by the small change in the particle fluxes with depth.

The maximum values from the inverse model for the opal fluxes produced flux densities in the subarctic of 54 g Si m^{-2} yr^{-1} which are nearly an order of magnitude greater than 5.5 g Si m^{-2} yr^{-1} determined for the subtropics. Selected sediment trap data for the North Pacific (Table 5.8) does show that the opal flux varies by nearly an order of magnitude between the subtropics and subarctic North Pacific. This agrees with the

Table 5.7: Sediment trap measurements of $CaCO_3$ fluxes in the North Pacific.

Location	$CaCO_3$ Flux (g C m^{-2} yr^{-1})	Reference
Subtropical Northeast Pacific (50m)	3.7	Martin and Knauer 1983
Subarctic Pacific (1000m)	1.4	Noriki and Tsunogai, 1986
Subarctic Pacific (1000 m)	2.3	Noriki and Tsunogai, 1986
Subtropical Eastern Pacific (500 m)	1.0	Noriki and Tsunogai, 1986
Subtropical Eastern Pacific (500 m)	0.3	Noriki and Tsunogai, 1986
Subarctic Pacific (200 m)	3.8	Wong unpublished
Subarctic Pacific (1000 m)	2.8	" "
Subarctic Pacific (3800 m)	2.1	" "

model maximum results but the model maximum opal fluxes are considerably greater than the sediment trap data. The comparison with sediment traps data is limited usefulness because of the very limited spatial and temporal sampling of the sediment trap data. Although the particle fluxes from the surface layer for the subarctic are high, measurements from the Antarctic have given particle fluxes of 87.6 g Si m^{-2} yr^{-1} (Noriki and Tsunogai, 1986).

Unlike $CaCO_3$, seawater is everywhere undersaturated with respect to opal. The solubility of opal decrease by about 30% for a fall in temperature from 25 to 5°C, though

Table 5.8: Sediment trap measurements of opal flux for the North Pacific.

Location	Opal Flux (g Si m^{-2} yr^{-1})	Reference
Subarctic Pacific (1000m)	2.7	Noriki and Tsunogai, 1986
Subarctic Pacific (2100 m)	1.8	Noriki and Tsunogai, 1986
Subtropical Eastern Pacific (500 m)	0.4	Noriki and Tsunogai, 1986
Subtropical Eastern Pacific (500 m)	0.04	Noriki and Tsunogai, 1986
Subarctic Pacific (200 m)	7.4	Wong unpublished
Subarctic Pacific (1000 m)	10.3	" "
Subarctic Pacific (3800 m)	7.0	" "

this is offset somewhat in the deep ocean because the high pressure acts to increase the opal solubility (Bearman, 1989). Inspection of samples from sediment data suggest a considerable amount of opal is dissolved at the ocean bottom (Bearman 1989). In order for this to occur the opal reaching the sea bed must be rapidly transport in large fast-sinking particles. The model results, like the sediment trap data at station P, do show that a significant amount of opal is dissolved at the ocean bottom, allowing up to 3.7 g Si m^{-2} yr^{-1} to redissolve in the bottom layer.

The model results for the particle fluxes and new production suggest a correlation between the particle fluxes and the mixing coefficients. The sensitivity of the new production rates to the change in mixing processes suggests that these mixing coefficients could be better determined by including data for new production and particle fluxes in the

model. The potential value of productivity data for the determination of isopycnal and diapycnal mixing coefficients was carried out using a simple experiment. New production rates and particle fluxes of organic carbon are incorporated into the model to estimate the improvement in the mixing coefficients. For this purpose, the minimal and maximal mixing coefficients have been recalculated for a model that constrained the new production to be 600 ± 300 Kmol s^{-1} for both regions. With the new constraints on new production, the acceptable bounds on the diapycnal mixing coefficients in the upper 4 layers are typically reduced by 30% and isopycnal mixing coefficients in the upper 4 layers are typically reduced by 10%. In the deeper ocean mixing coefficients are unaffected.

5.3 MODEL INCLUDING DISSOLVED ORGANIC MATTER

In addition to the inorganic components of phosphate, nitrate, and carbon, recent measurements have shown that significant amounts of dissolved organic nitrate (DON) and dissolved organic carbon (DOC) compounds are found in seawater (Sugimura and Suzuki, 1988, and Suzuki *et al.*, 1985) (Fig. 5.13). The new method of Sugimura and Suzuki (1988) of high temperature catalytic oxidation (HTCO) of dissolved organic carbon (DOC) extracted up to four times more organic carbon from the near-surface water oceanic waters and two times more carbon from deep waters than the existing wet-chemical oxidation methods. Sugimura and Suzuki claimed that much of the new DOC is high-molecular-mass material ($M_r > 20{,}000$). The additional DOC extracted by the Sugimura and Suzuki method appears to have high surface concentrations and large gradients within

the ocean's main thermocline. These qualities suggest that the new DOC must be produced and broken down by open ocean plankton communities within a decade or two. Throughput of such a large amount of carbon would make the new DOC one of the most active carbon reservoirs on the planet. The new higher concentrations of DON and DOC are suspected to play a role in the oceanic nutrient and carbon cycles (Williams and Druffel, 1988).

At present the measurement techniques are controversial and the distribution of dissolved organic compounds in the ocean are not well determined. Recently three papers have been published that re-examine the results of Sugimura and Suzuki. Martin and Fitzwater (1992) used the HTCO method to analyze vertical profiles of seawater from 59.5°N in the North Atlantic, from the Drake Passage and from the equatorial Pacific. They find very little differences between stations for the DOC concentrations in the deep water in spite of large differences in ^{14}C age and dissolved oxygen at the three locations. This result suggests that the bacterial consumption of DOC in the ocean's interior does not account for much of the observed consumption of oxygen. Martin and Fitzwater do, however, find a very strong DOC gradient in surface water between the equator (130 μM) and 9°N (230 μM) in the equatorial Pacific. Overall, Martin and Fitzwater report that their HTCO measurements produced excellent agreement with Suzuki's when the same water is analyzed.

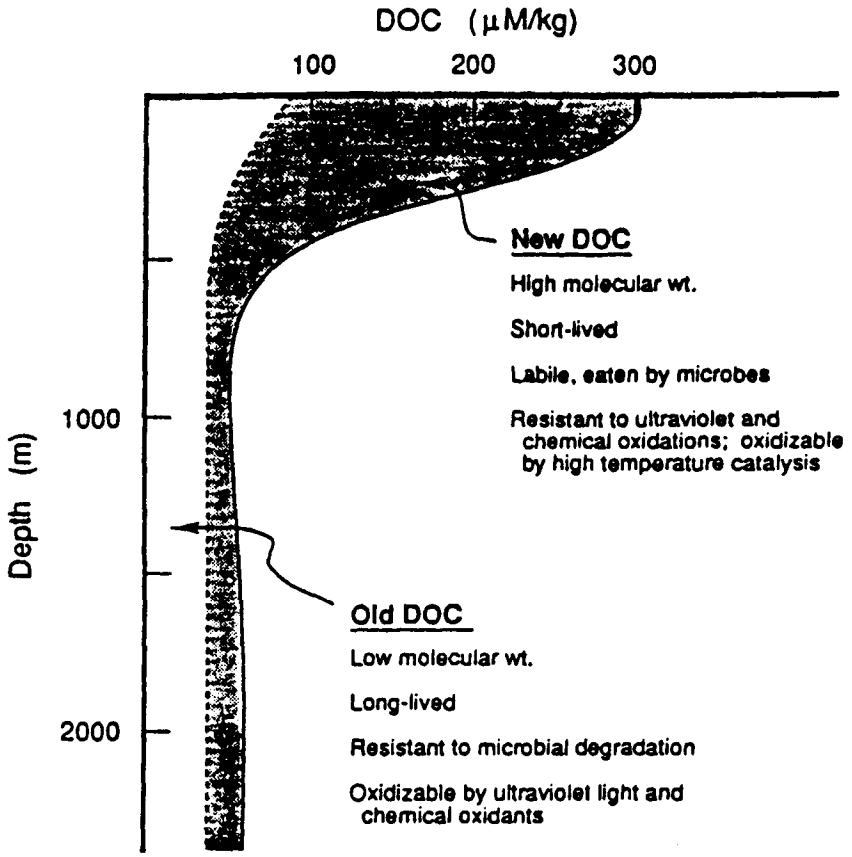

Figure 5.13: Illustration of an oceanic DOC profile indicating the "new" DOC, additional DOC found by the HTCO method of Sugimura and Suzuki, (1988), and the "old" DOC, that found by older methods (redrawn from Bacastow and Maier-Reimer, 1991).

Ogawa and Ogura (1992) compared the HTCO method with the wet chemical oxidation method and found the HTCO extracted only about one-third more carbon than the wet chemistry method. Using the process of ultrafiltration, Ogawa and Ogura found little DOC with molecular masses above 10,000. Contrary to Sugimura and Suzuki, these authors suggest that there might be no chemically refractory, high-M_r DOC in seawater.

Benner *et al.* (1992) attempt to characterize the $M_r > 1000$ fraction using the same ultra filtration technique as Ogawa and Ogura. They find that a third of the surface-water DOC falls in this size fraction, a result that agrees very well with Ogawa and Ogura's. Although they disagree with many of Sugimura and Suzuki's results, Benner *et al.*, "concur that the high-M_r in the upper ocean are reactive and support much of the heterotrophic activity in the surface ocean".

The one consistent conclusion drawn from these new measurements is that the AOU is not linearly correlated with DOC. In these new reported measurements only two direct comparisons can be made. Both Martin and Fitzwater (1992) and Benner *et al.*, (1992) measured water from the Hawaii Ocean Time Series station. Martin and Fitzwater report 152 μM for the surface water whereas Benner *et al.*, report only 82 μM. Similarly, large difference exists for the water at the O_2 minimum (86 compared to 38 μM) and for deep water (112 compared to 41 μM). In part some of the differences in the measurements can be attributed to whether one subtracts a system blank or not. Benner *et al.*, subtract a system blank of 22 μM from their raw data; Martin and Fitzwater do not subtract any blank. The same differences for both the surface and deep water samples (70 μM) between Benner *et al.*, and Martin and Fitzwater suggest that system blanks may be

at the heart of the disagreement. Studies by Benner and Stom (reference from Toggweiler 1992) showed that the observed blanks ranged from 10 to 50 μM for the different catalysts.

The most intriguing aspects of Sugimura and Suzuki's and of Martin and Fitzwater's data are the large vertical and horizontal DOC gradients revealed in the upper ocean. These gradients cannot be maintained unless large amounts of DOC production and remineralization are taking place. This reflects Toggweiler's (1992) conclusion that the actual size of the DOC pool is less interesting than the role DOC may be playing in the carbon cycle and marine ecosystems.

To address the question of the importance of the dissolved organic nutrients in the nutrient budgets of the ocean, a model was developed that implemented the data from Sugimura and Suzuki (1988) and Suzuki *et al.*, (1985) in a simple way. Toggweiler (1989) showed that a more appropriate correlation for DOM was obtained by plotting DON versus nitrate concentration rather then the AOU versus DOC plot of Sugimura and Suzuki (1988). The plot of DON versus nitrate for the Northwest Pacific is shown in Figure 5.14 (Toggweiler, 1989). The least squares linear fit to this data (r^2=0.96) is

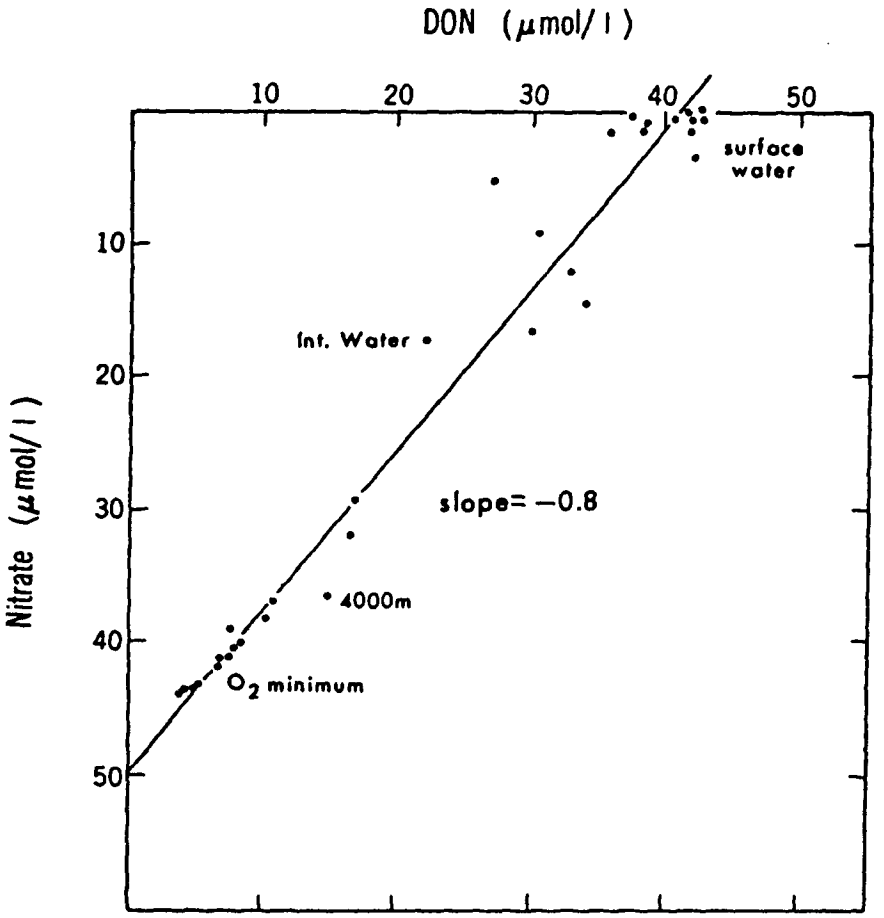

Figure 5.14: DON concentration versus the nitrate from Toggweiler (1989).

given by (Najjar *et al.*, 1992)

$$[DON] = 40.4\mu mol/kg - 0.806[NO_3]. \quad (5.1)$$

By using the $[NO_3]$ in the North Pacific, the corresponding DON concentrations ([DON]) is calculated using the linear equation above. The vertical profiles of DON at 24°N and 47°N are shown in Figure 5.15. The addition of the DON to the model requires that the tracer budgets of phosphate, DIC, alkalinity and oxygen be modified to include the DOM. This is accomplished by assuming a constant molecular ratio of $P:N:C:O_2$ = 1:16:102:-172 for the individual constituents of the DOM.

With the inclusion of the DOM as described above, to the model with the inorganic tracers one is able to obtain a feasible solution. The inverse solutions obtained from this model are nearly identical with the solutions without DOM. The ranges in acceptable values for the horizontal transport of DON into the subtropics and subarctic are -0.62 to 7.8 Kmol s^{-1} and -8.9 to 0.16 Kmol s^{-1} respectively. The highly productive subarctic region is capable of exporting a small amount of DOM into the subtropics. The small range of acceptable values for the horizontal transport of DON for the two regions emphasizes the modest role played by the horizontal transport of DOM in the carbon and nutrient cycles. This is contrary to Rintoul and Wunsch's (1991) budget studies in the North Atlantic which required a southward transport of DON of 119 $\pm$ 35 Kmol s^{-1} across 36°N.

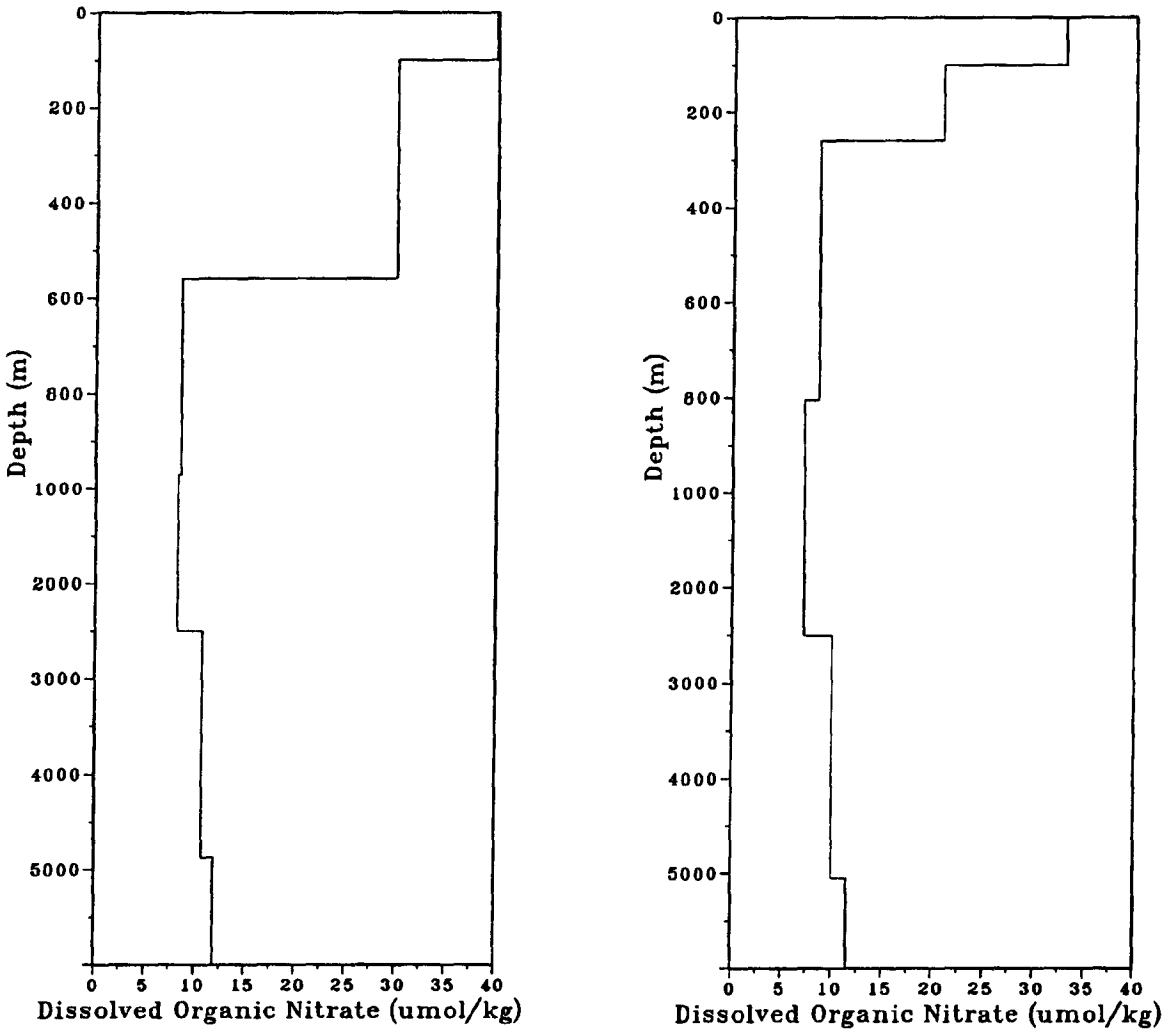

Figure 5.15: The vertical profiles of DON at 24° and 47°N.

CHAPTER 6. CONCLUSION

The work presented in this thesis was based on the analysis of tracer fields to infer information about the ocean carbon cycle. This work will be summarized in three parts:

1) the study of the tracer transports through the 35°N sections;

2) the assessment of the performance of the inverse box models when applied to the model data generated by the Hamburg model; and

3) the factors influencing the carbon, nutrient, heat, and salt content of the North Pacific Ocean.

In the first part of the thesis (chapter 2), the tracer transports across 35°N were computed using the hydrographic data from a synoptic section (INDOPAC) and from the Levitus annual mean section. The computations from the two sections produced significant differences in the mass and tracer transports. The study suggested that the Levitus section was inadequate for calculating tracer transports. The tracer transports calculated from the INDOPAC section were better able to close the tracer budgets of the North Pacific than the Levitus section. The transports calculation performed in this chapter pointed out the need to use highly resolved hydrographic data to accurately determine the tracer transports. The calculations reveal the sensitivity of the tracer transports to the estimated Ekman transports and air-sea exchanges of freshwater. The budget calculations from the INDOPAC sections suggested that dissolved organic matter (DOM) may play a significant role in the budgets of the nutrient tracers. The limited resolution of the INDOPAC section made it difficult to confidently assert this conclusion.

In the second part of the thesis (chapter 3), the inverse box model was applied to data generated from the Hamburg LSGOC-biogeochemical model. In this model, the mixing transport of tracers played an important role in closing the tracer budgets. Applying the inverse box model to the temperature, salinity, total CO_2, alkalinity, phosphate, oxygen, POC, calcite, and ^{14}C fields produced poor results. With the addition of velocity shear information, the inverse box model extracted the correct velocity fields and produced air-sea exchanges and detrital rain rates comparable to the known values from the Hamburg model. This provides some confidence that the inverse box model is capable of extracting information about the carbon cycle from the tracer fields.

In the third part of the thesis (chapters 4-5), inverse box models were formulated for the nutrient and carbon budgets of the North Pacific Ocean, and water flow rates, eddy mixing coefficients, particle fluxes and air-sea exchange rates of freshwater, heat, CO_2 and O_2 were calculated. The model incorporates geostrophy, wind-driven Ekman transports and budget equations for a suite of seven tracers (temperature, salinity, phosphate, DIC, oxygen, alkalinity, and silicate). As suggested in chapter 2, two highly sampled hydrographic sections across the Pacific at 24°N and 47°N are used to calculate the geostrophic transports. Historical station data are used and the budgets of mass, heat, salt, phosphate, oxygen, silicate, carbon and alkalinity are simultaneously satisfied in the North Pacific Ocean.

Feasibility studies using the inverse model showed that feasible solutions existed for a model that satisfied geostrophy, Ekman transport, and the prescribed Redfield ratios. A reference model was formulated by relaxing constraints on the Ekman transports and

Redfield ratios; this model satisfied the Ekman transports to within ±25% and the prescribed Redfield ratios to within ±20%. Tracer studies with the reference model showed that the unknowns are much better constrained when all 7 tracers are included in the model than by using only a subset of the tracers. Investigation showed the inverse solutions to be insensitive to the model layering and to the prescribed reference level used in the calculating the geostrophic transports.

From the reference inverse box model, the acceptable maximum and minimum bounds for the advective transports, mixing coefficients, air-sea exchanges and particle fluxes were determined. These bounds were determined using the LP algorithm and the calculated errors in the conservation equations.

The deep water transports of the model showed that 3.2 - 7.2 Sv of AABW and 3.0 - 11.9 Sv of AAIW enters the North Pacific at 24°N, and 7.3 - 12.1 Sv of NPDW leaves the North Pacific. The estimated transport by the Kuroshi through 24°N was 25 ± 5 Sv. In the upper ocean the flow pattern is much more confusing, reflecting the more zonal flow pattern of the North Pacific.

The northward transports of freshwater and heat by the model into the North Pacific were 0.05 ± .06 Sv and 0.12 ± 0.08 PW respectively. The model showed that the North Pacific Ocean was not a significant source of heat for the atmosphere. The model determined the North Pacific to be a sink of atmospheric CO_2. It was calculated that 0.1 ± 0.1 Gt C yr^{-1} enters the North Pacific, predominently between 24°N and 47°N. The model was unable to resolve the direction of the air-sea exchange of oxygen in the North Pacific, the calculated uptake of oxygen by the ocean was -467 to 497 Kmol s^{-1}.

The inverse model produced horizontal mixing terms that were greatest in the surface layer and decreased with depth. The vertical mixing coefficients were smallest in the surface layer and increased with depth. The inverse model showed a close connection between the unknown mixing coefficients and the particle fluxes of organic and inorganic carbon, and opal. By specifying the new production in the two regions of the model to be 600 $\pm$ 300 Kmol s^{-1}, the variance in the vertical and horizontal mixing coefficients are reduced by 30% and 10% respectively.

The new production determined in the subarctic region (21 $\pm$ 21 g C m^{-2} yr^{-1}) was 3.5 times greater than the subtropical region (6 $\pm$ 6 g C m^{-2} yr^{-1}). The model was not able to resolve the lower limit of new production.

The minimum bounds for all particle fluxes of organic and inorganic carbon and opal was zero. The decreases in particle fluxes with depth were consistent with sediment trap data. The maximum particle fluxes of $CaCO_3$ were 16.5 and 43.5 mg C m^{-2} yr^{-1} for the subtropics and subarctic regions respectively. The maximum particle fluxes of opal showed the subarctic region capable of producing nearly an order of magnitude larger flux than the subtropical region, 148 to 15 mg Si m^{-2} yr^{-1} respectively.

The large ranges in the acceptable values for the air-sea exchange of heat, CO_2 and O_2, and of the particle fluxes of organic carbon, $CaCO_3$ and opal material reflect the fact that these processes transport significantly less tracers than horizontal advection. Ideally, the determination of the air-sea exchanges and the biological processes can be thought of as small residual terms necessary to offset the tracer budget imbalances caused by the much larger horizontal transports. Two points should be emphasized as a consequence of

this situation. One, the horizontal advective transports of the tracers must be very accurately determined in order to extract useful estimates of the air-sea exchanges and the biological processes. Two, additional information to constrain the air-sea exchanges or biological processes will play an important role in the model solutions. In the future, as the measurements of biological productivity and air-sea exchanges of CO_2 increase, this information can easily be incorporated into the inverse model to demand more realistic solutions.

The role of dissolved organic matter (DOM) in the carbon and nutrient budgets in the North Pacific was investigated. The model used dissolved organic nitrogen (DON) data determined from the nitrate using the linear relationship of DON to nitrate derived from Suzuki *et al.*, (1985) data. For this model, the inclusion of DOM played a small part in the carbon and nutrient budgets. The subarctic region lost 4.4 ± 4.5 Kmol s^{-1} of nitrogen and the subtropical region gained 3.6 ± 4.2 Kmol s^{-1} of nitrogen. The net effect for the North Pacific was nearly zero. This contradicts the results from the tracer transports across 35°N. The results of the inverse model are much more believeable because these results do close the tracer budgets in the North Pacific. The different results obtained from the tracer transports across 35°N are attributed to the inadequancy of this section in calculating the tracer transports as was discussed in chapter 2.

In conclusion I would like to emphasize that further work should be done to investigate the role of DOM in the carbon and nutrient budgets. At present there is insufficient data available to directly include the fields of DON or dissolved organic carbon in the inverse model. It is expected that this problem will be rectified in the future

as more laboratories develop the ability to reproduce the measurements of Sugimura *et al.*, (1988) and Suzuki *et al.*, (1985). It is also apparent that the inverse box model approach should be applied to data that will be acquired by WOCE cruises.

APPENDIX A. THE NUMERICAL DIFFUSION OF THE IMPLICIT UPWIND ADVECTION SCHEME USED IN THE LSGOC MODEL

In one dimension, with u assumed positive and constant the implicit upwind advection scheme used in the LSGOC-biogeochemical model is given by (Bacastow and Maier-Reimer, 1990)

$$T_i^n = T_i^{n-1} + \frac{\Delta t}{\Delta x}\left(T_{i-1}^n - T_i^n\right) u \qquad \text{(A.1)}$$

In order to satisfy the continuity of mass in one dimension u must be constant. The numerical diffusion of this scheme is obtained by expanding T^n_i and T^n_{i-1} in (A.1) around the point T^n_i using Taylor series expansions. For clarity the i's and n's are dropped to give the expanded equation

$$T_t + uT_x = \frac{\Delta t}{2}T_{tt} + u\frac{\Delta x}{2}T_{xx} - \frac{\Delta t^2}{6}T_{ttt} - u\frac{\Delta x^2}{6}T_{xxx} + \ldots \quad . \qquad \text{(A.2)}$$

The 2nd order and higher time derivatives are removed by subtracting various differentiated equations of (A.2) from (A.2) to give

$$T_t+uT_x=\frac{u\Delta x}{2}\left(1+\frac{u\Delta t}{\Delta x}\right)T_{xx} - \frac{u\Delta x^2}{6}\left(1+\frac{3u\Delta t}{\Delta x} + \frac{2u^2\Delta t^2}{\Delta x^2}\right)T_{xxx} + \ldots \quad . \qquad \text{(A.3)}$$

The first term on the RHS of (A.3) is a diffusion term with a diffusivity coefficient given by

$$K = u\frac{\Delta x}{2}(1+u\frac{\Delta t}{\Delta x}) \ . \qquad \text{(A.4)}$$

For comparison, the numerical diffusion of the explicit advection scheme is (Smolarkiewicz, 1983)

$$K = u\frac{\Delta x}{2}(1-u\frac{\Delta t}{\Delta x}) \ . \qquad \text{(A.5)}$$

The numerical diffusion of the implicit upwind advection scheme is (u^2 Δt) greater than the numerical diffusion of the explicit scheme.

To estimate the apparent diffusivities of the model from (A.4), for comparison with the inverse model results I used the rms velocities of the LSGOC model along each of the box faces defined in the inverse box model.

By considering the implicit upwind advection equation in three dimensions additional cross derivatives terms are generated. In three dimensions with the (u,v,w) assumed positive (for simplicity) the expanded equation would be

$$\begin{aligned} T_t+uT_x+vT_y+wT_z \quad = & \frac{u\Delta x}{2}(1+\frac{u\Delta t}{\Delta x})T_{xx} + \frac{v\Delta y}{2}(1+\frac{v\Delta t}{\Delta y})T_{yy} + \\ & \frac{w\Delta z}{2}(1+\frac{w\Delta t}{\Delta z})T_{zz} + \qquad \text{. . . (A.6)} \\ & (uv\Delta t)T_{xy} + (uw\Delta t)T_{xz} + (vw\Delta t)T_{yz} + \ldots \ . \end{aligned}$$

This equation is presented to show that additional numerical diffusion is generated in three dimensions from the cross derivative terms. In my evaluation of the numerical diffusion, I will neglect these terms and evaluate (A.4).

BIBLIOGRAPHY

Anderson L.G., D.W. Dryssen, E.P. Jones, and M.G. Lowings, 1983: Inputs and Outputs of salt, freshwater, alkalinity and silica in the Arctic Ocean. *Deep Sea Res.*, **30**, 87-94.

Bacastow, R., and E. Maier-Reimer, 1991: Dissolved organic carbon in modeling oceanic new production, *Global Biogeochemical Cycles,* **5,** 71-85.

Bacastow, R., and E. Maier-Reimer, 1990; Ocean circulation model of the carbon cycle, *Climate Dynamics*, **4**, 95-125.

Bacastow, R., and C. Keeling, 1981; Atmospheric Carbon Dioxide concentration and observed airborne fraction, in Bolin B. (ed.) Carbon Cycle Modelling, SCOPE 16, Chichester, Wiley, 103-112.

Baumgartner, A. and E. Reichel, 1975: *The World Water Balance,* Elsevier, New York, 179p.

Bearman, G., 1989: *Ocean Chemistry and Deep-Sea Sediments,* The Open University, Pergamon Press, Oxford, England, 134pp.

Benner R., J.D. Pakulski, M. McCarthy, J. Hedges, and P. Hatcher, 1992: Bulk chemical characteristics of dissolved organic matter in the ocean. *Science,* **255,** 1561-1564.

Berger W., 1989: Global Maps of Ocean Productivity, in Berger, W., V. Smetacek and G. Wefer (eds) *Productivity of the Ocean: Present and Past,* John Wiley and Sons, 429-455.

Bien G., N. Rakestraw, and H. Suess, 1965: Radiocarbon in the Pacific and Indian Oceans and its relation to deep water movements, *Limnol. and Oceanog.*, **10,** R25-R37.

Bingham F., and L. Talley, 1991: Estimates of Kuroshio transport using an inverse technique, *Deep Sea Res.*, **38 suppl 1.**, S21-S43.

Bolin B., A. Björkström, K. Holmén, and B. Moore, 1987: On inverse methods for combining chemical and physical oceanographic data: A steady-state analysis of the Atlantic Ocean, Rep. CM-71, Dep of Meteorol., Stockholm.

Bolin, B. 1986; How much CO_2 will remain in the atmosphere?, in Bolin B. and D. Jäger (ed.) The Greenhouse Effect Climatic Change and Ecosystems, SCOPE 29, Chichester, Wiley, 93-153.

Bolin, B., A. Björkström, K. Holmén, and B. Moore, 1983: The simultaneous use of tracers for ocean circulation studies, *Tellus,* **35B**, 206-236.

Brewer P.G., C. Goyet, and D. Dryssen, 1989: Carbon Dioxide transport by ocean currents at 25°N latitude in the Atlantic Ocean. *Science*, **246**, 477-479.

Broecker, W., J. Ledwell, T. Takahashi, R. Weiss, L. Merlivat, L. Memery, T.H. Peng, B. Jähne and K. Munnich, 1986: Isotopic versus micrometeorological ocean CO_2 fluxes: a serious conflict, *J. Geophys. Res.*, **91**, 1431-1438.

Broecker, W., Taro Takahashi, and Timothy Takahashi, 1985: Sources and flow patterns of deep-ocean waters as deduced from potential temperature, salinity, and initial phosphate concentrations, *J. Geophys. Res.*, **90**, 6925-6939.

Broecker, W., and T-H. Peng, 1982: *Tracers in the Sea,* Columbia University, Palisades, New York, 690pp.

Coachman, L., and K. Aagaard, 1988: Transport through Bering Strait: annual and interannual variability, *J. Geophys. Res.*, **93**, 15,535-15,539.

Cochrane J., 1956: The frequency distribution of surface-water characteristics in the Pacific Ocean. *Deep Sea Res.*, **4**, 45-53.

Codispoti, L., G. Friedrich, D. Hood, 1986: Variability in the inorganic carbon system over the southeastern Bering Sea shelf during spring 1980 and spring-summer 1981, *Cont. Shelf Res.* **5**, 133-160.

Craig H., and T. Hayward, 1987: Oxygen supersaturation in the ocean: biological versus physical contributions. *Science* **235**, 199-201.

Craig H., W. Broecker, and D. Spencer, 1981: GEOSECS Pacific Expedition, vol 4 Sections and Profiles, U.S. Government Printing Office, Washington D. C., 1981.

de Boor, C., 1978: *A Practical Guide to Splines,* Springer-Verlag, New York, 445pp.

Dickinson, R. E., 1986; The climate system and modelling of future climate, in Bolin B. and D. Jäger (ed.) The Greenhouse Effect Climatic Change and Ecosystems, SCOPE 29, Chichester, Wiley, 206-270.

Dugdale, R., and J. Goering, 1967: Uptake of new and regenerated production forms of nitrogen in primary productivity, *Limnol. Ocean.* **23,** 196-206.

Feely, R., R. Byrne, P. Betzer, J. Gendron, and J. Acker, 1984: Factors influencing the degree of saturation of the surface and intermediate waters of the North Pacific with respect to aragonite, *J. Geophys. Res.*,

Feely, R., and C. Chen, 1982; The effect of excess CO_2 on the calculated calcite and aragonite saturation horizons in the northeast pacific, *Geophysical Research Letters*, **9**, 1294-1297.

Garçon, V., and Minster, J., 1988: Heat, carbon and water fluxes in a 12-box model of the world ocean, *Tellus,* **40B**, 161-177.

Gill A., 1982: *Atmosphere-Ocean Dynamics*, Academic Press, New York, New York, 662pp.

Gordon, L., P. Park, S. Hager, and T. Parsons, 1971: Carbon dioxide partial pressure in the North Pacific surface waters- time variations, *J. Oceanogr. Soc. Japan,* **27,** 81-90.

Hasselmann, K., 1982: An Ocean Model for Climate Variability Studies. *Progr. Oceanogr.*, **11**, 69-92.

Hellerman, and Rosenstein, 1983: Normal monthly wind stress over the world ocean with error estimates, *J. Phys. Oceanogr.*, **13**, 1093-1104.

Houghton, R. A., 1986; Estimating changes in the carbon content of terrestrial ecosystems form historical data, in Trabalka J. R., and D. E. Reichle (ed.) The Changing Carbon Cycle A Global Analysis, New York, Springer-Verlag, 175-193.

Johnson G.C., 1990: Near-equatorial deep circulation in the Indian and Pacific Oceans, Ph.D. Thesis, MIT-WHOI Joint Program, 157pp.

Kelly J., and D. Hood, 191: Carbon dioxide in the Pacific Ocean and Bering Sea: Upwelling and mixing, *J. Geophys. Res.*, **76,** 745-752.

Kenyon K., 1983: Sections along 35°N in the Pacific. *Deep Sea Res.*, **30,** 349-369.

Knauer G., D. Redalje, W. Harrison, and D. Karl, 1990: New Production at the VERTEX time-series site, *Deep Sea Res.*, **37,** 1121-1134.

Koblentz-Mishke, O.J., V.V. Volkovinsky and J.G. Kabanova, Plankton primary production of the world ocean, in *Scientific Exploration of the South Pacific,* edited by W.S. Wooster, pp 183-193, National Academy of Science, Washington, D.,C., 1970.

Lawson, C. L., and R. J. Hanson, 1974; Solving Least Squares Problem, Prentice-Hall, Englewood Cliff, N.J., 1054pp.

Levitus, S., 1982: Climatological atlas of the world ocean, Prof Pap 13, Natl. Oceanic and Atmos. Admin, Rockville, Md.

Luenberger, D. G., 1984; Linear and Nonlinear Programming, Addison-Wesley, Reading, Mass.

Longhurst A., W. Harrison, 1989: The biological pump: Profiles of plankton production and consumption in the upper ocean, *Prog. Oceanog.*, **22,** 47-123.

Maier-Reimer E., and R. Bacastow, 1990: Modelling of geochemical tracers in the ocean. *Climate-Ocean Interaction*, M.E. Schlesinger (ed.), Kluwer, 233-267.

Maier-Reimer, E., K. Hasselmann 1987; Transport and storage of CO_2 in the ocean - an inorganic ocean-circulation carbon cycle model, Climate Dynamics, 2:63-90.

Mantyla, A., and J. Reid, 1983: Abyssal characteristics of the world ocean waters. *Deep Sea Res.*, **30,** 805-833.

Martin, J. and S. Fitzwater, 1992: Dissolved organic carbon in the Atlantic, Southern and Pacific oceans, *Nature,* **356,** 699-700.

Martin, J.H., G.A. Knauer, D. M. Karl, and W.W. Broenkow, 1987: VERTEX: The carbon cycling in the northeast Pacific, *Deep Sea Res.*, **34**, 267-285.

Martin, J. and G. Knauer, 1983: VERTEX: manganese transport with $CaCO_3$, *Deep Sea Res.*, **30,** 411-425.

Matear, R. 1989: Circulation of the northeast Pacific Ocean inferred from temperature and salinity data, M.Sc. Thesis, University of British Columbia, 121pp.

McAllister, c. D. 1969. Aspects of estimating zooplankton production from phytoplankton production. J. Fish. Res. Board. Can. 26:199-220.

McBean G., 1991: Estimation of the Pacific Ocean meridional heat flux at 35°N. *Atmosphere-Oceans,* **29,** 576-595.

McBean G., 1989: Global energy and water cycles. *Weather,* **44,** 285-291.

Meméry L., and C. Wunsch, 1990: Constraining the North Atlantic circulation with Tritium data. *J. Geophys. Res.*, **95**, 5239-5256.

Merlivat L., J. Etcheto, and J. Boutin, 1991: CO_2 exchange at the air-sea interface: time and space variability, *Adv. Space Res.*, **11,** 77-85.

Metzl N., B. Moore, and A. Poisson, 1990: Resolving the intermediate and deep advective flows in the Indian Ocean by using temperature, salinity, oxygen and phosphate data: the interplay of biogeochemical and geophysical tracers. *Palaeogeography, Palaeoclimatology, Palaeoecology (Global and Planetary Change Section,* **89**, 81-111.

Metzl, N., B. Moore, A. Papaud, and A. Poisson, 1989: Transport and carbon exchanges in Red Sea, inverse methodology. *Global Biogeochemical Cycles,* **3**, 1-26.

Miller, C.B. and SUPER GROUP, 1988: Lower trophic level production dynamics in the subarctic Pacific Ocean, (eds. T. Memoto and W. Pearcy), in *Bulletin of the Ocean Research Institute of University of Tokyo,* Tokyo Japan, Nakas.

Montgomery, R., 1958: Water characteristics of Atlantic Ocean and world oceans. *Deep Sea Res.*, **5,** 134-148.

Najjar R., 1992: Marine Biogeochemistry, in Trenberth, K. (ed.), *Climate System Modelling,* Cambridge University Press, 241-277.

Najjar R., J. Sarmiento, and J. Toggweiler, 1992: Downward transport and fate of organic matter in the ocean: simulations with a general circulation model, *Global Biogeochemical Cycles,* **6,** 45-76.

Nitani H. 1972: Beginning of the Kuroshio, In: Stommel H., and K. Yoshida (eds.) *Kuroshio, physical aspects of the Japan Current,* University of Washington Press, Seattle, 129-164.

Noriki S., and S. Tsunogai, 1986: Particle fluxes and major components of settling particles from sediment trap experiments in the Pacific Ocean. *Deep Sea Res.*, **33,** 903-912.

Ogawa H. and N. Ogura, 1992: Comparison of two methods for measuring dissolved organic carbon in sea water. *Nature,* **356,** 696-698.

Olbers, D. J., M. Wenzel, and J. Willebrand, 1985; The inference of north Atlantic circulation patterns form climatological hydrographic data, Reviews in Geophysics, 23:313-356.

Peng, T-H., T. Takahashi, W. Broecker and J. Olafsson, 1987: Seasonal variability of carbon dioxide, nutrients and oxygen in the northern North Atlantic surface water: Observations and a model, *Tellus,* **39B,** 439-458.

Platt, T. and D. Subba Rao, 1975: Primary production marine microphytes, in Copper J. (ed) *Photosynthesis and Productivity in Different Environments,* Cambridge University Press, London, 249-280.

Post, W., T-H. Peng, W. Emanuel, A. King, V. Dale, and D. DeAngelis, 1990: The Global Carbon Cycle, *American Scientist,* **78,** 310-326.

Ramanathan, V., 1988; The greenhouse theory of climate change: A test by an inadvertent global experiment, Science, 240:293-299

Redfield, A., B. Ketchum, and F. Richards, 1963; The influence of organisms on the composition of sea water, in Hill, M. (ed.), The Sea, vol 2, Interscience, New York, 26-77.

Reid, J., and R. Lynn, 1983: On the influence of the Norwegian-Greenland and Weddell Seas upon the bottom waters of the Indian and Pacific Oceans, *Deep Sea Res.*, **18,** 1063-1088.

Rintoul, S.R., and C. Wunsch, 1991: Mass, heat, oxygen and nutrient fluxes and budgets in the North Atlantic Ocean, *Deep Sea Res.*, **38 suppl. 1,** s355-s377.

Rintoul, S.R., Mass, heat, and nutrient fluxes in the Atlantic Ocean determined by inverse methods. Ph.D. thesis, Mass. Inst. of Tech. and Woods Hole Oceanogr. Inst., Cambridge, 1988

Riser S., and D. Swift, 1989: Ventilation and North Pacific Intermediate water formation in the Sea of Okhotsk. Abstract T1.DW.07 presented at the Oceanography Society Inaugural Meeting.

Roemmich D., T. McCallister, and J. Swift, 1991: A transpacific hydrographic section along latitude 24°N: the distribution of properties in the subtropical gyre. *Deep Sea Res.*, **38 suppl 1,** S1-S20.

Roemmich D., and T. McCallister, 1989: Large scale circulation of the North Pacific Ocean. *Prog. Oceanogr.*, **22**, 171-204.

Roemmich D., 1983: Optimal estimation of hydrographic station data and derived fields. *J. Phys. Oceanogr.*, **13**, 1544-1549.

Schlitzer, R., 1989: Modeling the nutrient and carbon cycle of the North Atlantic 2. New production, particle fluxes, CO_2 gas exchange and the role of organic nutrients, *J. Geophys. Res.*, **94**, 12,781-12,794.

Schlitzer, R., 1988: Modeling the nutrient and carbon cycle of the North Atlantic 1. Circulation, mixing coefficients and heat fluxes, *J. Geophys. Res.*, **93**, 10,699-10,723.

Scripps Institution of Oceanography, University of California, 1978: Physical Chemical, and Biological Data, INDOPAC expedition, Legs I, II, III, VII, VIII, XV, XVI. SIO Reference 78-21 (unpublished data report).

Siegenthaler, U., 1983; Uptake of excess CO_2 by an outcrop-diffusion model of the ocean, Journal of Geophysical Research, 88(C6):3599-3608.

Smolarkiewicz, P., 1983: A simple positive definite advection scheme with small implicit diffusion, *Monthly Weather Review,* **111,** 479-486.

Sugimura, Y., and Y. Suzuki, 1988: A high temperature catalytic oxidation method of non-volatile dissolved organic carbon in seawater by direct injection of a liquid sample. *Mar. Chem.*, **24,** 105-131.

Suzuki, Y., Y. Sugimura, and T. Itoh, 1985: A catalytic oxidation method for the determination of total nitrogen dissolved in seawater, *Marine Chem.*, **16,** 83-97.

Takahashi T., 1989: The carbon dioxide puzzle, *Oceanus,* **32,** 2, 22-29.

Takahashi T., J. Goddard, S. Sutherland, D. Chipman, and J. Ledwell, 1985: Seasonal and geographic variability of carbon dioxide sink/source in the oceanic areas: observations in the North and equatorial Pacific ocean, 1984-1986 and global summary, *Final report to CO_2 research division,* Office of Energy Research U.S.A., Department of Energy, 52pp.

Takahashi, T., W. Broecker, and S. Langer, 1985: Redfield ratio based on chemical data from isopycnal surfaces, *J. Geophys. Res.*, **90,** 6907-6924.

Takahashi, T., W. Broecker, A. Bainbridge, and R. Weiss, 1980: Carbonate chemistry of the Atlantic, Pacific, and Indian Oceans: Results of the GEOSECS Expedition 1972-1978, *Tech. Rep, ICU-l-8,* Lamont-Doherty Geol. Observ., Palisades, N.Y.

Talley L.D., T.M. Joyce, and R.A. DeSzoeke, 1991: Transpacific sections at 47°N and 152°W: distribution of properties. *Deep Sea Res.*, **38, Suppl 1,** S63-S82.

Talley L.D., M. Martin, P. Salameh and Oceanographic Data Facility, 1988: Trans-Pacific section in the subpolar gyre (TPS47); physical, chemical, and CTD data. Scripps Institute of Oceanography, Reference 88-9, 245pp.

Talley, L., 1984: Meridional heat transport in the Pacific Ocean. *J. Phys. Oceanogr.*, **14,** 231-241.

Tans, P., I. Fung, and T. Takahashi, 1990: Observational constraints on the global atmospheric CO_2 budget. *Science,* **247**, 1431-1438.

Thomas, F., V. Garçon, and J-F Minster, 1990: Modelling the seasonal cycle of dissolved oxygen in the upper ocean at Ocean Weather Station P. *Deep Sea Res.*, **37,** 463-491.

Thomas, F., C. Perigaud, L. Merlivat, and J-F Minster, 1988: World-scale monthly mapping of the CO_2 ocean-atmosphere gas-transfer coefficient, *Phil. Trans. R. Soc. Lond. A.*, **325,** 71-83.

Toggweiler J.R., 1992: Catalytic conversions. *Nature,* **356,** 665-666.

Toggweiler, J., K. Dixon and K. Bryan, 1989a; Simulation of radiocarbon in a coarse-resolution world ocean model 1. Steady state prebomb distributions, Journal of Geophysical Research, 94(C6):8217-8242.

Toggweiler, J., K. Dixon and K. Bryan, 1989b; Simulation of radiocarbon in a coarse-resolution world ocean model 2. Distribution of bomb-produced carbon 14, *J. Geophys. Res.*, **94**, 8243-8264.

Van Scoy, K., D. Olson, and R. Fine, 1991: Ventilation of North Pacific Intermediate Water: the role of the Alaskan Gyre, *submitted to J. Geophys. Res.*,.

Volk, T. and M. Hoffert, 1985: Ocean carbon pumps: analysis of relative strengths and efficiencies in ocean-driven atmospheric pCO_2 changes, in Sundquist E. and W. Broecker (eds.) *Carbon Dioxide and the Carbon Cycle, Archean to Present,* Geophys. Monogr. Ser. **32,** 99-110, AGU, Washington, D.C.

Warren, B., 1981: Deep circulation of the World Ocean, in Warren B. and C. Wunsch (eds.) *Evolution of Physical Oceanography,* The MIT Press, Cambridge, Mass. and London England, 42-69.

Washington, W., and G. Meehl, 1989; Climate sensitivity due to increased CO_2: experiments with a coupled atmosphere and ocean general circulation model, Climate Dynamics, **4**, 1-38.

Weiss, R. 1974: Carbon dioxide in water and seawater: The slubility of a non-ideal gas, *Marine Chem.*, **2, 203-215.**

Wheeler, P. A., and S. A. Kokkinakis. 1990. Ammonium recycling limits nitrate use in the oceanic subarctic Pacific. Limnol. Oceanogr. 35:1267-1278.

Williams P.M. and E. Druffel, 1988: Dissolved organic matter in the ocean: comments on a controversy. *Oceanography,* **1,** 14-17.

Wong C.S., and Y-H. Chan, 1991: Temporal variations in the partial pressure and flux of CO_2 at Ocean Station P in the subarctic northeast Pacific Ocean. *Tellus,*

Wong, C. S., 1978; Atmospheric input of carbon dioxide from the burning of wood, Science, 200: 197-200.

Wong, C.S., D.R. Green and W.J. Cretney, 1974: Quantitative tar and plastic waste distribution in the Pacific Ocean. *Nature,* **247**, 30-32.

Wunsch, C., 1984; An eclectic Atlantic Ocean circulation model, Part I: The meridional flux of heat, Journal of Physical Oceanography, 14:1712-1733.

Wunsch, C., and J. Minster, 1982; Methods for box models and ocean circulation tracers: Mathematical programming and nonlinear inverse theory, Journal of Geophysical Research, 87(C8):5647-5662.

Yi S., 1966: Seasonal and secular variations of the water volume transport across the Korea Strait, *J. of Oceanographic Soc. of Korea,* **1**, 7-13.

Yoon, J-H., 1982: Numerical experiments on the circulation in the Japan Sea. Pt I. *J Oceanogr. Soc. Japan,* **38**, 43-51.